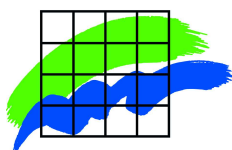
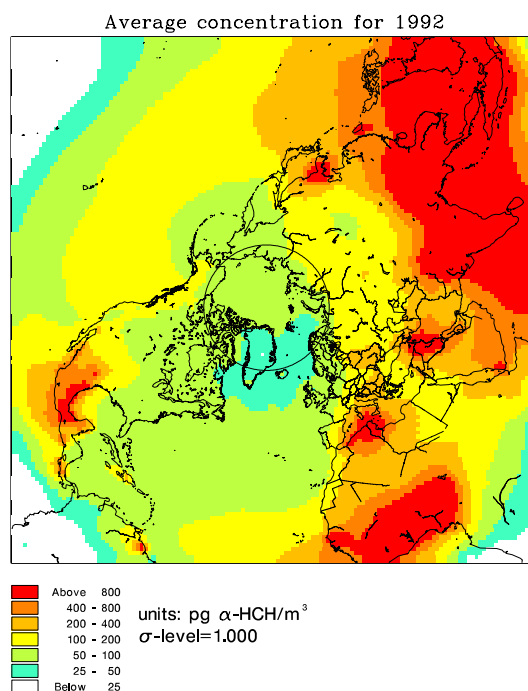


# Transport of persistent organic pollutants into the Arctic

by

Kaj Mantzius Hansen



PhD thesis



Copenhagen Global Change Initiative, Faculty of Science and  
Niels Bohr Institute for Astronomy, Physics and Geophysics  
University of Copenhagen  
and

National Environmental Research Institute  
Department of Atmospheric Environment

May 2006



# Transport of persistent organic pollutants into the Arctic

*PhD Thesis*  
2006

Kaj Mantzius Hansen

Copenhagen Global Change Initiative, Faculty of  
Science, University of Copenhagen

Niels Bohr Institute for Astronomy, Physics and  
Geophysics, University of Copenhagen

and

Department of Atmospheric Environment  
National Environmental Research Institute

## Data sheet

Title: Transport of persistent organic pollutants into the Arctic  
Subtitle: PhD thesis

Author: Kaj Mantzius Hansen  
Department: Department of Atmospheric Environment

University: Copenhagen Global Change Initiative and The Niels Bohr Institute for Astronomy, Physics and Geophysics, Faculty of Science, University of Copenhagen

Publisher: Ministry of the Environment  
National Environmental Research Institute

URL: <http://www.dmu.dk>

Date of publication: May 2006

Please cite as: Hansen, K. M., 2006: Transport of persistent organic pollutants into the Arctic. PhD thesis. Department of Atmospheric Environment, National Environmental Research Institute, Roskilde, Denmark. 250 pp.

Reproduction permitted only when quoting is evident

ISBN: 978-87-7772-928-7

Number of pages: 250

Internet version: The report is available only in electronic format from NERI's homepage.  
Internet-version:  
[http://www2.dmu.dk/1\\_viden/2\\_Publikationer/3\\_Ovrige/rapporter/KMH\\_phd.pdf](http://www2.dmu.dk/1_viden/2_Publikationer/3_Ovrige/rapporter/KMH_phd.pdf)

Supplementary notes: This PhD thesis was submitted to the Faculty of Science, University of Copenhagen in November 2005. In February 2006 it was recommended for acceptance by an international evaluation committee.

Front page figure:  
Annual average a-HCH concentrations in the lowermost atmospheric layer for 1992 predicted by the POP version of the Danish Eulerian Hemispheric Model (DEHM-POP).

To my family:

Pernille, the air that I breathe.

Veronika, the sunshine of my life.

Sigrid, a star on the sky at night. I miss you.



# Contents

<b>1</b>	<b>Introduction</b>	<b>1</b>
1.1	The objectives of this project . . . . .	2
1.2	Structure of the thesis . . . . .	3
1.3	Appendices . . . . .	5
<b>2</b>	<b>Persistent organic pollutants</b>	<b>7</b>
2.1	Groups of POPs . . . . .	7
2.1.1	Intentionally produced chemicals . . . . .	7
2.1.2	Accidentally formed chemicals . . . . .	8
2.2	History of POPs . . . . .	8
2.3	Characteristics of POPs . . . . .	9
2.3.1	Environmental partitioning of POPs . . . . .	10
2.3.2	Physical-chemical properties of POPs . . . . .	12
2.3.3	Environmental fate of POPs . . . . .	14
2.4	Modelling the environmental fate of POPs . . . . .	15
2.4.1	Multi-compartment mass balance models . . . . .	17
2.4.2	Atmospheric chemistry transport models . . . . .	18
2.5	Hexachlorocyclohexane . . . . .	20
2.5.1	Physical-chemical properties of hexachlorocyclohexanes . . . . .	20
2.5.2	Environmental partitioning of hexachlorocyclohexanes . . . . .	22
2.5.3	Modelling the environmental fate of HCH . . . . .	24
<b>3</b>	<b>The model set-up</b>	<b>25</b>
3.1	General description of the model . . . . .	27
3.2	The basic equation . . . . .	29
3.3	Numerical techniques . . . . .	29
3.3.1	Splitting . . . . .	29
3.3.2	Filtering . . . . .	31
3.3.3	Time step . . . . .	31
3.3.4	Boundary and initial conditions . . . . .	31
3.4	Horizontal and vertical diffusion . . . . .	31
<b>4</b>	<b>Environmental sources and sinks</b>	<b>33</b>
4.1	Air . . . . .	33
4.1.1	Partitioning between gas phase and particles . . . . .	34
4.1.2	Dry deposition of particles . . . . .	36

4.1.3	Wet deposition . . . . .	37
4.1.4	Chemical transformation in the atmosphere . . . . .	41
4.2	Soil . . . . .	42
4.2.1	The soil module in DEHM-POP . . . . .	43
4.2.2	Air-soil exchange in DEHM-POP . . . . .	44
4.2.3	Soil degradation in DEHM-POP . . . . .	46
4.3	Ocean water . . . . .	46
4.3.1	Air-water gas exchange . . . . .	47
4.3.2	Loss processes in the surface ocean compartment . . . . .	48
4.3.3	Oceanic transport of POPs . . . . .	49
4.4	Snow . . . . .	50
4.4.1	Air-snow exchange . . . . .	54
4.4.2	Particles within the snowpack . . . . .	56
4.4.3	Meltwater . . . . .	56
4.4.4	Air-meltwater gas exchange . . . . .	57
4.4.5	Degradation . . . . .	57
4.5	Vegetation . . . . .	57
4.5.1	Air-vegetation exchange . . . . .	58
4.5.2	Precipitation-vegetation exchange . . . . .	60
4.5.3	Influence of vegetation on soil . . . . .	60
4.5.4	Degradation . . . . .	61
4.6	Sea ice . . . . .	61
4.6.1	Sea ice in DEHM-POP . . . . .	62
4.7	Other compartments . . . . .	62
4.7.1	Fresh water . . . . .	62
4.7.2	Sediments . . . . .	63
4.7.3	Organic films in urban areas . . . . .	63
<b>5</b>	<b>Model input</b>	<b>65</b>
5.1	Meteorological data . . . . .	65
5.2	Land use and topography data . . . . .	66
5.3	Emissions . . . . .	67
5.4	Initial environmental concentrations . . . . .	68
5.4.1	Air . . . . .	71
5.4.2	Soil . . . . .	71
5.4.3	Ocean water . . . . .	71
<b>6</b>	<b>Model evaluation methods</b>	<b>73</b>
6.1	Available measurements . . . . .	74
6.1.1	Air . . . . .	74
6.1.2	Other media . . . . .	78
6.1.3	Extraction of data from the model simulations . . . . .	78
6.2	Evaluation tools . . . . .	79
6.2.1	Statistics . . . . .	79

<b>7</b>	<b>Results and model performance</b>	<b>81</b>
7.1	Reference simulation . . . . .	81
7.1.1	Temporal trends . . . . .	81
7.1.2	Seasonal patterns . . . . .	83
7.1.3	Particle-phase concentration . . . . .	86
7.1.4	Vertical distribution . . . . .	86
7.1.5	Surface compartment concentrations . . . . .	88
7.2	Evaluation . . . . .	95
7.2.1	Long-term averages . . . . .	95
7.2.2	Source area . . . . .	97
7.2.3	IADN stations . . . . .	100
7.2.4	Québec . . . . .	109
7.2.5	European stations . . . . .	109
7.2.6	Stations in the Arctic . . . . .	120
7.2.7	Vertical distribution . . . . .	134
7.3	Importance of the ocean . . . . .	134
7.3.1	Rörvik . . . . .	135
7.3.2	Stórhöfði . . . . .	137
7.3.3	Alert . . . . .	138
7.4	Importance of the vegetation . . . . .	138
7.4.1	Source area . . . . .	139
7.4.2	Mid-latitude stations . . . . .	140
7.4.3	Arctic stations . . . . .	141
7.4.4	Previous model studies . . . . .	142
7.5	Importance of the snowpack . . . . .	142
7.5.1	The Arctic stations . . . . .	143
7.5.2	North American and European stations . . . . .	145
7.5.3	The role of the snowpack in the environmental cycling of $\alpha$ -HCH . . . . .	147
7.6	Previous DEHM-POP results . . . . .	151
7.7	Comparison with results from other models . . . . .	151
7.8	Summary of the results and model performance . . . . .	152
<b>8</b>	<b>Applications of DEHM-POP</b>	<b>155</b>
8.1	Transport episodes . . . . .	155
8.2	Long-term simulation: 1945-2000 . . . . .	159
<b>9</b>	<b>Summary, conclusions and future perspectives</b>	<b>167</b>
9.1	Summary and conclusions . . . . .	167
9.2	Future perspectives . . . . .	168
<b>10</b>	<b>Acknowledgements</b>	<b>171</b>
	<b>Bibliography</b>	<b>173</b>
<b>A</b>	<b>Paper I</b>	<b>189</b>

<b>B Paper II</b>	<b>205</b>
<b>C Paper III</b>	<b>223</b>
<b>D Paper IV</b>	<b>233</b>

# Chapter 1

## Introduction

Previously, the Arctic was considered to be a pristine environment with little or no industrial production or other pollution sources. However, in the 1950s US Air Force pilots flying Arctic missions began observing murky bands of pollution on the horizon during spring, a phenomenon that was named Arctic haze. Research in the 1970s revealed that the Arctic haze was due to sulphur compounds and black carbon particles originating from iron, nickel and copper smelters and inefficient coal-burning plants in sub-Arctic regions reaching the Arctic through long-range atmospheric transport.

Other pollutants of concern observed but not used or emitted in the Arctic are the persistent organic pollutants (POPs), which are persistent, bioaccumulating compounds with a potential for long-range transport and with harmful effects on human health and the environment, even in small quantities. The first reports of POPs in the Arctic came in 1972 with the detection of dieldrin, dichlorodiphenyltrichloroethane (DDT) and polychlorinated biphenyls (PCBs) in blubber of ringed seals from the Canadian and Norwegian Arctic [Holden, 1972] as cited in Muir *et al.* [1992]. There is now a large number of reports on POPs in Arctic biota, see e.g. Muir *et al.* [1992] for a review. POPs are of particular concern in the Arctic because they up-concentrate in the food chain, and may reach harmful levels in the top predators and the traditional diet of the indigenous people.

POPs are introduced to the Arctic by long-range transport mainly through the atmosphere [e.g. Barrie *et al.*, 1992]. The earliest report of hexachlorocyclohexane (HCH) and other chlorinated compounds in Arctic air dates back to 1979 [Tanabe and Tatsukawa, 1980] as cited in Barrie *et al.* [1992]. Several types of POPs were found in air and sea water in the Arctic in the 1980s, see e.g. Barrie *et al.* [1992] for a review. The detection of POPs in remote regions and the increasing awareness of their harmful effects lead to restrictions or bans of several of the POP compounds. International agreements on ban and reduction of POPs, e.g. the Stockholm convention on persistent organic pollutants, have also been put in place. Environmental concentrations of the ‘classic’ POPs have therefore decreased during the last decades, but they are still measured in most environmental media.

Concentrations of POPs in the environment are generally low compared to other pollutants. Large samples are thus required to quantify the environmental concentrations, e.g. air samples are collected over days and snow samples require snow equivalent to 50 L of meltwater, which makes the measurements time consuming and expensive. The result is a low spatial and temporal resolution of the available measurements. Concurrent to the measurements, modelling exercises can be applied to examine the environmental distri-

bution and thus be an aid to understand the environmental processes that affect the fate of POPs. Traditionally these studies are done using low resolution multi-compartment mass balance models with homogeneous and long-term averaged environmental variables as input [e.g. *Strand and Hov*, 1996; *Wania et al.*, 1999b; *Scheringer et al.*, 2000; *MacLeod et al.*, 2001; *Prevedouros et al.*, 2004b; *Toose et al.*, 2004]. As *Wania* [1999] states: “It is important to note that this low spatial and temporal resolution often is a deliberate restriction rather than a regrettable shortcoming. This is based on the belief that the predictive capability of numerical models of environmental POP behaviour is not limited by the resolution of atmospheric transport processes, but rather by the uncertainties inherent in emission estimates, physical-chemical properties, degradation rates, and air-surface exchange descriptions of POPs”. However, in recent years our understanding of the processes involved in the environmental cycling of POPs has increased, which may justify the attempt to describe the environmental fate of POPs with more detailed models than previously attempted.

## 1.1 The objectives of this project

The aim of this project is to develop a high-resolution 3-D dynamical model that can be used to study the atmospheric transport and environmental fate of POPs within the Northern Hemisphere and especially with focus on the transport into the Arctic. With the characteristics of POPs, an environmental concentration for a given time at a given place is not only the result of an emission event and a subsequent atmospheric transport episode, but also the result of a complex interaction between the air mass and different surface compartments that the air passes over, which may contain previously deposited chemicals. A high-resolution 3-D dynamical model including the most important environmental processes thus potentially can increase our understanding of the environmental fate of POPs. It is also the aim of the study to investigate the role of different environmental compartments or processes in the environmental fate of POPs to increase our understanding of the role of these processes.

The model developed for this purpose is named DEHM-POP and will be a further development of the Danish Eulerian Hemispheric Model (DEHM), which is an atmospheric chemistry transport model covering the majority of the Northern Hemisphere. This model was originally developed to study the transport and deposition of sulphur and sulphate to the Arctic [*Christensen*, 1997]. DEHM has successfully been applied to study the atmospheric transport of these compounds as well as other compounds such as CO<sub>2</sub>, Hg, and various air pollutants [e.g. *Christensen*, 1997; *Geels et al.*, 2004a; *Christensen et al.*, 2004; *Geels et al.*, 2005]. The main work in this project is to expand the DEHM model to include modules describing the POP-related atmospheric processes and the air-surface exchange processes of POPs for the most important surface compartments: soil, water, snow and vegetation, and to test the model for one of the most abundant POPs. The predicted atmospheric concentrations will be evaluated against available measurements of this compound from the Northern Hemisphere.

There are several reasons for choosing a model that only covers the Northern Hemisphere. POPs are of anthropogenic origin and as the Northern Hemisphere accommodate the largest population most major sources of POPs will be included in the model domain.

For example, the major part of both usage and emissions of PCBs are in the Northern Hemisphere [Breivik *et al.*, 2002a, 2002b]. This is also the case for the POPs used in the agriculture, such as the insecticide hexachlorocyclohexane (HCH). The percentage of the global emissions of  $\alpha$ -HCH in the Northern Hemisphere was about 93% in 1980 and 90% in 1990 [Li *et al.*, 2000]. The atmospheric mixing time between the Northern and the Southern Hemisphere is on the order of 1-2 years due to the presence of the intertropical convergence zone at the equator [Seinfeld and Pandis, 1998]. Given this information it is not very likely that there are major sources of POPs on the Southern Hemisphere that influences atmospheric concentrations in the Arctic notably. Finally, Ballschmiter and Wittlinger [1991] concluded that inter-hemispheric exchange of the POPs: DDT, HCH, HCB and PCBs was negligible, although this investigation was made using only a sparse number of air measurements. Excluding the Southern Hemisphere furthermore have the advantage of reducing the computation time in the simulations.

The DEHM-POP model is developed using the  $\alpha$ -isomer of the insecticide hexachlorocyclohexane (HCH) as tracer.  $\alpha$ -HCH is chosen as trace chemical because it is the most abundant POP measured in air, water and snow in the Arctic [AMAP, 1998] and reliable emission estimates exists for this compound [Li *et al.*, 2000].  $\alpha$ -HCH is one of the ‘old’ POPs that are under regulations and the environmental concentrations are thus decreasing. Although  $\alpha$ -HCH is not of imminent concern compared to POPs of more recent origin, it is important to study to get an increased understanding of the environmental processes involved in the environmental cycling of POPs, which eventually will help in the study of the environmental fate of more modern compounds. Several environmental processes that are general for most POPs are included in the model even though they are not important for  $\alpha$ -HCH, e.g. gas-particle partitioning in the atmosphere. The model should thus also be capable of modelling the environmental fate of other POPs. The model has also been applied to study the atmospheric transport of three PCB congeners (although these model simulations are not fully evaluated) and the general applicability for other POPs is therefore possible.

The focus of this study will be the atmospheric transport into the Arctic in the 1990s. There are several ways to define the extent of the Arctic region, e.g. by the Arctic Circle (66°32’N), by floristic boundaries or by the 10°C July isotherm. In this thesis the Arctic is considered to be the Arctic Monitoring and Assessment Programme (AMAP) area, as defined in AMAP [1998] (see Figure 1.1).

## 1.2 Structure of the thesis

- A short introduction to the properties of persistent organic pollutants (POPs) and previous work on modelling atmospheric transport and environmental fate of POPs is given in chapter 2.
- Chapter 3 is a general description of the Danish Eulerian Hemispheric Model applied in this study.
- In chapter 4 the main environmental sources and sinks including the air-surface exchange processes are described in detail.

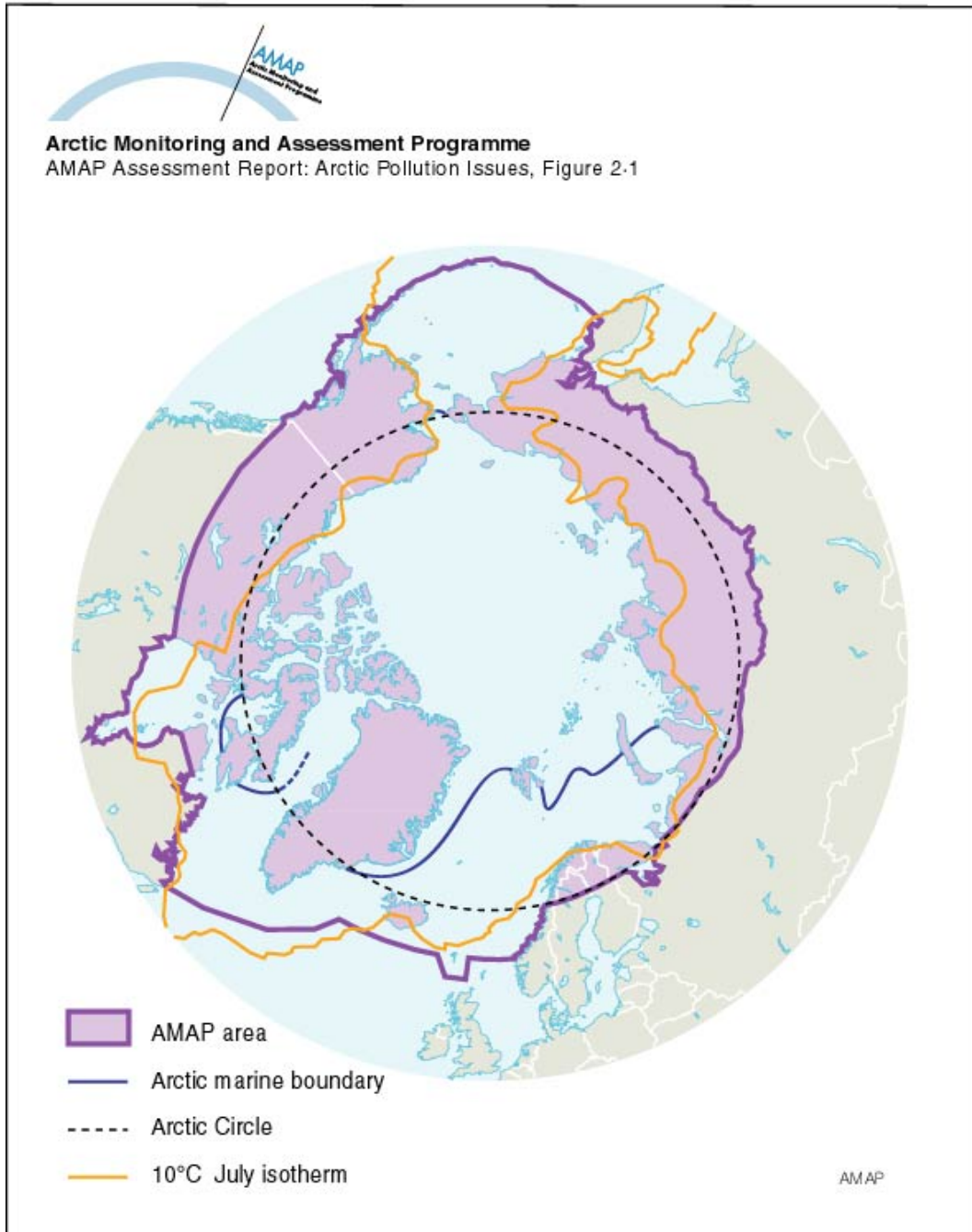


Figure 1.1: The Arctic as defined by the Arctic Monitoring and Assessment Programme. From *AMAP* [1998].

- The various model input required for simulating the environmental fate of POPs are presented in chapter 5.
- Chapter 6 includes a description of the model evaluation tools applied in this study.
- Results of the simulations as well as the performance of the model is described in chapter 7.
- In chapter 8 the application of the model to study specific questions on the environmental fate of POPs is shown.
- Finally, chapter 9 includes a summary of the main findings in this study as well as the future perspectives and applications of this type of models.

### 1.3 Appendices

Four papers written within the PhD-study are included in the Appendices of this thesis. Two of the papers concern results from previous versions of the models (Appendix A and C) and one paper is about the development of a sub-module of DEHM-POP (Appendix B). The fourth paper describes the inter-comparison of DEHM-POP with a fugacity based multi-compartment mass balance model, both in terms of process description and model performance (Appendix D), which is a subject that is not discussed further in this thesis. A short overview of the included papers is given in the following.

1. The paper ‘Modelling atmospheric transport of  $\alpha$ -hexachlorocyclohexane in the Northern Hemisphere using a 3-D dynamical model: DEHM-POP’ (Appendix A) describes the first version of the DEHM-POP model including the two surface modules: soil and ocean water. The atmospheric transport of  $\alpha$ -HCH is simulated for the years 1991-1998 and the results are evaluated against measurements. The paper is published in *Atmospheric Chemistry and Physics*.
2. The paper ‘A dynamic model to study the exchange of gas-phase POPs between air and a seasonal snowpack’ (Appendix B) describes an arctic snow model that was developed to predict the exchange of vapour-phase POPs between the atmosphere and the snowpack over a winter season. Net fluxes for six different gas-phase POPs were predicted based on their wet deposition and vapour exchange between the snow and atmosphere. This snowpack module is developed to be included in the DEHM-POP model. The paper was accepted subject to minor changes by *Environmental Science & Technology* on November 17, 2005.
3. The paper ‘Modelling the atmospheric transport and environmental fate of persistent organic pollutants in the Northern Hemisphere using a 3-d dynamical model’ (Appendix C) is a short description of the further development of DEHM-POP including additional surface compartments: snow and sea ice. The paper is in press, Kluwer Academic/Plenum Publishers.
4. The paper ‘A process-oriented inter-comparison of a box model and an atmospheric chemistry transport model: insights into model structure using  $\alpha$ -HCH as the modelled substance’ (Appendix D) is a comparison of the DEHM-POP model with a

fugacity based multi-compartment mass balance model. The models are compared both in terms of environmental process description and of predicted environmental concentrations. The paper is published in *Atmospheric Environment*.

I have furthermore participated in the development of other models at the National Environmental Research Institute (NERI) related to the objectives of this PhD-study. These model developments have been documented in several publications, which are listed here:

- Frohn, L. M., J. H. Christensen, J. Brandt, C. Geels and K. M. Hansen, 2003: 'Validation of a 3-D hemispheric nested air pollution model'. *Atmospheric Chemistry and Physics Discussions*. Vol. 3, pp. 3543-3588, 2003.
- Geels, C., J. H. Christensen, J. Brandt, L. M. Frohn, K. M. Hansen, 2004: 'A nested hemispheric model for simulations of atmospheric CO<sub>2</sub>'. *In: Air Pollution Modelling and Its Application*, Borrego and Incecik (eds.), Kluwer Academic/Plenum Publishers, New York, pp. 215-223.
- Brandt, J., J. H. Christensen, L. M. Frohn, C. Geels, K. M. Hansen and C. Ambelas Skjøth, 2004: 'The THOR integrated air pollution forecast system - current status and ongoing developments'. *Proceedings from the 2nd GLOREAM/EURASAP Workshop, Modern developments in modelling and chemical data analysis*, Copenhagen, September 6-8, 2004. pp. 10.
- Geels, C., J. Brandt, J. H. Christensen, L. M. Frohn, K. M. Hansen, C. Ambelas Skjøth, 2005: 'Long-term calculations with a comprehensive nested hemispheric air pollution transport model'. *In: Advances in Air Pollution Modeling for Environmental Security*, Farago et al. (eds.), Springer, Netherlands, pp. 11.
- Brandt, J., J. Christensen, L. M. Frohn, R. Berkowicz, C. A. Skjøth, C. Geels, K. M. Hansen, J. Frydendall, G. B. Hedegaard, O. Hertel, S. S. Jensen, M. Hvidberg, M. Ketzel, H. R. Olesen, P. Løfstrøm, and Z. Zlatev, 2005: 'THOR - an operational and integrated model system for air pollution forecasting and management from global to local scale', *Proceedings from the First ACCENT Symposium*, Urbino, Italy, 12th-16th September 2005, pp. 10.

The DEHM-POP model is furthermore part of an ongoing international POP model inter-comparison project under the Cooperative Programme for Monitoring and Evaluation of the Long-Range Transmission of Air Pollutants in Europe (EMEP). Two of the three stages are completed: stage I, concerning the comparison of descriptions of main processes determining POP behaviour in various environmental compartments [Shatalov *et al.*, 2004], and stage II, concerning comparison of mass balance estimates and calculated deposition and concentration fields of POPs in different environmental compartments and a sensitivity study with respect to physical-chemical parameter values used in basic process descriptions and mass balance estimates [Shatalov *et al.*, 2005]. The reports can be found on the internet site: <http://www.msceast.org/publications.html> (as of November 2005).

## Chapter 2

# Persistent organic pollutants

The term ‘persistent organic pollutants’ (POPs) is denoting a group of chemical compounds with different origin but with several common characteristics. The 1998 Aarhus Protocol on Persistent Organic Pollutants under the 1979 Geneva Convention on Long-range Transboundary Air Pollution (CLRTAP) defines POPs in the following way [UN-ECE, 1998]: “Persistent organic pollutants (POPs) are organic substances that: (i) possess toxic characteristics; (ii) are persistent; (iii) bioaccumulate; (iv) are prone to long-range transboundary atmospheric transport and deposition; and (v) are likely to cause significant adverse human health or environmental effects near to and distant from their sources”. The 1998 Aarhus Protocol on Persistent Organic Pollutants is an agreement under the United Nations Economic Commission for Europe (UNECE) to control, reduce or eliminate any discharges, emissions and losses of POPs to the environment. This chapter describes the properties and environmental behaviour of POPs in general and of  $\alpha$ -HCH in particular, as well as the different types of models used to study the environmental partitioning of POPs.

The term POPs is widely used in the literature, also to denote chemicals not included in the CLRTAP protocol [e.g. *AMAP*, 1998, 2004; *Jones and de Voogt*, 1999]. Another name regularly used for this group of compounds is Persistent, Bioaccumulative, Toxic substances (PBTs) [e.g. *Klán and Holoubek*, 2002]. PBTs can be of local, regional or global concern depending on their environmental mobility, and POPs can therefore be considered to be a subset of PBTs prone to long-range transport [*Vallack et al.*, 1998]. In this thesis the term POPs will be used in the broad sense encompassing a large number of compounds, although the modelled compound HCH is included in the CLRTAP protocol.

### 2.1 Groups of POPs

POPs are generally divided into two groups according to their sources; they are either intentionally produced for one or more purposes or they are accidentally formed in production or combustion processes [e.g. *Brevik et al.*, 2004].

#### 2.1.1 Intentionally produced chemicals

The group of intentionally produced chemicals can further be divided into two groups: organochlorine pesticides and industrial compounds.

### Organochlorine pesticides

The organochlorine pesticides were developed in the 1940s and 1950s and widely used until the 1970s and 1980s, where most of them were restricted or banned and they are now to a large extent replaced with less persistent products. The organochlorine pesticides constitute the largest group of chemicals subject to the international agreements, 11 of the 16 substances on the CLRTAP list are pesticides (see section 2.2). These include mainly insecticides such as dichlorodiphenyltrichloroethane (DDT), hexachlorocyclohexane (HCH), mirex, dieldrin and chlordanes.

### Industrial compounds

The group of chlorinated industrial compounds includes the polychlorinated biphenyls (PCBs), consisting of 209 different congeners with different degree of chlorination. PCBs were used for example for hydraulic, transformer and heat-exchange fluids. Of more recent concern are the polybrominated diphenyl ethers (PBDEs) and the polychlorinated naphthalenes (PCNs). The PBDEs are used as flame retardants in polymeric materials and the PCNs are used in several industrial applications e.g. as insulation in capacitors, transformers, cable, and wires.

#### 2.1.2 Accidentally formed chemicals

The main classes of unintentionally by-products are the polychlorinated dibenzo-*p*-dioxins (PCDDs), the polychlorinated dibenzofurans (PCDFs) and the polycyclic aromatic hydrocarbons (PAHs). The PCDD/Fs consist of 75 and 115 different congeners respectively, which are formed as by-products during chlorination processes and combustion. PAHs are important components of both crude and refined oil and are produced during the incomplete combustion of coal, wood and oil. Unlike the other POPs, PAHs also have natural sources, such as forest fires and natural losses or seeps of petroleum, which complicates the estimation of anthropogenic PAH pollution. Another substance released accidentally to the environment is hexachlorobenzene (HCB), which is a by-product in the production of several pesticides and a large number of chlorinated industrial compounds. HCB was also used as a fungicide to a limited extent.

## 2.2 History of POPs

Most of the POPs now subject to regulations were developed in the 1930s and 1940s and their usage expanded rapidly. A growing environmental concern in the 1960s and 1970s, especially with the emergence of the bestselling book "*Silent spring*" [Carson, 1962], led to a reconsideration of the use of POPs and many countries put restrictions on usage or bans on some of the POPs. A typical history of usage and emission to the environment of the POPs is depicted in Figure 2.1.

Increasing awareness of the long-range transport potential and harmful environmental effects of POPs led to the initiation of international agreements on the ban of production and usage and/or reduction of POP-emissions. The 1998 Aarhus Protocol on Persistent Organic Pollutants under the 1979 Geneva Convention on Long-range Transboundary Air Pollution is signed by 36 and ratified by 24 governments within the UNECE region (As

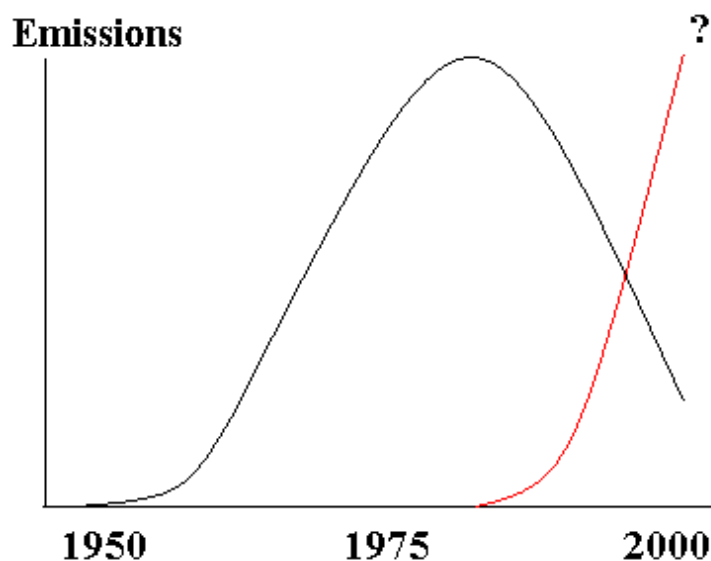


Figure 2.1: Typical usage and environmental emission history of POPs. The black line corresponds to the ‘classic’ POPs now under restrictions, such as the HCHs and the PCBs, while the red line corresponds to compounds of more recent concern, such as the PBDEs. Modified from *Jones and de Voogt* [1999].

of 5 September 2005) [UNECE, 1998]. There are at present 16 priority substances on the list. The production and use of the pesticides aldrin, chlordane, chlordecone, dieldrin, endrin, heptachlor, mirex, and toxaphene and the industrial compound hexabromobiphenyl is banned. The use of DDT, HCHs and PCBs is severely restricted and DDT, heptachlor, hexachlorobenzene (HCB), and PCBs are scheduled for elimination at a later stage. Finally, the emissions of PCDD/Fs, PAHs and HCB are to be reduced to below 1990-levels [UNECE, 1998].

Several other local initiatives were taken to reduce emissions to the environment, e.g. the North American Commission for environmental co-operation and several agreements to protect the marine environments of the North Sea, the North-East Atlantic Ocean, the Baltic Sea and the Mediterranean Sea [Vallack *et al.*, 1998].

A global international agreement is the Stockholm Convention on Persistent Organic Pollutants under the United Nations Environment Programme (UNEP), which aim to eliminate or control 12 specific substances worldwide (aldrin, chlordane, DDT, dieldrin, endrin, heptachlor, HCB, mirex, toxaphene, PCBs, PCDDs and PCDFs) [UNEP, 2005a]. The Stockholm Convention on POPs is signed by 151 governments and ratified by 113 (as of November 2005) and has therefore been enforced by 17 May 2004 [UNEP, 2005b].

## 2.3 Characteristics of POPs

The CLRTAP protocol and the Stockholm convention operates with similar definitions of POPs as persistent, bioaccumulating compounds with a potential for long-range transport

and with toxic effects on human health and the environment [UNECE, 1998; UNEP, 2005a]:

- The definition of persistence is that the half-life in water is greater than two months or the half-life in soil or sediments is greater than six months or that there is other evidence that the chemical is sufficiently persistent to be of concern.
- A compound bioaccumulates if the logarithm of the octanol-water partition coefficient ( $\log K_{ow}$ )<sup>1</sup> is greater than 5 or if the bioconcentration factor (BCF)<sup>2</sup> or the bioaccumulation factor (BAF)<sup>3</sup> is greater than 5000 or if there is other evidence that the chemical bioaccumulates.
- There is potential for long-range transport if the half-life of a compound in air is greater than two days or if it is detected in remote regions.
- If there is evidence of adverse effects or indications of potential damage to human health or the environment a compound is said to be toxic. Observed adverse effects are e.g. effects on the reproduction, development and the immune system and the promotion of tumors.

Both protocols also include references to detailed procedures developed to expand the list of priority substances [UNECE, 1998; UNEP, 2005a]. Following the procedure for the CLRTAP protocol *Lerche et al.* [2002] investigated four compounds and nominated polychlorinated naphthalenes (PCNs) as a candidate to be included in the priority list. Several compounds have also been suggested to be included in the Stockholm convention, e.g. HCH, chlordecone, hexabromobiphenyl and pentabromodiphenyl ether (one of the PBDEs) [UNEP, 2005a].

### 2.3.1 Environmental partitioning of POPs

The environmental partitioning of POPs depends on their mode of entry into the environment, their transport and reactions in the environmental compartments and on environmental conditions, such as temperature, humidity and soil organic carbon content.

#### Release of POPs to the environmental compartments

POPs are released to the environmental compartments by different means depending on their origin. Pesticides are mainly released into or onto agricultural soils or onto crops. Fractions of the used compounds can be emitted into the air, either during the application through spray drift or through post-application processes such as tilling and wind erosion of soils. Partitioning into the water within the soil and subsequent run-through can lead to contamination of ground water, rivers and marine waters.

Industrial products are primarily released to the atmosphere either during production or during disposal of products containing the compounds. Industrial production can also

---

<sup>1</sup> $K_{ow}$  is defined in section 2.3.2.

<sup>2</sup>BCF is defined as the concentration of a chemical in an organism (plants, microorganisms, animals) divided by the concentration in a reference compartment, e.g. food or surrounding water.

<sup>3</sup>BAF is defined as the ratio of the concentration of a substance in an organism to the concentration in water, based on uptake from the surrounding medium and food.

lead to local contamination of soil and thereby fresh water around the production or disposal sites, e.g. land fills. Combustion by-products are also emitted to the atmosphere.

Pesticide emissions are seasonally variable, with few major emission events often during spring or summer depending on agricultural practice. The emission of industrial organochlorines from production is more or less constant throughout the year, whereas emissions from disposal are higher during summer than winter due to temperature dependence of emission factors. For the combustion by-products the emissions are presumably higher during winter than summer due to increase in combustion heat sources.

### **Transport of POPs in the environmental compartments**

The atmosphere is the fastest environmental transport path, and most POPs are believed to enter the Arctic through the air [e.g. *Barrie et al.*, 1992]. It can take a few days or weeks for the air from source regions to reach into the Arctic [*AMAP*, 2004].

Pollutants are also transported in the oceans by the ocean currents. Although the transport is slow, it can be important depending on the partitioning into water compared to the partitioning into air [*AMAP*, 2004].

Soil is a stagnant medium, so there is no horizontal transport of POPs in soil. Partitioning into the water within the soil and subsequent run-through can though lead to transport of POPs within the soil. A recent model study has suggested that vertical movement of chemicals sorbed to soil particles, by e.g. bioturbation, cryoturbation and erosion into cracks in dry soil is of importance for the environmental fate of POPs [*McLachlan et al.*, 2002].

Fresh water transport through major rivers is considered to be an important source of contamination of the Arctic Ocean [e.g. *Barrie et al.*, 1992; *Macdonald et al.*, 2000; *AMAP*, 2004]. Sea ice may also be a mean of POPs re-distribution. POPs sorbed to particles bound to sea ice can be transported out of the Arctic Ocean to melt regions in the Fram Strait [*AMAP*, 2004]. Another transport pathway that may be of importance for the transport into the Arctic is through migratory animals, e.g. seabirds, cetaceans, salmon, and Arctic cods [*AMAP*, 2004].

### **Exchange of POPs between the environmental compartments**

There are several environmental processes that lead to exchange of POPs between the different environmental compartments. In the air POPs can associate with particles. Both gas-phase and particle-phase POPs are scavenged by rain and snow and are thus transferred to the underlying surface. Particles are also deposited on the surface by dry deposition, and gas-phase POPs can be deposited as well as re-emitted from the surface. Contaminated water can run through soil into a fresh water compartment and from there through rivers into the ocean. POPs sorbed to particles in water are deposited to sediments and re-suspension of sediments can transfer them back into the water in some areas. Finally, POPs are uptaken by animals, in the terrestrial food web from air or soil to vegetation, to herbivores and then to carnivores and in the marine food web from the water to phytoplankton, to zooplankton, to fish, and then to sea birds, and marine mammals.

## Reactions with other environmental constituents

Although termed as persistent, POPs do react with other environmental constituents and they are thereby degraded or transformed into other and, often, less persistent products. In air there are mainly two types of reactions, photolysis and oxidation. Photolysis happens when chemical reactions or rupture of chemical bonds are sparked by the energy in sun light. The main oxidation of POPs are reactions with OH radicals, but there can also be reaction with other radicals, such as the nitrate ( $\text{NO}_3$ ) radical and ozone ( $\text{O}_3$ ). In water POPs are subject to hydrolysis, a process in which the compounds reacts with water, hydrogen ion or hydroxyl ion. Finally, POPs undergo biodegradation, which occur in both water and soil. This term covers a wide range of processes in microbial organisms.

### 2.3.2 Physical-chemical properties of POPs

One of the main factors determining the environmental behaviour of POPs is their physical-chemical properties, such as the vapour pressure and solubilities into different environmental matrices, e.g. water, soil, and lipids.

Evaporation of a compound into air is primarily determined by its vapour pressure and dissolution into water by its aqueous solubility. The partitioning of the compound between air and water can then be described by the air-water partition coefficient,  $K_{aw}$ , which is given by the ratio of the vapour pressure to the aqueous solubility.  $K_{aw}$  is related to the Henry's law constant,  $H$  by:

$$K_{aw} = \frac{H}{RT}, \quad (2.1)$$

where  $R$  is the universal gas constant and  $T$  is temperature.  $K_{aw}$  is often referred to as the dimensionless Henry's law constant.

It has turned out that *n*-octanol is a good surrogate for both natural organic matter in soils and sediments, for lipids and for plant waxes [Mackay, 2001]. Environmental partitioning can therefore be described by partitioning in a three-phase system: air, water and octanol with three partition coefficients: the partition coefficient between octanol and water,  $K_{ow}$ , between octanol and air,  $K_{oa}$ , and  $K_{aw}$  [Mackay, 2001]. In such a system only two of the partition coefficients are independent [Mackay, 2001], since e.g.

$$K_{aw} = \frac{K_{ow}}{K_{oa}}. \quad (2.2)$$

POPs typically have partition values of  $K_{aw}$  between  $10^{-1}$  and  $10^{-4}$ ,  $K_{ow}$  between  $10^3$  and  $10^8$ , and of  $K_{oa}$  between  $10^5$  and  $10^{12}$  (see Figure 2.2). POP partitioning into organic phases is thus higher than into water by 3 to 8 orders of magnitude and higher than into air by 5 to 12 orders of magnitude.

The physical-chemical properties are more or less temperature dependent. Solubilities into water and octanol, and thus  $K_{ow}$ , are generally only slightly temperature dependent, whereas the vapour pressure, and therefore also  $K_{aw}$  and  $K_{oa}$ , are highly temperature dependent. There are several ways to describe the temperature dependence of a partition coefficient,  $K_{xx}$ , but it is often described by a modified van't Hoff equation of the form [e.g. Xiao *et al.*, 2004]:

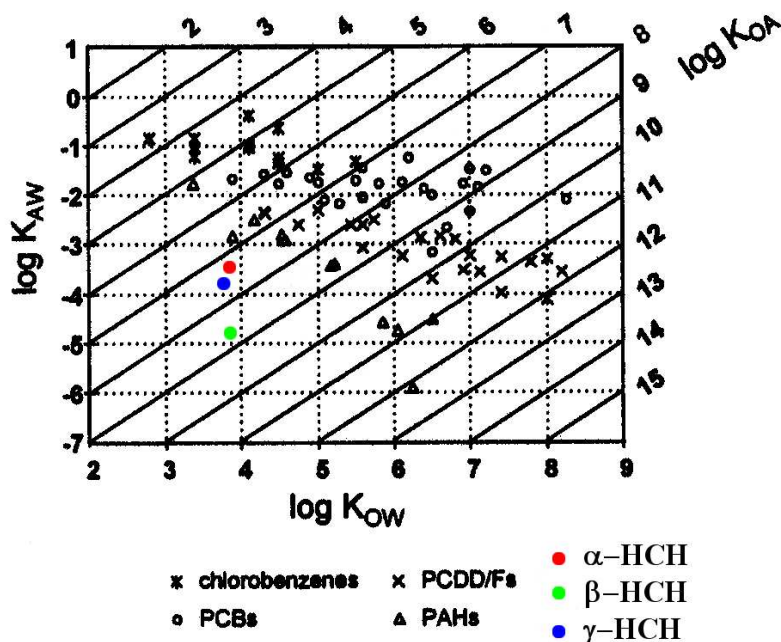


Figure 2.2: The  $K_{ow}$ (x-axis),  $K_{aw}$ (y-axis), and  $K_{oa}$ (diagonal) partitioning space. Symbols denote classes of selected POPs. Modified from *Wania and Mackay [1999a]*.

$$\log(K_{xx}(T)) = \log(K_{xx}(T_0)) - \frac{\Delta U_{xx} + RT_0}{\ln(10)R} \left( \frac{1}{T} - \frac{1}{T_0} \right), \quad (2.3)$$

where  $K_{xx}(T_0)$  is the partition coefficient at a reference temperature  $T_0$  and  $U_{xx}$  is the internal energy of phase transfer for the corresponding partition coefficient. This equation rests on the assumption that  $\Delta U_{xx}$  is independent of temperature, which is not the case for all properties for all organic compounds [*Shiu and Ma, 2000a, 2000b; Beyer et al., 2002*]. The expression is thus in general only valid within a relatively small temperature interval [*Beyer et al., 2002*], but alternative expressions can be used for those chemicals where the equation is not applicable [*Shiu and Ma, 2000a, 2000b*].

Vapour pressure and solubilities can be measured, although not all compounds have measurable solubilities due to miscibility. The partition coefficients can be estimated from the vapour pressure and solubilities [e.g. *Paasivirta et al., 1999*], if such data are available. Or they can be measured directly in laboratory studies, which has been done for a range of compounds, e.g. temperature dependent Henry's law constants for HCHs [*Kucklick et al., 1991; Sahuvar et al., 2003*]. Finally, there are various techniques to estimate the partition coefficients from molecular properties, e.g. molecular structure [e.g. *Chen et al., 2002*] and molecular connectivity index [*Zhao et al., 2005*].

When partition coefficients calculated from measured solubilities and vapour pressures are compared to measured partition coefficients or when partition coefficients measured in different experiments are compared they are typically not consistent, i.e., the relationship between the three phases (Equation 2.2) is not fulfilled. To overcome this problem

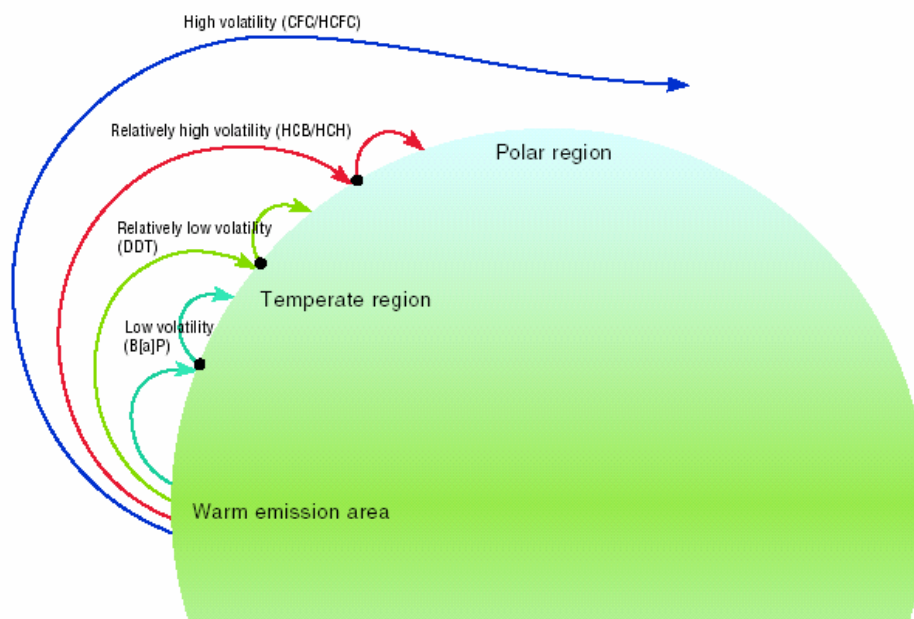


Figure 2.3: An illustration of ‘the global fractionation’ hypothesis. Differences in volatility leads to a global fractionation of POPs. From *AMAP* [2004].

an adjustment technique was developed in which measured properties are corrected by an evenly distribution of an eventual deviation from equilibrium between the measured properties [Beyer *et al.*, 2002]. This technique was applied for 50 compounds including several PCBs, PAHs and organochlorine pesticides [Beyer *et al.*, 2002]. The technique was further developed to include a procedure for compiling and evaluating measured data from the literature and selecting literature-derived values through averaging or linear regressions and by estimating uncertainties of the literature-derived values which are used in the adjustment procedure [Li *et al.*, 2003a]. This procedure was used to derive consistent physical-chemical properties for 16 PCB congeners [Li *et al.*, 2003a] and for  $\alpha$ -,  $\beta$ -, and  $\gamma$ -HCH [Xiao *et al.*, 2004].

### 2.3.3 Environmental fate of POPs

All the above mentioned factors interact to determine the environmental fate of POPs. Although POPs are referred to as a group, the differences in usage pattern and particularly in physical-chemical properties leads to divergent fate of the different POPs. It is thus not possible to state a general theory of the global fate of all POPs. There are however a few hypotheses that are generally accepted to increase our understanding of the environmental distribution of POPs. According to the ‘global fractionation hypothesis’ differences in volatility arising from different physical-chemical properties (especially the vapour pressure) leads to different atmospheric transport distances, and thereby a fractionation of the compounds (see Figure 2.3) [e.g. Wania and Mackay, 1993].

POPs are deposited to the surface through either wet or dry deposition. On the ground, POPs may be sorbed onto the surface of vegetation or soil or be dissolved in water. If the temperature rises, the surface-sorbed or dissolved POPs may re-volatilise into the atmosphere due to their temperature dependent physical-chemical properties, and here they can undergo further atmospheric transport. This effect is termed the ‘grasshopper effect’ (also indicated in Figure 2.3) [e.g. *Wania and Mackay*, 1996]. In this way POPs can undergo several cycles of transport, deposition and re-volatilisation, which complicates the description of their fate, since they are not easily tracked from source to eventual observation.

The temperature dependence of the volatility has another effect. When POPs reach cold environments such as the Arctic the low temperatures make it difficult for them to escape the region and they are thus ‘trapped’. This phenomenon has been named ‘cold condensation’ [e.g. *Wania and Mackay*, 1993, 1996]. The fate of  $\alpha$ -HCH is frequently mentioned as a good example of the ‘cold condensation’ process with higher measured concentrations in Arctic and North Pacific ocean water than closer to primary source regions, such as the southeast Asia (see Figure 2.4). This pattern prevails although only less than 1% of the emitted  $\alpha$ -HCH is estimated to reach the Arctic [*Wania and Mackay*, 1999b; *Li et al.*, 2004a]. This is due to the relatively small size of the Arctic as a whole and especially of the environmental organic phases with capacity of retaining POPs [*Wania and Su*, 2004]. Measurements have shown that mountain regions also can act as cold traps of POPs [e.g. *Blais et al.*, 1998].

The environmental system is complex and POPs do not behave simply according to these general ideas. For example, despite having the same source,  $\beta$ -HCH is shown to behave differently than  $\alpha$ -HCH [*Li et al.*, 2002].  $\beta$ -HCH has slightly lower  $K_{aw}$ -values than  $\alpha$ -HCH, which leads to a faster atmospheric depletion of  $\beta$ -HCH by precipitation and gaseous deposition to the ocean water and it is thus stripped out of the atmosphere before the air reaches the Arctic resulting in higher concentrations in the North Pacific Ocean than in the Arctic Ocean [*Li et al.*, 2002].

## 2.4 Modelling the environmental fate of POPs

Numerous models have been developed to study the environmental fate of POPs. These models of varying complexity can be a help in the understanding of the environmental processes that are influencing the fate of POPs. There are generally two different types of environmental fate models: multi-compartment mass balance models (also called box models) and atmospheric chemistry transport models (CTM).

In a box model the environment is described by a number of well-mixed compartments with homogeneous environmental characteristics. Relatively simple mathematical expressions are used to calculate the exchange and distribution of a compound between the compartments.

The CTMs are generally characterized by having a high spatial resolution of the atmosphere with less focus on the surface as this only acts as receptor for regular air pollutants. The models are adjusted to account for the two-way air-surface exchange processes that are involved in the environmental cycling of POPs. The high spatial resolution makes them very computationally demanding.

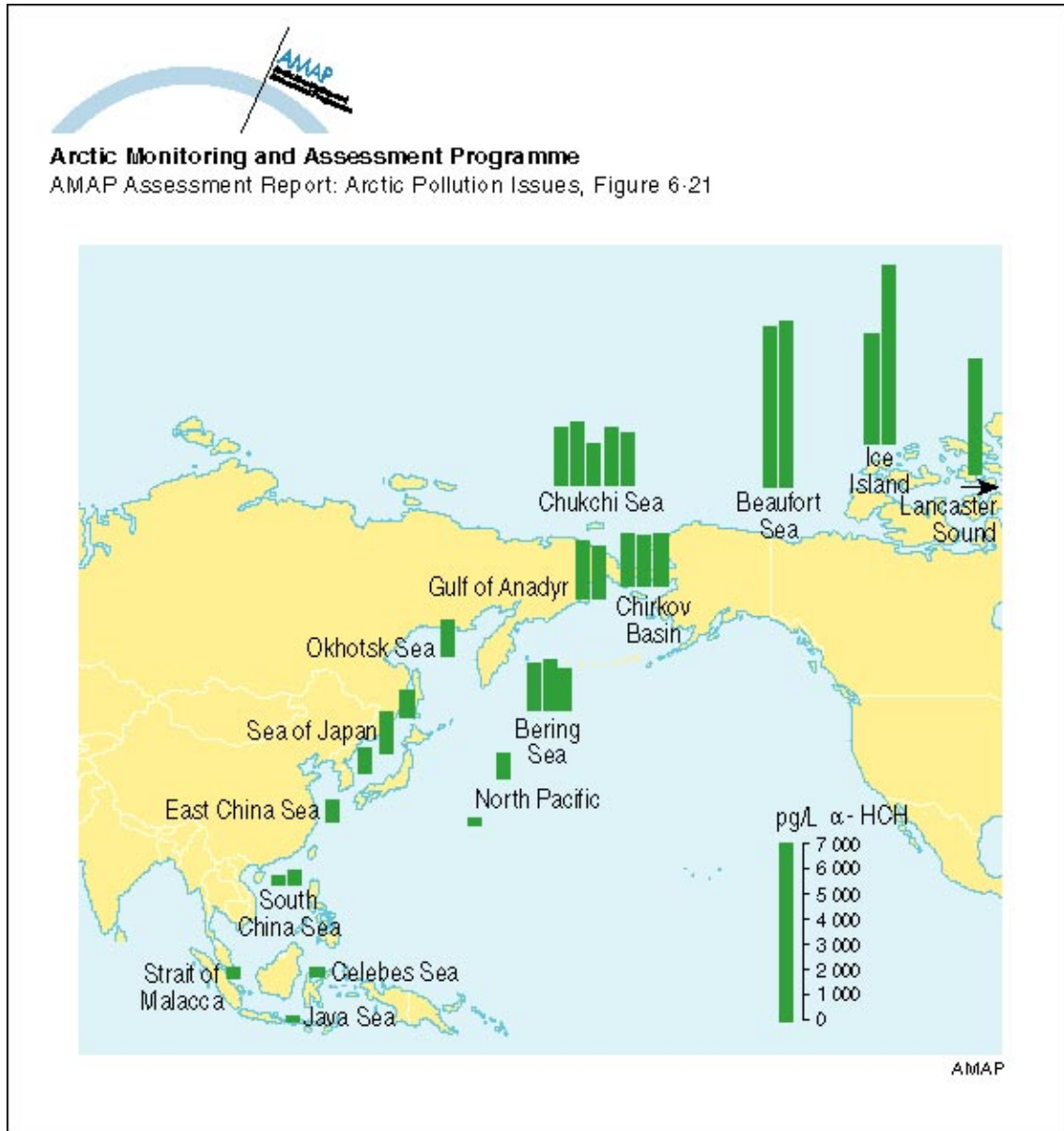


Figure 2.4: Measured  $\alpha$ -HCH concentrations in Pacific and Arctic Ocean water from the late 1980s and early 1990s, illustrating the ‘cold condensation’ effect. From *AMAP* [1998].

The two types of models can be seen as supplementing each other; box models are well suited to study long-term environmental fate and large scale patterns, whereas CTMs offer the opportunity to study short-term fluctuations and particular long-range transport episodes [Wania, 1999]. However, the two types of models seem to converge in recent years with a more and more increased spatial resolution of the box models and more focus on the surface modules as well as adoption of box model features by the CTMs.

The proper choice of model depends on the aim of the conducted study. To classify a range of substances for long range transport potential, which requires a large number of similar model simulations with slightly different input, a simple evaluative box model may be more suitable than a computationally demanding CTM. The latter may be more appropriate to use if the objectives of the study is short-term environmental variations of a specific compound, and CTMs also seem more appropriate for highly resolved predictions of source-receptor relationships.

#### 2.4.1 Multi-compartment mass balance models

The vast number of multi-compartment mass balance models can be classified into biological uptake models, models describing individual environmental processes, evaluative models, and models describing actual chemical fate on local, regional or global scale [Wania and Mackay, 1999a]. Below a short description of the four classes, with the focus on the last class, is given; a comprehensive review on the development of mass balance models can be found in Wania and Mackay [1999a] and references therein.

Biological uptake models describe the uptake of POPs in vegetation, in individual organisms, most often fish, or the uptake and transfer in entire food chains.

The individual environmental process models describes e.g. the partitioning between two environmental phases or the transport between two environmental compartments or transformation within an environmental compartment. These process models are often used as building blocks of the more complex evaluative models.

The evaluative models describe the behaviour of POPs in a purely hypothetical environment. These models can be focused on a few environmental processes or they can include several environmental compartments, typically air, soil, water and sediment, to evaluate the environmental distribution and partitioning behaviour of POPs. They are primarily used for classifying and ranking chemicals.

Most multi-compartment mass balance models aim to describe the environmental fate and behaviour of POPs in real environmental settings, either on a local, regional or global scale. These models can be regionalised versions of the evaluative models, where the input parameters have been adjusted to reflect regional conditions. A further development of this type of model is the spatially resolved model, which covers a region or the entire globe with several zones each consisting of a set of environmental compartments. The individual zones are connected through flow of air and water, where long-term average wind speeds and ocean currents typically are used.

There is a great diversity in the extent of the model domains, the number of modelled zones, and the methods to acquire and include data on the environmental conditions. The size and extent of the zones can be defined either from climatic zones [e.g. Wania and Mackay, 1995, 1999b], continental or political boundaries [e.g. Toose et al., 2004], major water basins [e.g. MacLeod et al., 2001] or they can be in regular grids [e.g. Scheringer

*et al.*, 2000; *Prevedouros et al.*, 2004b; *MacLeod et al.*, 2005]. The models can cover specific regions such as North America [*MacLeod et al.*, 2001], the Baltic area [*Breivik and Wania*, 2002a, 2002b], Europe [*Prevedouros et al.*, 2004b, 2004a] or they can cover the entire globe [e.g. *Wania and Mackay*, 1995, 1999b; *Scheringer et al.*, 2000; *MacLeod et al.*, 2005].

Information on size and extent of each compartment and exchange between climate zones and between environmental compartments is inferred from geographical reference databases and climatic averages of meteorological data. A recent development has been to integrate GIS-based environmental information, which is used e.g. in the Berkeley-Trent (BETR) framework [*MacLeod et al.*, 2001; *Woodfine et al.*, 2001]. From this concept models covering the North American continent (BETR-NA) [*MacLeod et al.*, 2001], the major part of Europe (EVn-BETR) [*Prevedouros et al.*, 2004b, 2004a] and the entire globe (BETR-World) [*Toose et al.*, 2004] and (BETR-global) [*MacLeod et al.*, 2005] have been developed. Another model based on GIS is the Grid-Catchment Integrated Modelling System (G-CIEMS) covering Japan and surroundings [*Suzuki et al.*, 2004].

The number of multi-compartment mass balance models has increased rapidly in recent years and the tendency is towards an increasing number of regions, e.g. for the global models from 10 [*Wania et al.*, 1999b] over 60 [*Scheringer et al.*, 2000] to 288 [*MacLeod et al.*, 2005].

Most of the multi-compartment mass balance models use the fugacity approach [*Mackay*, 2001]. Fugacity has the unit of pressure and describes the tendency of a chemical to escape from a medium. At low concentrations fugacity is proportional to concentrations, with the proportionality coefficient called the fugacity capacity, which describes the capacity of a chemical to remain in the medium. If a chemical's fugacities for two media are equal the media are in equilibrium and there is thus no exchange, which is not necessarily the case for equal concentrations. The use of the fugacity approach also facilitates the calculation of phase-transfer and comparison of important loss processes [*Wania*, 1999]. A thorough description of the principles of fugacity box modelling is given by *Mackay* [2001].

## 2.4.2 Atmospheric chemistry transport models

Another mean of studying the environmental distribution of POPs is by adapting classical atmospheric chemistry transport models (CTM) to POPs. This implies the addition of surface modules to describe the two-way air-surface exchange processes of POPs. CTMs often use high-resolution meteorological data as drivers, either observational, re-analyzed or from a numerical weather prediction model. There are two groups of CTMs: Lagrangian models and Eulerian models.

### Lagrangian models

The Lagrangian models are based on a number of air trajectories, which are calculated with a time interval from a source point or a receptor point and followed for a number of days. The models typically operates by calculating air trajectories from a number of source/receptor points to estimate the concentration or deposition in a number of receptor points or the origin of the receptor point concentrations. This type of model is well suited for determining the path of air from a specific source region to a contaminated area. The disadvantage of the Lagrangian models is that the trajectories can be very

uncertain depending on the meteorological situation and that the models become computational demanding if a large number of trajectories are calculated. The limitation of the trajectories makes the Lagrangian model regional/continental in extent rather than hemispheric/global. *Voldner and Schroeder* [1989] used a modified trajectory model to study the transport and deposition of toxaphene to the Great Lakes. The distribution of Lindane and B[a]P in parts of Europe was estimated by *van Jaarsveld et al.* [1997], and recently the deposition of PCDD/Fs to the great Lakes was studied with a model using a high number of source points [*Cohen et al.*, 2002].

Air trajectories can also be calculated backwards, i.e. from a receptor point to track the source of an observed concentration. This has been used in several studies [e.g. *Poissant and Koprivnjak*, 1996; *Halsall et al.*, 1997; *Bailey et al.*, 2000].

### Eulerian models

In Eulerian models, the concentrations of the studied compound is calculated in regular grids, and the models have generally a high horizontal and vertical resolution of the atmosphere. The high atmospheric resolution is retained for the POP versions of the Eulerian CTM with the addition of surface modules.

The Eulerian CTMs can be of regional, hemispheric and global scale. *Ma et al.* [2003a] coupled a regional CTM with fugacity based soil-air and water-air exchange modules. The model is covering the majority of Canada and the central and northern part of the United States with a horizontal resolution of  $35 \text{ km} \times 35 \text{ km}$  and with 12 vertical layers up to a height of 7 km. The model was used to study the impact of Lindane usage in the Canadian prairies on the Great Lakes Ecosystem [*Ma et al.*, 2003a, 2004b].

A regional model covering the majority of Europe and a model covering the Northern Hemisphere were developed concurrent under the Cooperative Programme for Monitoring and Evaluation of the Long-Range Transmission of Air Pollutants in Europe (EMEP) [e.g. *Malanichev et al.*, 2004; *Gusev et al.*, 2005]. The models have the same modules describing the atmospheric removal and air-surface exchange processes but with different air transport modules. The regional model is covering the EMEP region with a horizontal resolution of  $50 \text{ km} \times 50 \text{ km}$ . The hemispheric model is in the horizontal defined in geographical coordinates with a spatial resolution of  $2.5^\circ \times 2.5^\circ$  and it has nine vertical layers up to a height of approximately 12 km [*Malanichev et al.*, 2004]. The model was for example used to study the environmental fate of four PCB congeners in the Northern Hemisphere [*Malanichev et al.*, 2004].

A global model with a horizontal resolution of  $2^\circ \times 2^\circ$  and 11 vertical layers up to a height of 15 km was developed to study the environmental fate of  $\alpha$ -HCH for the years 1993 and 1994 [*Koziol and Pudykiewicz*, 2001]. Another model with global coverage is the model developed by Lammel and co-workers [*Lammel et al.*, 2001; *Semeena and Lammel*, 2003, 2005]. This model is based on an atmospheric general circulation climate model, which implies that the meteorological data used as driver are climatic representative for the model period but does not reflect the actual atmospheric constitution. The horizontal resolution is  $2.8^\circ \times 2.8^\circ$  and it has 19 vertical layers up to a height of about 30 km [*Semeena and Lammel*, 2005]. The model has been used to study different emission scenarios for DDT and  $\gamma$ -HCH [*Semeena and Lammel*, 2003] and the significance of the grasshopper effect on atmospheric distributions of DDT and  $\gamma$ -HCH [*Semeena and Lammel*, 2005].

Using non-averaged data as meteorological driver for the Eulerian models has the advantage of reflecting the actual atmospheric circulation pattern. Recent statistical studies have shown correlations between mid-latitude air concentration measurements of POPs and climatic indices reflecting the general atmospheric circulation pattern such as the El Niño–Southern Oscillation (ENSO) [Ma *et al.*, 2003b, 2004c], the North Atlantic Oscillation (NAO) and the Pacific North American pattern (PNA) [Ma *et al.*, 2004a, 2004c].

## 2.5 Hexachlorocyclohexane

DEHM-POP is developed using  $\alpha$ -hexachlorocyclohexane ( $\alpha$ -HCH) as tracer. The chemical formula of HCH is  $C_6H_6Cl_6$ . HCH was previously misnamed benzene hexachloride (BHC) in the literature because the six carbon atoms are placed in a ring-like structure. However, the ring is not planar and the chlorine and hydrogen atoms are placed in either equatorial or axial positions in eight different combinations. The isomers are denoted with Greek letters:  $\alpha$ -,  $\beta$ -,  $\gamma$ -,  $\delta$ -,  $\epsilon$ -,  $\eta$ -, and  $\theta$ -HCH, with two enantiomeric forms of  $\alpha$ -HCH (see Figure 2.5).

HCH was first synthesized in 1825 by Michael Faraday and in 1942 its pesticidal properties were discovered [Smith, 1991] as cited in Willett *et al.* [1998]. HCH is used worldwide in two different formulations: Technical HCH and Lindane. Technical HCH contains five stable isomers in a mixture with typical percentages of:  $\alpha$ : 60–70%,  $\beta$ : 10–12%,  $\gamma$ : 6–10%,  $\delta$ : 3–4%,  $\epsilon$ : 3–4% depending on the manufacturer [Willett *et al.*, 1998]. Lindane is a refined product containing almost pure  $\gamma$ -HCH, the isomer that exhibits the highest insecticidal activity [Willett *et al.*, 1998].

Technical HCH is the most used insecticide worldwide [Li *et al.*, 2000], with an estimated usage of  $9.4 \times 10^6$  tonnes between 1947 and 1997 with maximum usage around 1980 [Li *et al.*, 2003b]. Li [1999] made an extensive review on the global usage of Technical HCH and the contamination consequences, and found e.g. that China is the country with the highest amount used (4464 ktonnes), followed by India (1057 ktonnes) and the former Soviet Union (693 ktonnes), whereas the countries with the highest usage-density is Egypt (182 tonnes  $kha^{-1}$ ), Japan (80 tonnes  $kha^{-1}$ ) and Kuwait (68 tonnes  $kha^{-1}$ ) [Li, 1999]. The most contaminated countries globally have been India, China and Japan, but in different periods, typically up to the year of ban [Li, 1999]. Technical HCH was banned in most countries during the 1970s and 1980s, e.g. 1972 in Japan, 1976 in USA, 1983 in China, 1988 in France and 1990 in the former Soviet Union [Li, 1999]. Only small amounts are used worldwide today, primarily for control against malaria mosquitos. Lindane is still in use as seed treatment in some countries, but is banned in most other countries [Li, 1999].

A review of the toxicologic effects of HCH can be found in Willett *et al.* [1998] and references therein. The HCHs primarily affect the central nervous system but have also effects on renal and liver functions and on the reproduction as well as developmental effects and there are also indications that  $\beta$ -HCH has estrogenic effects [Willett *et al.*, 1998].

### 2.5.1 Physical-chemical properties of hexachlorocyclohexanes

The HCHs are some of the most volatile POPs with relatively high vapour pressures compared to other POPs. In general they also partition more readily into water with low

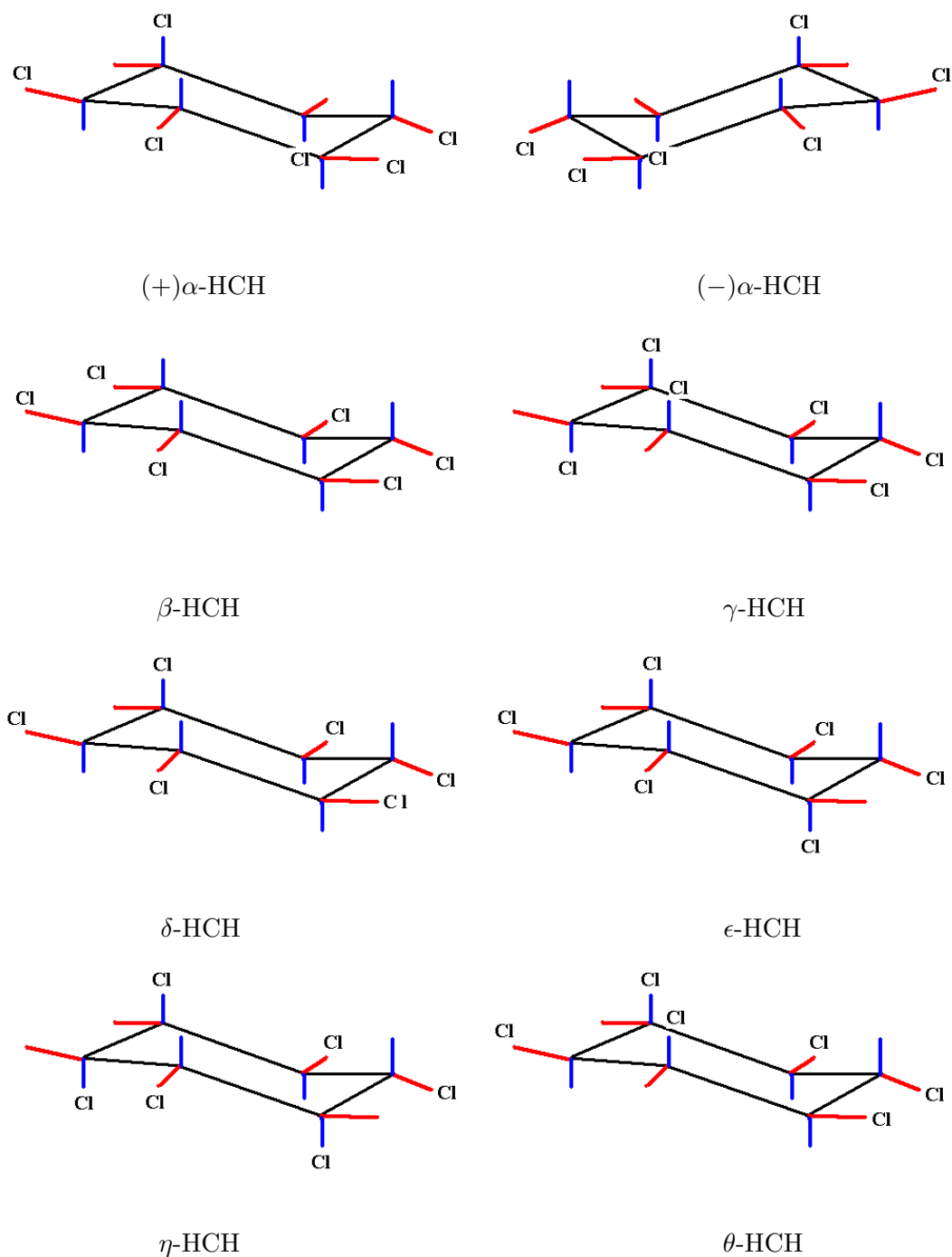


Figure 2.5: The structure of the two enantiomers of  $\alpha$ -HCH, and the  $\beta$ -,  $\gamma$ -,  $\delta$ -,  $\epsilon$ -,  $\eta$ -, and  $\theta$ -HCH isomers. The axial (blue — a) and equatorial (red — e) positions of the chlorine atoms are:  $\alpha$ , aeceea;  $\beta$ , eeeeee;  $\gamma$ , aaacee;  $\delta$ , aeceee;  $\epsilon$ , aeaeae;  $\eta$ , aaeae; and  $\theta$ , aeaece. Modified from *Willet et al.* [1998].

Table 2.1: Selected physical-chemical properties of  $\alpha$ -,  $\beta$ -, and  $\gamma$ -HCH at 25°C. All values are taken from *Xiao et al.* [2004] except for  $K_{aw}$  which is calculated from Equation 2.1.

Parameter	$\alpha$ -HCH	$\beta$ -HCH	$\gamma$ -HCH
Melting point (°C)	158	315	114
Liquid vapour pressure (Pa)	0.245	0.0529	0.0757
$K_{ow}$	$8.63 \times 10^3$	$8.22 \times 10^3$	$6.79 \times 10^3$
$K_{oa}$	$2.91 \times 10^7$	$5.54 \times 10^8$	$5.50 \times 10^7$
Henry's law constant, $H$ (Pa m <sup>3</sup> mol <sup>-1</sup> )	0.735	0.037	0.306
$K_{aw}$	$2.97 \times 10^{-4}$	$1.53 \times 10^{-5}$	$1.27 \times 10^{-4}$

$K_{aw}$ -values and relatively low  $K_{oa}$ -values resulting in low partitioning to particles in the atmosphere (see Figure 2.2). The main physical-chemical parameters used in this study ( $K_{aw}$ ,  $K_{ow}$ , and  $K_{oa}$ ) are chosen from *Xiao et al.* [2004] (see Table 2.1). The temperature dependence of the partition coefficients is described using Equation (2.3). An eventual temperature dependence of the energy of phase transfer is not discussed by *Xiao et al.* [2004]. The partition coefficients are given over a temperature interval from 277 K to 323 K. Care should, thus, be taken when evaluating results for environmental extremes, e.g. at the top of the model domain in approximately 18 km height, where the temperature can be as low as 200 K.

## 2.5.2 Environmental partitioning of hexachlorocyclohexanes

HCH appear to be omnipresent in the environment and has been measured in numerous environmental matrices such as air, water, snow, soil, and sediments and different types of vegetation and biota, see e.g. *Willett et al.* [1998] for a review. The HCHs are the most abundant POPs measured in air, water, snow, and zooplankton in the Arctic, whereas it is less abundant higher in the food web (see Figure 2.6). This pattern arise as a combination of the large emitted amount compared to some of the other POPs and of the physical-chemical properties of HCH, i.e. the high volatility, the low  $K_{aw}$  and the strong temperature dependence of  $K_{aw}$  favouring the partitioning into air and water. The result is a high concentration in Arctic Ocean water compared to concentrations at lower latitudes (see Figure 2.4), although this only applies to  $\alpha$ -HCH as discussed earlier. The uptake in biota is limited by the relatively low  $K_{ow}$ . Although  $\alpha$ -HCH constitutes the largest fraction of the emitted HCHs, the  $\beta$ -isomer is relatively more abundant in biota due to higher  $K_{oa}$ - and  $K_{ow}$ -values and a greater persistence towards bio-degradation.

The sorption to particles in the atmosphere can be correlated to either the vapour pressure or the  $K_{oa}$  (see section 4.1.1 on page 34). The high vapour pressure and relatively low  $K_{oa}$ -values for the HCHs should result in only little sorption of HCHs to particles [e.g. *Bidleman*, 1988]. This is confirmed by measurements, e.g. at the Canadian station Alert in the high Arctic with temperatures as low as -40°C, where the average fraction sorbed on particles is less than 1% of the measured gas-phase fraction [*Halsall et al.*, 1998].

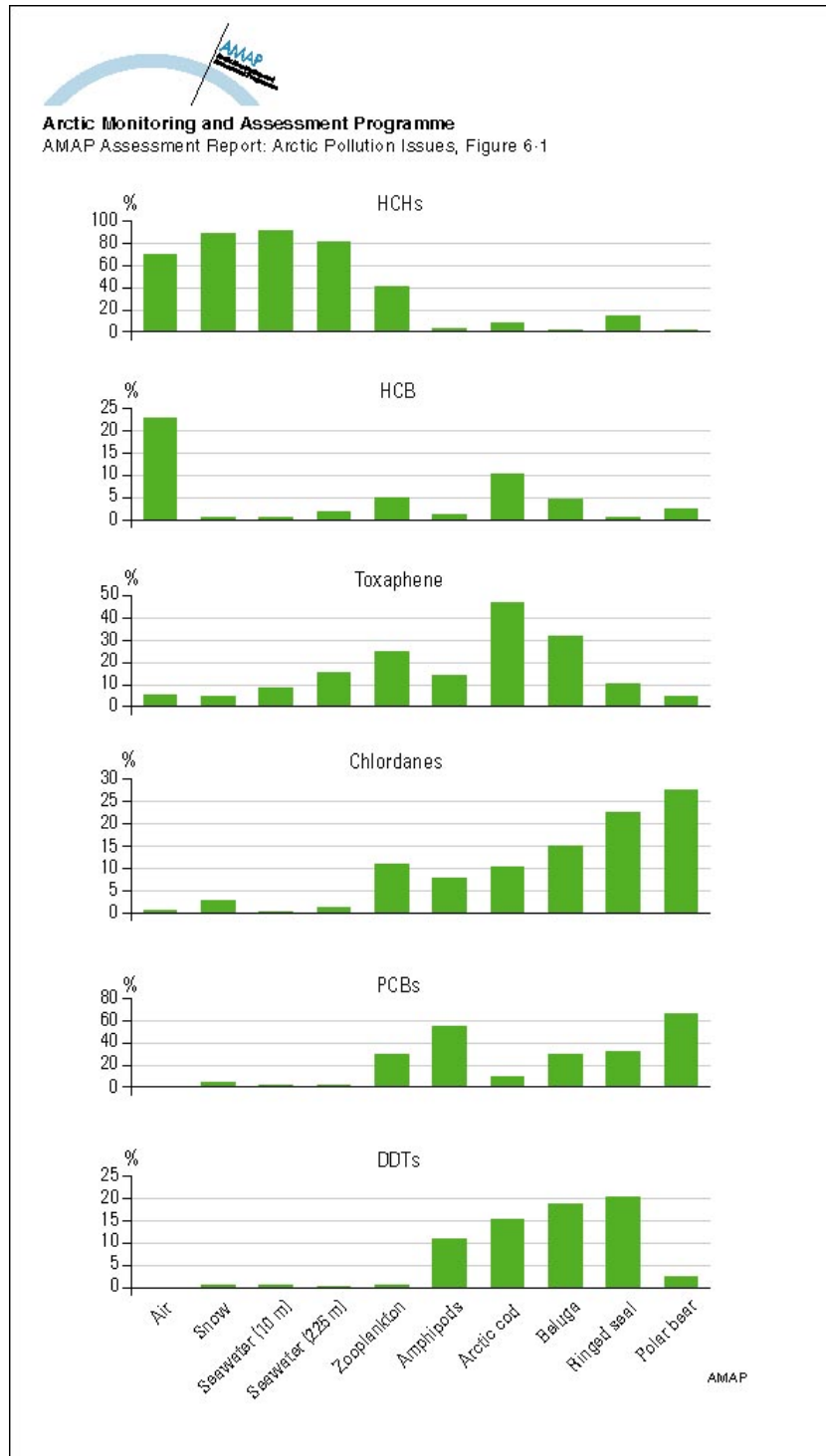


Figure 2.6: The abundance of HCHs relative to other major POPs in various media in the Arctic. From *AMAP* [1998].

### 2.5.3 Modelling the environmental fate of HCH

Several models have been used to study the environmental fate of  $\alpha$ -HCH. A regional non-steady-state multi-compartment mass balance model covering the Baltic Sea region based on the global distribution model of *Wania et al.* [1999b], was used to study the environmental fate of  $\alpha$ -HCH for the years 1970–2000 [Breivik and Wania, 2002a, 2002b]. This model obtains very good predictions of both seasonally averaged and individual measured air concentrations at Lista, Norway and Rörvik, Sweden for the 1980s and 1990s [Breivik and Wania, 2002a].

Three different global box models were used previously to study the global fate of  $\alpha$ -HCH. Two models have 6 and 10 zonally averaged regions, respectively [Strand and Hov, 1996; Wania et al., 1999b]. The third model is divided into 25 zones following both climatic and continental or political borders [Toose et al., 2004]. The results from the Strand and Hov model are given as annual average concentrations for the year 1985 [Strand and Hov, 1996]. The other two models were run for a 50 year period.

Only one atmospheric chemistry transport model using dynamic meteorological data as input was used to study the environmental fate of  $\alpha$ -HCH [Koziol and Pudykiewicz, 2001]. The model is a global atmospheric transport model with a horizontal resolution of  $2^\circ \times 2^\circ$  and 11 vertical layers, and it has been used to study the atmospheric transport of  $\alpha$ -HCH for the years 1993–1994 [Koziol and Pudykiewicz, 2001]. A clear seasonal pattern with higher values during summer than winter is seen in the model results for the four studied stations: Alert and Tagish in Canada, Spitzbergen in Svalbard, and Dunai Island in Russia [Koziol and Pudykiewicz, 2001].

## Chapter 3

# The model set-up

The model applied in this study is the Danish Eulerian Hemispheric Model (DEHM), a three-dimensional Eulerian atmospheric chemistry transport model. DEHM was initially developed at the National Environmental Research Institute (NERI) in the mid-1990s with the main purpose to study long-range transport of SO<sub>2</sub> and SO<sub>4</sub><sup>2-</sup> into the Arctic. For a thorough description of the original model see *Christensen* [1995, 1997].

The model setup and design has been further developed to study other air pollutants and to include up-to date numerical methods. Several versions of the model now exists each dedicated to the study of specific pollutants:

- DEHM-SO<sub>X</sub>, the original model developed to study atmospheric transport of SO<sub>2</sub> and SO<sub>4</sub><sup>2-</sup> [*Christensen*, 1997].
- DEHM-Pb, a version describing the atmospheric transport of lead [*Christensen*, 1999].
- DEHM-Hg, used to study transport, transformation and deposition of reactive and elemental mercury [*Christensen et al.*, 2004; *Skov et al.*, 2004; *Heidam et al.*, 2004].
- DEHM-CO<sub>2</sub>, modelling transport and exchange of atmospheric CO<sub>2</sub> [*Geels et al.*, 2001, 2002; *Geels*, 2003; *Geels et al.*, 2004a, 2004b].
- DEHM-REGINA, applied to study concentrations and depositions of various pollutants through the inclusion of an extensive chemistry scheme including 63 compounds at present [*Frohn et al.*, 2002, 2003; *Frohn*, 2004; *Geels et al.*, 2005].
- DEHM-POP, the model described in this thesis developed to study atmospheric transport and environmental fate of persistent organic pollutants [*Hansen et al.*, 2004, 2006a].

Several air pollutants have a long life-time in the atmosphere so a large model domain is necessary in order to include the effect of long-range transport from distant sources. Applying the desired high spatiotemporal resolution in the full large domain would, nevertheless, be very computer demanding, and it is not necessary as often the focus is on specific regions within the model domain. DEHM has therefore been extended to include one or multiple two-way nested domains over e.g. Europe and/or Greenland, to study

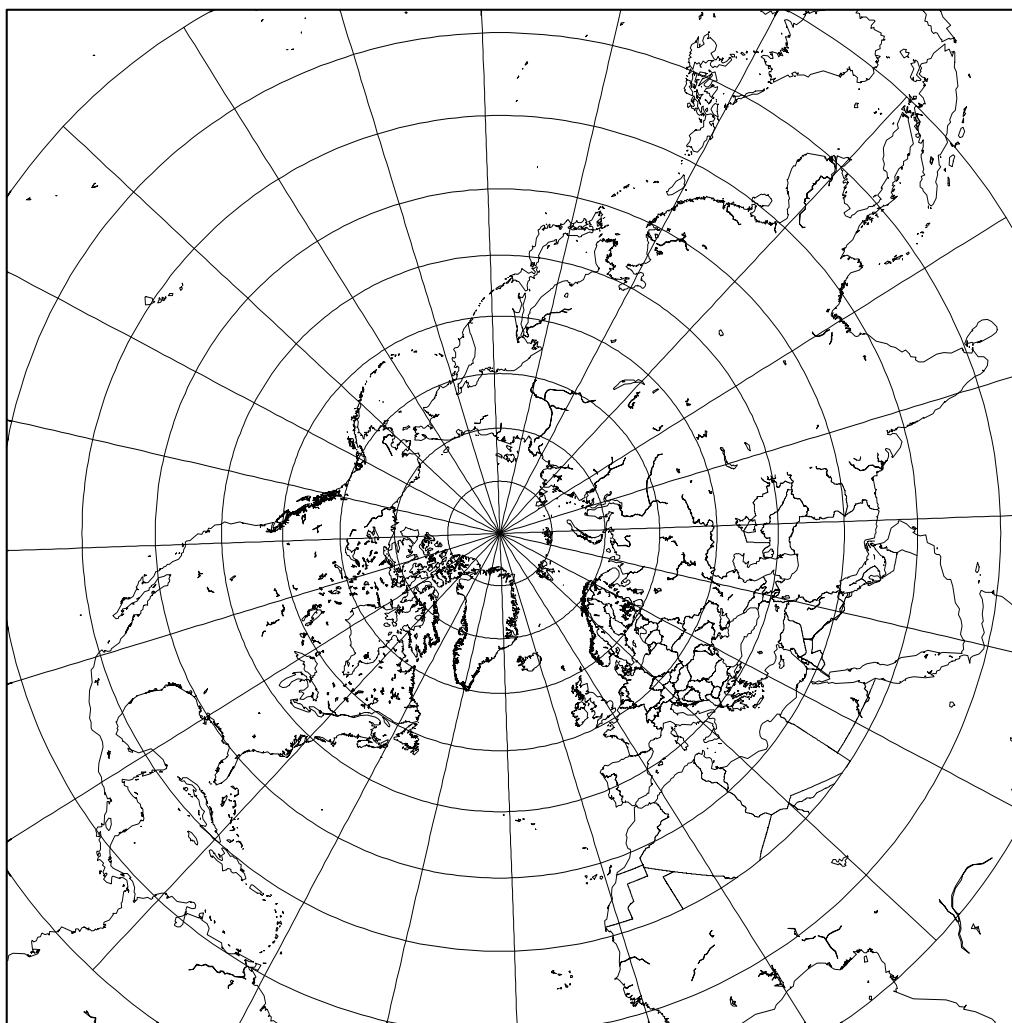


Figure 3.1: The horizontal DEHM-POP model domain. A polar stereographic projection centered around the Arctic Ocean is applied. Circles depict latitudes spaced with  $10^\circ$ .

detailed spatiotemporal variations of air pollutants at a higher resolution. The nesting options have been used in DEHM-CO<sub>2</sub> [Geels *et al.*, 2001, 2004b] and DEHM-REGINA [Frohn *et al.*, 2002]. Details about the implementation of nests can be found in Frohn *et al.* [2002]; Geels [2003]; Frohn [2004]. The implementation of the Fifth-Generation NCAR/Penn State Mesoscale Model (MM5v2) [Grell *et al.*, 1995] as meteorological driver of DEHM allows for the use of multiple nests and the use of grid resolutions alternative to the meteorological input data obtained from the European Center for Medium-range Weather Forecasts (ECMWF) previously used in DEHM. A description of the numerical methods used in the nested version of DEHM, and a thorough and very successful testing of the model system including two nests is described in detail by Frohn *et al.* [2002].

DEHM has also been combined with other models in order to broaden its usage; the model is part of the integrated model system THOR, recently developed at NERI [Brandt

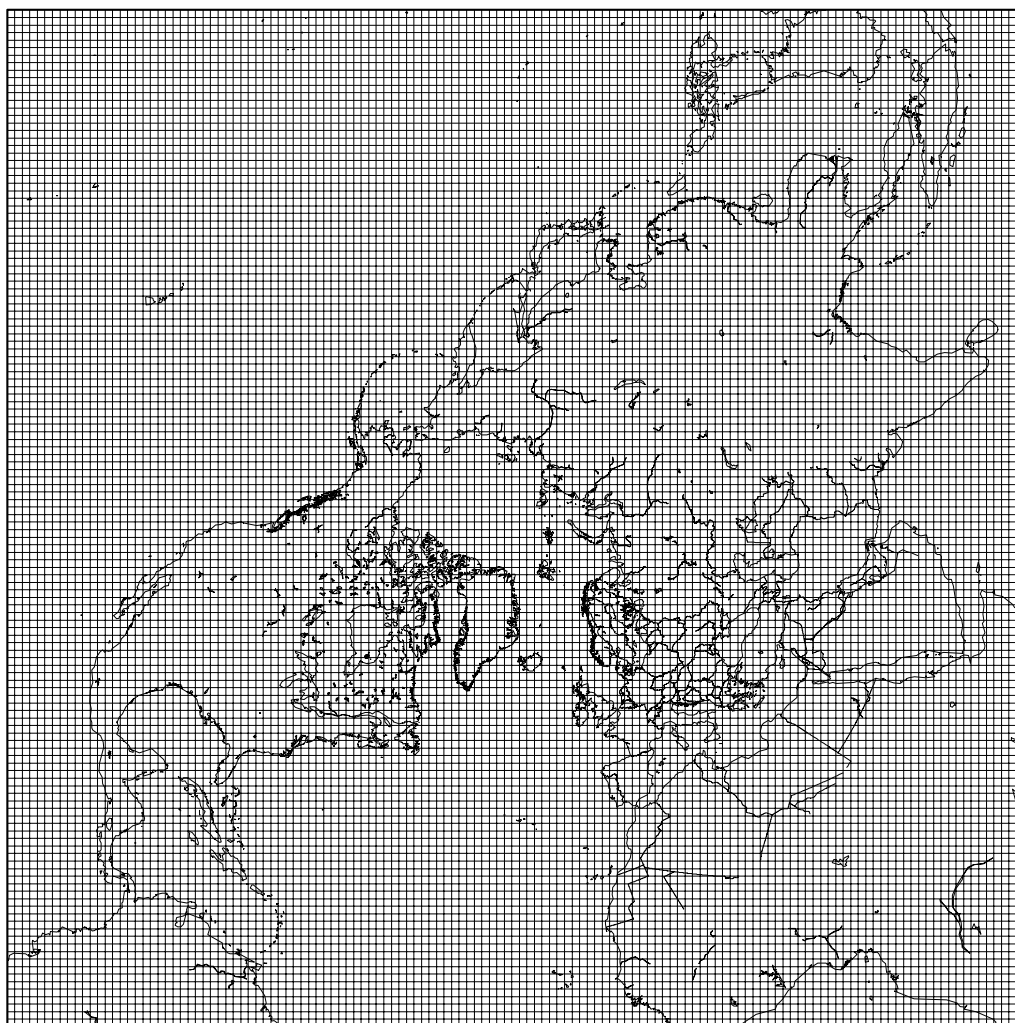


Figure 3.2: The DEHM-POP model domain and the associated horizontal grid with a resolution of  $150 \text{ km} \times 150 \text{ km}$  at  $60^\circ \text{N}$ .

*et al.*, 2001, 2004, 2005]. The THOR system is an operational air pollution forecasting system covering regional, local and street scales.

In the present study the model is used without nests. The atmospheric transport model, the applied numerical methods as well as the relevant parameterization of boundary conditions etc. will shortly be described in the following sections. The parameterizations of the air-surface exchange processes of POPs are described in detail in chapter 4.

### 3.1 General description of the model

The domain of the DEHM-POP model covers almost the whole of the Northern Hemisphere and extends into the Southern Hemisphere (Figure 3.1). The model is defined on a regular  $135 \times 135$  grid in the horizontal, an expansion of the original  $96 \times 96$  grid.

Table 3.1: The 20 vertical layers in the DEHM-POP model with the matching  $\sigma$  levels and approximate height in meters above the ground for the middle of the layers, the approximate thickness of the layers and density of air within the layers. The heights are estimated for a standard atmosphere.

Model layer	$\sigma_{middle}$	Height $z$ [m]	Thickness $\Delta z$ [m]	Density [kg m <sup>-3</sup> ]
20	0.040	~16030	~3250	~0.17
19	0.115	~12780	~2710	~0.31
18	0.185	~10610	~1990	~0.41
17	0.260	~8800	~1780	~0.53
16	0.350	~7050	~1660	~0.59
15	0.450	~5480	~1450	~0.74
14	0.550	~4160	~1220	~0.82
13	0.650	~3030	~940	~0.91
12	0.725	~2280	~610	~0.96
11	0.775	~1810	~450	~1.00
10	0.825	~1380	~380	~1.06
9	0.863	~1060	~260	~1.11
8	0.888	~860	~200	~1.11
7	0.913	~660	~200	~1.14
6	0.938	~460	~180	~1.17
5	0.960	~290	~140	~1.20
4	0.974	~190	~80	~1.20
3	0.982	~130	~60	~1.20
2	0.989	~80	~70	~1.22
1	1.000	~20	~40	~1.22

DEHM-POP is expanded to include the whole of India, a major source of  $\alpha$ -HCH in the Northern Hemisphere with one of the largest historically usage of Technical HCH. The spatial resolution is 150 km  $\times$  150 km at 60°N (Figure 3.2).

In the vertical, the model is divided into 20 unevenly distributed layers with the upper boundary at approximately 18 km. The model has the highest vertical resolution in the lowest  $\sim$  2 km due to the importance of the processes in the atmospheric boundary layer. The vertical model layers are discretized using terrain-following  $\sigma$ -coordinate i.e. the lowest grid level follows the terrain, which simplifies the boundary conditions. Height and thickness of the model layers are, thus, variable both spatially and temporally. In Table 3.1 the vertical model layers, the corresponding  $\sigma$  values and approximate heights above the surface of the middle of the layers, the thickness of the layers and the approximate density of air in the layers are shown for a standard atmosphere. The vertical velocity is always zero at the ground ( $\sigma = 1.0$ ), and the only flux at the lower boundary will therefore

be due to surface emissions and air-surface exchanges.

## 3.2 The basic equation

Using the Eulerian approach, the continuity equation for a chemical compound in the air takes the form:

$$\begin{aligned} \frac{\partial \bar{q}}{\partial t} = & - \left( m \left( \bar{u} \frac{\partial \bar{q}}{\partial x} + \bar{v} \frac{\partial \bar{q}}{\partial y} \right) + \bar{\sigma} \frac{\partial \bar{q}}{\partial \sigma} \right) \\ & + \left( \frac{\partial}{\partial x} \left( m^2 K_x \frac{\partial \bar{q}}{\partial x} \right) + \frac{\partial}{\partial y} \left( m^2 K_y \frac{\partial \bar{q}}{\partial y} \right) + \frac{\partial}{\partial \sigma} \left( K_\sigma \frac{\partial \bar{q}}{\partial \sigma} \right) \right) \\ & + \bar{P}(x, y, \sigma, t, \dots) - \bar{Q}(x, y, \sigma, t, \dots), \end{aligned} \quad (3.1)$$

where:

- $q = c/\rho$  is the mixing ratio, with  $c$  being the air concentration of the modelled compound and  $\rho$  the air density.
- $t$  is time,
- $x$  and  $y$  are the horizontal coordinates in the plane,
- $u$  and  $v$  are the corresponding horizontal velocities,
- $\sigma$  is the vertical coordinate, and
- $\dot{\sigma}$  is the vertical velocity in  $\sigma$ -coordinates.
- $m$  is the polar stereographic projection map scale factor used to convert lengths defined on a sphere to lengths defined on the plane.
- $K_x$  and  $K_y$  are the horizontal eddy diffusion coefficients described in detail in section 3.4,
- $K_\sigma$  is the vertical eddy diffusion coefficient, described in detail in section 3.4.
- $P$  and  $Q$  are the source and sink term, respectively.

This form of the continuity equation is derived from the general form using Reynolds decomposition, averaging, and gradient transport theory ( $K$ -theory), by converting horizontal coordinates using the polar stereographic projection and by converting the vertical coordinates to  $\sigma$ -coordinates. A thorough derivation can be found in *Christensen* [1995]; *Frohn* [2004]. Bars denote average values arising from the Reynolds decomposition.

## 3.3 Numerical techniques

### 3.3.1 Splitting

The physical processes represented by the different terms in Equation (3.1) act over different time scales. Therefore it can be an advantage to split the continuity equation into

sub-models that are solved consecutively. The most efficient numerical technique can be chosen for each sub-model and applied separately in every time step during the time integration. This will generally result in a more stable and efficient numerical scheme, which is assumed to be more important than the error caused by the splitting. For a detailed discussion on typical splitting procedures and the associated error see *Lanser and Verwer [1999]*; *Sportisse [2000]*; *Blom and Verwer [2000]*. Equation (3.1) is here divided into five sub-models according to the different physical processes:

1. Three-dimensional advection:

$$\frac{\partial \bar{q}^{(1)}}{\partial t} = - \left( m \left( \bar{u} \frac{\partial \bar{q}^{(1)}}{\partial x} + \bar{v} \frac{\partial \bar{q}^{(1)}}{\partial y} \right) + \bar{\sigma} \frac{\partial \bar{q}^{(1)}}{\partial \sigma} \right) \quad (3.2)$$

2. and 3. Horizontal diffusion:

$$\frac{\partial \bar{q}^{(2)}}{\partial t} = \frac{\partial}{\partial x} \left( m^2 K_x \frac{\partial \bar{q}^{(2)}}{\partial x} \right) \quad (3.3)$$

$$\frac{\partial \bar{q}^{(3)}}{\partial t} = \frac{\partial}{\partial y} \left( m^2 K_y \frac{\partial \bar{q}^{(3)}}{\partial y} \right) \quad (3.4)$$

4. Vertical diffusion:

$$\frac{\partial \bar{q}^{(4)}}{\partial t} = \frac{\partial}{\partial \sigma} \left( K_\sigma \frac{\partial \bar{q}^{(4)}}{\partial \sigma} \right) \quad (3.5)$$

5. Atmospheric sources and sinks:

$$\frac{d\bar{q}^{(5)}}{dt} = \bar{P}(x, y, \sigma, t, \dots) - \bar{Q}(x, y, \sigma, t, \dots) \quad (3.6)$$

Sub-model 1, the three-dimensional advection, is solved by an accurate space derivatives (ASD) scheme for the horizontal part and a finite element scheme for the vertical part. These are described in detail in *Christensen [1995]* and *Frohn et al. [2002]*. The time integration of the advection is solved by a Taylor series expansion to third order.

The horizontal and vertical diffusion (sub-model 2–4) are solved by applying a finite elements scheme for the spatial discretizations and the  $\theta$ -method with  $\theta = 0.5$  (i.e. the Crank-Nicolson method) for the integration in time [*Christensen, 1993, 1995, 1997*].

By assuming that  $P$  and  $Q$  are constant within a given time step sub-model 5 is solved analytically. The numerical methods for sub-model 1-4 have been carefully tested [see *Christensen, 1995*; *Frohn et al., 2002*, and references herein]. At each time step the set of differential equations (3.2)-(3.6) is coupled as the mixing ratio ( $\bar{q}^{(1)}$ ) estimated in sub-model 1 is used as input in sub-model 2 ( $\bar{q}^{(2)}$ ), which is then used as input in sub-model 3 and so on.

### 3.3.2 Filtering

The choice of numerical methods for each sub-model is mainly determined by the requirement of high accuracy of the model results. This is obtained e.g. by solving the advection with the ASD method, which is an accurate high-order numerical scheme. Solutions from this scheme are, though, affected by high frequency computational noise, which result in spurious oscillations especially in areas with sharp mixing ratio gradients. The noise can propagate through the domain and affect the surrounding grid points, which can possibly lead to unrealistic solutions e.g. with negative concentrations. When a high-order numerical scheme is combined with a filtering technique, high accuracy solutions without or at least with less computational noise can be obtained. In DEHM a horizontal mass-conservative Forester filter [Forester, 1977] is applied at each time step in order to smooth out possible oscillations in the concentration field. To deal with negative mixing ratios a mass-conservative Bartnicki filter is applied, which redistributes possible negative values over the positive solution [Bartnicki, 1989].

### 3.3.3 Time step

The time step ( $\Delta t$ ) is determined in sub-model 1 and the time integration is calculated using a Taylor series expansion to third order, with a Courant-Friderich-Levy stability criterion for numerical stability equal to 0.49. The lowest of the three following values is used as time step:

$$\Delta t = \frac{0.49}{u/\Delta x}; \Delta t = \frac{0.49}{v/\Delta y}; \Delta t = \frac{0.49}{\dot{\sigma}/\Delta \sigma} \quad (3.7)$$

where  $\Delta x$ ,  $\Delta y$  and  $\Delta \sigma$  are the resolutions in the  $x$ -,  $y$ - and  $z$ -direction, while  $u$ ,  $v$  and  $\dot{\sigma}$  are the maximum wind speeds in the respective direction over the whole domain [Bartnicki, 1989]. A typical time step is between 10 and 20 minutes, shortest in winter where the highest wind speeds typically occurs.

### 3.3.4 Boundary and initial conditions

The lower atmospheric boundaries of the model domain, i.e. the surface, are influenced by input from emissions and exchange processes at the surface. Emissions and exchange fluxes between the atmosphere and the surface compartments are included in sub-model 5, which is described in detail in chapter 4. The vertical dissolution of the emissions can be varied; it is possible to assume an evenly distribution of the emissions within e.g. the entire boundary layer.

The concentration at the lateral boundaries of the domain at all levels is assumed to be half the value of the neighbouring grid cell inside the domain. The concentration at the upper boundary of the domain is set to zero. No initial air concentration is used in the model. Initial concentrations for the surface media are described in section 5.4 on page 68.

## 3.4 Horizontal and vertical diffusion

The diffusion is a parameterization of the fluctuations and uncertainties that are not resolved in the meteorological data and it depends, thus, on the meteorological input.

The variations are, however, only small and the horizontal eddy diffusion coefficients can be approximated by constant values [e.g. *Gifford, 1982; Elliott et al., 1996*]. In this study the horizontal eddy diffusion coefficients are assumed to be:  $K_x = K_y = 2 \times 10^5 \text{ m}^2 \text{ s}^{-1}$ .

The vertical diffusion in the boundary layer is parameterized using the Monin-Obukhov similarity theory. The vertical eddy diffusion coefficient is given by:

$$K_\sigma = \Gamma^2 K_z, \quad (3.8)$$

where hydrostatic equilibrium is assumed and the ideal gas law is used:  $\Gamma = d\sigma/dz = -g\sigma/RT$ , where  $g$  is the acceleration of gravity,  $R$  is the gas constant, and  $T$  the air temperature. The vertical diffusion for the surface layer is calculated as:

$$K_z = \frac{\kappa u_* z}{\phi(z/L)}, \quad (3.9)$$

where  $\kappa$  is the von Karman constant,  $u_*$  is the friction velocity, and  $z$  is the height above the surface.  $\phi(z/L)$  is the similarity function for heat, and  $L$  is the Monin-Obukhov length. These are defined as:

$$\phi(z/L) = \begin{cases} 1 + 4.7z/L & , \text{for } z/L > 0 \text{ ("stable")} \\ 1 & , \text{for } z/L = 0 \text{ ("neutral")} \\ (1 - 15z/L)^{-1/2} & , \text{for } z/L < 0 \text{ ("unstable")} \end{cases} \quad (3.10)$$

and

$$L = \frac{u_*^3 T_2}{\kappa g \left( -\frac{H_{sen}}{c_p \rho} \right)}, \quad (3.11)$$

where  $T_2$  is the temperature at 2 m above the surface,  $c_p$  is the specific heat of dry air at constant pressure and  $H_{sen}$  is the sensible heat flux, which is positive/negative for unstable/stable conditions. The corresponding atmospheric conditions e.g. stable or unstable, are indicated in brackets in the expression for  $\phi(z/L)$  in Equation (3.10).

The  $K_z$  profile is extended from the surface layer to the top of the boundary layer by a simple extrapolation, where a decreasing tendency with  $z$  in the upper part of the planetary boundary layer is included:

$$K_z = \max \left[ \frac{\kappa u_* z}{\phi(z/L)} \left( 1 - \frac{z}{z_{pbl}} \right), 0.1 \text{ m}^2/\text{sec} \right], \quad (3.12)$$

where  $z_{pbl}$  is the depth of the mixing layer, described in detail in *Geels [2003]*. Due to the simple expression for  $K_z$  in equation (3.12) the vertical diffusion is restricted to be small above the mixing layer.

## Chapter 4

# Environmental sources and sinks

DEHM-POP is developed from the atmospheric chemistry transport model, DEHM. Apart from the advective and diffusive transport described in chapter 3, the fate of POPs in the atmosphere is governed by the sources and sinks. The major atmospheric sinks are wet deposition, chemical transformation, dry particle deposition, and dry gas deposition. These processes are described in section 4.1. Due to the long environmental life time and the physical-chemical properties of POPs they can re-volatilise after deposition and undergo further atmospheric transport and deposition (see section 2.3.3 on page 14). The dry gas deposition is more correctly described as a two-way gas exchange process and this process is a key to understand the environmental fate of POPs due to the ‘grasshopper transport’. This process is dependent on the surface type, and other processes within the surface compartment may influence the available amount for exchange with the atmosphere. The main work in this study has been to include surface compartments reflecting the composition of the environment and to include the most relevant processes for each compartment in the DEHM-POP model. Five environmental compartments were considered: soil, water, snow, vegetation and sea ice. The included environmental processes for each compartment are described in detail in sections 4.2 – 4.6 in this chapter. For each compartment a short review of the most important processes associated with that compartment is given, followed by a description of the possible parameterisations of the processes and the choice of parameterisation in DEHM-POP. A few other environmental compartments may also be of relevance when modelling the environmental fate of POPs. These are described in section 4.7 but are not included in the present version of DEHM-POP.

### 4.1 Air

The atmosphere has long been considered the dominant pathway for  $\alpha$ -HCH and other POPs into the Arctic. This is supported by studies linking the  $\alpha$ -HCH concentrations in Arctic air with the global  $\alpha$ -HCH usage and emissions from 1979 to the late 1990s [Li *et al.*, 1998, 2004a; Li and Macdonald, 2005].

POPs can be associated with particles in the atmosphere, and the distribution between the gas phase and the particle phase is probably the most important process for determining the atmospheric transport and fate of POPs [Bidleman, 1988]. This process is described in section 4.1.1.

The atmospheric sources and sinks are different for the gas- and particle-phase compounds. The processes that acts as sources and sinks to the gas-phase air concentration,  $C_g$  in each grid cell in DEHM-POP can be described as:

$$\frac{dC_g}{dt} = F_{emis} - F_{wet} - F_{exc,surface} - k_{air}C_g, \quad (4.1)$$

where  $F_{emis}$  is the emission input, which is described in section 5.3 on page 67,  $F_{wet}$  is the wet deposition flux described in section 4.1.3,  $F_{exc,surface}$  is the air-surface gas exchange, which only acts in the lowermost grid cells and depends on the type of surface (see sections 4.2.2, 4.3.1, 4.4.1 and 4.5.1), and  $k_{air}C_g$  is the chemical transformation, described in section 4.1.4.

The concentration of particle phase POPs,  $C_p$  has only two sink terms in the DEHM-POP model:

$$\frac{dC_p}{dt} = -F_{wet} - F_{dry}, \quad (4.2)$$

where  $F_{dry}$  is the dry deposition of particles from the lowermost atmospheric layer to the surface described in section 4.1.2. Chemical transformation of particle-phase POPs is disregarded in DEHM-POP as discussed in section 4.1.4.

#### 4.1.1 Partitioning between gas phase and particles

The first theoretical description of the association of semi-volatile organic compounds (SVOCs) with particles suggest that they are adsorbed to the surface of the particles and that the process depends on the available particle surface area [Junge, 1977] as cited in e.g. Lohmann and Lammel [2004]. Also based on the adsorption theory and assuming that the available surface area for sorption is proportional to the total suspended particle concentration in air ( $TSP$ ), Yamasaki *et al.* [1982] developed an expression for the equilibrium partitioning between particle phase,  $P$  and gas phase,  $A$ :

$$K_p = \frac{P}{A} \frac{1}{TSP}, \quad (4.3)$$

where  $K_p$  is the particle-air partition coefficient, and this expression was found to fit with concurrent gas- and particle-phase measurements of PAHs from Tokyo [Yamasaki *et al.*, 1982]. An inverse correlation of  $K_p$  with temperature was furthermore observed [Yamasaki *et al.*, 1982]. Assuming equilibrium between the gas-phase and the particle phase, the fraction of a compound sorbed to particles,  $\phi$  can then be described as:

$$\phi = \frac{P}{P + A} = \frac{K_p TSP}{K_p TSP + 1}. \quad (4.4)$$

According to the Junge adsorption theory, the fraction adsorbed to the particles are inversely dependent on the solid vapour pressure [Junge, 1977, as cited in e.g. Lohmann and Lammel [2004]]. The expression for the inverse dependence of  $K_p$  on the vapour pressure was further refined by Pankow [1987, 1988]. This description (known as the Junge-Pankow adsorption theory) was shown to be a good approximation to measurements, although the liquid vapour pressure gave better regression results than the solid vapour pressure originally suggested by Junge [Bidleman, 1988; Pankow, 1988].

It was later suggested that the association of SVOCs with particles can be described by absorption into the fraction of organic matter ( $f_{OM}$ ) in the particles rather than adsorption to the particle surface. *Pankow* [1994b, 1994a] showed that the absorption theory was not inconsistent with correlation between  $K_p$  and the liquid vapour pressure. The absorption theory was supported by laboratory studies, see e.g. *Lohmann and Lammel* [2004] and references therein. The octanol-air partition coefficient,  $K_{oa}$  was suggested as predictor for the particle-air partition coefficient and a theoretical relation as well as empirical relations for the two groups PAHs and organochlorines (PCBs and organochlorine pesticides combined) were developed [*Finizio et al.*, 1997]. Based on this study *Harner and Bidleman* [1998] suggested a more general form of the relationship between the particle-air partition coefficient and  $K_{oa}$ :

$$\log(K_p) = \log(K_{oa}) + \log(f_{OM}) - 11.91, \quad (4.5)$$

by assuming that the activity coefficients of octanol and organic matter are equal and that the molecular weight of octanol and organic matter also are equal [*Harner and Bidleman*, 1998]. Using this expression, better agreement between predicted and measured gas-particle partitioning of PCBs, PAHs, and PCNs were obtained than when using the liquid vapour pressure [*Harner and Bidleman*, 1998].

*Pankow* [1998] investigated the relationships between  $K_p$ ,  $K_{oa}$  and the liquid vapour pressure and concluded that  $K_{oa}$  is expected to be a more universal correlating parameter for  $K_p$  than the liquid vapour pressure. In a review, *Xiao and Wania* [2003] argued that the choice of vapour pressure or  $K_{oa}$  for descriptor of partitioning into organic matter depends on whether the interaction of the organic compound with the organic matter more resembled that of pure liquid than that of liquid octanol. It was concluded that with the present accuracy of vapour pressure and  $K_{oa}$  measurements it is not possible to determine which descriptor is the best for determining the partitioning between gas phase and organic matter [*Xiao and Wania*, 2003]. However, there is a good case for using  $K_{oa}$ , since it is directly measurable [*Xiao and Wania*, 2003].

Some experimental studies have shown higher measured PAH concentrations in particles than predicted by the  $K_p$  models [e.g. *Harner and Bidleman*, 1998]. This has been interpreted as the presence of a nonexchangeable fraction trapped inside combustion aerosols [*Harner and Bidleman*, 1998]. However, in a recent review *Lohmann and Lammel* [2004] argued that this fraction can be described by adsorption onto black carbon. A dual organic matter absorption and black carbon adsorption model was recommended for atmospheric long-range transport studies [*Lohmann and Lammel*, 2004].

### Gas-particle partitioning in DEHM-POP

The physical-chemical properties of  $\alpha$ -HCH results in very low concentrations sorbed to particles (see section 2.5.2 on page 22), and in several model studies  $\alpha$ -HCH is treated as a gas-phase compound only [e.g. *Strand and Hov*, 1996; *Wania et al.*, 1999b; *Koziol and Pudykiewicz*, 2001]. This is also the case for the first version of DEHM-POP used in the studies that are presented in [*Hansen et al.*, 2004, 2006a, 2006c]. However, the gas-particle partitioning process is now included in DEHM-POP for the general applicability of the model. The fraction sorbed to particles is described using Equation (4.4). The partitioning between the gas- and particle-phase is described using the  $K_{oa}$  approach suggested by

*Harner and Bidleman* [1998] (Equation 4.5). The fraction of organic matter is set equal to 20% in DEHM-POP, which is in the upper range expected for urban aerosols [*Harner and Bidleman*, 1998]. The best available possibility to estimate the *TSP* concentration was to estimate it from the sulphate particle concentrations predicted by the DEHM-SO<sub>X</sub> model, and this is applied as a first approximation of the *TSP* concentration. Monthly averaged sulphate particle concentrations are extracted for each grid cell from the DEHM-SO<sub>X</sub> model [*Christensen*, 1997]. Concentrations in grid cells outside the original 96 × 96 grid are assumed equal to the closest cell in the original domain. The sulphate particle concentration only accounts for a fraction of the total *TSP* and the concentration in each grid cell is therefore multiplied by a factor of 7 to reach *TSP* concentrations within a range of observed values as cited by *Shatalov et al.* [2004]. Alternatively, monthly averaged *TSP* concentrations can be extracted from the DEHM-REGINA model, which includes *TSP* as one of the modelled components in the chemical scheme. This may be tested in a future version of DEHM-POP.

The dual organic matter absorption and black carbon adsorption model recommended by *Lohmann and Lammel* [2004] is not used in DEHM-POP due to the lack of a soot-air partition coefficient for  $\alpha$ -HCH. A method to derive this coefficient for organic compounds has recently been developed [*Roth et al.*, 2005], and the dual model may be tested in a future version of DEHM-POP.

#### 4.1.2 Dry deposition of particles

POPs sorbed to particles can settle to the surface by dry particle deposition. The flux can be expressed as the product of a dry deposition velocity,  $v_d$  and the particle-phase concentration,  $C_p$ :

$$F_{dry} = v_d C_p, \quad (4.6)$$

where  $v_d$  depends on the particle size and density, surface properties, such as roughness and humidity, and meteorological variables, mainly the wind speed [*Wania et al.*, 1998a].

The distribution of POPs on particle size is mainly studied for the PAHs, see *Wania et al.* [1998a] for a review. The PAHs are mainly associated with the fine aerosol fraction, i.e. particles less than 2.5  $\mu\text{m}$  in diameter [*Wania et al.*, 1998a], which is confirmed by recent measurements [e.g. *Shimmo et al.*, 2004], who observed a single-modal peak around 1  $\mu\text{m}$ . A seasonal variation, where smaller particles are more important during winter is also observed [*Wania et al.*, 1998a; *Miguel et al.*, 2004]. It has been found that coarse particles are dominating the dry deposition flux for PAHs and PCBs close to urban sites resulting in a much higher dry deposition velocity [*Wania et al.*, 1998a]. Higher dry deposition velocities are also expected over water because of particle growth due to water vapour condensation [*Wania et al.*, 1998a]. Dry deposition velocities for POPs have been measured directly with values in the range 0.0013-0.011  $\text{m s}^{-1}$  with a geometric mean of 0.0046  $\text{m s}^{-1}$  [*Wania et al.*, 1998a].

#### Dry particle deposition in DEHM-POP

It is assumed that  $\alpha$ -HCH is associated with particles of the same size as the PAHs, i.e. around 1  $\mu\text{m}$ , and these are the same size as the sulphate particles [*Christensen*, 1997]. The dry particle deposition module from the DEHM-SO<sub>X</sub> model is therefore also used in

the DEHM-POP model. This module distinguishes between dry deposition to open water, to forest covered land surface and to non-forest covered land surface. The dry deposition velocity to open water,  $v_{d,o}$ , is given by:

$$v_{d,o} = 1.3 \times 10^{-3}U, \quad (4.7)$$

where  $U$  is the horizontal wind speed. Over non-open water, the dry deposition velocity depends on the atmospheric stability:

$$v_d = \begin{cases} \frac{u_*}{a} \left( 1 + \left( \frac{-300}{L} \right)^{2/3} \right) & \text{for } L < 0 \\ \frac{u_*}{a} & \text{for } L \geq 0, \end{cases} \quad (4.8)$$

where  $u_*$  is the surface friction velocity,  $L$  is the Monin-Obukhov length and  $a$  is a parameter which is equal to 100 for forest and 500 for the rest of the land covered surface [Christensen, 1997]. The dry deposition to forest-covered land is higher because of the larger available surface area of a forest canopy compared to grass or bare soil. The particles around  $1 \mu\text{m}$  are too small to undergo gravitational settling [Wania *et al.*, 1998a], and this process is thus not taken into account.

### 4.1.3 Wet deposition

Both particles and gas-phase POPs are episodically scavenged from the atmosphere by precipitation. The relative importance of gas-phase and particle scavenging depends on the gas-particle partitioning [e.g. Bidleman, 1988]. The magnitude of the wet deposition flux furthermore depends on the type of precipitation and the precipitation intensity. Precipitation generally has two forms, rain and snow.

The wet deposition intensity is often described by defining a dimensionless scavenging ratio,  $W_T$  given by:

$$W_T = \frac{C_{precip}}{C_{air}}, \quad (4.9)$$

where  $C_{precip}$  is the concentration in the precipitation and  $C_{air}$  is the concentration in air. Individual scavenging ratios for the gas-phase and particle fractions can also be defined, with a total scavenging ratio given by the sum of the gas-phase and particle scavenging ratios weighed with the fraction of particle sorption [e.g. Ligocki *et al.*, 1985b]. The magnitude of the scavenging ratio can be estimated by concurrent air and precipitation samples [e.g. Ligocki *et al.*, 1985a, 1985b].

### Rain scavenging of POPs sorbed to particles

Particles are scavenged either by acting as cloud condensation nuclei or by being intercepted by rain drops in or below the cloud formation. The description of particle scavenging is often limited to empirically determined particle scavenging ratios, which are variable. Measured scavenging ratios range from  $10^2$  to  $2.0 \times 10^5$  for various POPs [Wania *et al.*, 1998a]. The scavenging of particles also depends on the particle size distribution, with higher scavenging ratios observed for large particles than for small [Wania *et al.*, 1998a].

### Scavenging of gas-phase POPs by rain

The vapour phase scavenging by rain can be described by assuming that equilibrium is attained rapidly between the vapour phase and the dissolved phase in a raindrop. This equilibrium is estimated to be attained during the time it takes a rain drop to fall a few meters [e.g. *Ligocki et al.*, 1985a; *Wania et al.*, 1998a]. In this case the scavenging ratio can be estimated by using the water to air partition coefficient,  $K_{wa}$ , which is the reciprocal of the dimensionless Henry's law constant,  $K_{aw}$ . Since most POPs have large Henry's law constants the wet scavenging of vapour phase is assumed to be relatively unimportant, except for compounds with high water solubility such as the HCHs [*Wania et al.*, 1998a]. Estimates of gas-phase scavenging ratios using the  $K_{wa}$  values are in good agreement with measured values for a range of organic compounds [*Ligocki et al.*, 1985a].

For  $\alpha$ -HCH a scavenging ratio of  $W_T = 31000$  was estimated from measurements in Portland, Oregon, US in 1984 [*Ligocki et al.*, 1985a]. The same scavenging ratio was obtained from measurements averaged over a five year period at Lista in Norway [*Wania and Haugen*, 1999]. However, calculated scavenging ratios using the  $K_{wa}$  description indicated higher-than-equilibrium partitioning, which could neither be explained by interfacial sorption nor temperature [*Wania and Haugen*, 1999].

### Sorption onto the surface of water droplets

It has been suggested that adsorption of organic compounds onto the surface of rain droplets may be of importance in several environmental situations, e.g. for small bubbles of air in water and for small droplets of water in air (for example, fogs), e.g. *Hoff et al.* [1993] and references therein. Experimental data on adsorption of naphthalene on fog droplets support this theory [*Raja and Valsaraj*, 2004].

In a recent study, *Simcik* [2004] expanded the scavenging ratio expression with a term describing the sorption of gas-phase SVOCs onto the surface of rain drops. With this formulation the amount of a compound scavenged by rain apart from the dimensionless Henry's law constant also depends on the diameter of the rain drops and the interface-air partition coefficient,  $K_{ia}$  [*Simcik*, 2004]. The expression was used to calculate scavenging ratios of PAHs, PCBs, and PCDDs, and the adsorption process was found to dominate the scavenging of the PCDDs, and the low-volatile PAHs and PCBs [*Simcik*, 2004]. The rain drop surface adsorption process is estimated to be of importance for the HCHs only if the water droplets are smaller than 50  $\mu\text{m}$  [*Wania and Haugen*, 1999].

### Gas-phase scavenging by snow

Surface adsorption is also assumed to play a role for gas scavenging by snow. Ice crystals at temperatures between the melting point and  $-30^\circ\text{C}$  are covered by a thin quasi-liquid layer, which at the melting point is approximately 10 nm thick, see e.g. *Hoff et al.* [1995] and references therein. Scavenging of gas-phase POPs by snow may thus be described as vapour adsorption onto a liquid surface [*Hoff et al.*, 1995]. Adsorption into the bulk water may also occur, but with the relatively little amount of water in the thin layer this process is assumed to be negligible [*Wania et al.*, 1998b].

Partitioning at the air-water interface can be described by the interface-air partition coefficient,  $K_{ia}$ , which is the ratio of the concentration sorbed to the surface to the con-

centration in air and thus has the dimension of length ( $\text{mol m}^2 / \text{mol m}^3 = \text{m}$ ) [Hoff *et al.*, 1993].  $K_{ia}$  values at the air-water interface can be measured directly, estimated from an extrapolation from other materials or estimated from different physical-chemical properties, typically the water solubility or the vapour pressure, see Wania *et al.* [1998b] for a review. Hoff *et al.* [1995] suggested to extrapolate the  $K_{ia}$  values for the air-water interface to apply at the air-snow interface as a first approximation and estimated them to be of the same order of magnitudes, but with  $K_{ia}$  for snow up to a factor 2 higher than for water [Hoff *et al.*, 1995]. Snow  $K_{ia}$  values were recently measured for a range of organic compounds in a laboratory study and an expression to derive  $K_{ia}$  values for other compounds was developed using the poly-parameter linear free energy relationship based on intermolecular interactions [Roth *et al.*, 2004]. High correlation with observed values was found with this expression, however it was not possible to assign the observed sorption to a specific process, i.e. adsorption to the snow crystal surface, incorporation in the solid ice crystal, absorption into a quasi-liquid layer, or grain boundary effects [Roth *et al.*, 2004]. Using the poly-parameter linear free energy relationship expression to calculate  $K_{ia}$  values at the air-water interface [Roth *et al.*, 2002], and applying the intermolecular interaction parameters collected by Lei and Wania [2004], the calculated  $K_{ia}$  value at the air-snow interface is 2.6 times higher than the  $K_{ia}$  values at the air-water interface, which is in line with the estimates of Hoff *et al.* [1995]. The snow scavenging ratio of gas-phase POPs can then be described with the expression [Lei and Wania, 2004]:

$$W = K_{ia}SSA_{ini}\rho_w, \quad (4.10)$$

where  $K_{ia}$  is the interface air partition coefficient,  $SSA_{ini}$  is the specific surface area of the snow flakes and  $\rho_w$  is the density of water. Snow flakes from new fallen snow have large surface areas up to  $154 \text{ m}^2 \text{ kg}^{-1}$  [Cabanes *et al.*, 2003], and the snow scavenging ratio of gas-phase compounds is thus potentially high for compounds with high snow interface-air partition coefficients.

### Scavenging of particles by snow

Cloud droplets contain the largest aerosol mass in the clouds and large settling snow flakes can intercept these as they sweep through a cloud, and thus accumulate particle-phase contaminants, furthermore additional particles can be intercepted below the cloud as the snow flakes settle to the ground, see e.g. Franz and Eisenreich [1998] and references therein. From concurrent air and snow or rain event samples it was concluded that particle scavenging by snow was the most important scavenging process for PCBs and PAHs [Franz and Eisenreich, 1998]. Calculated particle scavenging ratios were in the range  $3.3 - 39 \times 10^5$  for PCBs and  $6.1 - 510 \times 10^5$  for PAHs [Franz and Eisenreich, 1998]. However, Wania *et al.* [1999a] pointed out that re-partitioning between particles and the dissolved phase in the meltwater might have occurred during the analysis, which may result in an erroneous conclusion of the gas-phase scavenging by snow being of little importance. A re-interpretation of the data suggests that vapour scavenging by snow is an important if not dominant scavenging for the more volatile PCBs and PAHs [Wania *et al.*, 1999a]. It was furthermore suggested that a constant particle scavenging ratio can be applied for chemicals within the same class in a precipitation event, which can be estimated from the scavenging of a predominantly particle-sorbed chemical [Wania *et al.*, 1999a]. Particle

scavenging ratios for snow were estimated to be  $5.4 \times 10^5$  for PCBs and  $30 - 98 \times 10^5$  for PAHs in the sampled precipitation event [Wania *et al.*, 1999a].

### Wet deposition flux in DEHM-POP

The wet deposition flux of  $\alpha$ -HCH is calculated in DEHM-POP using a simple parameterisation based on a scavenging coefficient formulation as in DEHM-SO<sub>X</sub> [Christensen, 1997]:

$$F_{wet} = W \frac{P}{h\rho_w} C_{air}, \quad (4.11)$$

where  $W$  is the scavenging coefficient,  $P$  is the precipitation rate, which is given at all levels by the meteorological input (see section 5.1 on page 65),  $h$  is the effective thickness for scavenging, which is set equal to 1000 m [Iversen, 1989],  $\rho_w$  is the density of water and  $C_{air}$  is the air concentration of  $\alpha$ -HCH (either gas- or particle-phase, which are treated separately, see below). The scavenging coefficient,  $W$  is equivalent to the above mentioned scavenging ratio,  $W_T$ , although the 3-D structure of the model render a direct comparison impossible.

In the first version of DEHM-POP the scavenging in clouds and below clouds was treated differently, where in-cloud scavenging is more efficient due to the higher density of water droplets in clouds than below clouds. As a first approximation the scavenging coefficients were assumed to be constant with values of  $7.0 \times 10^5$  and  $1.0 \times 10^5$  for in-cloud and below-cloud scavenging respectively as in DEHM-SO<sub>X</sub> [Christensen, 1997]. This wet deposition parameterisation was used for the studies described in Hansen *et al.* [2004, 2006c].

When particles and gas-particle partitioning was introduced in the model, the scavenging of gas-phase and particle sorbed  $\alpha$ -HCH was treated separately. The scavenging of particle-sorbed  $\alpha$ -HCH was described using constant scavenging coefficients with values for in-cloud and below-cloud scavenging as above. The model does not distinguish between rain and snow scavenging of particles. For gas-phase  $\alpha$ -HCH, a more refined approach was taken by assuming equilibrium between the rain drops and the surrounding air as described above. The model distinguishes between rain and snow scavenging of gas-phase  $\alpha$ -HCH. The rain scavenging coefficient was then replaced by  $K_{wa}$ , where the  $K_{wa}$  is calculated by Equation (2.1) on page 12 using the temperature dependent Henry's law constant reported by Xiao *et al.* [2004]. The scavenging of snow is described using Equation (4.10). Initial specific surface area is chosen to be:  $SSA_{ini} = 120 \text{ m}^2 \text{ kg}^{-1}$ , which corresponds to observed values for freshly fallen snow in calm weather conditions [Legagneux *et al.*, 2002]. Temperature dependent  $K_{ia}$  values were taken from Hoff *et al.* [1995]. Lei and Wania [2004] calculated  $K_{ia}$  values from the poly-parameter linear free energy relationship empirically derived by Roth *et al.* [2004]. These values were applied in the snowpack model developed by Hansen *et al.* [2006b] and also tested in DEHM-POP, but it was found to disturb the correlations between measured and simulated  $\alpha$ -HCH concentrations.

Atmospheric observations indicate that water readily supercools, and liquid water is frequently found in clouds at temperatures below 0°C [Seinfeld and Pandis, 1998]. To account for this a fraction of supercooled liquid is assumed to decrease linearly between 0°C and -31°C. Scavenging of the supercooled liquid fraction is described as the scavenging of water. According to Lei and Wania [2004], there is an upper limit of the application

of scavenging ratios, where the aqueous phase becomes a dominant reservoir in the cloud. This occurs at a precipitation-air partition coefficient of about  $1.0 \times 10^6$  for gas phase compounds [Lei and Wania, 2004]. A maximum scavenging coefficient of  $1.0 \times 10^6$  is thus introduced in DEHM-POP, although the effect on the atmospheric concentrations is very small.

#### 4.1.4 Chemical transformation in the atmosphere

The chemical transformation of a compound in air depends on the fractions in gas-phase and in particle-phase respectively.

##### Transformation of gas-phase POPs

The transformation process of gas-phase POPs can be photolysis or reactions with OH radicals, nitrate radicals or ozone and a few other atmospheric constituents which are of minor importance [Atkinson *et al.*, 1999]. Of these processes, reaction with OH radicals is assumed to be the most important transformation of  $\alpha$ -HCH in the atmosphere [Atkinson *et al.*, 1999].

OH-reaction rates of  $\alpha$ -HCH were measured in a laboratory experiment for temperatures between 346 and 386K [Brubaker and Hites, 1998]. The reaction rates were extrapolated outside this temperature interval using an Arrhenius expression:

$$k_{OH} = A \exp\left(\frac{-E_a}{RT}\right), \quad (4.12)$$

where the pre-exponential factor  $A = 1.4 \times 10^{-11} \text{ cm}^3 \text{ s}^{-1}$  and the activation energy  $E_a = 11.2 \text{ kJ mol}^{-1}$  were determined by the regression of the measured values [Brubaker and Hites, 1998]. The reaction rate at 277K is  $k_{OH} = 1.0 \times 10^{-13} \text{ cm}^3 \text{ s}^{-1}$  and the degradation rate in air is then [Brubaker and Hites, 1998]:

$$k_{air} = \frac{1}{k_{OH}[\text{OH}]}, \quad (4.13)$$

where [OH] is the averaged OH concentrations. Using a global 24 h averaged OH concentration an atmospheric lifetime of 120 days for  $\alpha$ -HCH was calculated from this expression for a temperature of 277 K [Brubaker and Hites, 1998].

A transformation of  $\gamma$ -HCH into  $\alpha$ -HCH by UV radiation has been observed in laboratory studies, see e.g. Pacyna and Oehme [1988] for references, and this process was therefore speculated to be a source of  $\alpha$ -HCH to Arctic air [Pacyna and Oehme, 1988]. However concurrent measurements of  $\alpha$ - and  $\gamma$ -HCH from Québec do not show signs of increased  $\alpha$ -HCH concentrations linked to the  $\gamma$ -HCH concentration, which indicates that this process is slower in the environment than the reactions of  $\gamma$ -HCH with OH radicals [Poissant and Koprivnjak, 1996]. A further indication of this is the close link between global emissions of technical HCH and atmospheric  $\alpha$ -HCH concentrations in the Arctic [Li *et al.*, 1998, 2004a; Li and Macdonald, 2005]. Apparently, this process is not taken into account in any other model studies and is also disregarded in this study.

### Transformation of particle-bound POPs

The major chemical transformations of particle phase POPs are reactions with OH radicals and ozone and photolysis, while the transformation probably depends on whether the POPs are adsorbed to the surface or absorbed in the organic phase of the particles [Atkinson *et al.*, 1999]. The higher measured PAH concentrations in particles than predicted by the gas-particle partitioning models have been interpreted as the presence of a nonexchangeable fraction trapped inside combustion aerosols [e.g. Harner and Bidleman, 1998]. A nonexchangeable fraction in the particles would influence the degradation process which presumably is a surface process.

Little is known about the actual degradation rates of HCHs and other POPs sorbed to particles. Only one datum has been published on the reaction of  $\gamma$ -HCH sorbed to particles with OH radicals:  $6.0 \times 10^{-13} \text{ cm}^3\text{s}^{-1}$  [Zetzsch, 1991] as cited in Atkinson *et al.* [1999]. This is of the same order of magnitude as the gas-phase reactions [Atkinson *et al.*, 1999]. However, there is a general belief that the degradation of particle-phase SVOCs is considerably slower than gas-phase reactions. In most models the degradation rate of POPs sorbed to particles is usually assumed smaller than the gas-phase degradation rate or it is set equal to zero [e.g. Scheringer, 1997; Scheringer *et al.*, 2000; Semeena and Lammel, 2005].

### Atmospheric transformation in DEHM-POP

As degradation by reactions with OH radicals dominates the atmospheric gas-phase transformation of  $\alpha$ -HCH, this process is described in DEHM-POP by the expression:

$$\frac{dC_g}{dt} = -k_{air}C_g, \quad (4.14)$$

where  $k_{air}$  is the degradation rate. In the first version of the model the degradation in air is estimated with a constant degradation rate [Hansen *et al.*, 2004, 2006a, 2006c]. This is calculated in the model using an estimated mean residence time in the atmosphere due to reactions with OH radicals of  $k_{air} = 1/(118 \text{ days})$  [Mackay, 2001]. This value compares favorably with the atmospheric lifetime of 120 days for  $\alpha$ -HCH calculated by Equation (4.13) for a temperature of 277 K using a global 24 h averaged OH concentration [Brubaker and Hites, 1998]. As a further development of the model a temperature- and OH-concentration dependent degradation rate is introduced using the expression given by Brubaker and Hites [1998] (Equation 4.13). Monthly averaged OH concentrations, [OH] are extracted for each grid point from the DEHM-REGINA model [Frohn *et al.*, 2002; Frohn, 2004]. Concentrations in grid cells outside the original  $96 \times 96$  grid are assumed equal to the closest cell in the original domain. It is assumed that there is no degradation of compounds sorbed to particles. Given the low degradation rates compared with other atmospheric loss processes, the parameterisation of this process does not influence the predicted concentrations to a high degree.

## 4.2 Soil

Soil is a complex organic matrix consisting of air, water, mineral matter and organic matter and there can be large variations in the fractions of these phases both over diurnal and

Table 4.1: Values of soil and chemical properties used in DEHM-POP, original values as suggested by *Jury et al.* [1983], and new values used in the latest version of the model (see text for details).

Parameter	Symbol	Units	Original values	New values
Soil depth	$z_s$	m	0.15	-
Water content	$l$	$\text{m}^3 \text{m}^{-3}$	0.3	-
Air content	$a$	$\text{m}^3 \text{m}^{-3}$	0.2	-
Bulk density	$\rho_s$	$\text{kg m}^{-3}$	1350	-
Water diffusion coefficient	$D_L^{water}$	$\text{m}^2 \text{s}^{-1}$	$5.0 \times 10^{-10}$	-
Air diffusion coefficient	$D_g^{air}$	$\text{m}^2 \text{s}^{-1}$	$5.0 \times 10^{-6}$	$4.59 \times 10^{-6}$
Organic carbon fraction	$f_{oc}$	$\text{kg kg}^{-1}$	0.0125	site specific

seasonal time scales but also over a few meters within a field [Mackay, 2001]. Soil is the major terrestrial reservoir of POPs [Cousins *et al.*, 1999]. Not surprisingly, soils receiving direct input e.g. from pesticide usage or sewage sludge disposal can be very contaminated with POPs. But also soils from remote locations receive input from atmospheric deposition and can reach high contamination levels [e.g. Meijer *et al.*, 2003a]. Soil receive input through wet deposition of both gas-phase and particle-phase compounds, through dry particle deposition and through gaseous exchange, see Cousins *et al.* [1999] for a review of air-soil exchange processes. Both field and laboratory studies have shown that the soil air partition coefficient,  $K_s$  can be approximated with an expression linearly dependent on  $K_{oa}$  and the fraction of organic matter [e.g. Hippelein and McLachlan, 1998; Meijer *et al.*, 2003b].  $K_s$  also depends on environmental factors such as temperature and relative humidity [e.g. Hippelein and McLachlan, 2000; Meijer *et al.*, 2003c].

Jury and colleagues presented a comprehensive work on modelling air-soil exchange of pesticides in a suite of papers [Jury *et al.*, 1983, 1984a, 1984b, 1984c, 1987]. This has formed the basis of the soil module in several multi-compartment mass balance models [e.g. Wania and Mackay, 1995; Strand and Hov, 1996; Wania *et al.*, 1999b; Mackay, 2001].

#### 4.2.1 The soil module in DEHM-POP

The soil module introduced in DEHM-POP is based on the soil module from the zonally averaged multi-compartment mass balance model developed by Strand and Hov [1996]. The land-covered surface in the model consists of a 0.15 m thick soil layer containing a mixture of soil, air and water in fractions kept constant with time. The soil layer is assumed to have the standard properties suggested by Jury *et al.* [1983] that are listed in Table 4.1, with a few parameters changed in the most recent version of the model. The change in  $\alpha$ -HCH concentration in soil,  $C_s$ , with time is expressed by:

$$\frac{\partial C_s}{\partial t} = \frac{1}{z_s} (F_{exc,soil} + F_{wet} + F_{dry} - F_{evap} - F_{run-through}) - k_{soil} C_s, \quad (4.15)$$

where  $z_s$  is the soil depth,  $F_{exc,soil}$  is the air-soil gas exchange flux,  $F_{wet}$  is the wet deposition,  $F_{dry}$  is the dry particle deposition,  $F_{evap}$  is the evaporative flux out of the soil,

$F_{run-through}$  is the amount of chemical running out with the excess water through the bottom of the soil layer, and  $k_{soil}$  is the degradation rate in soil. Application input is also included in the original soil module [Strand and Hov, 1996]. However, the amount of  $\alpha$ -HCH applied to the soil is taken into account when emissions to air are calculated (see section 5.3 on page 67) and it is therefore disregarded in this context.

#### 4.2.2 Air-soil exchange in DEHM-POP

The air-soil gas exchange flux in DEHM-POP is given by:

$$F_{exc,soil} = v_{soil} \left( C_g - \frac{C_s}{K_s} \right), \quad (4.16)$$

where  $v_{soil}$  is the exchange velocity, and  $K_s$  is the partition coefficient between soil and air in the soil. The exchange velocity is given by [Strand and Hov, 1996]:

$$v_{soil} = \frac{(D_G^{air} a^{10/3} + D_L^{water} l^{10/3} K_{wa})(1 - l - a)^{-2}}{z_s/2}, \quad (4.17)$$

where  $D_G^{air}$  is the molecular air diffusion coefficient,  $D_L^{water}$  is the liquid diffusion coefficient,  $l$  and  $a$  is the water and air fractions in soil respectively, and  $K_{wa}$  is the reciprocal of the dimensionless Henry's law constant. The value for the molecular air diffusion coefficient  $D_G^{air} = 5.0 \times 10^{-6}$  was a general value suggested to apply for pesticides [Jury *et al.*, 1983]. However,  $D_G^{air}$  is temperature dependent and can be calculated from a semi-empirical relation depending on the molar volume and molecular masses of air and the compound [Schwarzenbach *et al.*, 1993]. This yields  $D_G^{air}$  values in the range  $4.0 - 5.5 \times 10^{-6}$  for the temperature interval between  $-30^\circ\text{C}$  and  $+30^\circ\text{C}$ . Using the temperature dependent expression only have little influence on air and soil  $\alpha$ -HCH concentrations, so a constant value of  $D_G^{air} = 4.6 \times 10^{-6}$  corresponding to a temperature of  $0^\circ\text{C}$  is applied, which applies better for the snowpack module (see section 4.4).

The partition coefficient between soil and air in the soil is given by [Strand and Hov, 1996]:

$$K_s = \rho_s f_{oc} K_{oc} K_{wa} + l K_{wa} + a, \quad (4.18)$$

where  $\rho_s$  is the soil density,  $f_{oc}$  is the organic carbon fraction, and  $K_{oc}$  is the organic carbon to water partition coefficient. The two latter parameters have been changed in the course of this study. The fraction of organic carbon,  $f_{oc}$  was taken to be constant throughout the model domain:  $f_{oc} = 0.0125$  as suggested by Jury *et al.* [1983] in the studies reported in Hansen *et al.* [2004, 2006a, 2006c]. A variable site specific  $f_{oc}$  on a  $1^\circ \times 1^\circ$  grid was obtained through the study reported by Shatalov *et al.* [2005], and this was introduced in the model (see Figure 4.1). The organic carbon-water partition coefficient was originally taken to be constant:  $K_{oc} = 1.3 \text{ m}^3 \text{ kg}^{-1}$  [Strand and Hov, 1996].  $K_{oc}$  is often approximated by a constant times the octanol-water partition coefficient as reviewed by Seth *et al.* [1999], who also suggested the proportionality factor 0.35 as the most appropriate. As a revised estimate  $K_{oc}$  is given by the expression:

$$K_{oc} = 0.35 K_{ow}. \quad (4.19)$$

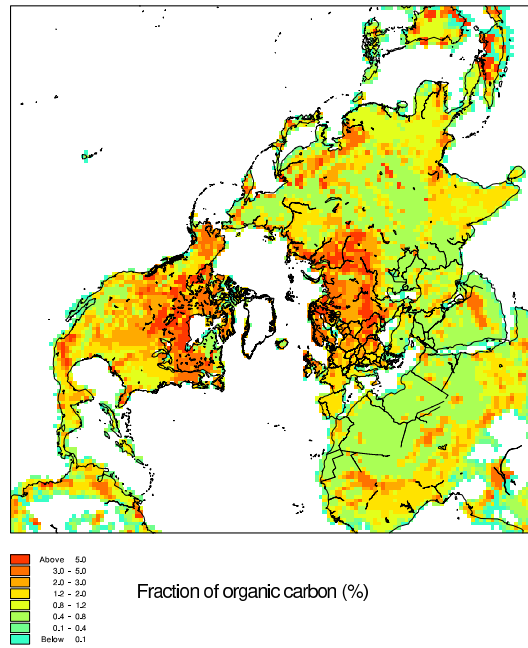


Figure 4.1: Fraction of organic carbon in the soil. The data have been redistributed to the DEHM-POP model grid.

By applying Equation (2.2) on page 12, the soil-air partition coefficient can then be expressed as:

$$K_s = 0.35\rho_s f_{oc} K_{oa} + lK_{wa} + a. \quad (4.20)$$

Temperature dependent  $K_{oa}$  values from *Xiao et al.* [2004] are used as input. Both of these changes are of little importance on the results reported here.

Two different expressions for the reciprocal of the dimensionless Henry's law constant,  $K_{wa}$ , are also used. In the studies reported in *Hansen et al.* [2004, 2006a, 2006c], the temperature dependent  $K_{wa}$  are calculated using the equation:

$$K_{wa} = RT \exp\left(\frac{2.303m}{T} - 2.303b\right), \quad (4.21)$$

where  $R$  is the molar gas constant,  $T$  is the temperature and  $m = 2810$  and  $b = 9.31$  are empirical constants determined for distilled water [*Kucklick et al.*, 1991]. The other expression is calculated using the reciprocal of Equation (2.1) on page 12 from the temperature dependent Henry's law constants reported by *Xiao et al.* [2004].

The  $\alpha$ -HCH flux out of the soil due to evaporation of water is not taken into account in the studies presented in the papers *Hansen et al.* [2004, 2006a, 2006c]. It has been introduced later estimated by the expression [*Strand and Hov*, 1996]:

$$F_{evap} = EC_s \frac{K_{wa}}{K_s}, \quad (4.22)$$

where  $E$  is the water evaporation rate, which is extracted from the numerical weather prediction model together with the other meteorological data (see section 5.1). This has

potentially a large effect locally in places with a strong latent heat flux. However, it is not seen to affect the distribution of  $\alpha$ -HCH to a large degree in the DEHM-POP model.

The excess run-through is calculated by:

$$F_{run-through} = F_{excess} C_s \frac{K_{wa}}{K_s}, \quad (4.23)$$

where  $F_{excess}$  is the flux of excess water, which in the model is equal to the precipitation rate minus the evaporation rate since the water content in the soil layer is kept constant.

### 4.2.3 Soil degradation in DEHM-POP

POPs are primarily degraded in soil by microbial activity. The degradation process is not well quantified and typical estimated degradation rates are very variable. In the DEHM-POP model the degradation is described using a first order degradation rate:

$$\frac{dC_s}{dt} = -k_{soil} C_s. \quad (4.24)$$

The degradation rate is estimated to be:  $k_{soil} = 1/(1 \text{ year})$  [*Strand and Hov*, 1996]. This value compares well with the half-life in soil of 260 days as used by *Jury et al.* [1983], but is generally higher than degradation rates used in more recent models. A half-life of 120 days at 20°C, increasing with decreasing temperatures, is used by *Wania et al.* [1999b] and *Brevik and Wania* [2002a]. Degradation rates of 1/(3 months) – 1/(4 months) are used for the temperature range –3°C – 28°C by *Scheringer et al.* [2000].

## 4.3 Ocean water

About 70% of the worlds surface is covered by oceans with a mean depth of about 4 km. Ocean currents continuously redistribute the water both horizontally and vertically. The oceans thus potentially constitute a major reservoir for POPs and have early been predicted to receive most of the globally applied amount of POPs [*Goldberg*, 1975] as cited in *Wania et al.* [1998a]. The main processes contributing to the exchange between air and ocean water are wet deposition of both gas- and particle-phase compounds, dry particle deposition and dry gas exchange at the surface, see *Wania et al.* [1998a] for a review. Several processes in the water column are also of importance to the fate of POPs in oceans, such as hydrolysis, biodegradation, partitioning between the dissolved phase and the fraction sorbed to suspended particulate matter and the vertical settling of such matter [*Wania et al.*, 1998a]. The ocean is in most environmental fate models described by a single surface ocean compartment for each region, with a model specific depth of between 20 m [*Wania and Mackay*, 1995] and 200 m [*Scheringer et al.*, 2000]. In these models the deep ocean acts as a sink only. *Strand and Hov* [1996] included deep ocean compartments with a parameterisation of upwelling in warm regions and inter-region deep ocean transport. A dynamic parameterisation of the oceans with full 3-D description of the transport processes and 15 vertical layers are included in the Eulerian hemispheric model by *Gusev et al.* [2005].

### The DEHM-POP water compartment

The ocean in DEHM-POP is assumed to consist of a 75 m deep well-mixed surface water compartment. The deep ocean and sediments are not taken into account in the model. The open water category from the land use data includes major lakes such as Lake Baikal in Russia and the Great Lakes in North America. The size of lakes included in the data is determined by the original resolution of the land use data of  $1^\circ \times 1^\circ$  (see section 5.2). The model does not distinguish between lakes and ocean water, although there is a salinity effect on the solubility (see section 4.3.1).

The change in  $\alpha$ -HCH concentration in water,  $C_w$ , with time can be expressed by:

$$\frac{\partial C_w}{\partial t} = \frac{1}{z_w} (F_{exc,water} + F_{wet} + F_{dry}) - k_{water} C_w, \quad (4.25)$$

where  $z_w$  is the depth of the ocean compartment,  $F_{wet}$  is the wet deposition,  $F_{dry}$  is the dry particle deposition,  $F_{exc,water}$  is the air-water gas exchange flux, and  $k_{water}$  is the loss rate in the surface ocean compartment.

#### 4.3.1 Air-water gas exchange

The air-water gas exchange is one of the most important exchange processes across the air-water interface. According to rough estimates this process accounts for 25-30% of the HCH deposition and 50-80% of the deposition of other organochlorine compounds to the sea, see *Wania et al.* [1998a] and references therein. The gas exchange direction can also be reversed and a net volatilisation to the atmosphere can take place, which has been observed for  $\alpha$ -HCH in the Bering and Chucki Seas and the Arctic Ocean in the early 1990s [*Jantunen and Bidleman*, 1995, 1996, 1997].

#### DEHM-POP air-water gas exchange

The air-water gas exchange flux in DEHM-POP is given by:

$$F_{exc,water} = v_w \left( C_g - \frac{C_w}{K_{wa}} \right), \quad (4.26)$$

where  $v_w$  is the exchange velocity calculated using the Whitman two-layer resistance method and is increasing for increasing wind speeds. As for the soil module two different expressions for the  $K_{wa}$  have been used. In the studies reported in *Hansen et al.* [2004, 2006a, 2006c] the  $K_{wa}$  is calculated using Equation (4.21) but with values for the empirical constants:  $m = 2969$  and  $b = 9.88$  determined for artificial ocean water [*Kucklick et al.*, 1991]. The Henry's law constant for ocean water are significantly higher than for distilled water at  $35^\circ\text{C}$  and  $45^\circ\text{C}$ , whereas there is no difference at  $0.5^\circ\text{C}$  [*Kucklick et al.*, 1991]. This is due to the effect of the salinity, which reduces the solubility of organic compounds in sea water as reviewed by *Xie et al.* [1997]. To ensure consistent partition coefficients the  $K_{wa}$  is in the most recent model version calculated by Equation 2.1 using the temperature dependent Henry's law constant reported by *Xiao et al.* [2004]. This does not include the salinity effect and the air-water gas exchange is thus probably underestimated in warm regions.

### 4.3.2 Loss processes in the surface ocean compartment

There are several loss processes of POPs in the surface ocean compartment: biodegradation, hydrolysis, and sedimentation. HCH can be degraded by microbial degradation in water, and is transformed to pentachlorocyclohexane (PCCH:  $C_6H_5Cl_5$ ), which again undergoes further degradation [Hühnerfuss *et al.*, 1992]. The degradation of  $\alpha$ -HCH is enantioselective. Whereas technical HCH is racemic, i.e.  $(+)\alpha$ -HCH/ $(-)\alpha$ -HCH = 1, the average enantiomeric ratio was found to be 0.87 in the eastern Arctic Ocean [Harner *et al.*, 1999]. Similar enantiomeric ratios were found in samples from the Baltic and North Sea [Hühnerfuss *et al.*, 1992], and even lower enantiomeric ratios were found in water samples from a lake in the high Arctic [Falconer *et al.*, 1995]. Biodegradation half-lives calculated from the study in the eastern Arctic Ocean are  $5.9 \pm 1.2$  years for  $(+)\alpha$ -HCH and  $23.1 \pm 4.7$  years for  $(-)\alpha$ -HCH [Harner *et al.*, 1999]. Microbial degradation is suggested to be the most important removal process in the eastern Arctic Ocean and possibly in other water bodies as well [Harner *et al.*, 1999].

Another important loss process of HCH in the surface ocean compartment is hydrolysis, in which HCH reacts with water and dehydrochlorinate to form PCCH [Ngabe *et al.*, 1993]. The hydrolysis process is depending on both temperature and pH of the water; in water with pH = 8 and at 5°C, a hydrolytic half-life of  $\alpha$ -HCH was estimated to be 26 years [Ngabe *et al.*, 1993]. An  $\alpha$ -HCH hydrolysis half-life of 63.6 years is calculated for conditions within the Arctic Ocean [Harner *et al.*, 1999].

POPs can also be transferred to the deep ocean by settling of particulate organic carbon (POC) in the water column. The importance of this process depends on the fraction of the POPs sorbed to the POC, which can be described by the average POC concentration and the organic carbon-water partition coefficient,  $K_{oc}$  [e.g. Wania *et al.*, 1998a], which can be parameterised using the  $K_{ow}$  partition coefficient, as mentioned in section 4.2.2. The bulk of POC in ocean water originates from phytoplankton, and a two-year long study in the Baltic Sea indicates that the partitioning of PCBs to POC is equilibrated and thus not limited by factors such as phytoplankton growth [Sobek *et al.*, 2004]. In a study combining measurements of PCBs, and PCDD/Fs and remote sensing estimates of temperature, wind speed and chlorophyll, it was concluded that the deposition of these compounds to oceans at mid-high latitudes was enhanced due to the sinking of POC rather than by the cold condensation effect [Dachs *et al.*, 2002]. In an investigation of the importance of different loss processes using a global multi compartment mass balance model, it was concluded that the transfer of particle-bound PCBs to the deep sea dominates the loss of the more chlorinated congeners [Wania and Daly, 2002]. Another global model study found that transfer to deep oceans affects the mass balance and the long-range transport potential for hydrophobic compounds, such as the PCBs [Scheringer *et al.*, 2004]. Only a small fraction of HCHs is sorbed to particles and the loss of  $\alpha$ -HCH due to sedimentation is insignificant compared to other loss processes with a sedimentation half-life estimated to be 700 years in the Arctic Ocean [Harner *et al.*, 1999]. When the POPs are transferred to the deep ocean waters they can be considered lost for further environmental cycling due to the small exchange between surface and deep ocean waters.

### Description of surface ocean loss in DEHM-POP

The loss from the surface water compartment is described in DEHM-POP using a first order reaction rate:

$$\frac{dC_w}{dt} = -k_{water}C_w. \quad (4.27)$$

A degradation rate of  $k_{water}=1/(10 \text{ years})$  is used. This value approximates the biodegradation half-life calculated by *Harner et al.* [1999]. The degradation rate used in DEHM-POP is generally higher than estimates used in other models. An  $\alpha$ -HCH half-life of 5 years for ocean water was used by *Strand and Hov* [1996]. A half-life of 4 months for  $\alpha$ -HCH in ocean water and 3 years in fresh water is used by *Wania et al.* [1999b]. *Breivik and Wania* [2002a] use an  $\alpha$ -HCH half-life of 1 year for both ocean and fresh water. Degradation rates for  $\alpha$ -HCH of  $1/(5.4 \text{ years})$  to  $1/(1.8 \text{ months})$  is used for the temperature range 270 – 301 K by *Scheringer et al.* [2000].

#### 4.3.3 Oceanic transport of POPs

In addition to the above mentioned loss processes in the surface ocean compartment, contaminated water is redistributed by ocean currents and by vertical advection, i.e. up- and down-welling of water. Although the oceanic transport is slow, it can be important depending on the partitioning between air and water. For example, oceanic transport is predicted to play a key role in the transport of  $\beta$ -HCH to the Arctic Ocean [*Li et al.*, 2002]. Based on studies with the Arctic Mass Balance Box Model (AMBBM) [*Li et al.*, 2004a], *Li and Macdonald* [2005] predicted that the major  $\alpha$ -HCH loading to the Arctic Ocean in the years 1945 to 1990 was gas-exchange (52%), whereas for the years 1991-2000 it was sea currents (50%). The largest removal was also due to sea currents in the latter period (more than 40%) so the net loading was still gas exchange.

Horizontal oceanic transport is included in most environmental fate models [e.g. *Wania and Mackay*, 1995; *Scheringer et al.*, 2000; *Prevedouros et al.*, 2004b]. These models also include a (one way) vertical transport from the surface ocean compartment to the deep ocean, in form of settling of particles and/or a vertical diffusion. *Strand and Hov* [1996] included a parameterisation of upwelling in warm regions from a deep ocean compartment and inter-regional deep ocean transport. The most comprehensive description of oceanic transport is included in a Eulerian model by *Gusev et al.* [2005], where full 3-D sea currents from a dynamic ocean transport model are included.

#### Oceanic transport in DEHM-POP

It was attempted to include ocean currents in the surface ocean compartment of DEHM-POP to account for the oceanic pollution transport. Monthly averaged horizontal ocean currents were extracted from a dynamic oceanic transport model (HOPE) [*Marsland et al.*, 2003] (see Figure 4.2). The HOPE model is described using an orthogonal curvilinear grid, which posed the problem of converting the sea currents to the polar stereographic projection used in DEHM-POP. A horizontal transport was calculated from the converted sea currents. Conservation of mass was imposed in the individual ocean grid cell, and divergence or convergence of sea currents in an ocean grid cell was counter-acted by subsequent down-welling or up-welling of excess water to or from the deep ocean. With the

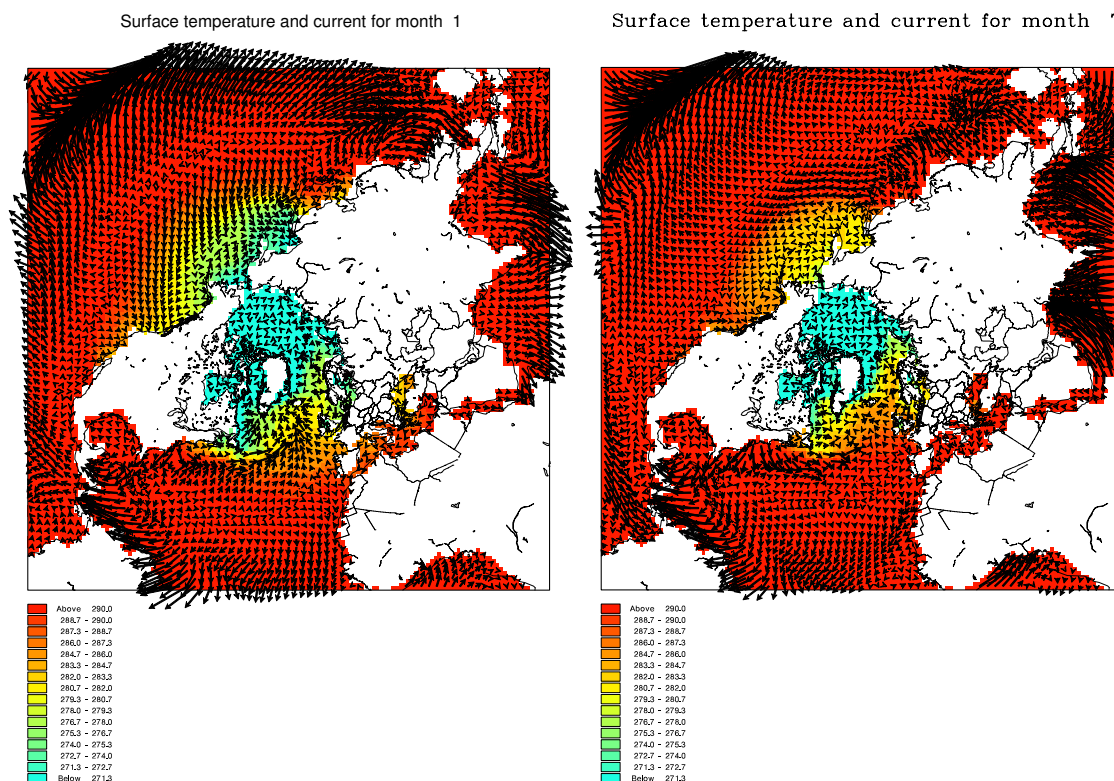


Figure 4.2: Monthly averaged ocean currents (arrows) and temperatures (colours) for January (left) and July (right) extracted from an oceanic chemistry transport model. The data have been redistributed to the DEHM-POP model grid.

simplistic description of the ocean compartments, strong divergence and convergence in some regions had the effect of diluting the contamination vary rapidly in these regions. The results from these experiments are not included in this project and the attempt of introducing oceanic transport in the present simple ocean module was thus abandoned.

A full coupling of the two models is currently under development. The two models will run simultaneously with an exchange of contaminants at a prescribed time interval, e.g. once a day. This work is still in the early stages and the results are not included in this project.

## 4.4 Snow

Due to the cold environment of the Arctic the precipitation primarily falls as snow resulting in the formation of a snowpack on the ground and on the ice-covered Arctic Ocean. A large part of the Arctic is therefore covered by snow for the majority of the year and even at lower latitudes the ground can be covered by snow for shorter or longer periods. The size and extent of terrestrial and sea-ice snowfields ensures that snow plays a major role in influencing atmospheric chemistry and ultimately the composition of the polar boundary layer [e.g. *Dominé and Shepson, 2002*]. The fate of POPs is also influenced by snow e.g. by

changes in the scavenging pattern and in the air-surface exchange processes [Wania *et al.*, 1998b]. This is also highlighted by the few modelling studies that have been published so far [Wania, 1997; Wania *et al.*, 1999c; Daly and Wania, 2004]. For example, incorporating a seasonal snowpack in a regional multi-compartment mass balance model resulted in lower  $\alpha$ -HCH concentrations in air during winter but higher concentrations during the melt season [Daly and Wania, 2004]. Therefore a snowpack module was developed to include in the DEHM-POP model [Hansen *et al.*, 2006b].

The horizontal extent of the snow cover can be extracted from the meteorological data delivered by the numerical weather prediction model that are used as input to DEHM-POP. However, these data do not include the depth of the snowpack, and thus not the total amount of snow. The surface area of the snowpack is of particular interest for the prediction of snowpack concentrations and air-snow interaction since it is assumed that gas-phase POPs are sorbed onto the surface of the snow crystals [e.g. Wania, 1997; Wania *et al.*, 1998b; Halsall, 2004]. Snow flakes have large surface areas; specific surface areas (*SSA*) of up to  $154 \text{ m}^2 \text{ kg}^{-1}$  have been measured for new fallen snow in the Arctic [Cabanes *et al.*, 2003]. Although the surface area decreases as a result of post-depositional processes, such as sublimation and settling of the snowpack [e.g. Cabanes *et al.*, 2003], the snowpack still has a large surface area and thus a large reservoir capacity for POPs. By measuring the densities, depth and *SSA* for all snow layers in a 50 cm deep snowpack at Alert, northern Canada, the total surface area (*TSA*) was estimated to be up to  $3710 \text{ m}^2$  of snow surface area per  $\text{m}^2$  of ground [Dominé *et al.*, 2002].

The snowpack module describes the physical evolution of a single-layer snowpack and comprises the three components of snow accumulation, settling and melting. The snowpack is considered to be homogeneous and is characterized by the following physical parameters; depth  $d$  (m), specific mass  $m$  ( $\text{kg m}^{-2}$ ), density  $\rho$  ( $\text{kg m}^{-3}$ ), specific surface area *SSA* ( $\text{m}^2 \text{ kg}^{-1}$ ), and total surface area *TSA* ( $\text{m}^2 \text{ m}^{-2}$ ).

### Snow accumulation

The snowpack accumulates by consecutive snowfall events, whereby for each time-step including a precipitation event a low-density snow layer is formed, which is assumed to mix instantaneously with the existing snowpack. Mass and *TSA* are conserved in this process, and the other physical parameters are then calculated from the following equations:

$$SSA = \frac{TSA}{m}, \quad (4.28)$$

$$\rho = 350.29 \exp(-0.0162SSA), \quad (4.29)$$

$$d = \frac{m}{\rho}. \quad (4.30)$$

The relationship between density and *SSA* has been empirically derived from snow observations and measurements [Legagneux *et al.*, 2002]. In this case, simultaneous measurements of density and *SSA* from 131 samples of different snow types, combined with grain observations, were made from a number of locations including Svalbard (Norwegian Arctic), Arctic Canada and the Alps. A number of linear *SSA*-density relationships were derived for the different snow types by Legagneux *et al.* [2002]. As the snowpack module operates with only one homogenous snow layer, then these data were pooled resulting in

a ‘best-fit’ exponential relationship given by Equation (4.29). An  $SSA$  value of  $120 \text{ m}^2 \text{ kg}^{-1}$  was selected as initial value, yielding a density of  $50.1 \text{ kg m}^{-3}$  (calculated from Equation 4.29), which corresponds to observed values for freshly fallen snow in calm weather conditions [Legagneux *et al.*, 2002; Paterson, 1994].

Snowpack depth may also be influenced by wind-blown snow, resulting in uneven accumulation. However, this process was disregarded due to the homogeneous (single layer) structure of the snowpack in the module and the relatively coarse resolution of the DEHM-POP grid in which the ground is flat within a  $150 \times 150 \text{ km}$  square.

### Settling

Changes to snow crystal structure, or snow metamorphosis, is brought about through the action of wind, changes in temperature and general snow ageing [Cabanes *et al.*, 2003]. This continuous ‘settling’ following snowfall results in increases in snow density and decreases in  $SSA$ . The settling process in the model is described using an empirically derived expression in which the  $SSA$  decreases with time,  $t$  [Cabanes *et al.*, 2003]:

$$SSA(t) = SSA(0) \exp(-at), \quad (4.31)$$

where the settling rate  $a$  is given by:

$$a = 8.87 \times 10^{-4} \exp\left(\frac{-1708}{T}\right), \quad (4.32)$$

where  $T$  is the temperature of the snowpack, which is considered to be the same as the boundary layer air temperature. New values for the density, depth and total surface area are then calculated from equations (4.28) – (4.30) in each time step.

A maximum depth of the snowpack over sea ice of 1 m has been imposed, since the model has a tendency to overestimate the sea ice snowpack depth. This is due to the low air temperature close to the surface which probably result in a too low melt rate as discussed in Hansen *et al.* [2006b]. Another process that would limit the snowpack depth is flooding of ice floes, in which the weight of the snowpack would press down the floe and the lowermost part of the snowpack would be flooded by the sea water and refreeze to form ice. This process is not included since the sea ice is not included as a compartment (see section 4.6) and e.g. the sea ice thickness is not known. A 1 m thick sea ice floe can support approximately 30 cm of snow before it gets flooded depending on the snow density [Granberg, 1998]. The sea ice thickness in the Arctic Ocean is variable both seasonally and on longer time scales. Mean sea ice thicknesses up to 7–8 m are observed north of Greenland and the Canadian Archipelago, in Baffin Bay the modal ice thickness is 0.5–1.5 m and in the southern Greenland Sea the ice thickness is about 1 m Wadhams [1998]. The mean sea ice thickness in the Arctic Ocean is estimated to be 3 m, so the sea ice can support a 1 m thick snow layer. When the snowpack depth exceeds 1 m the ice floe is assumed to be flooded and the excess snow including contamination is transferred to the water compartment below.

The predicted physical parameters of the snowpack module, i.e. snowpack depth, density,  $SSA$  and  $TSA$  are difficult to assess. The monthly averaged snowpack depth of January, April, July, and October 1992 are plotted in Figure 4.3 as an example of the predicted depths of the snowpack. The predicted snowpack depths are of realistic

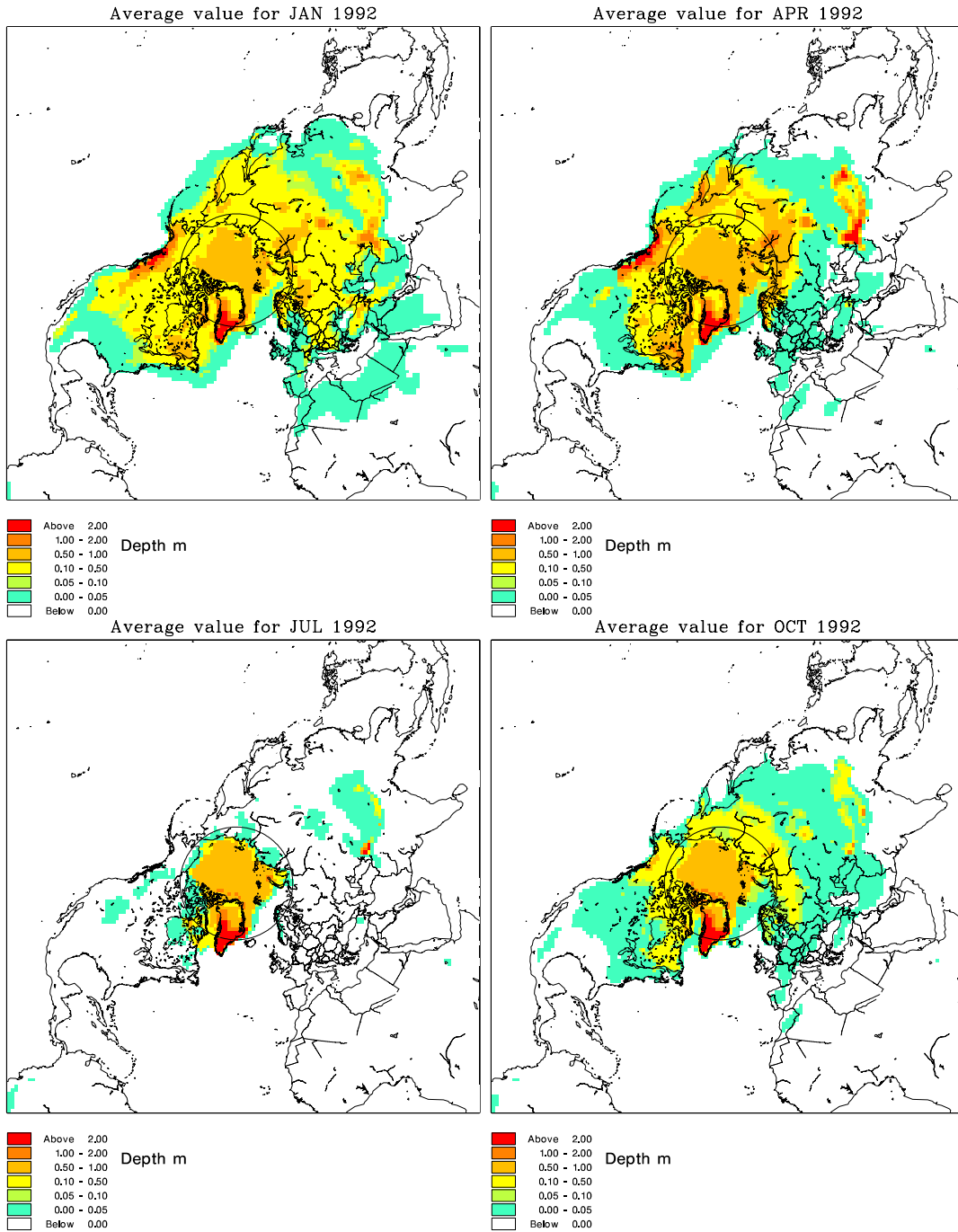


Figure 4.3: Monthly averaged snowpack depth for January 1992 (upper left), April 1992 (upper right), July 1992 (lower left), and October 1992 (lower right).

magnitudes but the extent of the snowpack generally appears to be too large and is probably unrealistic at certain locations, such as in the Hudson Bay in July. The extent of the sea ice also appears to be too large in the North Atlantic Ocean off the North American coast and off the Siberian coast in the North Pacific Ocean in January. It should be noted that the data in figure 4.3 are monthly averages and that the lower boundary of the colour scale is zero, i.e. even a very thin snowpack present for only one time step would be displayed in the Figure. The monthly averaged *TSA* for January, April, July, and October 1992 is plotted in Figure 4.4 as an example of the predicted surface area. The predicted *TSA* values are of the same order of magnitude as the few measurements made during winter in the high Arctic around Alert, Canada, which range from 1160 to 3710 m<sup>2</sup> m<sup>-2</sup> [Dominé *et al.*, 2002].

#### 4.4.1 Air-snow exchange

The chemistry within the snowpack module details the interaction of  $\alpha$ -HCH with snow, and describes fluxes into and out of the snowpack, based on changes in snow physical parameters, the partitioning of the chemical to snow surfaces and the chemical concentration.

The dry gas exchange flux at the surface was derived as the gradient between the boundary layer air concentration and the concentration in the snow pore space multiplied by an exchange velocity,  $v$ :

$$F_{exc,snow} = v(C_g - \frac{C_{snow}}{K_{sa}}), \quad (4.33)$$

where  $C_{snow}$  is the snowpack concentration and  $K_{sa}$  the snow-air partition coefficient, which is calculated by:

$$K_{sa} = K_{ia}SSA\rho, \quad (4.34)$$

where  $SSA$  and  $\rho$  are the specific surface area and density of the snowpack. The exchange velocity,  $v$  was calculated using the Whitman two-layer resistance method equivalent to the expression for the air-water interface [Wania *et al.*, 1998a]:

$$\frac{1}{v} = \frac{1}{v_{air}} + \frac{1}{v_{snow}K_{sa}}, \quad (4.35)$$

The air side exchange velocity,  $v_{air}$  is calculated as [Seinfeld and Pandis, 1998]:

$$v_{air} = \frac{k^2U}{\ln(\frac{z_w}{z_0}) \ln(\frac{z_{ref}}{z_0})}, \quad (4.36)$$

where  $k$  is the von Karman's constant ( $k = 0.4$ ),  $U$  is the wind speed,  $z_w$  is the height of the wind ( $z_w = 10$  m),  $z_{ref}$  is the reference height ( $z_{ref} = 2$  m) and  $z_0$  is the surface roughness for snow ( $z_0 = 0.001$  m).  $v_{snow}$  is given by the snow diffusion coefficient,  $D_{snow}$ , divided by half the thickness of the snowpack, which represents the average diffusion path given the evolution of snowpack depth over the course of a winter season.  $D_{snow}$  depends on the air diffusion coefficient ( $D_{air}$ ) and the density of the snow and was determined according to:

$$D_{snow} = D_{air} \left(1 - \frac{\rho_{snow}}{\rho_{ice}}\right)^n, \quad (4.37)$$

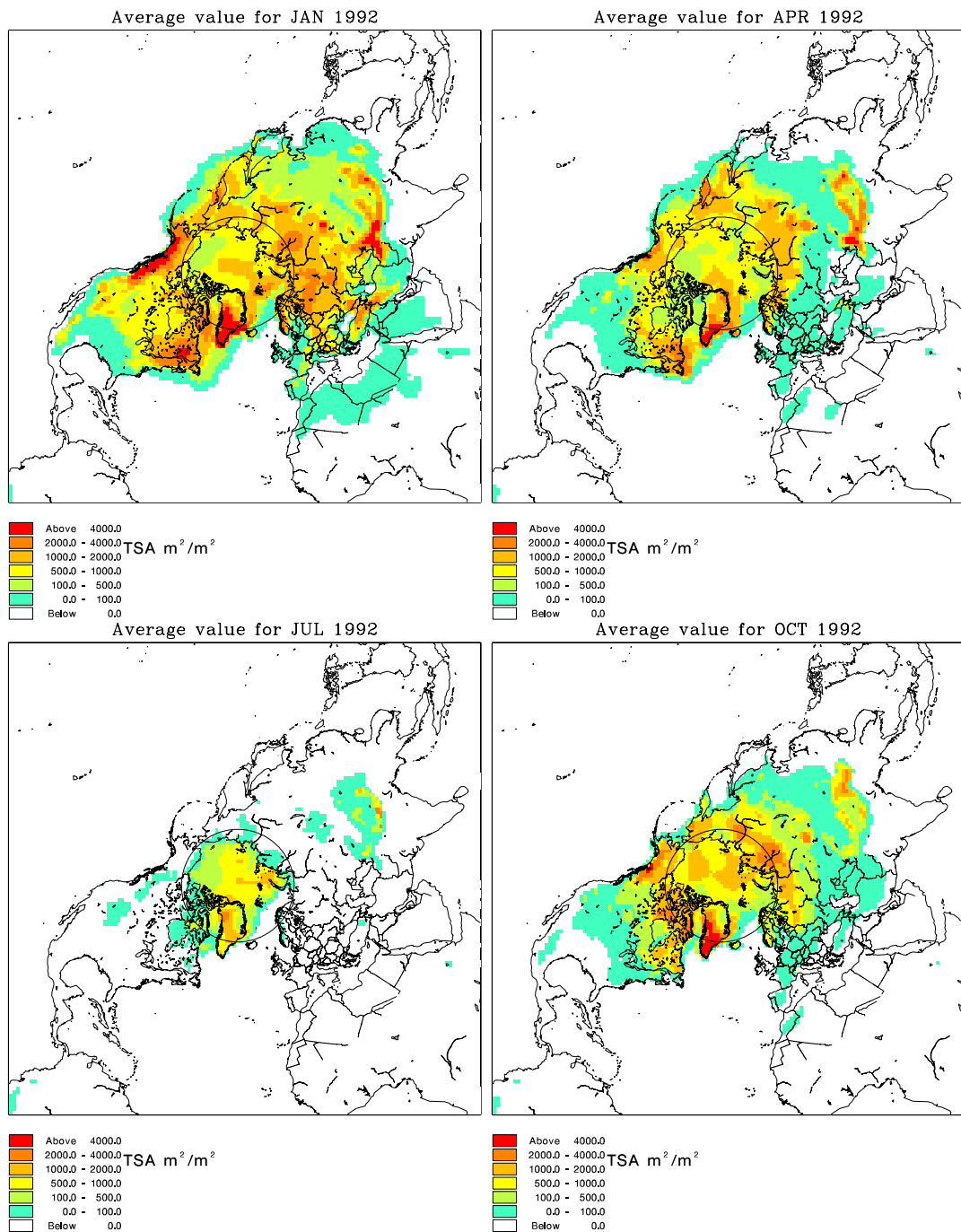


Figure 4.4: Monthly averaged total surface area of the snowpack (*TSA*) for January 1992 (upper left), April 1992 (upper right), July 1992 (lower left), and October 1992 (lower right).

where  $n = 1.5$  was empirically determined for a volatile tracer, sulphur hexafluoride ( $\text{SF}_6$ ), from field experiments conducted at Summit, Greenland [Albert and Shultz, 2002]. A constant air diffusion value of  $D_{air} = 4.59 \times 10^{-6} \text{m}^2 \text{s}^{-1}$  is used in the snowpack module, corresponding to a temperature of  $0^\circ\text{C}$  as calculated by the expression given by Schwarzenbach *et al.* [1993]. The temperature-dependent  $D_{air}$  values used in the snowpack module described in Hansen *et al.* [2006b] was seen to influence the snowpack concentrations too much by retaining the  $\alpha$ -HCH in the snowpack at low temperatures, thereby decreasing the air concentrations.

When wind blows across the snow surface it gives rise to pressure variations in the snowpack, which can result in the movement of interstitial air within the snow. This ventilation process can lead to enhanced chemical exchange between the air and the snowpack [e.g. Waddington *et al.*, 1996; Albert and Shultz, 2002]. The ventilation was described in the model by calculating an effective snow diffusion coefficient depending on the wind speed. The description is based on measurements from Summit, Greenland where  $\text{SF}_6$  diffusion in snow was examined at different wind speeds [Albert and Shultz, 2002]. The diffusion coefficient was measured for calm ( $3 \text{ m s}^{-1}$ ) and windy ( $9 \text{ m s}^{-1}$ ) conditions, with an observed increase of the  $\text{SF}_6$  diffusion coefficient of about a factor 6 for the higher wind speed [Albert and Shultz, 2002]. Therefore, for wind speeds at or below  $3 \text{ m s}^{-1}$  the diffusion coefficients for  $\alpha$ -HCH were assumed to be constant, with a linear increase between  $3$  and  $9 \text{ m s}^{-1}$  with  $D_{snow}$  derived according to Equation (4.37). This process is included in the snowpack module although it was shown to have only small effects on the  $\alpha$ -HCH snowpack and air concentrations [Hansen *et al.*, 2006b].

#### 4.4.2 Particles within the snowpack

Particles are not included in the original version of the snowpack module [Hansen *et al.*, 2006b]. However, as the particles are introduced in the atmosphere they are also deposited to the snowpack by both dry and wet deposition. The particle concentration in the snowpack ( $TSP_{snow}$ ) is estimated from the monthly mean deposition of sulphate particles as calculated by the DEHM-SO<sub>X</sub> model. The particle concentration is assumed to increase linearly through the month, with the increase rate for each time step equal to the fraction of the total deposition that month.

It is likely that there is re-partitioning between the different phases within the snowpack [Wania *et al.*, 1998b]. Re-partitioning between particle concentrations and snowpack concentrations is calculated by Equations (4.4) and (4.5) on page 34 and 35 as for the gas-particle partitioning in air but using the  $TSP_{snow}$  concentration instead of  $TSP$ .

The particles are assumed to remain in the snowpack until it is completely melted at which time they are transferred to the underlying surface. This approach is also used by Wania [1997] and Daly and Wania [2004].

#### 4.4.3 Meltwater

The snow melts when  $T > 0^\circ\text{C}$ . When a snowpack is present in a grid cell in the numerical weather prediction model, the temperature in the lowermost atmospheric layer is low. This may be a problem when the air temperature is used to melt away snow in the snowpack module. To counteract the low temperature close to the surface, the melt

rate is increased to  $10 \text{ cm day}^{-1} T^{-1}$  compared to the snowpack module [Hansen *et al.*, 2006b]. The meltwater is assumed to be lost from the snowpack as run-off with the amount of meltwater within the snowpack reduced to  $1/e$  after 24 hours. The run-off, including eventual contamination, is transferred to the underlying compartment, i.e. soil or water. The meltwater refreezes if  $T < 0^\circ\text{C}$  and the refreeze rate is determined by the amount of heat supplied by the temperature difference between the meltwater ( $0^\circ\text{C}$ ) and the snowpack. Instantaneous mixing is enforced, where the refrozen melt layer is assumed to have a  $TSA = 0$ .

#### 4.4.4 Air-meltwater gas exchange

During melt, the meltwater rapidly fills the pore spaces in the snowpack thereby ‘shutting off’ chemical exchange between air and the snow surface. It is assumed that the air-snow gas exchange during periods of melting is replaced by an air-meltwater gas exchange. This exchange is calculated using the same expression as for the air-water interface (Equation 4.26).

#### 4.4.5 Degradation

The chemical transformation processes in snow and ice are not well known. POPs in snow are not likely to undergo biodegradation, but there are possibilities of photochemical reactions. This has been studied for a number of organic compounds both in the laboratory and in field studies [e.g. Klán and Holoubek, 2002; Klán *et al.*, 2003; Klánová *et al.*, 2003]. However, reaction rates and half-lives from these studies are not well suited as model input parameters since they were made with higher than environmental concentrations and constant sample irradiation [Daly and Wania, 2004]. Higher concentrations of hydroxyl radicals (OH) are observed following  $\text{NO}_x$  photochemistry, which potentially could affect the degradation of POPs in the snowpack [e.g. Dominé and Shepson, 2002]. As a first approximation of degradation rates in snow, air degradation rates are thus assumed to apply in the snowpack module in DEHM-POP. Degradation on the particle-sorbed fraction is not included similarly to the assumptions in air. Degradation half-lives in water were used as a first estimate of degradation in snow by Daly and Wania [2004].

### 4.5 Vegetation

The role of vegetation in the global cycling of POPs is very complex. Although the subject of many studies, several aspects of the process are not well understood, see Barber *et al.* [2004] for an extensive review. Plants can take up contaminants from air through the leaves or from soil through the roots, although the latter process is believed to be of little importance for POPs due to their physical-chemical properties [Simonich and Hites, 1995]. As for other surface media, POPs may be released to the atmosphere after being taken up in or deposited to the vegetation. The exchange of POPs between air and vegetation depends on many different parameters such as the temperature, and there is a large variability in plant characteristics such as leaf area and thickness, structure, chemical composition, and transpiration rates [Barber *et al.*, 2004]. POPs are believed to primarily enter plants by sorption into the cuticle, a thin lipid surface layer covering leaves

to protect against water loss [Barber *et al.*, 2004]. Recent studies suggest that stomata (pores allowing the exchange of gases between the leaf interior and the surrounding air) also may act as a pathway of POPs into plants [Barber *et al.*, 2002, 2004].

The high deposition velocities to vegetation and the large canopy densities of forest may lead to a ‘forest filter effect’, where gas-phase POPs are scavenged from the air by the vegetation and transferred to the soil by subsequent leaf litter fall [McLachlan and Horstmann, 1998]. Including vegetation in a multi-compartment mass balance model resulted in up to a factor 5.5 lower air concentrations of SVOCs during summer than without vegetation [Wania and McLachlan, 2001]. In another model study, the transport of SVOCs into the Arctic was shown to be reduced due to vegetation at lower latitudes [Su and Wania, 2005].

The inclusion of vegetation in multi-compartment mass balance models has been the subject of several studies [e.g. Severinsen and Jager, 1998; Cousins and Mackay, 2001; Wania and McLachlan, 2001; Wegmann *et al.*, 2004]. Most models are based on the assumption that POPs are taken up through the lipophilic cuticle which covers the plant surface [Barber *et al.*, 2004].

### The vegetation module in DEHM-POP

A very simple vegetation module with only one type of vegetation is introduced in DEHM-POP. The module describes the absorption of gas-phase POPs by the cuticle of leaves. The vegetation coverage is calculated from a data set of the global monthly average leaf area index (LAI) with a  $0.5^\circ \times 0.5^\circ$  resolution [Myneni *et al.*, 1997]. These data are redistributed to the DEHM-POP model grid and it is assumed that there is a vegetation cover in grid cells with positive LAI values (see Figure 4.5). The rate of change in the concentration in vegetation,  $C_v$ , is given by:

$$\frac{\partial C_v}{\partial t} = F_{exc,vege} + f_{vege}F_{wet} - F_{litter-fall} - k_{vege}C_v, \quad (4.38)$$

where  $F_{exc,vege}$  is the dry gas exchange,  $f_{vege}$  is the vegetation interception fraction of precipitation,  $F_{wet}$  is the wet deposition flux,  $F_{litter-fall}$  is the vegetation to soil transfer of litter fall, and  $k_{vege}$  is the degradation rate in vegetation.

#### 4.5.1 Air-vegetation exchange

The air-vegetation gas exchange in DEHM-POP is calculated from the equation:

$$F_{exc,vege} = v(C_g - \frac{C_v}{K_{va}}), \quad (4.39)$$

where  $v$  is the exchange velocity and  $K_{va}$  is the vegetation-air partition coefficient.

The exchange velocity is calculated using the Whitman two-layer resistance method:

$$\frac{1}{v} = \frac{1}{v_{air}} + \frac{1}{v_{vege}}, \quad (4.40)$$

The air side exchange velocity,  $v_{air}$  is calculated from Equation 4.36 as for the air-snow gas exchange. The vegetation side resistance is calculated as:

$$v_{vege} = \frac{LAI}{P_{cut}K_{wa}}, \quad (4.41)$$

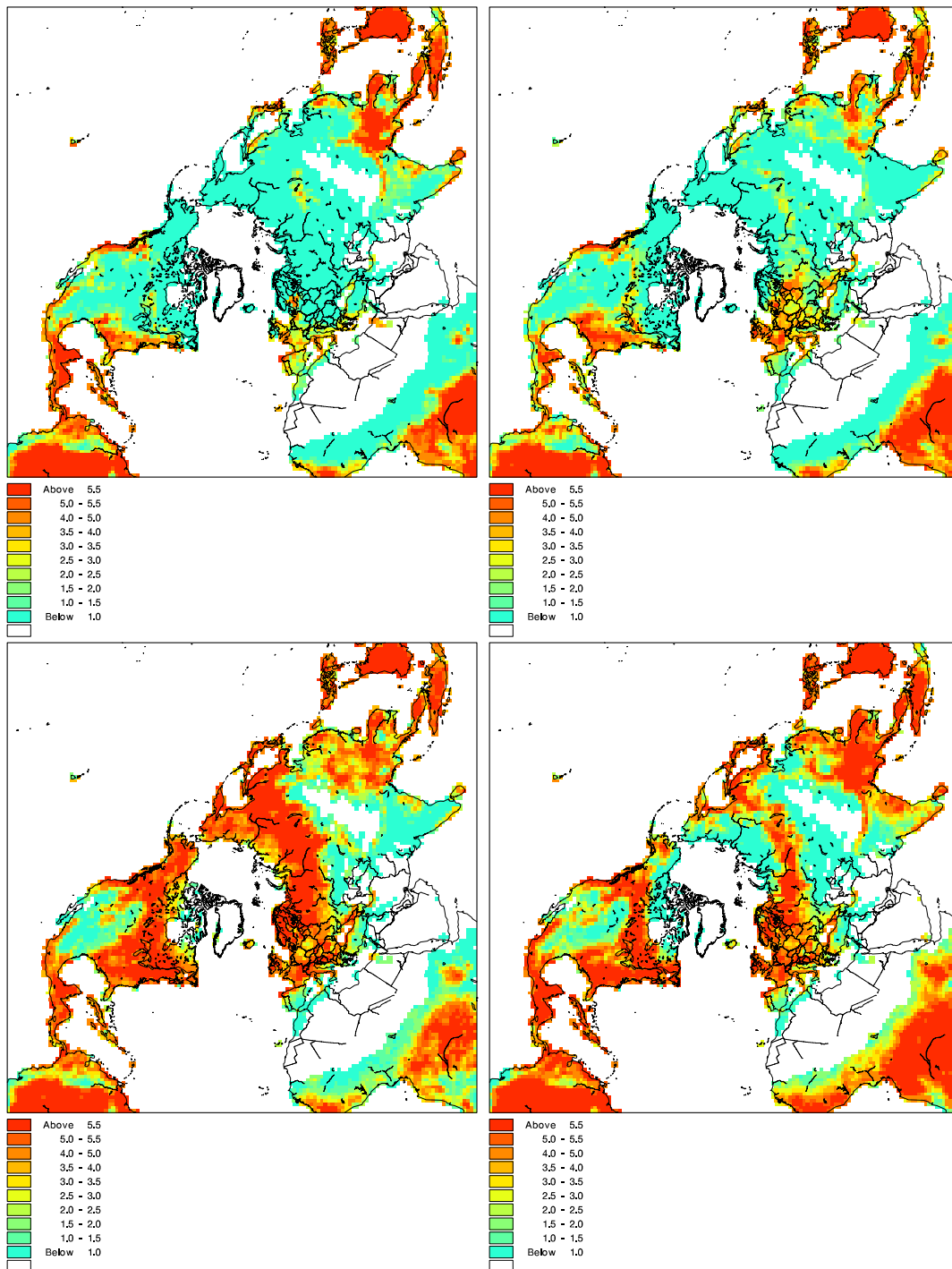


Figure 4.5: Monthly averaged leaf area index (LAI) for January (upper left), April (upper right), July (lower left), and October (lower right). The data have been redistributed to the DEHM-POP model grid.

where  $P_{cut}$  is the cuticle permeance, which is estimated experimentally from one plant species [see *Barber et al.*, 2004, for reference]:

$$\log P_{cut} = 0.704 \log K_{ow} - 11.2. \quad (4.42)$$

The vegetation-air partition coefficient can be described using the octanol-air partition coefficient, however the relationship is not linear [e.g. *McLachlan and Horstmann*, 1998]:

$$K_{va} = m(K_{oa})^n, \quad (4.43)$$

where  $m$  and  $n$  are plant specific coefficients that can be determined experimentally. For the DEHM-POP vegetation module  $m = 26$  and  $n = 0.72$  is chosen as the average value between the values determined for coniferous and deciduous forest by *McLachlan and Horstmann* [1998]. Temperature dependent  $K_{oa}$  values from *Xiao et al.* [2004] are used as input.

When there is a snow cover, it is assumed that the air-vegetation exchange is ‘shut off’. The experiments with a multi compartment mass balance model including snow by *Daly and Wania* [2004] operate with a similar assumption, but includes air-vegetation gas exchange during the melting of the snowpack.

#### 4.5.2 Precipitation-vegetation exchange

The canopy is intercepting the falling precipitation and a fraction of it is absorbed by the vegetation, whereas the rest is assumed to drip or flow off the vegetation and is thus transferred to the underlying soil. The vegetation interception fraction,  $f_{vege}$ , is in DEHM-POP calculated using the leaf area index (LAI) scaled with a factor 0.05. It attains a maximum value for maximum LAI, which is approximately equal to  $6 \text{ m}^2 \text{ m}^{-2}$ , so a maximum vegetation interception fraction is equal to 0.3. In other models the interception fraction is not included [*Severinsen and Jager*, 1998] or described either as a constant, e.g. with values of 0.1 [*Cousins and Mackay*, 2001], 0.35 [*Wania and McLachlan*, 2001], 0.14 [*Wegmann et al.*, 2004], or it is scaled to the change in canopy volume and vegetation type distribution and attains values between 0.01 and 0.3 [*Wegmann et al.*, 2004].

#### 4.5.3 Influence of vegetation on soil

The vegetation cover has two effects on the soil, it reduces the air-soil gas exchange and when dead leaves fall upon the ground the leaf litter is incorporated into the soil and the vegetation thus acts as an input of organic material to the soil. The decrease in air-soil gas exchange is scaled with the LAI value in each grid cell, so that a maximum LAI value is reducing the air-soil exchange to zero.

The input of chemical to soil from leaf litter is in DEHM-POP calculated at the beginning of each month. If the monthly average LAI in a grid cell is smaller than the LAI from the previous month, it is assumed that leaves are lost as litter fall. The fraction of contamination corresponding to the difference between the old and new LAI value is transferred from the vegetation into the underlying soil compartment, where it is assumed to be immediately incorporated into the soil.

#### 4.5.4 Degradation

Several degradation mechanisms in vegetation has been proposed, e.g. photodegradation on the surface of plants and metabolism within the plants, see *Barber et al.* [2004] and references therein. There are several problems in quantifying the effect of these processes, such as knowledge on how and where the contamination enters the plants, and various studies also show different results [*Barber et al.*, 2004]. However, using a new methodology which combines PAH autofluorescence with two-photon excitation microscopy, *Wild et al.* [2005] has examined photodegradation on vegetation of PAHs and the results suggest that this process may be a more important loss mechanism for PAHs than previously thought.

In DEHM-POP degradation rates as in air are used as suggested by *Cousins and Mackay* [2001]. Other models use various approaches to describe vegetation degradation rates. For example, experimental degradation rates were adopted for the study by *Wegmann et al.* [2004], and *Semeena and Lammel* [2003] used the same degradation rates in vegetation as in soil. In an investigation of the forest filter effect, *Wania and McLachlan* [2001] used a degradation rate in vegetation equal to zero, while a sensitivity study showed that the degradation rate was an important parameter in vegetation modelling.

## 4.6 Sea ice

Sea ice is created by water as this freezes in areas with temperatures below 0°C. The major part of the Arctic Ocean is covered by sea ice most of the year. Sea ice can have three different effects on the environmental distribution of POPs. Sea ice acts as a lid on the water that prevents or highly reduces the air-water exchange processes, a snowpack can form upon the ice, which can increase the possible snow covered area, and POPs trapped within the sea ice or in the overlying snowpack may be re-distributed when the ice is transported with the wind and the surface ocean currents.

When sea ice is formed in shelf area regions of the Siberian seas with shallow water, sediments and organic materials and thus associated contaminants may be incorporated into the ice [*Pfirman et al.*, 1995]. Some of the ice may be transported into the Arctic Ocean and further into the marginal ice zone, e.g. it is estimated that sea ice formed in the Kara Sea with 50% probability drifts into the Barents Sea within two years [*Korsnes et al.*, 2002]. Surface melting as well as additional deposition to the sea ice during this transport may increase the concentration of particles and contaminants, and they are released when melting in the biologically active marginal ice zones and thus easily enters the food chain [*Pfirman et al.*, 1995]. Measurements north of Svalbard and in the Fram Strait indicate that the sea ice drift route influences the concentrations of POPs in ice-associated amphipods [*Borgå et al.*, 2002]. However, other measurements from the Barents Sea marginal ice zone and the North Pole area indicate that the sea ice is not an important long-range transport medium [*Gustafsson et al.*, 2005].

The incorporation of sea ice in multi-compartment mass-balance models is variable. It is not included as a compartment in the global zonally averaged model by *Scheringer et al.* [2000], whereas the model described by *Wania and Mackay* [1995]; *Wania et al.* [1999b] includes sea ice to reduce the air-water exchange processes. A full sea ice module including both transport and exchange between air, sea, ice and overlying snow is included in the atmospheric chemistry transport model described by *Gusev et al.* [2005].

### 4.6.1 Sea ice in DEHM-POP

Sea ice is only partly included in DEHM-POP, i.e.  $\alpha$ -HCH is not accumulating in the sea ice and only the first two of the above mentioned effects of sea ice are thus included in the model (reduced air-water exchange and foundation for snowpack). Data on the extent of sea ice within the model domain are extracted from the MM5v2 model together with the meteorological data.

Sea ice is transported around by ocean currents and wind, which may lead to break-up of the ice floes, thereby creating leads, i.e. strips of open water. Leads typically occupy 1–5% of the ice cover in the central Arctic Ocean in winter, a percentage that increases to 10–20 for the marginal ice zone and for divergent drift currents such as the East Greenland Current [Wadhams, 1998]. In DEHM-POP it is assumed that leads on average occupy 5% of the sea ice cover in all sea ice covered grid cells at all times. The air-water exchange is thus reduced to 5% in sea ice covered grid cells. As there are no ocean currents included in the model, the sea ice drift and concurrent re-distribution of the POPs is not taken into account.

## 4.7 Other compartments

A few other environmental compartments and processes within them may be of importance to the environmental fate of POPs, and will be described in this section. However, they are not included in the present version of DEHM-POP.

### 4.7.1 Fresh water

Rain or snow consist of fresh water, and when it falls upon the land-covered surface it seeps through the soil or form streams or rivers that can discharge the water into lakes or into the ocean.

#### Fresh water bodies

The open fresh water bodies, whether it is a lake or a river affects the environmental cycling of POPs differently than ocean water. The air-water gas exchange process acts slightly differently over fresh water than over ocean water due to the salinity effect on the water solubility and thus on the Henry's law constant (see section 4.3.1). Biodegradation rates may also be different in fresh water bodies than in ocean water [e.g. Falconer *et al.*, 1995].

#### Fresh water transport

The transport of contamination with fresh water may also be of importance to the fate of relatively water soluble POPs. For example approximately 10% of the loading of  $\alpha$ -HCH to the Arctic Ocean between 1945 and 2000 is estimated to come from transport through rivers [Li *et al.*, 2004a]. Wania and Mackay [1999b] estimated that 2.3 % of the global usage of  $\alpha$ -HCH was transferred to the oceans through fresh water transport, about one third of the total input to the oceans.

Fresh water transport is also included in several multi-compartment mass balance models. This is typically parameterised by including fresh water flow rates from one region of the model to the neighbouring regions. For example, *Prevedouros et al.* [2004b] extracted water flow rates from a network of gauging stations on the European continent for the EV<sub>n</sub>-BETR model. This work is manageable for a model with 25 or 50 regions but will be quite extensive in a model with several thousands grid cells. The fresh water transport is thus not included in the present version of DEHM-POP.

### 4.7.2 Sediments

As described in section 4.3.2, POPs can be lost from surface waters by settling with particulate organic carbon. Ocean or lake sediments mainly act as ultimate sinks of POPs and the continental shelf sediments are estimated to contain up to 80% of the estimated maximum cumulative global emissions of the higher chlorinated PCB congeners [*Jönsson et al.*, 2003]. There are however a possibility that sediment-bound POPs may enter the environmental cycling by re-suspension of sediments. For example, sediment re-suspension is large in the Venice Lagoon, Italy and this possibly influences the environmental cycling of PCCD/Fs [*Dalla Valle et al.*, 2003].

Sediment compartments are included in most multi-compartment mass balance models [e.g. *Wania et al.*, 1999b; *MacLeod et al.*, 2001; *Prevedouros et al.*, 2004b], and is important to include in mass-balance estimates and assessments of the environmental distribution of POPs. Sediments are not included in DEHM-POP, since the model does not include a description of the ocean below the surface compartment and the settling of particulate organic carbon.

### 4.7.3 Organic films in urban areas

An organic film has been observed on impervious urban surface, and it is suggested that this film may constitute a site for exchange of SVOCs in urban environments [*Law and Diamond*, 1998; *Diamond et al.*, 2000]. PAHs and PCBs were measured in organic films on windows from downtown Toronto, Canada, and the measured film to air partition coefficient for selected congeners was comparable to  $K_{oa}$  values suggesting that gas-phase SVOCs may partition into the organic films [*Diamond et al.*, 2000]. Recent measurements of the composition of window surface films from Toronto, Canada have shown that the surface films consist of 94% inorganic material and 5% organic carbon, thus significant different composition than particulate matter [*Lam et al.*, 2005].

*Diamond et al.* [2001] developed a multi-compartment urban model (MUM) including the organic surface films as a compartment together with air, surface water, sediment, soil, and vegetation compartments. Illustrative calculations using selected PAHs and PCDDs indicate that the organic surface films act as a transient sink that increases the chemical mobility in urban areas by allowing the more volatile chemicals to re-volatilise into the air, and facilitates the removal to surface waters by wash-off [*Diamond et al.*, 2000]. A comparison of the MUM model with a model set-up simulating a forested watershed confirmed the increased mobility of SVOCs in urban areas [*Priemer and Diamond*, 2002]. The primary loss-mechanism from the organic films of compounds with  $K_{oa} < 10^{7.5}$  is re-volatilisation, whereas it is wash-off and subsequent transfer to surface waters for compounds with  $K_{oa} > 10^{7.5}$  [*Priemer and Diamond*, 2002]. Urban area organic surface films

are not included in DEHM-POP, although urban area is one of the land-cover classes in the land use data (see section 5.2 on page 66). It may be an important medium to include in a future version of model, especially for studies of chemicals with urban origin.

## Chapter 5

# Model input

Atmospheric chemistry transport models require input to simulate the environmental distribution of pollutants. These input are meteorological data, land use and topography data, and data on emissions of the simulated compounds. Depending on the simulated period and compounds it can also be necessary to use initial environmental concentrations as input. The input used in DEHM-POP is described in this chapter.

### 5.1 Meteorological data

The numerical weather prediction model, MM5v2 [Grell *et al.*, 1995] is used as the meteorological driver for the current DEHM model system. The MM5v2 model is run for slightly larger domains and implemented on the same projections as the transport model (see Figure 3.1 on page 26). The horizontal MM5v2 domain is thus divided into  $136 \times 136$  grid points for the DEHM-POP version. Both horizontal and vertical resolutions are the same in MM5v2 as in DEHM.

The MM5v2 model requires input such as gridded atmospheric data on pressure, wind velocity, temperature, relative humidity and geopotential height at pressure levels from the surface and up to 100 hPa. This information is obtained from the European Center for Medium Range Weather Forecasts (ECMWF) with a horizontal resolution of  $2.5^\circ \times 2.5^\circ$  and a 12-hour temporal resolution. The applied ECMWF/TOGA Basic Level III Consolidated data set consists of uninitialized analyzed data for the surface and 14 upper levels.

The MM5v2 model includes hydrostatic dynamics and various options for the parameterisations of atmospheric processes designed for simulations at different scales. The following are chosen as appropriate for the grid resolutions applied in DEHM-POP: The Reisner mixed phase for explicit moisture. The Betts-Miller convective parameterization and the MRF boundary layer parameterization, including a five layer soil model and a cloud-radiation scheme (see *Dudhia et al.* [1999] for details). High resolution (30 arc sec) data on topography and land use from United States Geological Survey (USGS) are also applied as input to MM5v2.

A four-dimensional data assimilation scheme based on Newtonian relaxation, or so called nudging, is included in the MM5v2 modelling sub-system. Artificial forcing functions are continuously added to the governing model equations thereby nudging the so-

lutions towards observations or analyzed fields. In the used model set-up the nudging is towards the ECMWF data (in 12 hours interval) and the forcing functions are based on differences between the two fields. The output of the MM5v2 modelling sub-system is a gridded meteorological data set with a higher spatiotemporal resolution than the ECMWF input and is thus considered to give a better representation of e.g. wind velocities and boundary layer meteorology than the original input. Effects of e.g. topography will also be represented in more detail. The effect of the nudging procedure is that the resolution of the resulting data field to some degree is maintained at the original  $2.5^\circ \times 2.5^\circ$  resolution. The advantage of the MM5v2 model's ability to generate mesoscale meteorological structures can therefore not be fully utilized as these features are not always sufficiently resolved in the analyzed ECMWF fields. The input and nudging towards an analyzed meteorological field with a higher resolution in time and space would be more optimal. Although analyzed data of higher resolution are available, the solution with low resolution analyzed data combined with a meteorological driver is chosen at NERI for economic reasons.

Meteorological data from the MM5v2 model are available from 1991 to 2000 for the set-up of the DEHM-POP version with  $135 \times 135$  grid points. For the original model domain with the  $96 \times 96$  grid points set-up meteorological data back to 1979 are available.

## 5.2 Land use and topography data

The dry deposition and the air-surface gas exchange modules in the DEHM-POP model operate with different set of land use classes. The main land use data applied in DEHM are derived from a global  $1^\circ \times 1^\circ$  gridded data set [Wilson and Henderson-Sellers, 1985]. The original 53 possible land cover classes are condensed to eight categories: coniferous forest, deciduous forest, cultivated land, grass land, urban, swamp, open water and snow following the ideas of Voldner *et al.* [1986]. Details on the land use condensation are described in Frohn [2004]. The eight land cover classes are further condensed in the DEHM-POP model to three categories: forest, non-forest covered land surface and open water. These three land surface classes are used in the dry particle deposition module (see section 4.1.2 on page 36). A further condensation of these data to the two classes: land covered surface and open water is made for the air-surface gas exchange module. Three additional land cover classes are used in this module: sea ice, snow, and vegetation. Information on the extent of snow is created in the snowpack module (see section 4.4 on page 50). Data on the extent of sea ice within the model domain are extracted from the MM5v2 model together with the meteorological data. The sea ice data are used to reduce the air-water exchange and to create snowpack on sea ice (see section 4.6 on page 61). The horizontal extent of the vegetation is derived from the leaf area index data (see section 4.5 on page 57). Although the original land cover classes are more detailed with several different types of vegetation, these were not possible to apply due to the simple structure of the vegetation module. Topographical features are included in the  $\sigma$ -coordinate introduced in DEHM-POP from the MM5v2 model; topographical data are, thus, not used directly as input to DEHM-POP.

### 5.3 Emissions

Emissions are essential input parameters in 3-D atmospheric chemistry transport models, but they are also the origin of some of the major uncertainties in the models [Russell and Dennis, 2000]. The uncertainties arise due to incomplete knowledge of the exact amount of production, usage or sources and due to the distribution process onto gridded surrogate data of these estimates that are often based on countries or counties [Russell and Dennis, 2000].

Emission estimates for POPs are generally more uncertain than emission estimates for regular air pollutants; while the uncertainties in annual  $\text{NO}_x$  emissions are 25–40% [Russell and Dennis, 2000], uncertainties in emissions are estimated to be a factor 2–5 for  $\gamma$ -HCH [van Jaarsveld *et al.*, 1997] and up to an order of magnitude for PCBs [Breivik *et al.*, 2002b]. These large uncertainties arise due to little knowledge on production and usage, the often complex application pattern, and the not well-known release processes and their contribution to the final emissions.

Significant progress has been made for a number of pesticides, while emission estimates for the non-pesticide POPs still are limited as stated in a review of existing emission estimates for POPs [Breivik *et al.*, 2004]. The spatial coverage is mainly regional with a few global scale estimates and only few of the published emission estimates are gridded, most are country based estimates [Breivik *et al.*, 2004]. In this project two global gridded emission estimates for  $\alpha$ -HCH are used.

The two sets of  $\alpha$ -HCH emission data have different temporal resolution and time span. The two data sets are prepared in the same way on the basis of compiled year by year usage data for each country, which are then distributed on a  $1^\circ \times 1^\circ$  gridded cropland as surrogate data [Li *et al.*, 2000]. The horizontal resolution of these data are thus  $1^\circ \times 1^\circ$ . Emissions into air are then calculated by estimating emission factors from the two events spraying and tiling. By using the Simplified Gridded Pesticide Emission and Residue Model (SGPERM) [Li *et al.*, 2004b], not only fresh usage but also usage from the previous up to 15 years are taken into account [Li *et al.*, 2000]. No quantitative uncertainty estimate of these emission data was made, but the contribution to uncertainties from the usage data, the gridding procedure, the assumed application modes and the used soil half-life was discussed qualitatively [Li *et al.*, 2000].

The first set of emissions is made from the global gridded emission estimates for the years 1990 and 2000 published by Li *et al.* [2000] (see Figure 5.1). Emissions for the years 1991–1999 are estimated by assuming a linear development of the emissions between 1990 and 2000 in each grid cell. The emissions for each year are distributed evenly throughout the year. This emission data set is used as input to the model simulation presented in Hansen *et al.* [2004].

The second data set consists of monthly averaged emissions spanning from 1945 to 2000 [Li, personal communication]. The long time span of this emission data set allows for long-term simulations of the environmental fate of  $\alpha$ -HCH. The monthly resolution of the data also allows for better evaluation of shorter-term air concentration fluctuations arising from different agricultural practise in different parts of the world (see Figure 5.2 for the year 1991 and Figure 5.3 for the year 1995 as examples). This data set is based on the same usage data as the first set, but it also includes a more recent estimate of the European usage from 1970 to 1996 [Breivik *et al.*, 1999]. The emissions for each month

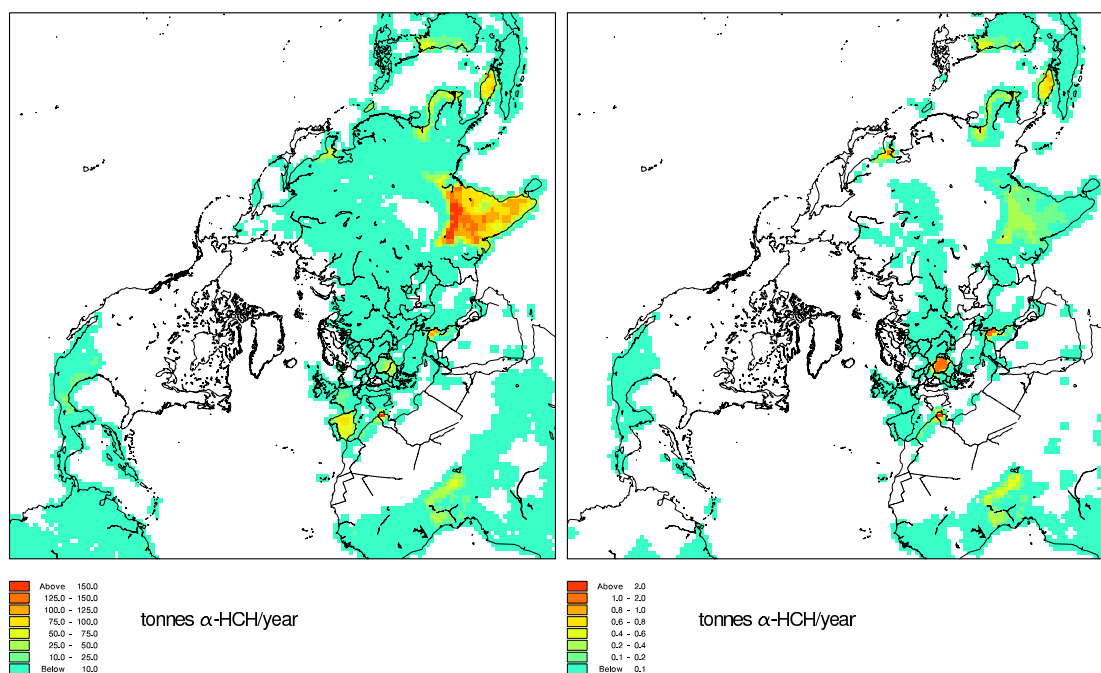


Figure 5.1: Emissions of  $\alpha$ -HCH for 1990 (left) and 2000 (right) [Li et al., 2000]. The data are redistributed to the DEHM-POP model grid. Note the different colour scales.

are distributed evenly throughout the month. These emission data are used as input in the model simulations presented in *Hansen et al.* [2006a] and in this thesis. It was later realized that the emission estimates for the former Soviet Union were too low for the second emission data set [Li, personal communication]. The results should thus be interpreted with this deficit in mind.

## 5.4 Initial environmental concentrations

Depending on the simulated compound and period it can be necessary to use initial concentrations in the environmental media as input together with the emissions and meteorological data. The focus in this project is on the environmental distribution in the 1990s, while the largest usage and emission of  $\alpha$ -HCH was before this period (see section 2.5 on page 20). Due to the great persistence of the compounds, residues of previous emissions are still cycling the environment. Initial concentrations in the environmental media are thus necessary to study the environmental fate of  $\alpha$ -HCH in the simulations presented in this thesis. Initial environmental concentrations can be estimated either from measurements of the environmental media or by spinning-up the simulation, i. e. running the model for a period up to the start of the simulation if the necessary emission input and meteorological data are available.

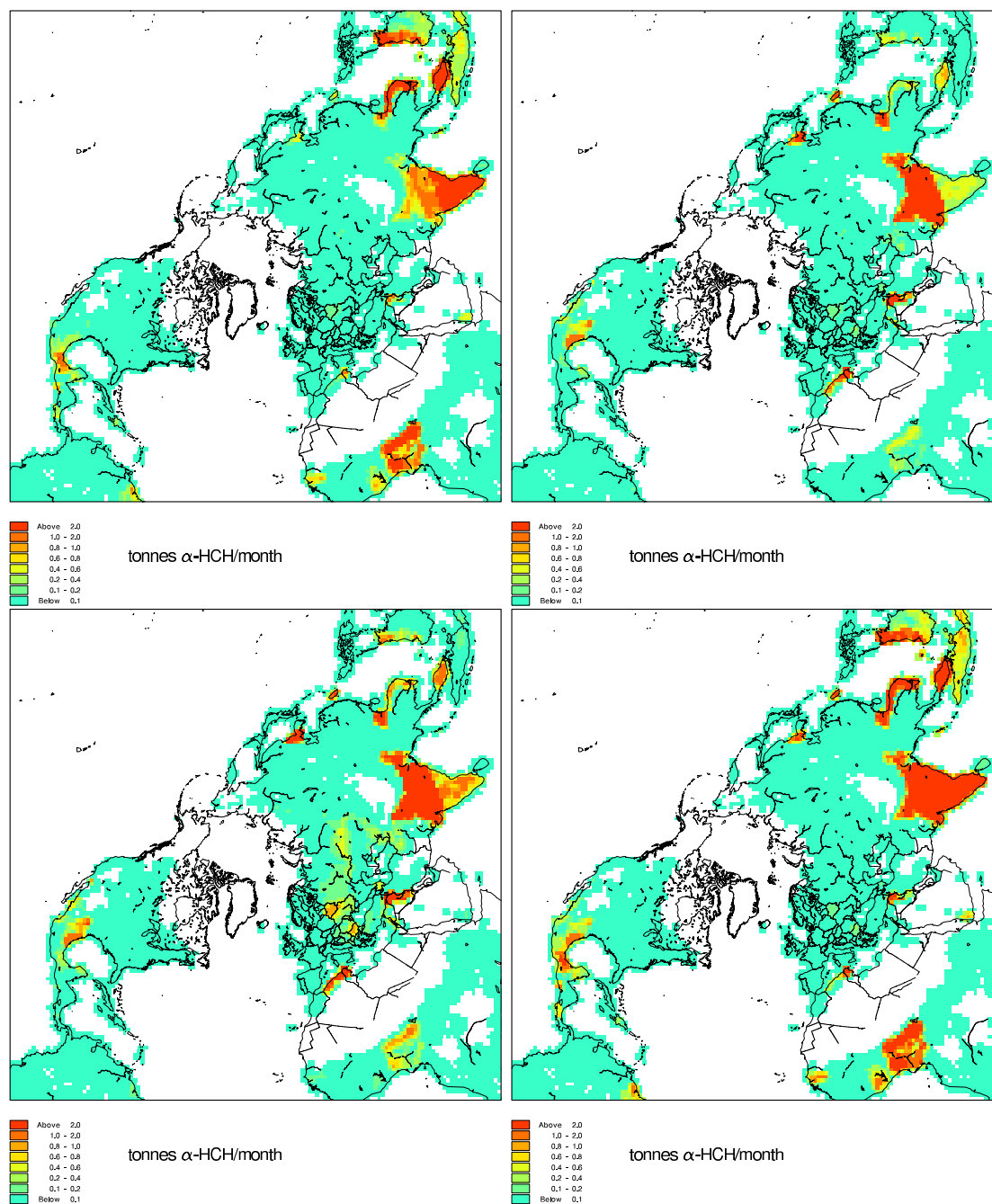


Figure 5.2: Emissions of  $\alpha$ -HCH for January 1991 (upper left), April 1991 (upper right), July 1991 (lower left) and October 1991 (lower right) [Li, personal communication]. The data are redistributed to the DEHM-POP model grid.

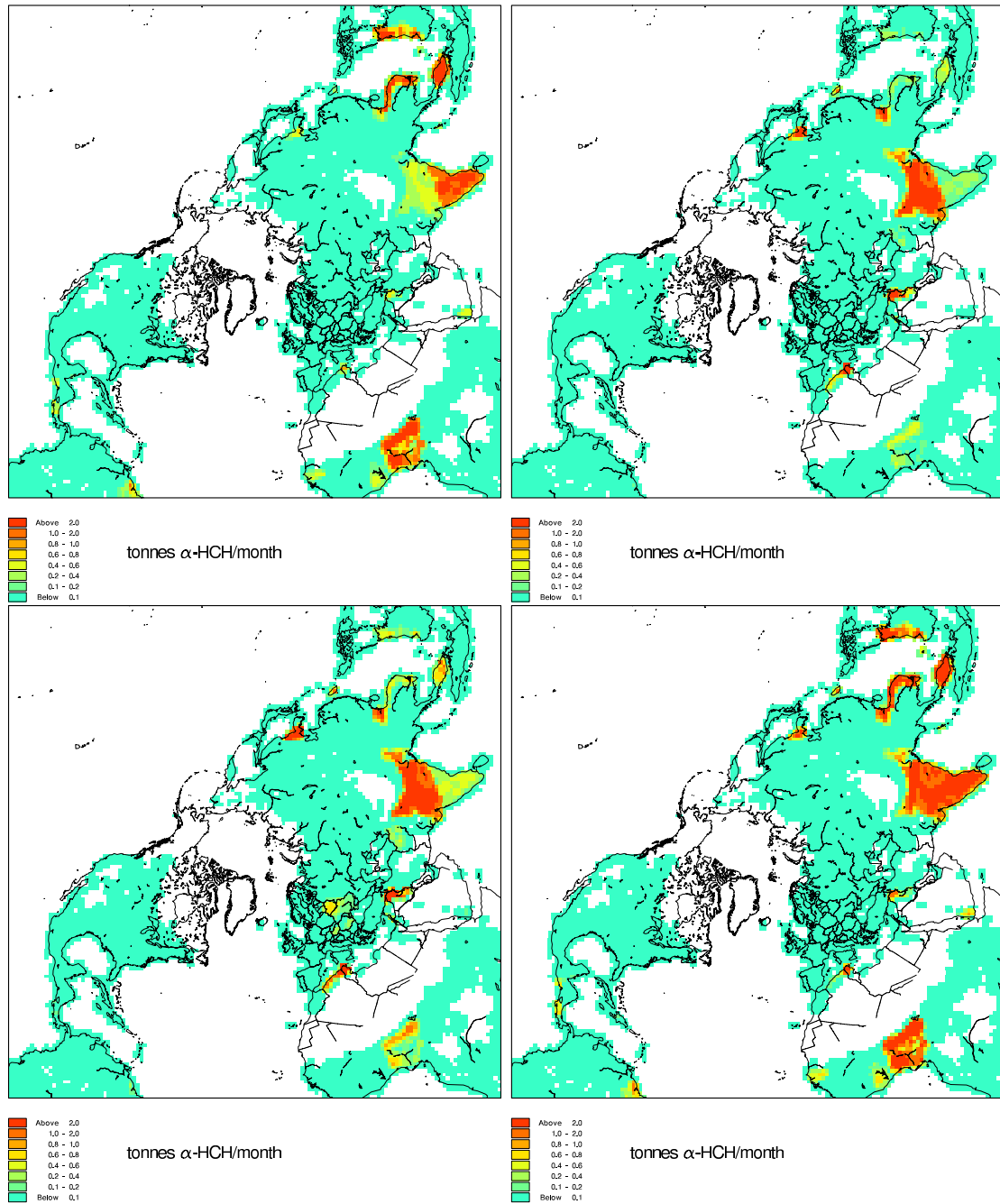


Figure 5.3: Emissions of  $\alpha$ -HCH for January 1995 (upper left), April 1995 (upper right), July 1995 (lower left) and October 1995 (lower right) [Li, personal communication]. The data are redistributed to the DEHM-POP model grid.

### 5.4.1 Air

The mixing time throughout one hemisphere is about 1–2 months [Seinfeld and Pandis, 1998]. Atmospheric concentrations thus rapidly disperse through the model domain, and the initial concentrations in the atmosphere are therefore set equal to zero in the model simulations in this study.

### 5.4.2 Soil

The main part of the  $\alpha$ -HCH contamination in soil derives from direct usage of Technical HCH, and large residues may remain in the soil several years after the usage in a particular area is stopped [Li *et al.*, 2004b]. However, these residues are taken into account when the emissions are calculated, and although not present in DEHM-POP as soil concentrations they are accounted for in the model. What is not accounted for is then the fraction of emissions from years prior to 1990 that has been deposited to the soil. However, this is very difficult to estimate from the very limited available data on  $\alpha$ -HCH measurements in soil. The initial concentration in soil is thus set equal to zero in the model simulations presented here.

### 5.4.3 Ocean water

The low  $K_{aw}$  of  $\alpha$ -HCH favour partitioning from air into water, especially at low temperatures. Oceans are therefore major sinks of  $\alpha$ -HCH [e.g. Macdonald *et al.*, 2000]. Measurements of  $\alpha$ -HCH concentrations are made in surface water from most of the worlds oceans [e.g. Iwata *et al.*, 1993]. Although the major sources are in tropical and temperate regions, up to an order of magnitude higher concentrations are found in Arctic sea water than closer to the source regions [e.g. Iwata *et al.*, 1993; Schreitmüller and Ballschmiter, 1995].

Several multi-compartment mass balance models have been used to estimate the total  $\alpha$ -HCH inventory of the worlds oceans. Using a zonally averaged model, the total  $\alpha$ -HCH ocean inventory at the end of 1985 was estimated to be 22661 tonnes in the surface ocean and 72914 tonnes in the deep ocean [Strand and Hov, 1996]. The total loading to the worlds oceans between 1947 and 1997 was estimated to be 408000 tonnes, corresponding to 6% of the global emitted amount with another zonally averaged model [Wania and Mackay, 1999b]. The surface ocean inventory in 1997 was estimated to be 10880 tonnes, corresponding to 0.16% of the amount emitted to the global environment [Wania and Mackay, 1999b]. Several mass balance estimates were made for the Arctic Ocean. The loadings of HCHs in the Arctic Ocean in the mid-1990s were estimated on the basis of measurements to be 3550 tonnes, where 2910 tonnes were  $\alpha$ -HCH [Macdonald *et al.*, 2000]. Loadings of  $\alpha$ -HCH in the Arctic Ocean were estimated with a mass balance box model from 1945 to 2000 with a peak of about 6700 tonnes in the beginning of the 1980s, decreasing to about 4220 tonnes in 1990 and to 1550 tonnes in 2000 [Li *et al.*, 2004a]. The total loading between 1945 and 2000 is estimated to be 27700 tonnes accounting for approximately 0.6% of the total global  $\alpha$ -HCH emissions [Li *et al.*, 2004a].

An initial ocean water concentration of  $\alpha$ -HCH was determined from measurements. A set of  $\alpha$ -HCH measurements from the late 1980s and early 1990s collected from the literature [Terry Bidleman, personal communication] was plotted in the DEHM-POP grid

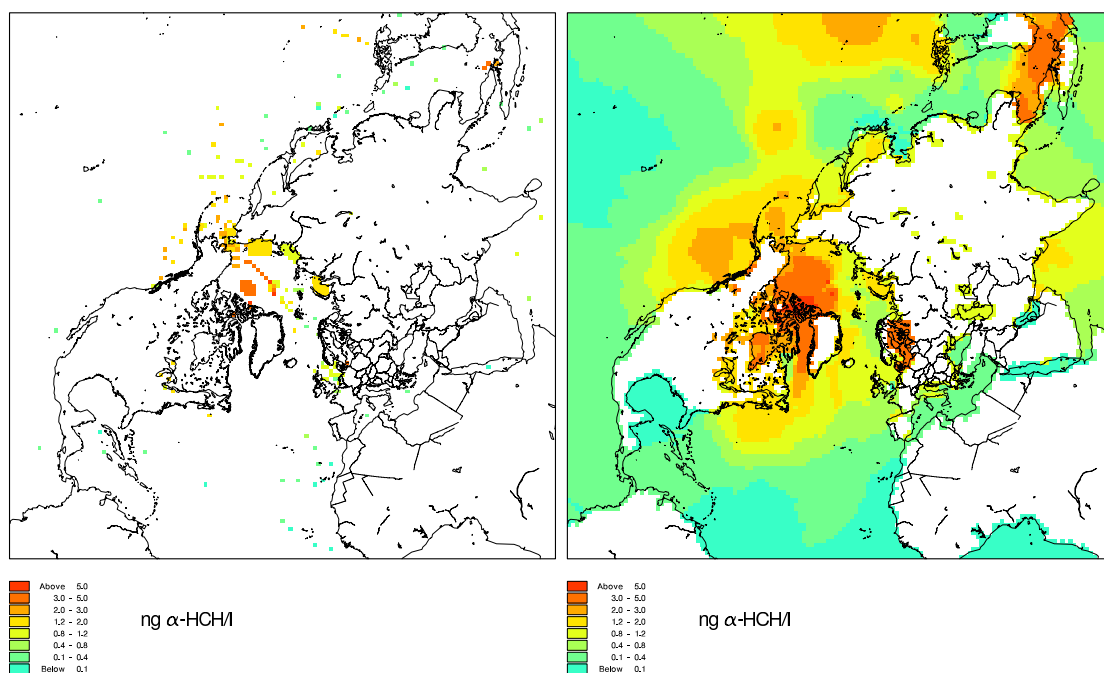


Figure 5.4: A collection of  $\alpha$ -HCH measurements from the late 1980s and early 1990s (left), initial concentration in ocean water derived from an inter- and extra-polation of the measurements (right).

(see left hand side of Figure 5.4). Measurements from between 1987 and 1996 were used to ensure a reasonable coverage of the world's oceans and as large a number of points for the interpolation as possible. In grid points with more than one measurement, the average value of the measurements was used.  $\alpha$ -HCH concentrations in all DEHM-POP grid cells were inter- and extrapolated from these (see right hand side Figure 5.4). This is used as initial condition for the model simulations presented in *Hansen et al.* [2004, 2006a] and in this thesis. It was later discovered that there was an error in the use of the initial ocean concentrations in the model simulation presented in *Hansen et al.* [2004]. Although this leads to slightly different  $\alpha$ -HCH air concentrations, average concentrations are of the same order of magnitude, and the conclusions made in the paper does not change due to this problem.

## Chapter 6

# Model evaluation methods

The evaluation of a model is a necessary part in the cyclic process of model development, testing and evaluation [Russell and Dennis, 2000]. In this context model development is changes in existing model elements or the addition of new modules, e.g. a new description of the wet deposition process or the addition of a snowpack module. There are two levels of testing the model, a purely technical testing of the model in terms of no bugs or errors in the model formulation and a scientific testing to secure an agreement with the accepted knowledge and theories of the involved numerical methods, physical and chemical processes, etc. The testing involves the transport model as an integrated system as well as its component parts. Evaluation is defined by Russell and Dennis [2000] as an: “...assessment of the adequacy and correctness of the science represented in the model through comparison against empirical data, such as laboratory tests, in situ tests and the analysis of natural analogs. Evaluation is a process of model confirmation relative to current understanding. Multiple, confirmatory evaluations can never demonstrate the veracity of a model: confirmation is a matter of degree. However, an evaluation can raise doubts about the science in a model”.

There are two other ways to evaluate the performance of a model, sensitivity studies and evaluation against other model results. In sensitivity studies the sensitivity of the results to changes in individual model input is tested. This is typically done for simpler models or sub-modules, e.g. the snowpack module [Hansen *et al.*, 2006b]. However, for a complex model as an atmospheric chemistry transport model it is difficult to quantify the sensitivity to model parameter changes, since different parts of the domain may behave differently to these changes and it is hence difficult to interpret the importance of sensitivity results. A sensitivity analysis for DEHM-POP was, thus, not made. Finally models can be evaluated by comparing their results to results from other models. This is a suitable way of evaluation if there is a bench-mark model for the area or if there is a model which is generally accepted to give reliable results. Model comparisons can also be conducted by comparing process descriptions or by running the models with similar conditions and compare predicted concentrations in specific regions. The purpose of this type of study is not to evaluate the models but to enhance the understanding of the environmental processes described by the models [Hansen *et al.*, 2006c; Shatalov *et al.*, 2004, 2005].

A thorough testing was previously conducted on the original version of the DEHM model both with and without nests [Christensen, 1995; Frohn, 2004]. For the DEHM-

POP model the addition of each module or additional process has led to a test and subsequent evaluation against observational data. The evaluations have then resulted in either acceptance or, for a few cases, rejections of the model changes (see e.g. section 4.4 on page 50). These evaluations are not reported in this thesis as it would be too extensive. The final evaluation of the DEHM-POP model is a direct comparison of model results and observations from monitoring stations within the model domain, presented in chapter 7.

## 6.1 Available measurements

While POPs have been measured in many different environmental media, such as wet deposition, soil, fresh water, ocean water, sediments, and many different types of biota, air is the most regularly monitored medium for POPs.

### 6.1.1 Air

Air is typically sampled for POPs by operating a pump to suck air through a glass fiber filter to collect particles and then through an adsorption medium, such as a polyurethane foam plug so the gas-phase compounds are retained. The sampled air volumes are variable, e.g. 280–400 m<sup>3</sup> of air is sampled at sampling stations in Québec [Aulagnier and Poissant, 2005], while 11.400 m<sup>3</sup> of air is sampled at sampling stations in the Canadian Arctic [Fellin *et al.*, 1996; Halsall *et al.*, 1997]. Several campaigns of short duration, e.g. 1–3 months have measured POPs in air, e.g. in the Arctic [Hargrave *et al.*, 1988; Patton *et al.*, 1991; Oehme, 1991]. Long-term monitoring of POPs in air started in the beginning of the 1990s with results from the first full year presented by Fellin *et al.* [1996] and Oehme *et al.* [1996].

### Long-term monitoring networks

Atmospheric monitoring networks have been established around the world to increase the understanding of the behavior of POPs in the environment. The parties of the Co-operative Programme for Monitoring and Evaluation of the Long-Range Transmission of Air Pollutants in Europe (EMEP) have set up several monitoring sites around Europe [see e.g. Berg *et al.*, 2001; Aas *et al.*, 2003; EMEP, 2005]. Stations to measure POPs in air in the Great Lakes basin in North America have been established within the Integrated Atmospheric Deposition Network (IADN) [Buehler and Hites, 2002]. The results are presented in several studies together with statistical analysis of the data to calculate e.g. temporal trends, especially for the data from the US side [e.g. Buehler *et al.*, 2002, 2004; Hafner and Hites, 2005]. As part of the Canadian commitment to assessing the occurrence, levels, and pathways of POPs to the Arctic, a multi-year systematic air sampling study was established in the framework of the Northern Contaminants Program [Fellin *et al.*, 1996]. Five different stations have been operated for shorter or longer periods since 1992; three stations in Canada (Alert, Tagish and Kinngait) and two on the Russian coast of the Arctic Ocean (Dunai Island and Amderma), see Hung *et al.* [2005] for a review. Concentration levels and temporal trends of organochlorine pesticides, PAHs and PCBs from these stations have been published in several studies [Fellin *et al.*, 1996; Stern *et al.*, 1997; Halsall *et al.*, 1997, 1998; Bailey *et al.*, 2000; Hung *et al.*, 2001, 2002, 2005]. A

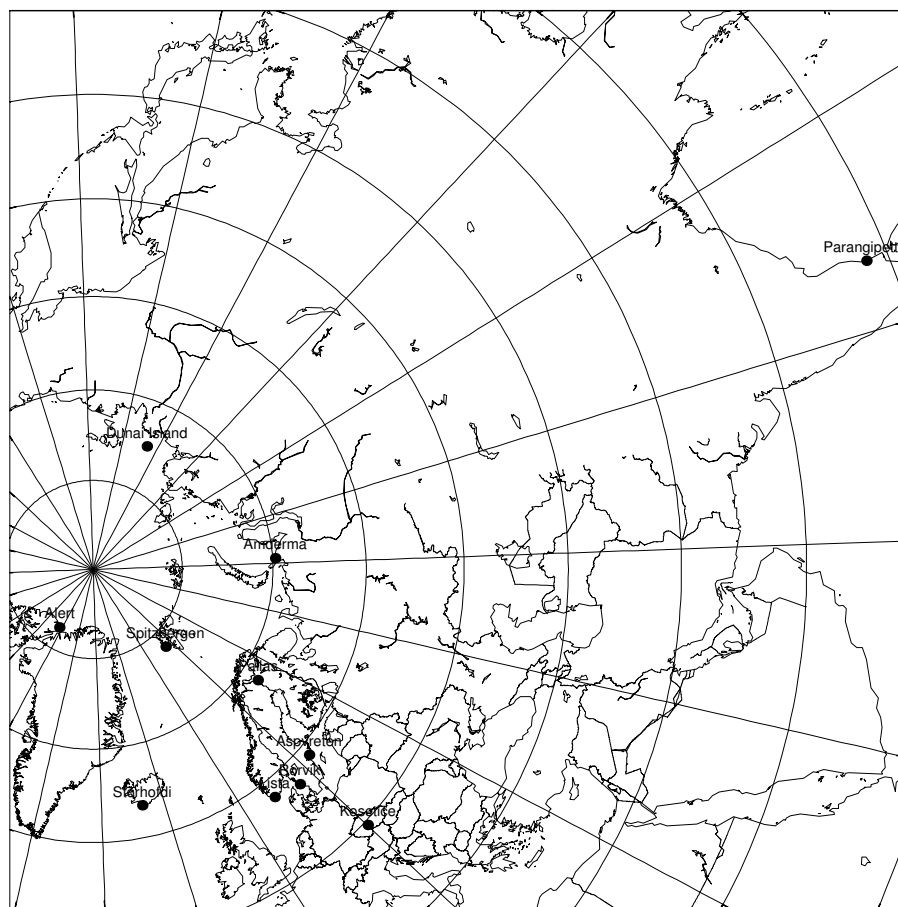


Figure 6.1: Location of the 10 European and Asian sites from which measured  $\alpha$ -HCH air concentrations are used in the model evaluation.

long-term campaign with measurements of HCHs was made at two rural and one remote site in Québec, Canada [Poissant and Koprivnjak, 1996; Garmouma and Poissant, 2004; Aulagnier and Poissant, 2005]. Measurements from these monitoring sites have been obtained for the model evaluation of DEHM-POP. The position of the sites are plotted in Figure 6.1 and 6.2 and the names are listed in table 6.1 together with the year of sampling, the number of measurements, the average deployment time and sampling frequency as well as the average and range of measured  $\alpha$ -HCH concentrations in air.

### Short-term campaigns

In addition to the long-term air monitoring stations many smaller campaigns have been made throughout most of the world. Generally a single or few air samples are taken at these campaigns, often in conjunction with samples from other media such as water, soil, snow, vegetation or biota. Results from one such short-term campaign are used for model evaluation in this study, since it is the only study in a source region. Air concentrations of  $\alpha$ -HCH were measured in Parangipetta at the southeast coast of India from August

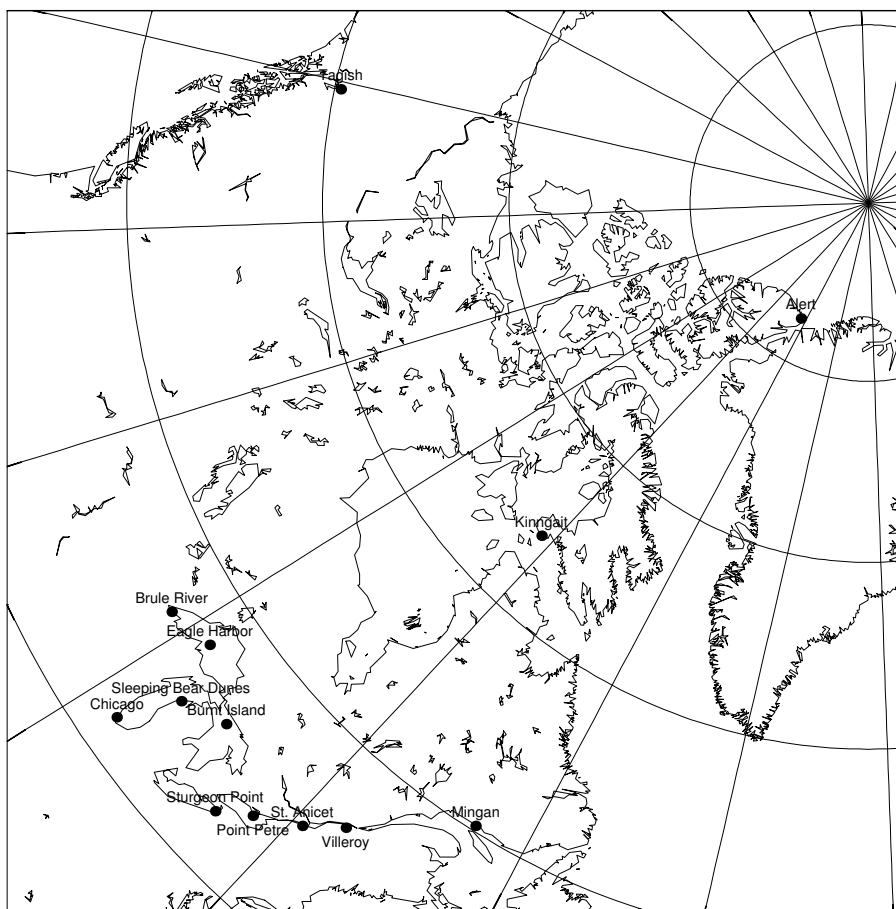


Figure 6.2: Location of the 13 North American sites from which measured  $\alpha$ -HCH air concentrations are used in the model evaluation.

1993 to October 1994 [Rajendran *et al.*, 1999].

### Particle phase concentrations

At most stations the particle-phase and gas-phase compounds are measured separately as described in the introduction to this section. However, for the HCHs the results are only given individually for a few stations. The predicted gas-particle partitioning of  $\alpha$ -HCH is thus not evaluated in this study, although the particle concentration results will be described briefly.

### Passive air sampling

Air concentrations of POPs can also be collected using passive samplers, where a collection medium is exposed to air for a longer time period. Passive samplers can be deployed at remote sites without power supply and simultaneous deployment of a large number of samplers is a cost-efficient way of evaluating the spacial contamination distribution.

Table 6.1: Years of sampling, number, typical deployment time and sampling frequency of the measurements, and mean and range of the measured air concentrations for each of the studied stations. <sup>1</sup>Measurements at Lista have been made once a week but only the results from 1992-1995 and 1999-2000 were available for this study. However, monthly mean values for 1991-1998 were also available. <sup>2</sup> Measurements at Kinnait were made once a week, while 16 of the reported values are for four combined samples.

Station	Years of sampling	Number of samples	Av. deploy. time	Average sampling frequency	Measurements Mean (range)
Alert	1992–1998	327	7 d	1/week	54.4 (0.1 – 310.7)
Kinnait	1994–1996	35	7/28 <sup>2</sup> d	1/week	76.0 (19.3 – 193.4)
	2000	9	7 d	1/week	34.4 (21.0 – 50.0)
Tagish	1992–1995	110	7 d	1/week	76.4 (0.3 – 757.2)
Dunai Island	1993–1995	88	7 d	1/week	50.3 (0.6 – 144.0)
Amderma	1999–2000	91	7 d	1/week	23.2 (4.5 – 78.0)
Spitzbergen	1993–2000	405	2 d	1/week	50.4 (0.1 – 203.1)
Lista <sup>1</sup>	1991–1998	95	1 d	1/month	67.1 (20.8 – 170.0)
Lista <sup>1</sup>	1992–1995	204	1 d	1/week	70.5 (4.0 – 296.7)
	1999–2000	104	1 d	1/week	22.0 (7.7 – 46.6)
Rörvik	1991–2000	90	7 d	1/month	26.0 (4.0 – 148.3)
Aspvreten	1995–2000	52	7 d	1/month	58.3 (17.0 – 163.0)
Pallas	1996–2000	60	7 d	1/month	20.3 (3.0 – 40.0)
Stórhöfði	1995–2000	140	14 d	2/month	13.7 (3.7 – 57.9)
Košetice	1999–2000	101	1 d	1/week	29.6 (4.0 – 95.0)
Point Petre	1992–2000	297	1 d	1/12 days	33.8 (4.2 – 109.0)
Burnt Island	1993–2000	226	1 d	1/12 days	29.7 (5.2 – 80.5)
Sleeping Bear Dunes	1991–2000	257	1 d	1/12 days	92.7 (0.4 – 694.3)
Sturgeon Point	1991–2000	268	1 d	1/12 days	99.0 (1.1 – 606.3)
Eagle harbor	1991–2000	278	1 d	1/12 days	114.1 (12.4 – 749.3)
Chicago	1996–2000	132	1 d	1/12 days	69.2 (3.6 – 274.6)
Brule River	1996–2000	142	1 d	1/12 days	65.4 (7.8 – 404.0)
Villeroy	1993–1996	168	1 d	1/6 days	89.6 (7.0 – 188.0)
St. Anicet	1994–1996	117	1 d	1/6 days	89.6 (27.0 – 191.8)
Mingan	1994–1995	26	1 d	1/12 days	96.0 (43.0 – 187.6)
Parangipettai	1993–1994	9	4 d	-	7860 (530 – 27400)

Passive air sampling campaigns have been conducted, where 71 samplers across Europe were deployed for a six week period [Jaward *et al.*, 2004], and where 40 samplers were deployed across the North American continent for a full year [Shen *et al.*, 2004, 2005]. It is not straight forward to convert the results from passive samplers to average atmospheric concentrations of contaminants over the deployment period, since the exact amount of air passing the sampler is not known [e.g. Jaward *et al.*, 2004]. However, for model evaluation purposes they can be used to evaluate the spacial pattern. This is done in the study described in Hansen *et al.* [2006c], where the normalised  $\alpha$ -HCH concentrations from the European passive air sampling campaign, from DEHM-POP, and from the multi-compartment mass balance model EVn-BETR are compared.

### 6.1.2 Other media

Soil, ocean water, snow and other media are not monitored regularly at specific sites. There is thus a lack of data sets to evaluate predicted concentrations in other media than air. The most comprehensive data set of HCHs in environmental compartments other than air are measurements in ocean water, but most of these are included in the construction of the initial ocean water concentration (see section 5.4.3 on page 71). It is thus not possible to use these measurements for an evaluation of the predicted water concentrations.

For soil concentrations there is the further complication that the majority of  $\alpha$ -HCH measurements is made on cultivated soils, where usage has taken place and these are thus containing residues of past usage, see Li [1999] for a collection of studies. The usage residues are taken into account in the calculation of emissions, but they are not present as concentrations in the soil compartment. The measurements from soil with documented previous usage can therefore not be compared to the modelled soil concentrations. A comprehensive study was made on HCB and PCB levels in global background soil [Meijer *et al.*, 2003a]. However, a similar study for the HCHs does not exist.

### 6.1.3 Extraction of data from the model simulations

The temporal resolution of the model results is chosen in the model set-up. Depending on the aim of the study, the resolution can be set to hours, but for the major part of this study daily averages are used. To compare the model results directly with the measurements, these daily averages are extracted for each station. To obtain the concentration at the locations of the monitoring stations, a horizontal bi-linear interpolation of the concentrations in the nearest model grid points is made.

For the measurements, only the starting and ending date of the sampler deployment is known, not the exact hour. Average values for each samples are thus calculated from all the daily averaged concentrations of the deployment period. This means that a model ‘sample’ consists of air from a longer time period than a measured sample, which may induce some uncertainty in the predicted concentrations.

Gas-phase and particle-phase concentrations are extracted separately, but as most measurements are reported as gas- plus particle-phase concentration, the two components are added in the model evaluation. When the expression ‘air concentrations’ is used in the remainder of this thesis it thus refers to the total concentration of gas- and particle-phase  $\alpha$ -HCH.

## 6.2 Evaluation tools

There are numerous ways of comparing model results and measurements. In this study it is mainly done by visual inspection of time series and scatter plots and by applying statistical tools.

### 6.2.1 Statistics

For statistical evaluations an appropriate hypothesis must be defined in accordance with the general purpose of the model study [Hanna, 1994]. In this study the main hypothesis must be that there is not a significant difference (at some predefined confidence level) between the observed and simulated atmospheric concentrations of POPs (within some time frame). This hypothesis then has to be tested by applying statistical tools.

In the following  $\bar{O}$  and  $\bar{S}$  refer to the mean of the observed ( $O$ ) and simulated ( $S$ ) time series each including  $N$  data points and  $O_i$  is the observed concentration at the  $i$ 'th step in the time series ( $i = 1, 2, \dots, N$ ).

The most used statistical tool in this study is the *coefficient of correlation* ( $r$ ), which can be used to estimate to what degree variables co-vary in time or space. It is commonly defined as:

$$r = \frac{\sum_{i=1}^N (O_i - \bar{O})(S_i - \bar{S})}{\sqrt{\sum_{i=1}^N (O_i - \bar{O})^2 \sum_{i=1}^N (S_i - \bar{S})^2}}, \quad (6.1)$$

and it is therefore proportional to the covariance between the two time series divided by the product of their standard deviations ( $\sigma_s$  and  $\sigma_o$ ).

To test if the hypothesis formulated above is true or false a null hypothesis,  $H_O$ , stating the opposite is often formulated, only to be rejected:

$$H_O : r = 0. \quad (6.2)$$

In this study the two-tailed  $t$ -test is used to reject or accept  $H_O$ . The  $t$  statistic is defined as:

$$t = r \sqrt{\frac{N-2}{1-r^2}}, \quad (6.3)$$

which has a Student's distribution with  $N - 2$  degrees of freedom. If  $t$  is above a critical value,  $t_c$ , the null hypothesis has to be rejected, which indicates that there is a correlation or anti-correlation between the two time series. The critical value depends on the significance level, e.g.  $t_c$  is higher for a 1% significance level than for a 10% significance level. The significance of the correlation thus depends on how high  $t$  is compared to the  $t_c$ -values for the various significance levels. This analysis is, however, based on several assumptions and requires e.g. that the data points in the two time series are independent. In this study it is not always possible to meet this requirement as both the simulated and observed  $\alpha$ -HCH concentration at one time step will be highly correlated with the concentration in the next. To rely on this test the degrees of freedom should be modified and set equal to the actual number of independent data points in the time series, otherwise the test would be less stringent. This 'effective number of degrees of freedom'  $N^* < N$ , can be estimated from knowledge of the autocorrelation etc., but it has not been included in this study. In table 6.2 critical values of the test statistics are given for different degrees

Table 6.2: Critical values of the test parameter  $t_c$  for different degrees of freedom,  $f$ , ranging from 15 to  $\infty$  and at two different significance levels (in brackets).

$f$	$t_c$ (10%)	$t_c$ (1%)
15	1.75	2.95
30	1.70	2.75
60	1.67	2.66
120	1.66	2.62
$\infty$	1.64	2.56

of freedom. In the following model evaluation (see chapter 7) these values will be applied to test for significance.

A few other statistical parameters were also used in this study especially in the above mentioned iterative process of model development, testing and evaluation to study and compare the performance of different model setups including new modules compared to previous versions. The *bias* is defined as:

$$bias = \frac{1}{N} \sum (S_i - O_i) = \bar{S} - \bar{O}, \quad (6.4)$$

and the *fractional bias (FB)* is given by:

$$FB = 2 \frac{\bar{S} - \bar{O}}{\bar{S} + \bar{O}}. \quad (6.5)$$

Both sign and numerical value of these two parameters give information on whenever the model over- or under-estimates the measured atmospheric  $\alpha$ -HCH concentration.

The *root mean square error (RMSE)*, defined as:

$$RMSE = \left( \sum_{i=1}^N \frac{(O_i - S_i)^2}{N} \right)^{1/2}, \quad (6.6)$$

is an estimate of the overall difference between observations and model results. It can be useful to subtract the constant bias and the resulting parameter is here referred to as the *root mean square error bias (RMSEB)*:

$$RMSEB = \left( \sum_{i=1}^N \frac{((O_i - S_i) - (\bar{S} - \bar{O}))^2}{N} \right)^{1/2}. \quad (6.7)$$

The above listed statistical parameters are more or less sensitive to the mean values of both observed and simulated time series, which for the latter are directly affected by the applied initial and boundary conditions. These parameters are, however, included in this study as they are valuable when the different model runs are compared and for quantifying differences in model performances.

## Chapter 7

# Results and model performance

Several simulations were performed with the DEHM-POP model in this study. All simulations cover a full decade from 1991 to 2000 and the meteorological data and the second emission data set described in chapter 5 were used as input. In this chapter results from the model simulations are presented. The results of the reference simulation are described in section 7.1 with focus on the distribution patterns and temporal trends. These results are thoroughly evaluated against measurements and discussed in section 7.2. The evaluation raise questions about the effect of some of the environmental processes in the model, and these processes are studied in section 7.3 for the ocean module, section 7.4 for the vegetation module, and in section 7.5 for the snowpack module. Previously published results from DEHM-POP and other models are briefly discussed in section 7.6 and 7.7. Finally the results will be summarized in section 7.8.

### 7.1 Reference simulation

The reference simulation includes all environmental processes described in chapter 4 and the initial ocean concentration described in chapter 5. In this section the results from this simulation will shortly be described in terms of temporal trends (section 7.1.1), seasonal patterns (section 7.1.2), and vertical distribution (section 7.1.4). This section will concentrate on the results for the gas-phase air concentration, although the particle-phase air concentrations are also briefly described in section 7.1.3 as well as the concentrations in the surface compartments (section 7.1.5).

#### 7.1.1 Temporal trends

The annual average gas-phase  $\alpha$ -HCH air concentrations for the years 1992, 1994, 1996, 1998, and 2000 are displayed in Figures 7.1 and 7.2. The  $\alpha$ -HCH air concentrations are generally high over areas with primary emissions such as India, southeast Asia, southern Europe, Mexico, and western Africa. Relatively high concentrations are also seen in air over areas without primary emissions such as the Atlantic and Pacific Oceans and the Arctic, which indicates atmospheric transport from source areas and/or re-volatilisation of previously deposited  $\alpha$ -HCH to these areas.

The  $\alpha$ -HCH concentration in air generally decrease through the modelled period, which reflect the decreasing usage of technical HCH as given by the emissions (see Figure 5.2

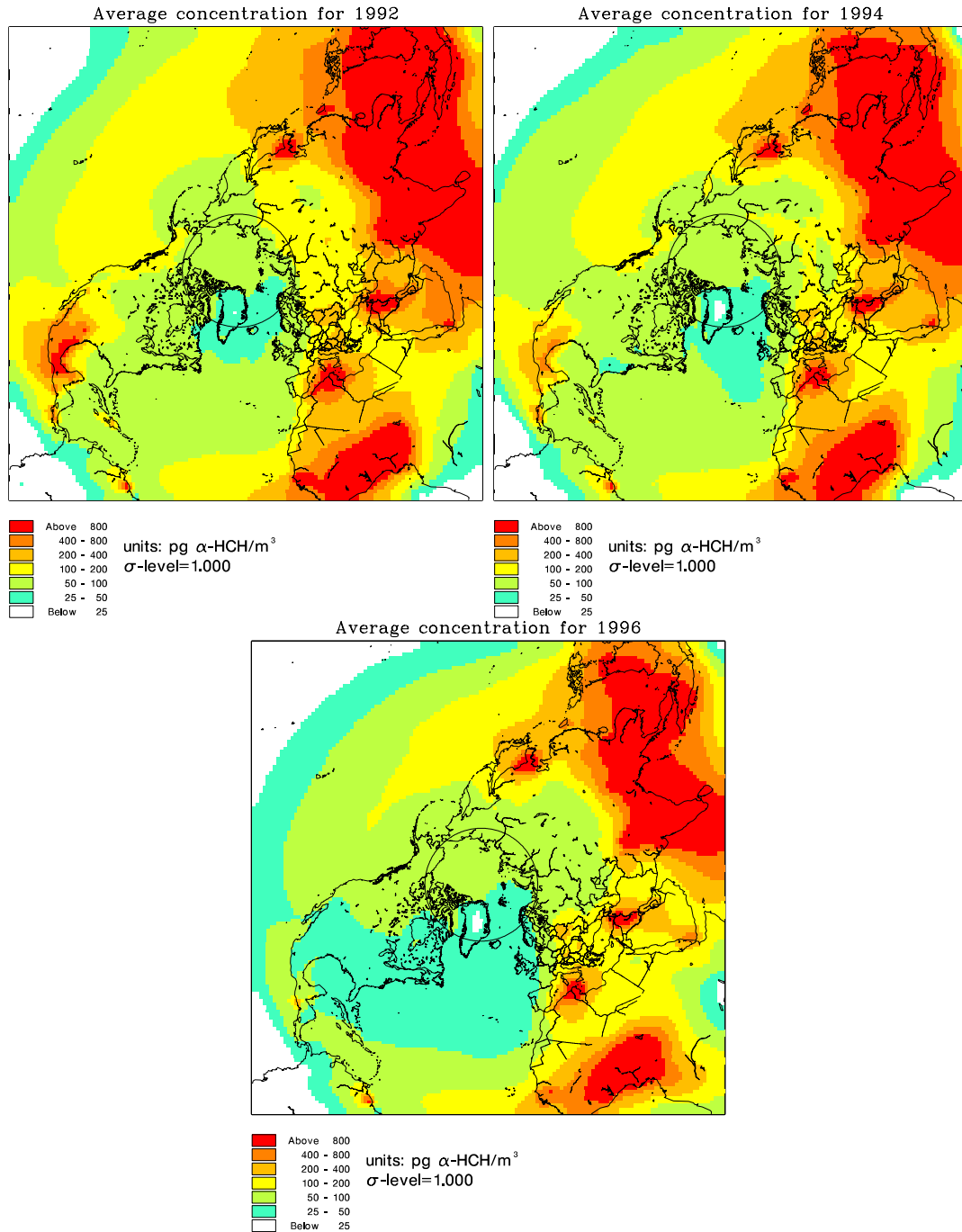


Figure 7.1: Annual average  $\alpha$ -HCH concentrations in the lowermost atmospheric layer for 1992 (upper left), 1994 (upper right), and 1996 bottom.

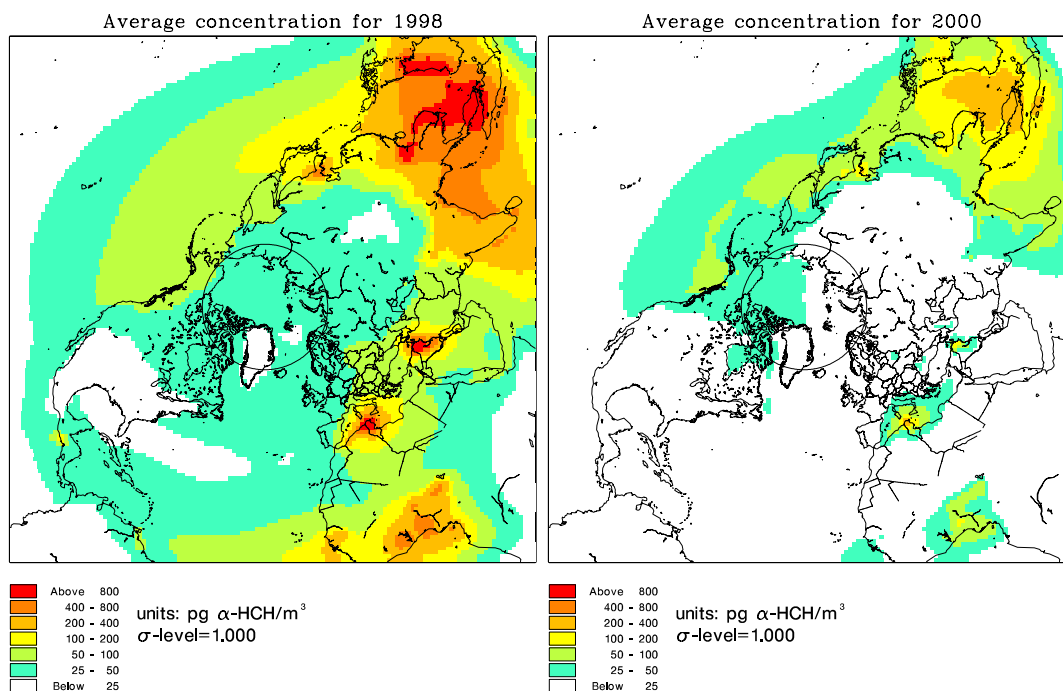


Figure 7.2: Annual average  $\alpha$ -HCH concentrations in the lowermost atmospheric layer for 1998 (left) and 2000 (right).

on page 69 and Figure 5.3 on page 70). The emissions from previous years usage are also notable in the results. Mexico banned the use of technical HCH in 1993 [Li, 1999], but the air concentrations from 1994 and 1996 indicate emissions from the Mexican area. Indications of re-volatilisation of previously deposited  $\alpha$ -HCH from ocean water are also found, e.g. over the Pacific Ocean off the Mexican Coast in 1996, and over the Hudson Bay and the Black and Caspian Seas in 2000.

### 7.1.2 Seasonal patterns

The seasonal pattern is essentially the same through the simulated period, which is illustrated in Figures 7.3 and 7.4, where the averaged gas-phase concentrations in the lowermost atmospheric layer are plotted for the months January, April, July and October for the years 1992 and 1998 respectively. There are clearly seasonal variations in air concentrations and they differ from region to region. In general high concentrations are seen over primary source areas, and these differences display the variable agricultural practice over the hemisphere (see figure 5.2 on page 69 for a comparison with source areas). High concentrations are found in air during fall and winter over source areas at low latitudes, e.g. India, south-east Asia, Mexico and the western part of Africa. In mid-latitude source regions, such as Tunisia, Iraq and North Korea high concentrations are found during the spring and summer months. Areas relatively close to primary source areas are influenced by the nearby sources and reflect similar seasonal patterns. They are though also influenced by the transport pattern for the given month and larger variability are generally

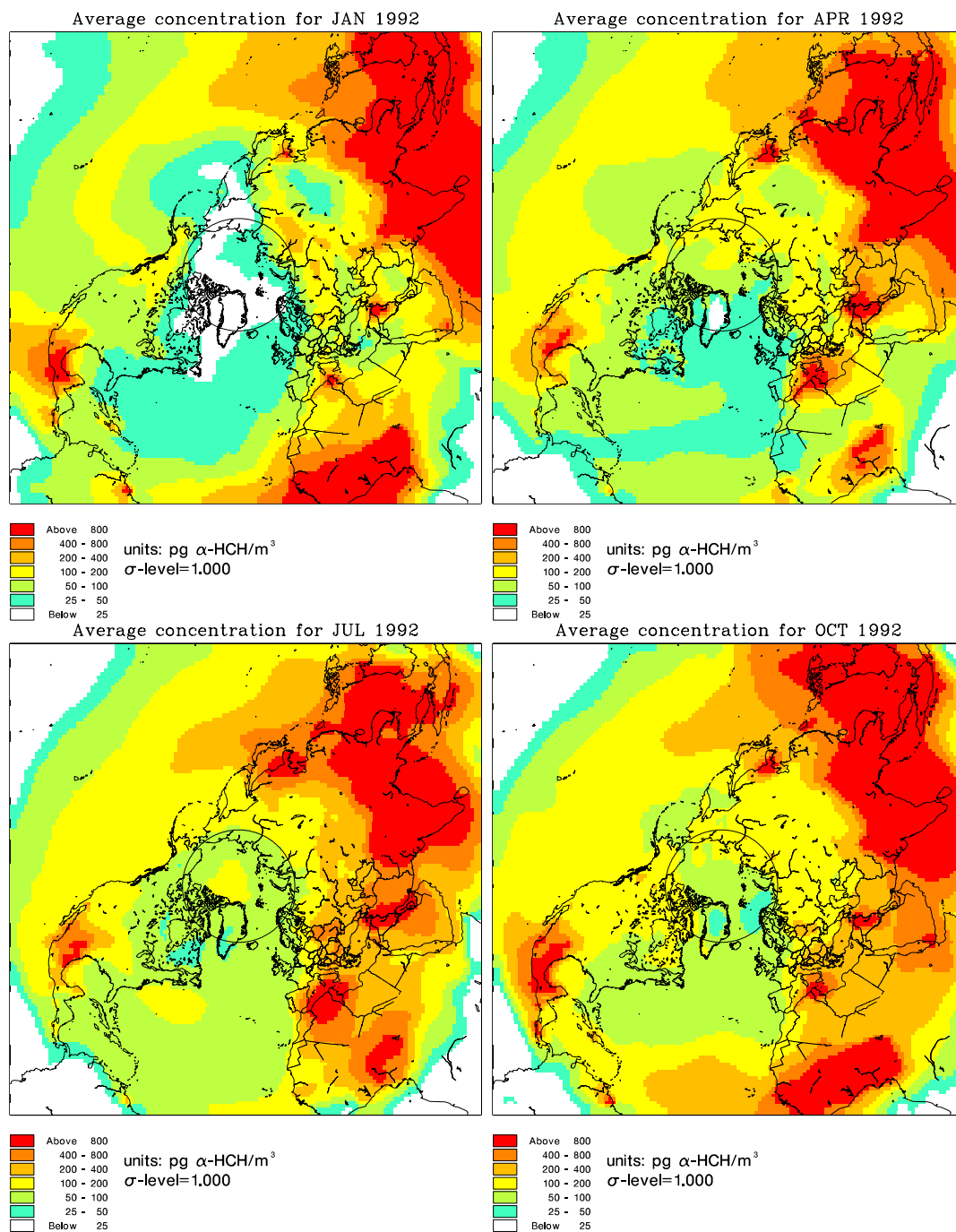


Figure 7.3: The monthly average air concentration in the lowermost atmospheric layer in January 1992 (upper left), April 1992 (upper right), July 1992 (lower left), and October 1992 (lower right).

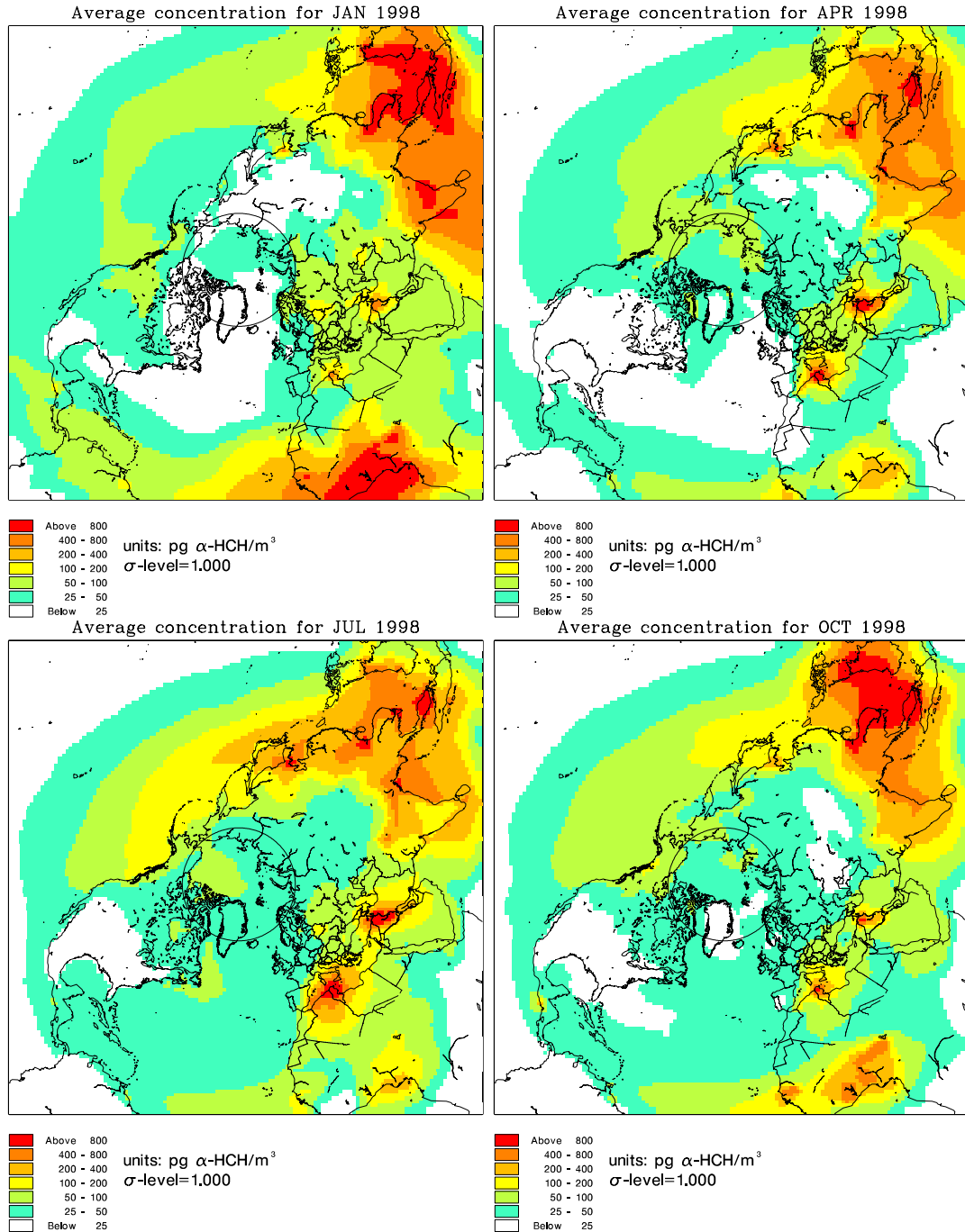


Figure 7.4: The monthly average air concentration in the lowermost atmospheric layer in January 1998 (upper left), April 1998 (upper right), July 1998 (lower left), and October 1998 (lower right).

seen in these regions than in the source regions.

Over the southern part of the North Atlantic Ocean the air concentrations are highest during the fall and winter months, due to the proximate source regions in Western Africa and South America and southern part of North America. Over the northern part of the North Atlantic Ocean and over the North Pacific Ocean there are generally higher  $\alpha$ -HCH air concentrations during summer and fall than during winter and spring. This pattern indicates relatively higher deposition to the ocean surface during winter and spring due to the relatively lower ocean temperatures compared to the air temperatures during these seasons. In the Arctic two different patterns are seen. In the central and western Arctic, north of Canada and Greenland, the air concentrations are highest during the summer months, whereas in the eastern part of the Arctic, north of Siberia, the highest air concentrations are found in the spring and autumn months. An interesting exception to this is the northern part of central Siberia, where the highest air concentrations for the beginning of the model simulation, e.g. 1992 are seen in January, whereas the area follow the pattern of the rest of the Arctic later in the simulated period.

### 7.1.3 Particle-phase concentration

As for the gas-phase, the annual averaged particle-phase  $\alpha$ -HCH air concentration is decreasing through the simulated period (not shown). Seasonal differences are also observed for the particle-phase concentrations, although they are somewhat different than for the gas-phase air concentrations. In low- and mid-latitude source regions the particle-phase concentrations are higher during periods of emissions, e.g. during autumn and winter for India and southeast Asia and during summer for Northern Africa and southern Europe (see Figure 7.5), which is also seen for the gas-phase  $\alpha$ -HCH. However, in central Arctic the seasonal variation is opposite to the gas-phase concentrations with highest concentrations during winter and lowest during summer. Highest overall particle-phase concentrations are seen in central Siberia and east Asia during winter with  $1 - 5 \text{ pg m}^{-3}$ , which is up to 5% of the gas-phase concentration found in the same area (see Figure 7.3 for comparison). In a low-latitude source area such as India the particle-phase air concentration is about 0.1% of the gas-phase air concentration or less. As the primary source areas mainly are in temperate and warm regions, the temperature appear to be a more important descriptor for the particle-phase concentrations than the source of primary emissions. Increasing particle concentrations in winter in the model may also be of importance for the increasing particle-phase  $\alpha$ -HCH concentrations.

### 7.1.4 Vertical distribution

The vertical distribution is very variable locally, depending on the meteorological conditions and local or nearby emissions. When looking at longer-term averages, such as monthly average concentrations, a few general patterns emerge. As for the surface concentrations the gas-phase and particle-phase behaves differently with height and they will be treated separately. Large concentration decreases are found in some regions in the uppermost model layer for both the gas- and particle-phase. This is probably due to the assumed top-boundary condition, where it is assumed that there is no  $\alpha$ -HCH in in-flowing air at the upper boundary (see section 3.3.4 on page 31). The results from the top layer is thus not described in this study.

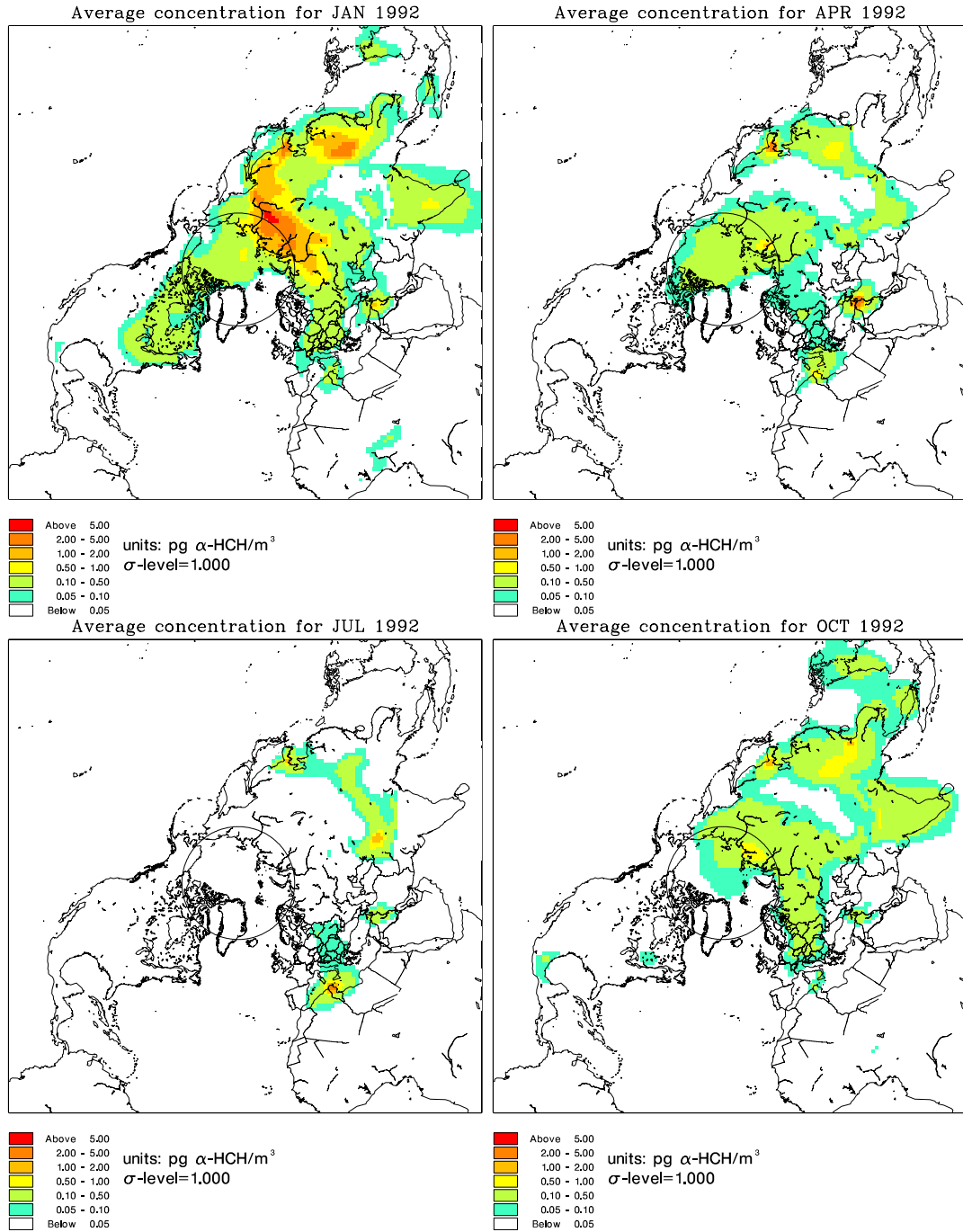


Figure 7.5: Particle-phase concentration in the lowermost atmospheric layer in January 1992 (upper left), April 1992 (upper right), July 1992 (lower left), and October 1992 (lower right).

### Gas-phase $\alpha$ -HCH

The gas-phase  $\alpha$ -HCH air concentration for the fifth, tenth, fifteenth, and nineteenth layer, approximately corresponding to the heights of  $\sim 290$  m,  $\sim 1380$  m,  $\sim 5480$  m, and  $\sim 12780$  m for a standard atmosphere is plotted in Figure 7.6. The gas-phase concentration in the lowermost atmospheric layer can be seen in the lower left part of Figure 7.3. In general the concentrations decrease with height within the model domain. The decrease is most rapid over areas with primary sources. An exception to the general pattern is found in some parts of the North Pacific Ocean, where the concentrations increase with height up to approximately 5 km, where it starts to decrease again. This indicates the influence of different air masses, e.g. from the nearby southeast Asian source areas.

### Particle-phase $\alpha$ -HCH

The particle-phase  $\alpha$ -HCH air concentration is plotted in Figure 7.7 for the same heights as the gas-phase concentration. The particle-phase concentration in the lowermost atmospheric layer can be seen in the lower left part of Figure 7.5. The concentrations generally increase with height, except very locally over areas with direct emissions. The increase is slow in the lowermost 5 km, while the particle-phase concentration increase more rapidly in the top 10 km. This is due to the decreasing temperatures with height, that favours partitioning to the particle phase. This supports the findings from the seasonal particle-phase distribution pattern that temperature is the main descriptor of the particle-phase concentration.

#### 7.1.5 Surface compartment concentrations

The soil and water compartments are stagnant and they have relatively large storage capacities, whereas the vegetation and snow compartments are variable in extent over the year and thus have variable storage capacities. There are therefore only small seasonal variations in the ocean and soil concentrations and only the long term trends are shown here. The vegetation and snowpack concentrations follow similar long-term trends as the soil and water compartments, however the largest variability is the seasonal and this will be shown here.

#### Water

The distribution of the annual averaged  $\alpha$ -HCH concentration in water ( $\text{ng L}^{-1}$ ) for the years 1991, 1994, 1997, and 2000 are displayed in Figure 7.8. The  $\alpha$ -HCH concentrations in water are quickly building up in waters close to the warm source regions, such as the Indian Ocean, Mediterranean Ocean off Tunis and the southern North Atlantic Ocean off the west African coast. As the emissions, and thus the deposition from air, decrease, the water concentrations in these areas also decrease rapidly. In the Arctic Ocean the  $\alpha$ -HCH concentration decrease through the modelled period, but more slowly than in warm regions.

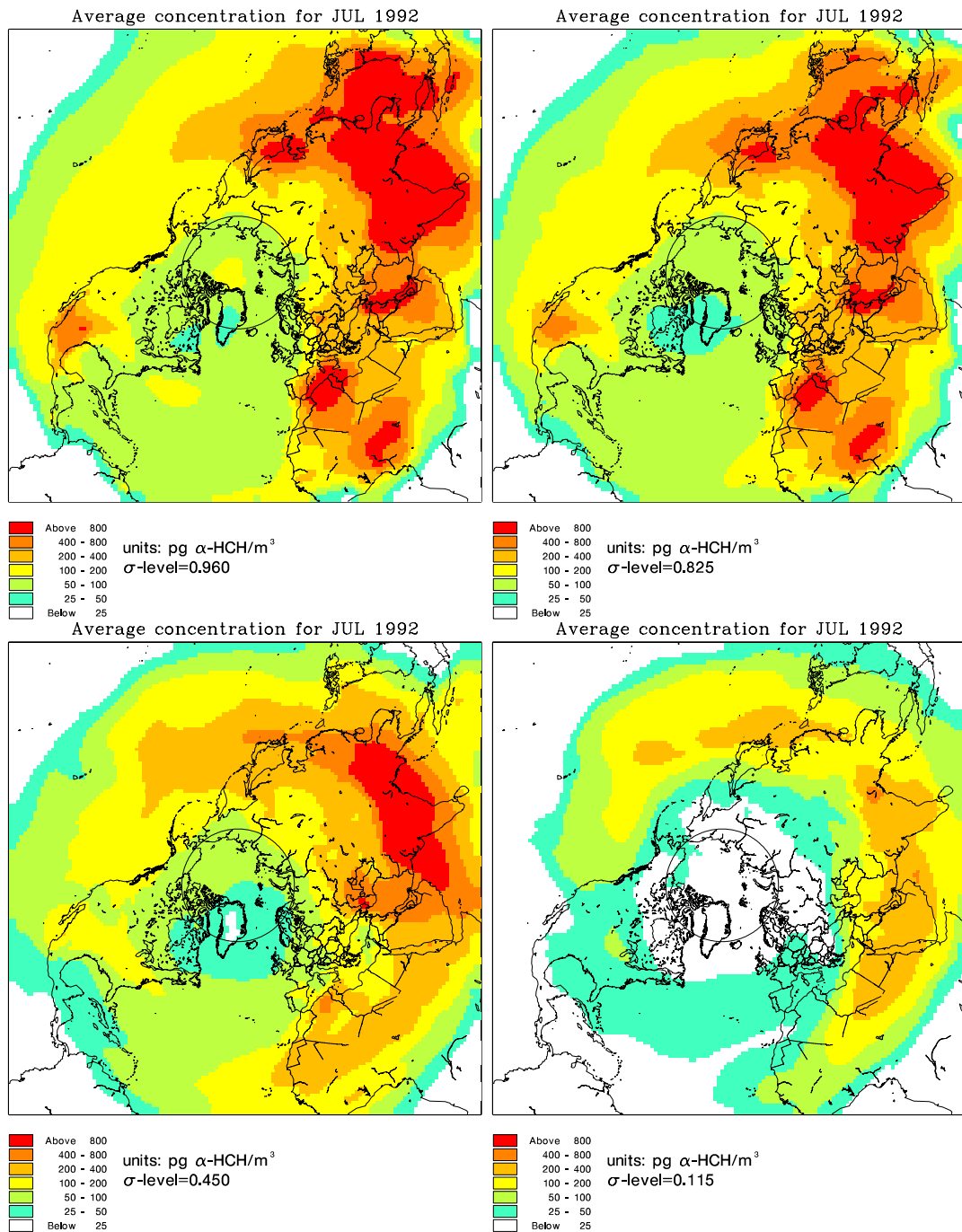


Figure 7.6: Vertical distribution of gas-phase  $\alpha$ -HCH for July, 1992 for the approximate heights  $\sim 290$  m (upper left),  $\sim 1380$  m (upper right),  $\sim 5480$  m (lower left), and  $\sim 12780$  m (lower right). The heights are given for the corresponding sigma levels in a standard atmosphere (see Table 3.1 on page 28).

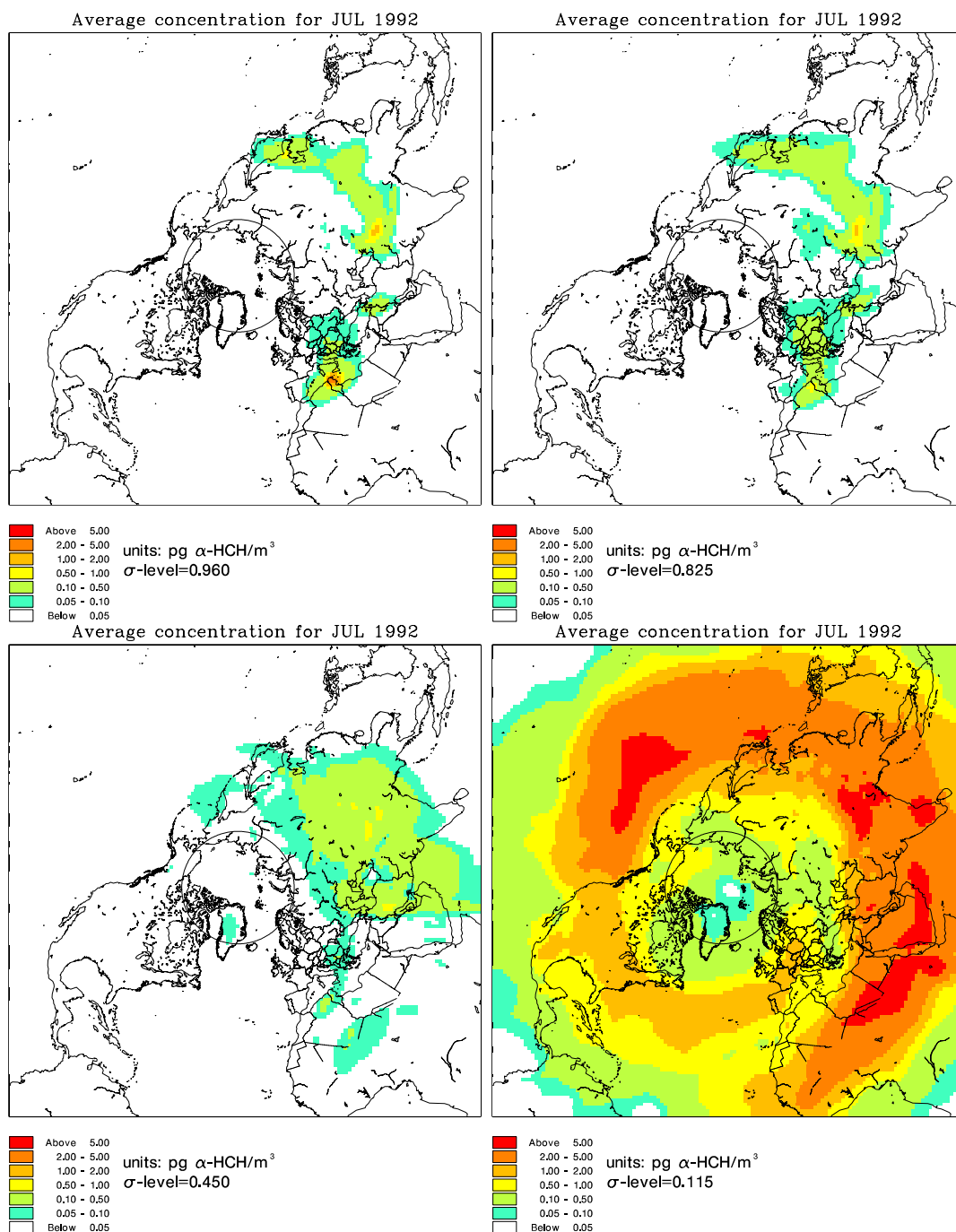


Figure 7.7: Vertical distribution of particle-phase  $\alpha$ -HCH for July, 1992 for the approximate heights  $\sim 290$  m (upper left),  $\sim 1380$  m (upper right),  $\sim 5480$  m (lower left), and  $\sim 12780$  m (lower right). The heights are given for the corresponding sigma levels in a standard atmosphere (see Table 3.1 on page 28).

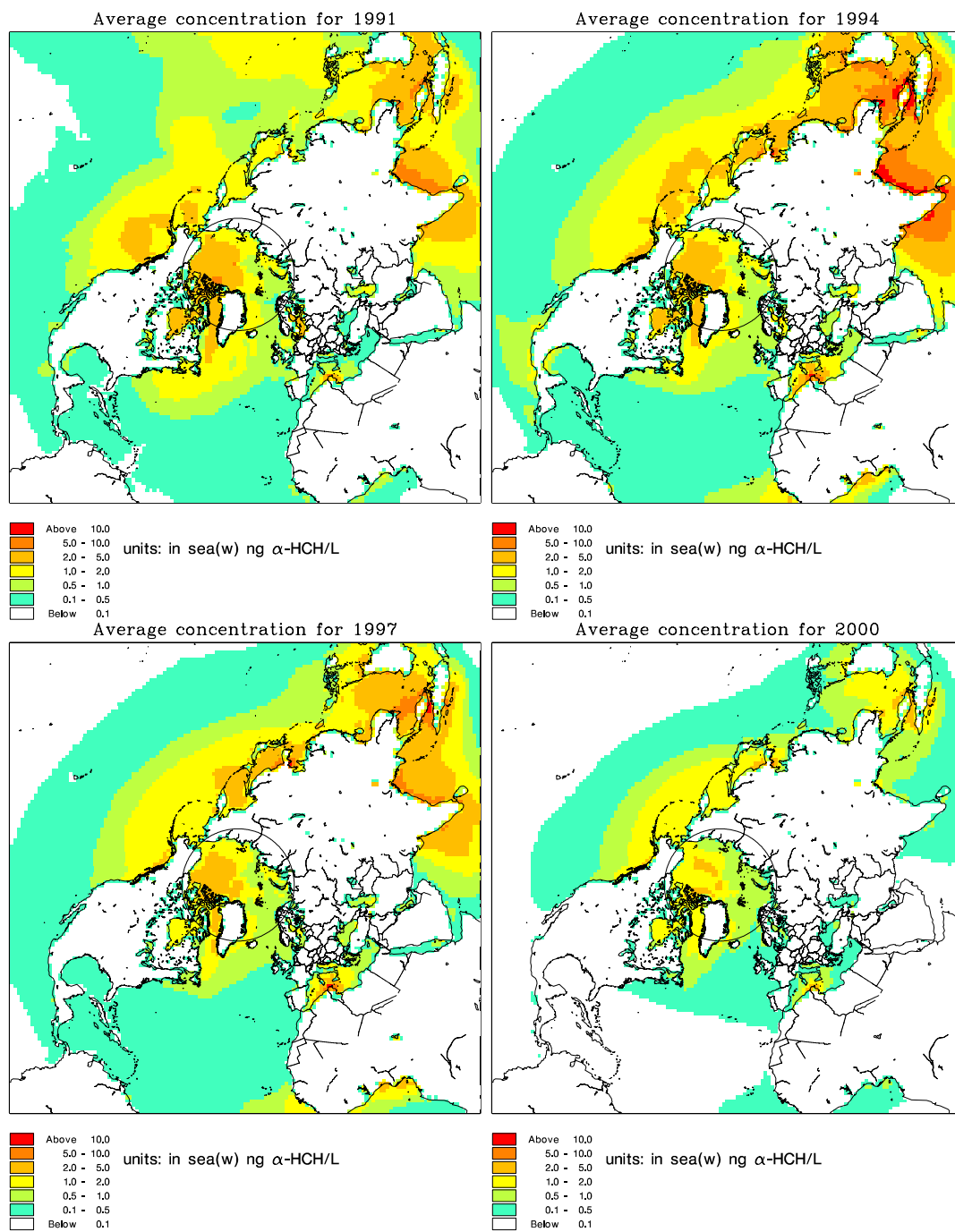


Figure 7.8: Distribution of  $\alpha$ -HCH in water for the years 1991 (upper left), 1994 (upper right), 1997 (lower left), and 2000 (lower right).

## Soil

The annual averaged  $\alpha$ -HCH soil concentration ( $\text{pg g}^{-1}$ ) for the years 1991, 1994, 1997, and 2000 are displayed in Figure 7.9. The soil follows the same pattern as the water with increasing concentrations close to source areas in the beginning of the simulated period. The soil concentrations in these areas decrease again towards the end of the simulated period, following the decreasing emissions. The chemical transformation rate is larger for soil than for water in the model, and the decrease in concentrations is thus more rapid. Soil concentrations outside source areas are also building up in the beginning of the model simulation with a following decrease, and there is a tendency for a slower decrease in cold areas, such as the north Siberia and north Canada. The Tibetan plateau contain the highest soil concentrations towards the end of the simulated period. This is a combination of the close proximity to the major source area: India, the low temperatures in the plateau, which favours the retention of chemicals in the soil, and the presence of a snowpack for all or most of the year (see Figure 4.3 on page 53), which shuts off re-volatilisation from the soil. When comparing with the fraction of organic carbon (Figure 4.1 on page 45) it can be seen that  $\alpha$ -HCH does not accumulate preferentially in the most carbon rich soils. An indication of this is seen e.g. in the eastern part of Canada, where the soil concentration does not follow the gradient in organic carbon content. This appear also to be the case in the Scandinavian soils and in the eastern Russia. The soil concentration difference in these regions are thus probably the result of different deposition processes and/or differences in the temperature and thus the air-soil exchange process.

It should be kept in mind that these soil concentrations only contains the deposited  $\alpha$ -HCH, not the usage residues from which the emissions are calculated, and not the residues from the depositions from previous years emissions. If these residues were included, the soil concentration pattern would probably look different than what is predicted by the present model.

## Vegetation

The monthly averaged  $\alpha$ -HCH concentration in vegetation ( $\text{ng g}^{-1}$  wet weight) for the months January, April, July and October 1992 are plotted in figure 7.10. Close to the major source areas, e.g. India and western Africa, there are large seasonal variations in the vegetation concentrations, with highest concentrations in winter and autumn, i.e. when the emissions take place. Far from major sources, such as in Siberia and in Canada, the vegetation concentrations are highest in summer, which corresponds to the period with highest air concentrations (see Figure 7.3) but also when the leaf area index values, and thus the extent of the vegetation compartment, are highest (see Figure 4.5 on page 59).

The data are converted from  $\text{pg m}^{-2}$  to  $\text{ng g}^{-1}$  by assuming a wet weight of phytomass in the foliage of  $1 \text{ kg m}^{-2}$  as given by *Cousins and Mackay* [2001] and may not easily be compared to measured concentrations. The predicted vegetation concentrations are not evaluated against measurements due to the lack of extensive data sets and due to the simple structure of the vegetation module, which operates with only one type of vegetation with average properties.

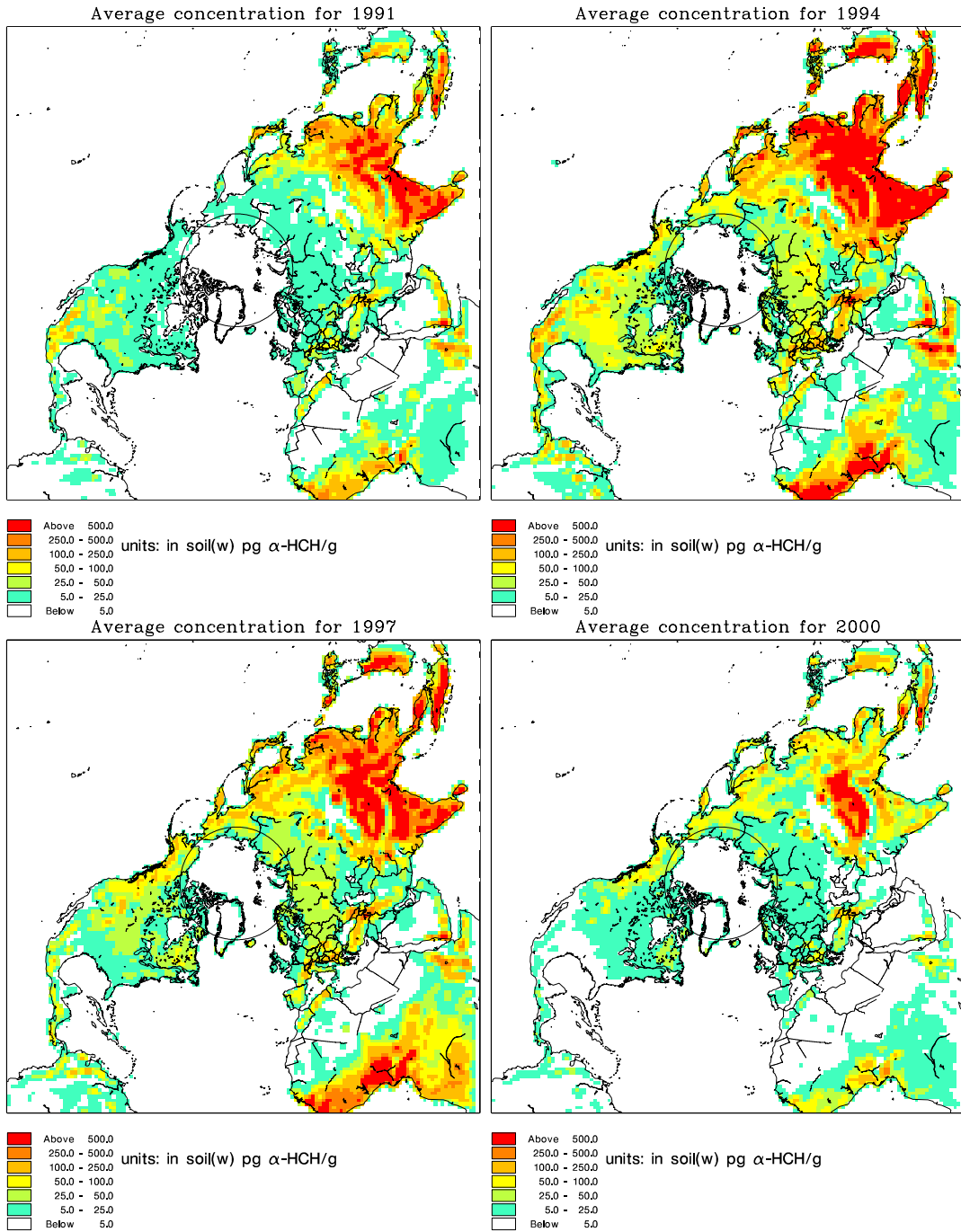


Figure 7.9: Distribution of  $\alpha$ -HCH in soil for the years 1991 (upper left), 1994 (upper right), 1997 (lower left), and 2000 (lower right).

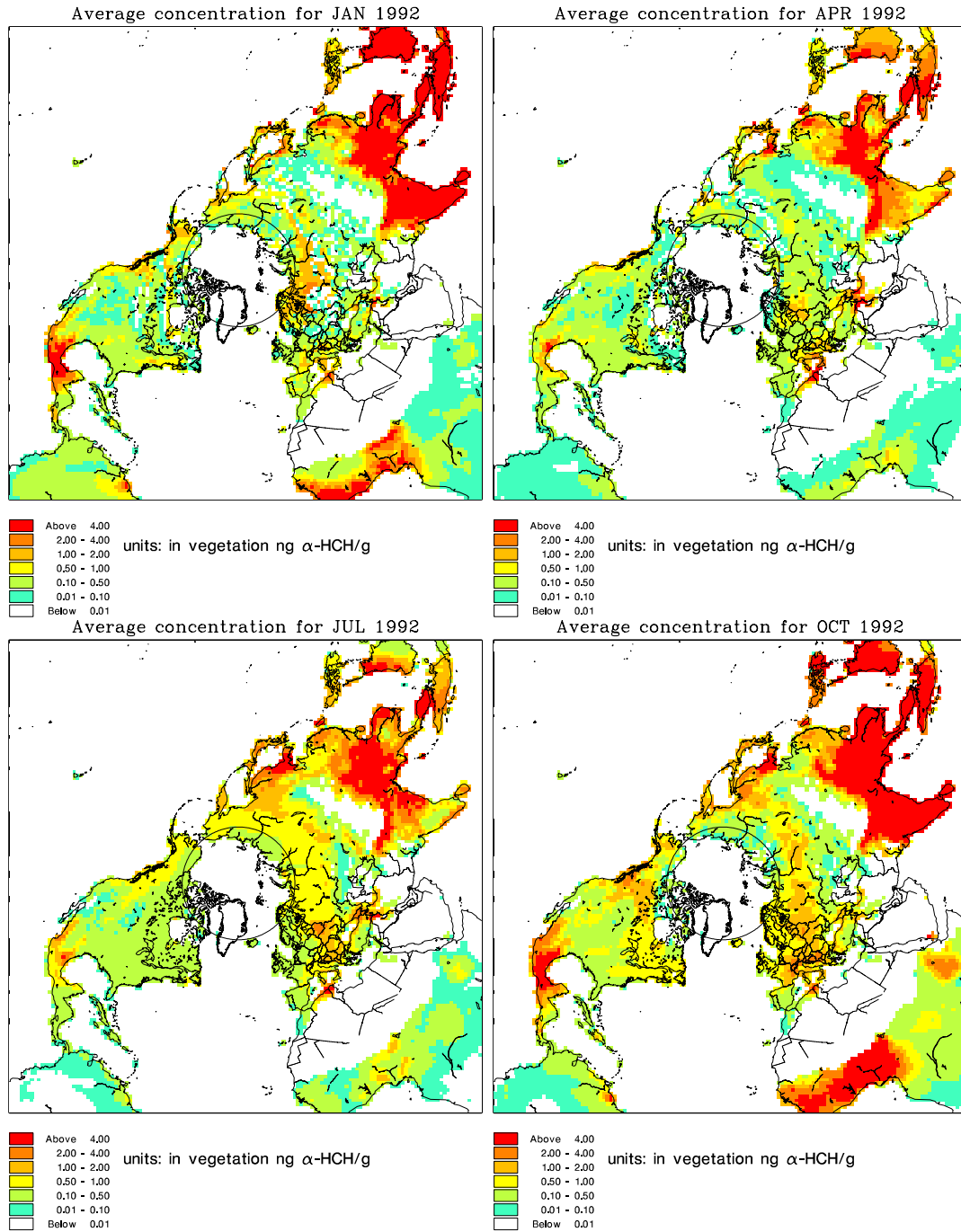


Figure 7.10: Distribution of  $\alpha$ -HCH in vegetation for January 1992 (upper left), April 1992 (upper right), July 1992 (lower left), and October 1992 (lower right).

## Snow

The monthly averaged  $\alpha$ -HCH concentration in the snowpack ( $\text{ng L}^{-1}$  meltwater) for the months January, April, July and October 1992 are plotted in figure 7.11. In winter, high concentrations are found close to the major source areas such as China, but also in remote regions such as the northern Russia and in the snowpack on the Arctic Ocean sea ice. Large variations are found spatially, but also temporally. In summer, when most of the snow is melted away, only moderate concentrations remain in the snowpack on the Arctic Ocean sea ice and very high concentrations in snow on the Tibetan Plateau, due to the proximity of the major sources in India. It should be noted that high concentrations in figure 7.11 not necessarily implicates high total burdens in the snowpack. To calculate the inventory in the snowpack the snow concentrations have to be combined with the depth and the density of the snowpack. For example the total loading of the Tibetan Plateau snowpack during summer is not very large due to the very thin snowpack (see Figure 4.3 on page 53), whereas the snowpack on the Arctic Ocean sea ice contains large amounts of  $\alpha$ -HCH, since it both is deep and has high concentrations.

## 7.2 Evaluation

The model is evaluated by comparing the predicted  $\alpha$ -HCH air concentrations with measurements as described in chapter 6. The annual averaged air concentrations are evaluated in section 7.2.1. Then the individual measurements are evaluated starting with the source area (section 7.2.2), the regions relatively close to source areas, i.e. Europe and North America (sections 7.2.3–7.2.5), ending with an evaluation of the predicted  $\alpha$ -HCH concentrations in the Arctic (section 7.2.6).

### 7.2.1 Long-term averages

To evaluate the predicted long-term average  $\alpha$ -HCH air concentrations the measured concentrations and the corresponding predicted concentrations are averaged within each year. The results from two of the stations are excluded in this exercise, Parangipettai, India, due to the few measurements and Stórhöfði, Iceland due to possible sampling artifacts (see section 7.2.6 for details). For the other stations some of the years are excluded because there were only a few measurements for these years. The annual averaged measured concentrations are plotted against the annual averaged predicted concentrations in Figure 7.12. There is a correlation between averaged measured and predicted concentrations of  $r = 0.5$  significant within a 0.1% significance level ( $p < 0.001$ ), while the predicted mean of all stations and all years is about two third of the measured. At some stations the annual averaged air concentrations appear to be consistently underestimated by the model, namely the five stations from US (Sleeping Bear Dunes, Sturgeon Point, Eagle Harbor, Chicago, and Brule River) and the three stations from Québec, Canada (Villeroy, St. Anicet, and Mingan). The annual averages from these stations are therefore plotted alone in the left hand side of Figure 7.13 and the other stations in the right hand side of Figure 7.13. When the US and Québec stations are excluded, the measured and predicted mean of all stations and all years are almost the same and there is a higher correlation ( $r = 0.68$ ,  $p < 0.001$ ), and for only a few data points the difference between measured and predicted

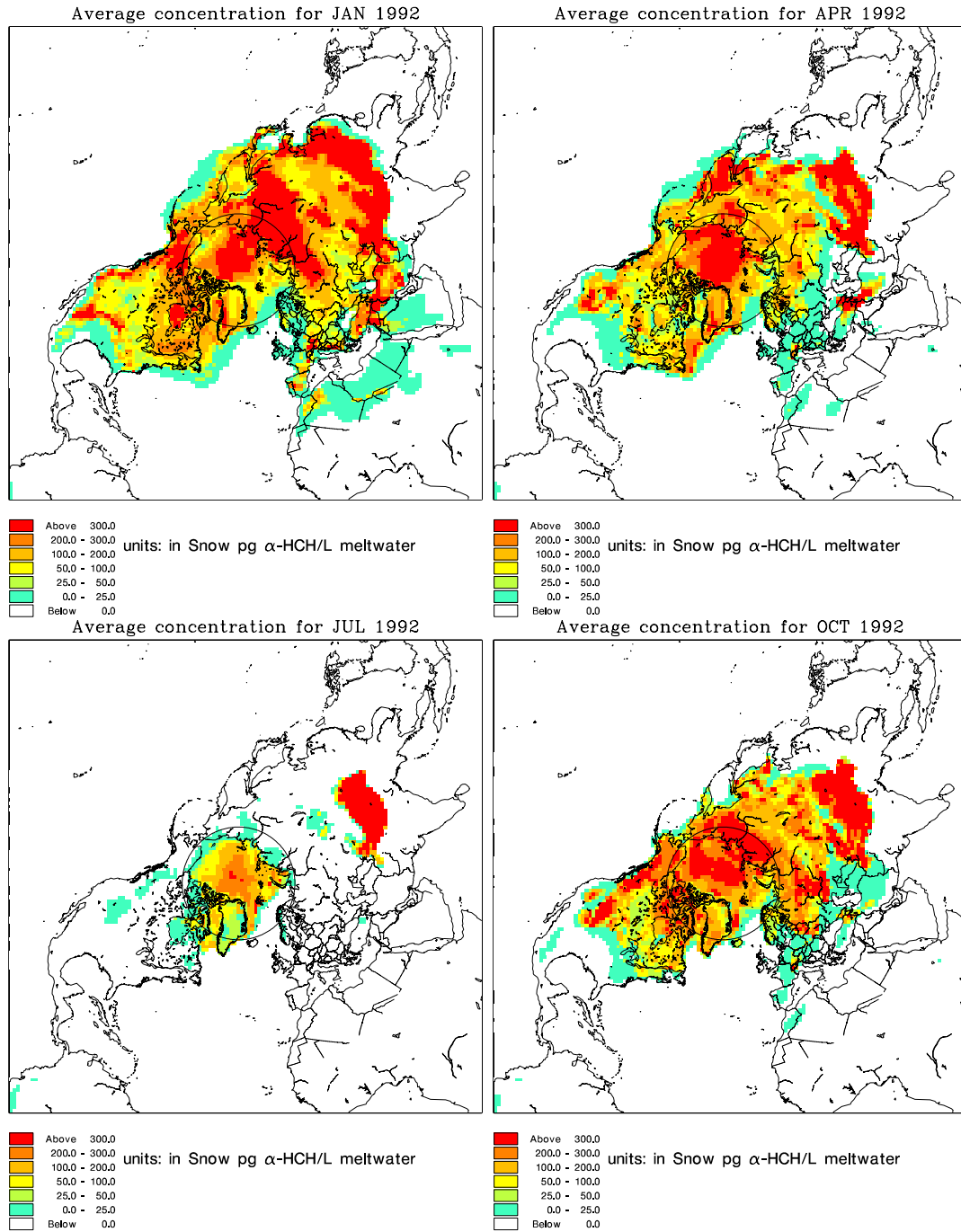


Figure 7.11: Distribution of  $\alpha$ -HCH in snow for January 1992 (upper left), April 1992 (upper right), July 1992 (lower left), and October 1992 (lower right).

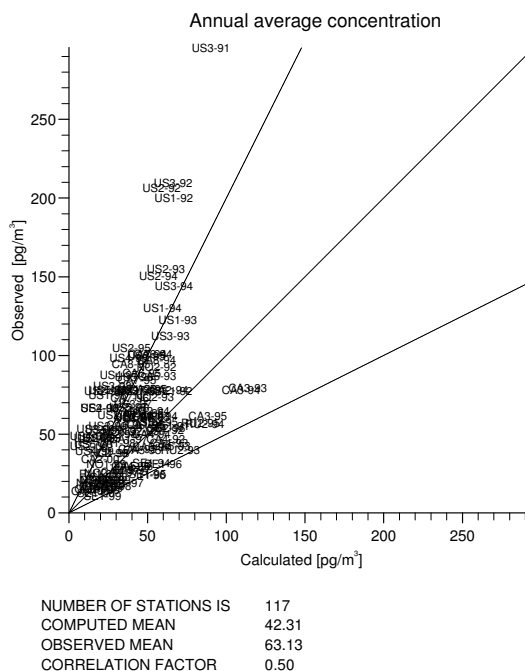


Figure 7.12: Annual averaged measured concentrations plotted against the annual averaged modelled concentrations for all stations. See caption to Figure 7.13 for station codes.

concentrations are more or less than a factor of two. There is also a high correlation of the annual averaged concentrations from the US and Québec stations ( $r = 0.85$ ,  $p < 0.001$ ), however, the predicted mean of all stations and all years is more than a factor of two lower than the measured. The difference in distribution pattern between the US and Québec stations and other stations will be discussed in sections 7.2.3 and 7.2.4.

### 7.2.2 Source area

There are only data from one station situated in an area known to be within a large source area. These are the nine measurements taken at the Indian coastal town of Parangipettai 230 km south of Madras between August 1993 and October 1994 [Rajendran *et al.*, 1999]. The measured concentrations range from 0.53 to 27.4 ng m<sup>-3</sup>, with highest concentrations July – October. The average for the nine measurements are 7.86 ng m<sup>-3</sup>. The modelled concentrations for the same nine sampled periods range from 2.2 to 11.7 ng m<sup>-3</sup> with an average of 6.1 ng m<sup>-3</sup>. Although the average measured and modelled concentrations are in good agreement the individual modelled concentrations are not in good agreement with the measurements (see Figure 7.14). However, this is not surprising since the model operates with monthly averaged emission data evenly distributed over the whole month. Since the measurements are made close to a major source area, the exact time of application may influence the measurements, but this can not be captured by the model. It would therefore be more appropriate to compare the predicted range for the years 1993 and 1994, which is 1.0 ng m<sup>-3</sup> to 21.5 ng m<sup>-3</sup>, with the above mentioned observed range. The range of the

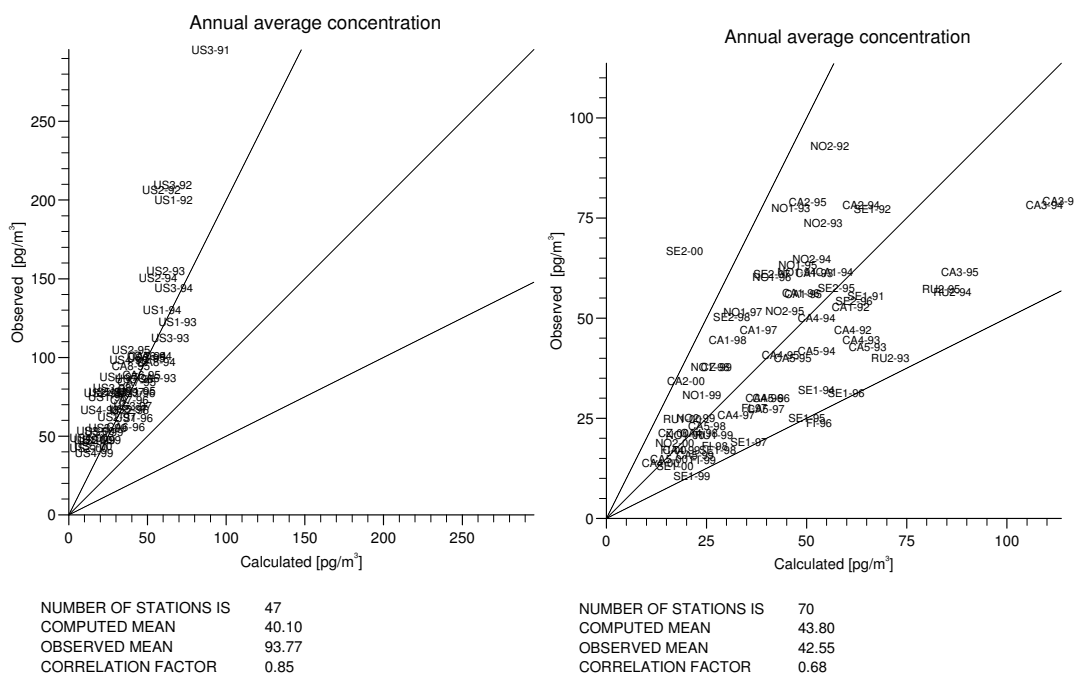


Figure 7.13: Annual averaged measured concentrations plotted against the annual averaged modelled concentrations for the stations in US and CA6, CA7, and CA8 from Québec, Canada (left) and for the other stations (right). The station codes are: -XX: year, CA1: Alert, CA2: Kinngait, CA3: Tagish, CA4: Point Petre, CA5: Burnt Island, CA6: Villeroy, CA7: St. Anicet, CA8: Mingan, CZ: Košetice, FI: Pallas, NO1: Spitzbergen, NO2: Lista, SE1: Rörvik, SE2: Aspvreten, RU1: Amderma, RU2: Dunai Island, US1: Sleeping Bear Dunes, US2: Sturgeon Point, US3: Eagle Harbor, US4: Chicago, US5: Brule River.

predicted and the measured concentrations are in good agreement.

The measurements of *Rajendran et al.* [1999] are concentrated in the summer and autumn of the two years. A more comprehensive data series was established by *Ramesh et al.* [1989], who measured the concentration of HCHs and DDT in air at the same site between December 1987 and January 1989. The model does not cover this time period so a direct comparison of measured and modelled concentrations can not be made, but the seasonal pattern can be evaluated by comparing with these data. The highest observed concentrations are from December 1987 and December 1988. The observed pattern is: low concentrations in January, (no observations from February,) increasing concentrations in March and low concentrations in April to July. In August the concentrations increase, reaching a peak in September/October and low concentration again in November before a narrow peak in December [*Ramesh et al.*, 1989]. The relatively high concentrations from August to January probably reflect the major application of HCHs during the flowering season of rice in the area [*Ramesh et al.*, 1989]. The modelled daily averaged  $\alpha$ -HCH concentration for the whole modelled period is plotted in Figure 7.15, where it can be seen that the modelled concentration for 1991 is representative for the first years of the

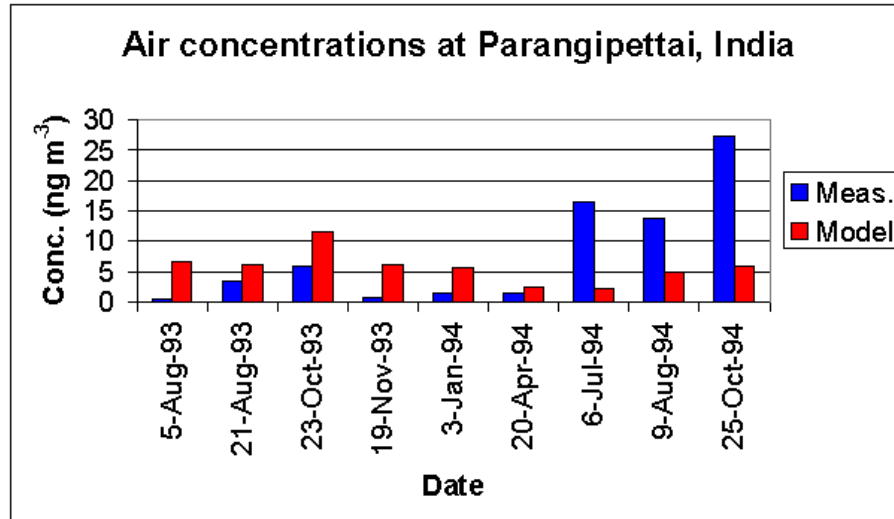


Figure 7.14: Measured and modelled concentrations at Parangipettai, India. Note that the concentrations are in  $\text{ng m}^{-3}$ .

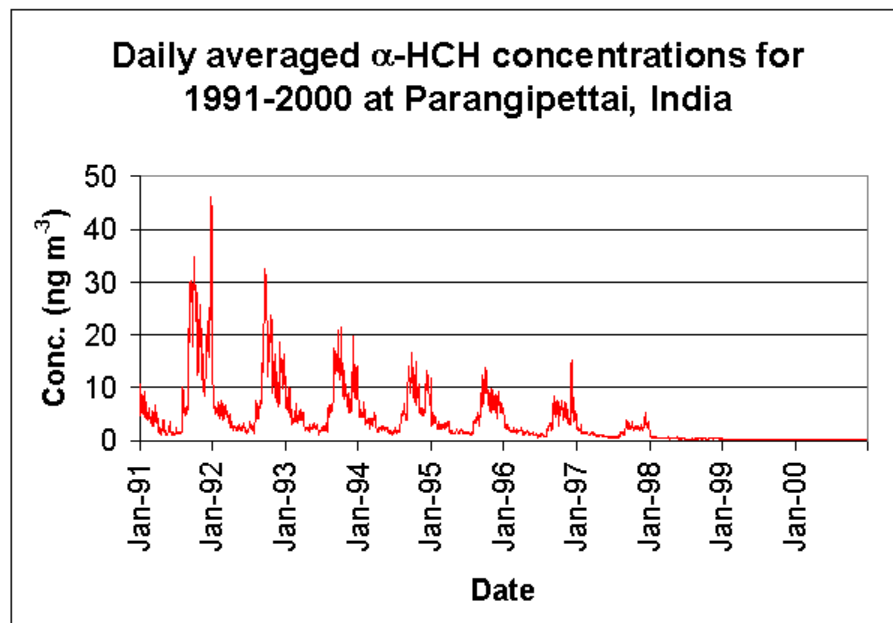


Figure 7.15: Daily averaged modelled concentrations at Parangipettai, India for the years 1991 to 2000. Note that the concentrations are in  $\text{ng m}^{-3}$ .

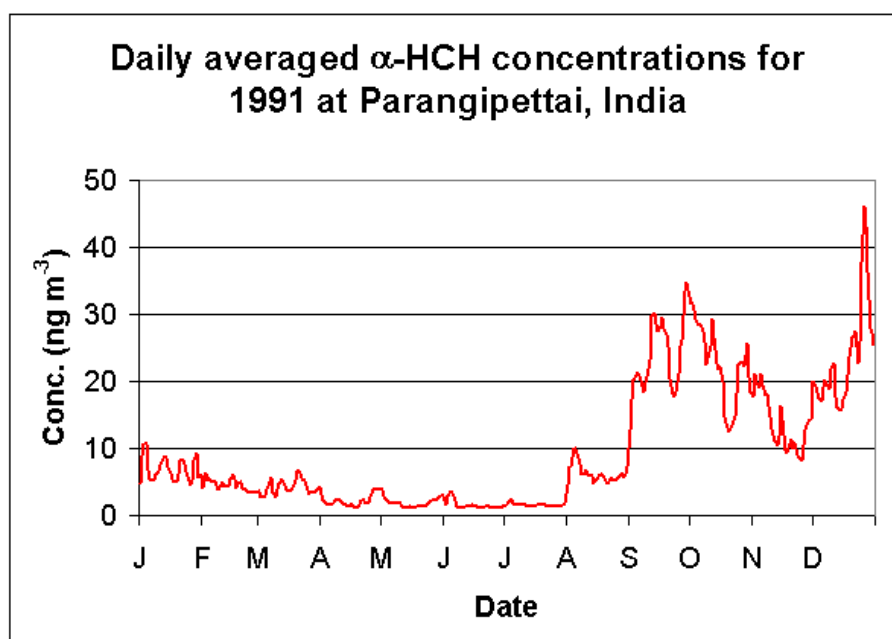


Figure 7.16: Daily averaged modelled concentrations at Parangipettai, India for the year 1991. Note that the concentrations are in  $\text{ng m}^{-3}$ .

modelled period and data from this year is plotted in Figure 7.16. It can be seen that the modelled concentration pattern is in good agreement with the observations of *Ramesh et al.* [1989], with low concentrations during April to July, and highest concentrations in September/October and December. This indicates that the applied monthly mean emission data are capturing the seasonal variation in emissions of  $\alpha$ -HCH following the agricultural practice in this area.

### 7.2.3 IADN stations

There are  $\alpha$ -HCH air measurements from seven of the Integrated Atmospheric Deposition Network (IADN) stations around the Great Lakes, two on the Canadian side of the lakes, and five on the US side. The stations are relatively close (see Figure 6.2 on page 76), and in the model they are separated by only a few grid cells. The results from these stations are therefore expected to be similar, but there are however differences between the Canadian and the US stations.

#### Canadian stations

Both Canadian stations are characterised as ‘remote sites’. Point Petre is a small peninsula on the eastern end of Lake Ontario where the station is located 50 m from the lake, and Burnt Island is situated in the northern part of Lake Huron where the sampling station is located 200 m from the lake [IADN, 2005]. Measured  $\alpha$ -HCH air concentrations are plotted against predicted concentrations for the two stations in Figure 7.17. There is a

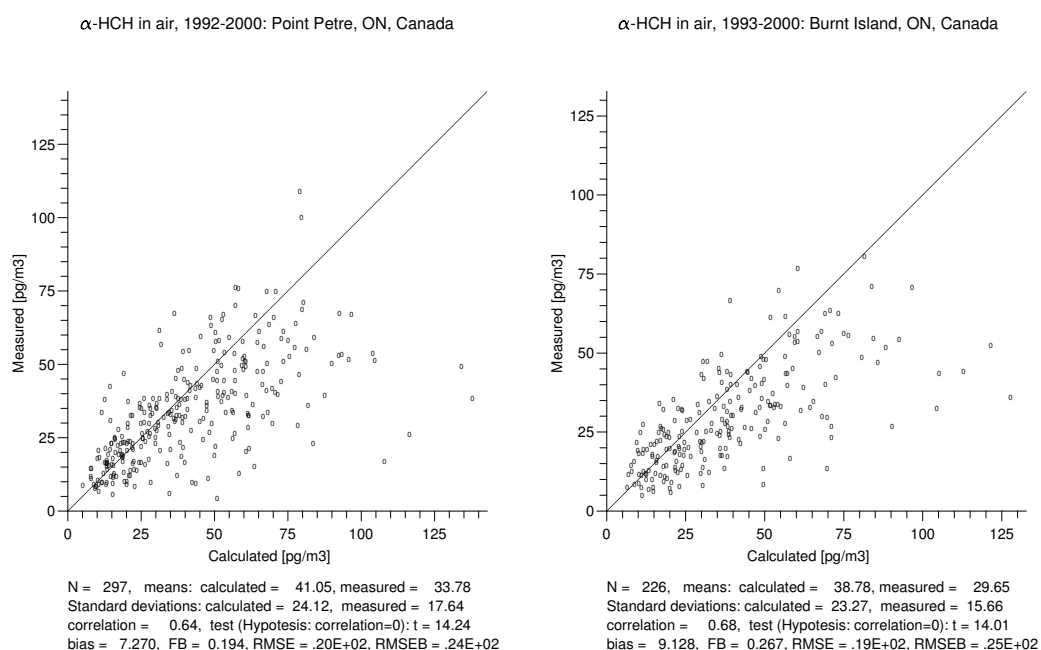


Figure 7.17: Measured  $\alpha$ -HCH air concentrations plotted against predicted concentrations for Point Petre, Ontario, Canada (left) and Burnt Island, Ontario, Canada (right).

high correlation between measured and calculated concentrations at the two stations:  $r = 0.64$  and  $r = 0.68$ , respectively, with both correlations significant within a 0.1% significance level ( $p < 0.001$ ). Only a few of the measured values are more than a factor of two higher than predicted concentrations (5 and 4 from the two stations, respectively), whereas there are several predicted concentrations that are more than a factor of two higher than the measured concentrations (34 and 32, respectively) and a few of these a much higher than measured. The averaged predicted concentrations are higher than the measured by about 25%.

The data from the two stations are also plotted as time series in Figures 7.18 and 7.19. There are clear seasonal patterns with higher concentrations during summer than during winter, and a decreasing trend through the simulated period is evident for both stations. The time series from Point Petre confirms the good agreement between measured and modelled concentrations seen in the scatter plots. The few very high predicted concentrations all occurs during late autumn or early winter. The results from Burnt Island are similar to the results from Point Petre, although there appear to be a more consistent model over-prediction of the concentrations during autumn and early winter. For the last years (1998–2000 for Point Petre and 1999–2000 for Burnt Island) the model has a tendency of underestimating the air concentrations during summer, while the air concentrations during winter are slightly overestimated.

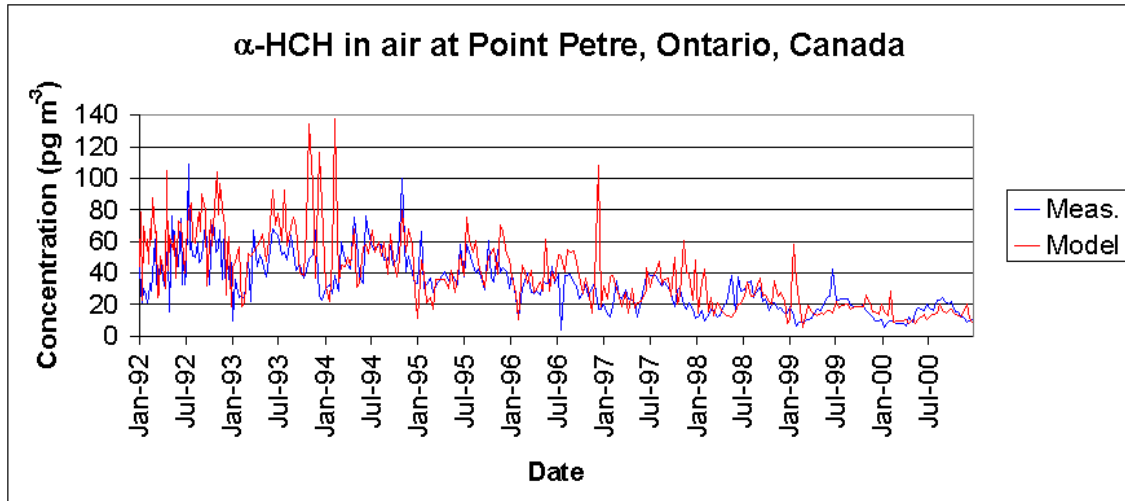


Figure 7.18: Measured and modelled concentrations at Point Petre, Ontario, Canada.

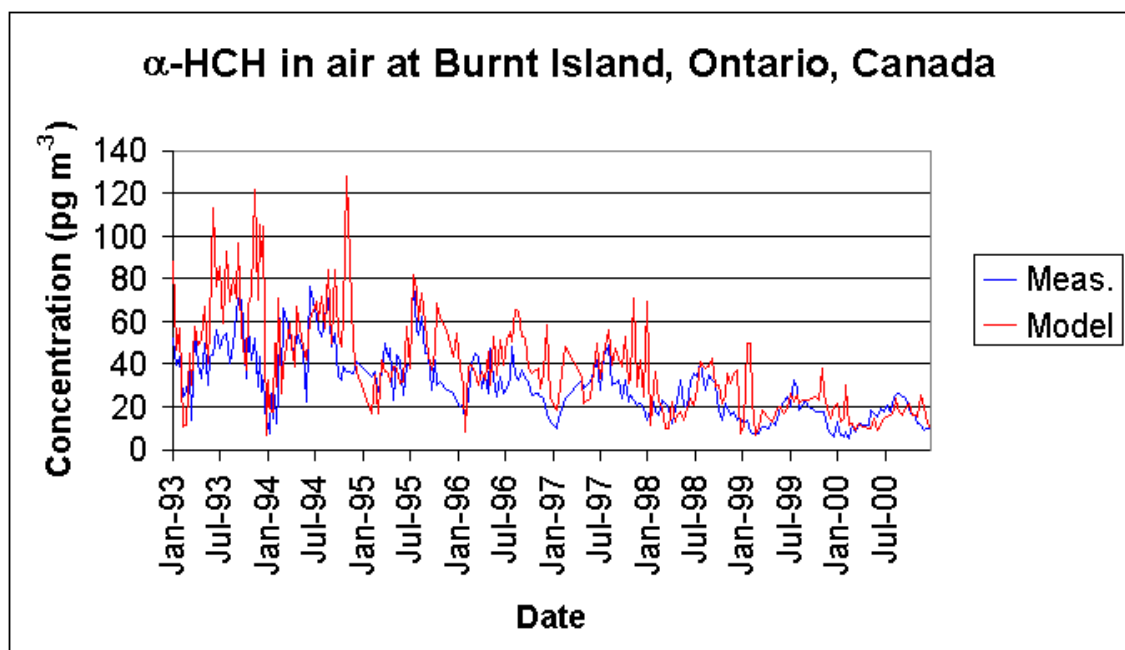


Figure 7.19: Measured and modelled concentrations at Burnt Island, Ontario, Canada.

### US stations

Sleeping Bear Dunes is a remote site on the eastern side of Lake Michigan. The station is placed in an abandoned farm field about 1.5 km from the lake [IADN, 2005]. Sturgeon Point is a rural/suburban site located about 100 m from Lake Erie in an area surrounded by residential, agricultural and commercial development [IADN, 2005]. Eagle Harbor is placed on the Keweenaw peninsula on the south side of Lake Superior. There are no major sources in the surroundings of Eagle Harbor [IADN, 2005]. Chicago is an urban site on the southwestern end of Lake Michigan, and the station is placed on the roof of the Illinois Institute of Technology, about 1.5 km west of the lake in a surrounding of heavy urban and industrial development [IADN, 2005]. Brule River is located on the western end of Lake Superior in an area of grassy meadows adjacent to mixed forest with some agriculture in the area [IADN, 2005].

As indicated by the annual average concentrations, the results from the five US stations from the IADN network display another pattern than the results from the Canadian stations. The measured  $\alpha$ -HCH air concentrations are plotted against predicted concentrations for Sleeping Bear Dunes in Michigan, Sturgeon Point in New York, Eagle Harbor in Michigan, and Chicago in Illinois in Figure 7.20. The correlations are lower than at the Canadian stations ( $r = 0.3 - 0.56$ ,  $p < 0.001$ ) and the model apparently systematically under-predicts the measured concentrations. The results from Brule River, Wisconsin (not shown), that spans only the last four simulated years display a similar pattern as the other four US stations, although the correlation is lower and less statistically significant ( $r = 0.15$ ,  $p < 0.1$ ). The averaged measured concentrations are a factor of two to three higher than the predicted for all stations.

The time series for the five US stations are plotted in Figures 7.21–7.25, with all stations displaying similar patterns. There are clear seasonal patterns in the measurements with higher concentrations during summer than winter, whereas the predicted air concentrations display less pronounced variations between summer and winter concentrations. The predicted air concentrations agree well with the measured during late autumn and winter, whereas the summer concentrations are up to a factor of seven lower than the measured concentrations. There is a clear decreasing trend in both measurements and model results through the modelled period, with the measured concentrations during summer 1998 as an exception at all US stations.

The higher measured concentrations than predicted could indicate that there are sources not accounted for by the emission data or initial environmental concentrations used as input in the model. The pattern could also be explained if a surface sink in the model (e.g. vegetation) locally was too strong.

### Discussion of the IADN results

There are several possible explanations for the difference between measured and predicted concentrations in the US stations. However, most of these would require that similar patterns in the difference between measurements and model results are found for both the US and the Canadian stations, which is not the case.

The model predicts similar concentrations at the seven IADN stations. The daily average concentrations at Point Petre, Canada and Eagle Harbor, USA, the two stations placed with the largest distance, are plotted for 1992 in Figure 7.26. The pattern at the

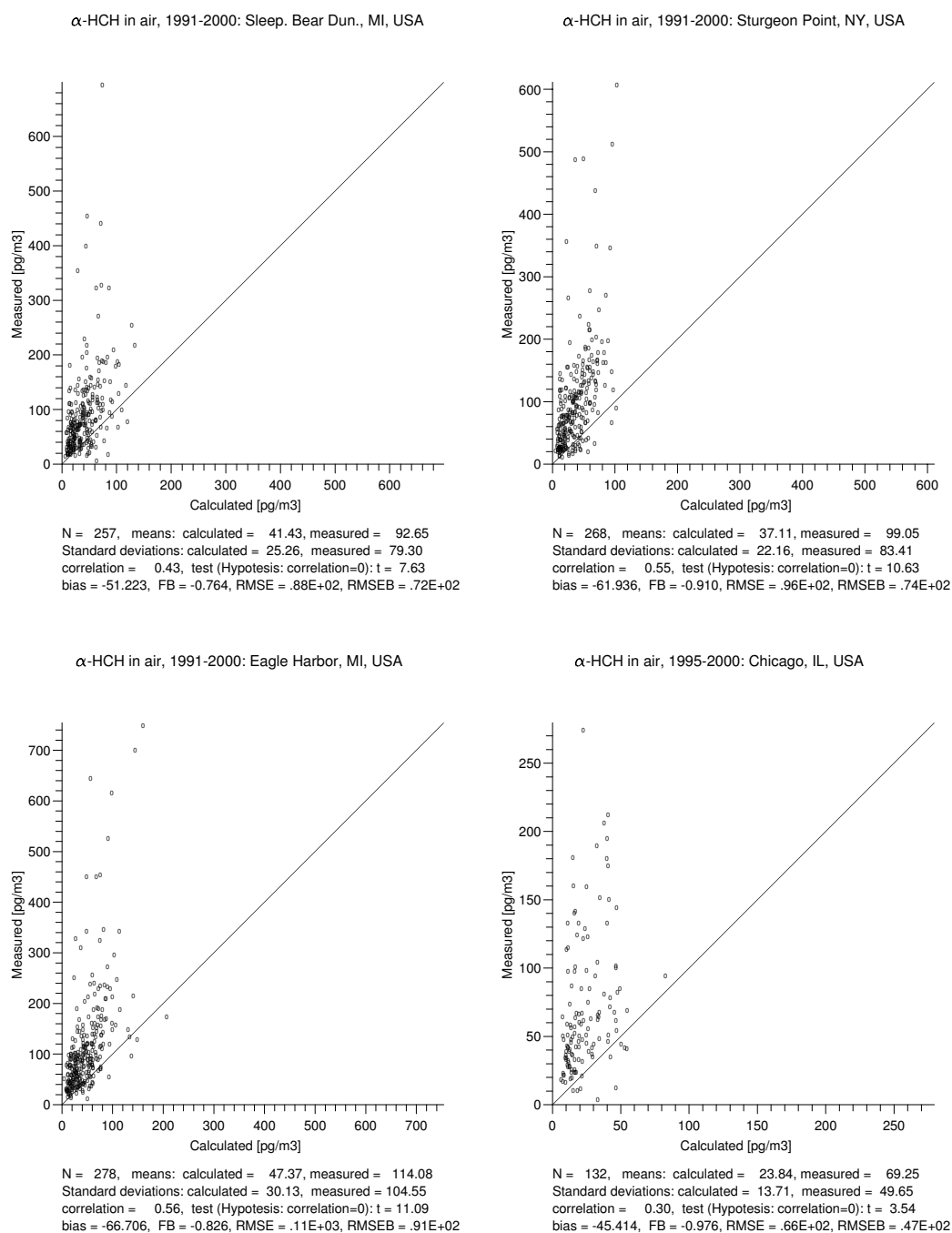


Figure 7.20: Measured  $\alpha$ -HCH air concentrations plotted against predicted concentrations for Sleeping Bear Dunes, Michigan, USA (upper left), Sturgeon Point, New York, USA (upper right), Eagle Harbor, Michigan, USA (lower left), and Chicago, Illinois, USA (lower right).

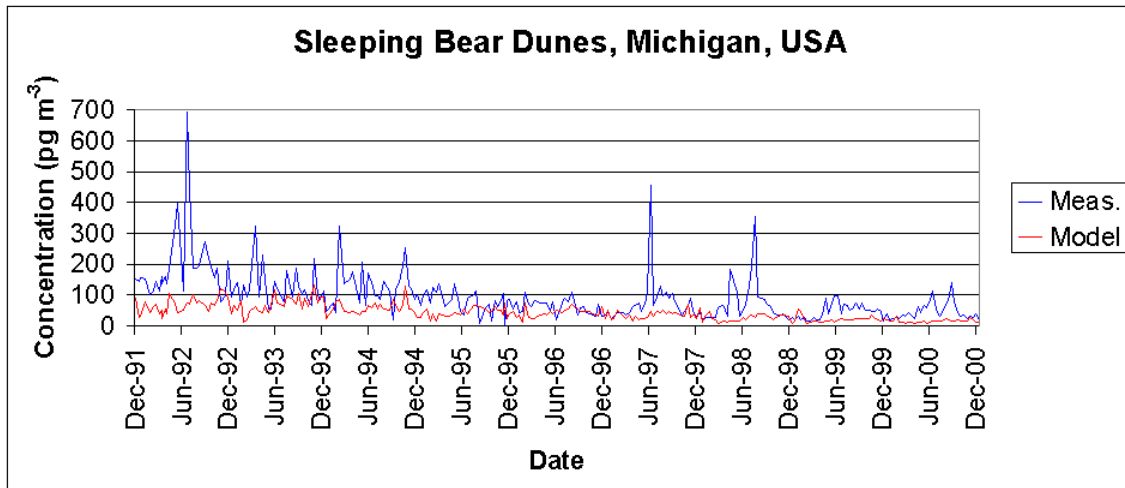


Figure 7.21: Measured and modelled concentrations at Sleeping Bear Dunes, Michigan, USA.

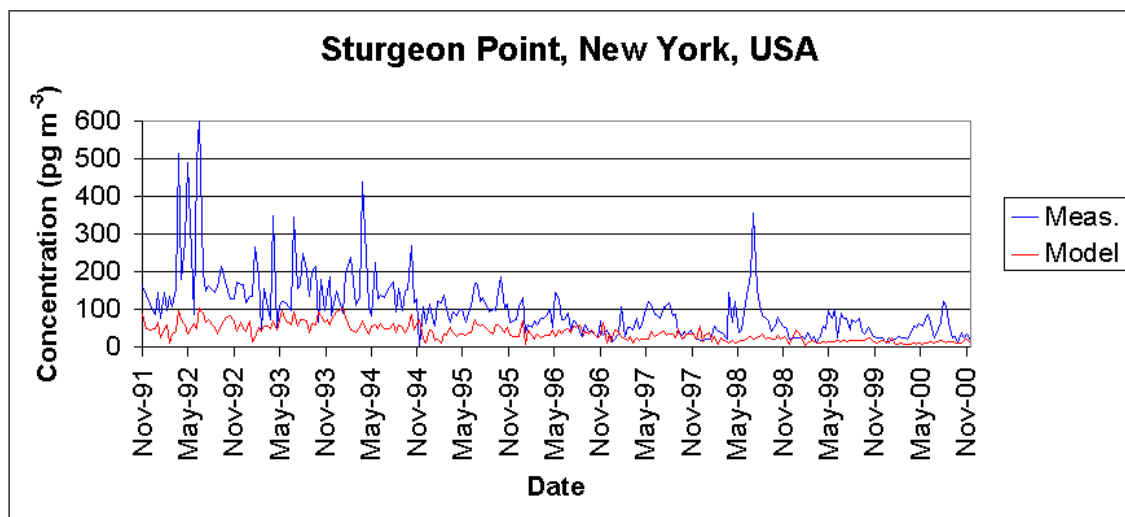


Figure 7.22: Measured and modelled concentrations at Sturgeon Point, New York, USA.

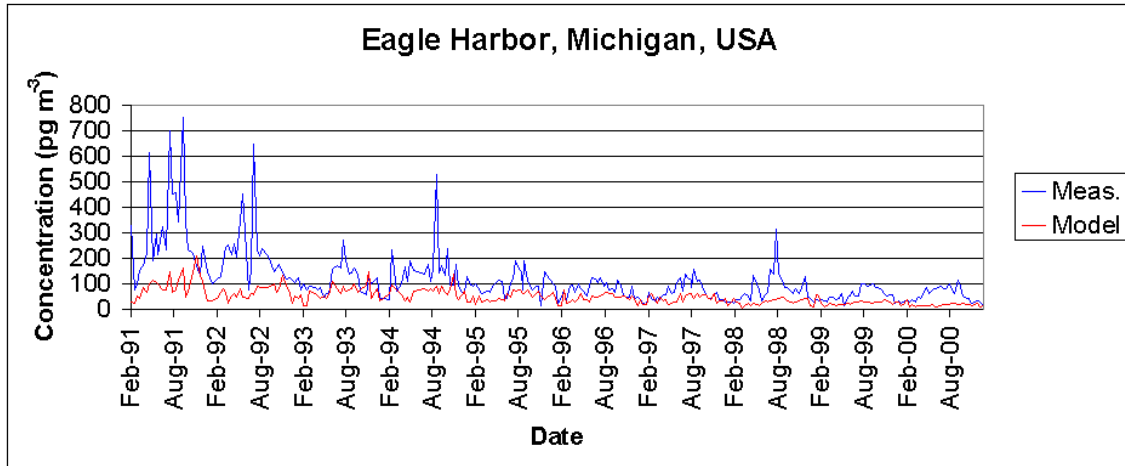


Figure 7.23: Measured and modelled concentrations at Eagle Harbor, Michigan, USA.

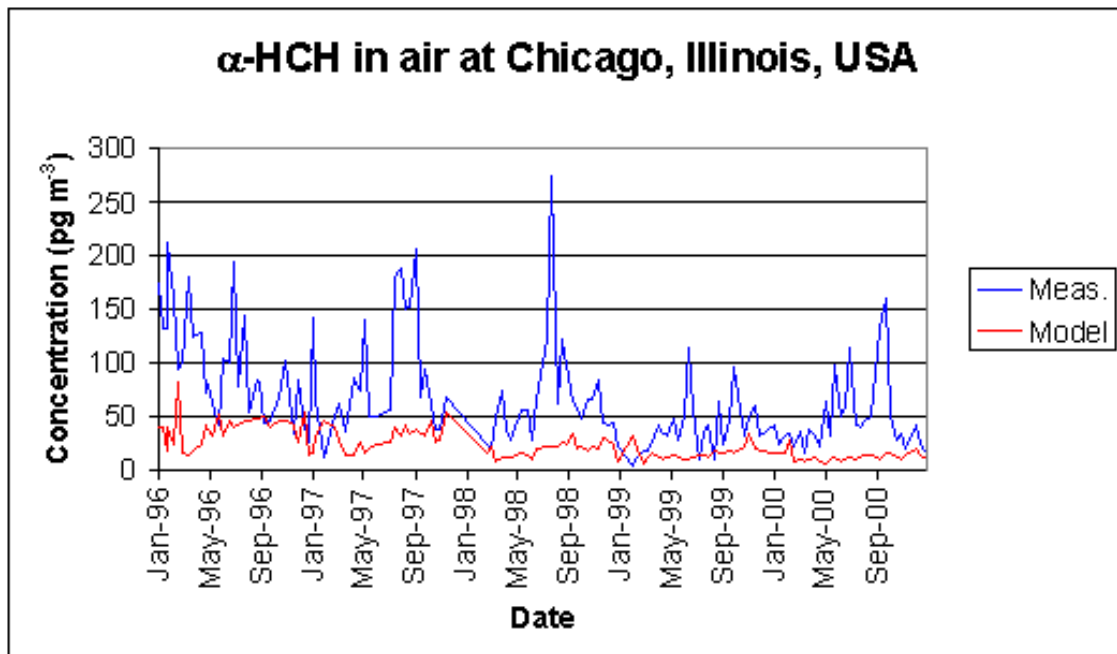


Figure 7.24: Measured and modelled concentrations at Chicago, Illinois, USA.

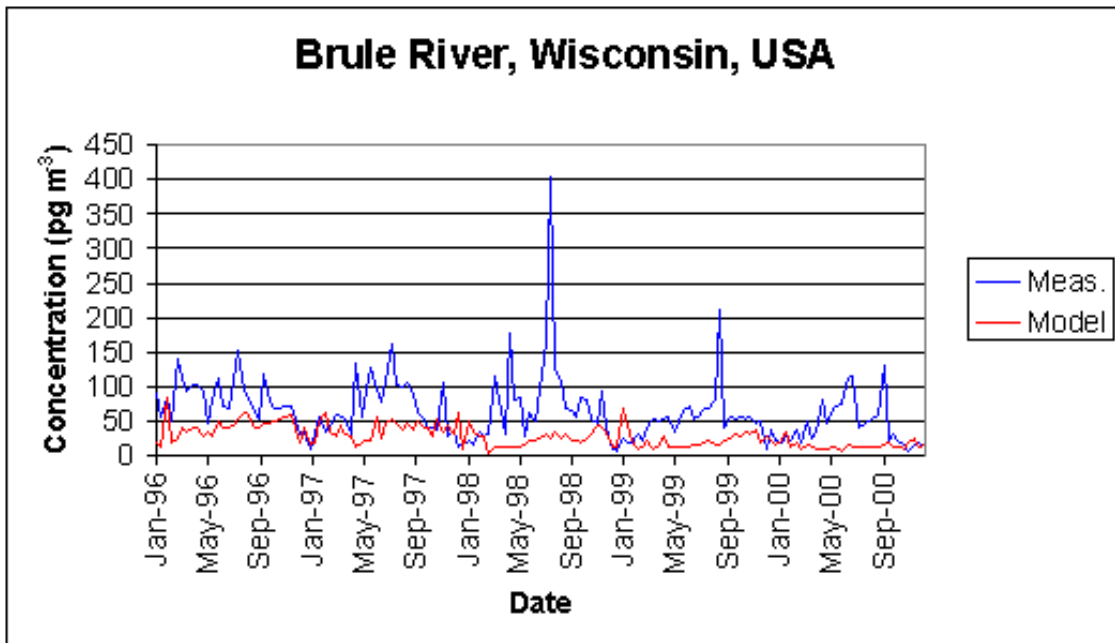


Figure 7.25: Measured and modelled concentrations at Brule River, Wisconsin, USA.

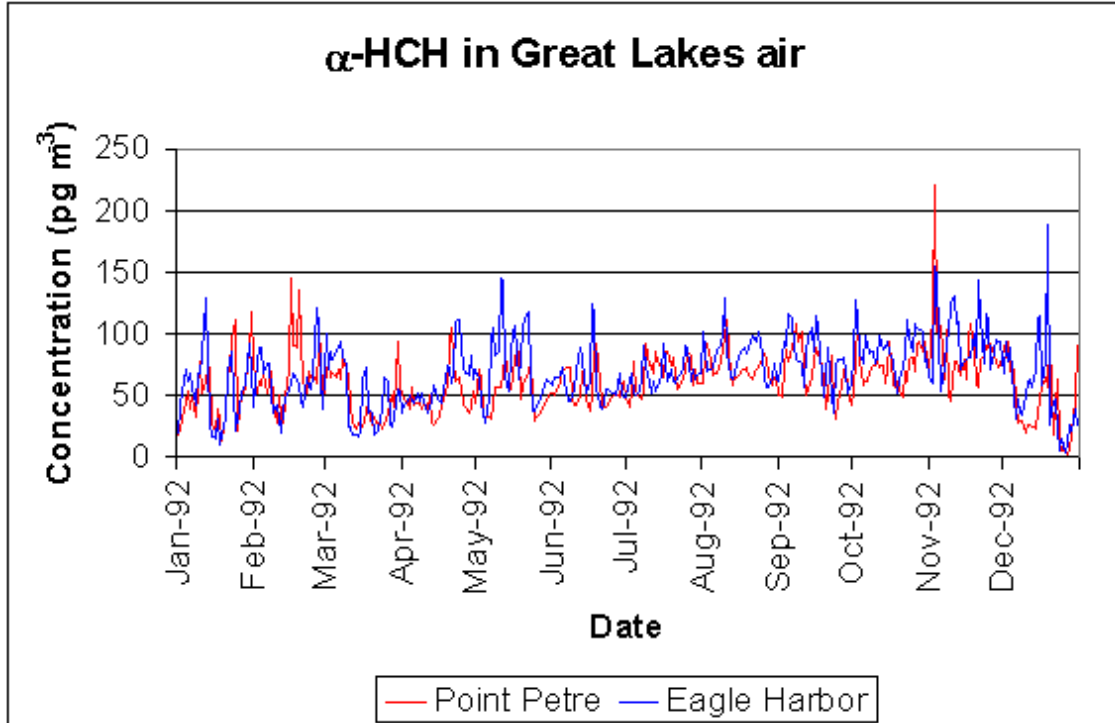


Figure 7.26: Predicted concentrations at Point Petre, Ontario, Canada and Eagle Harbor, Wisconsin, USA.

two stations is very similar, although differences up to a factor of two periodically are seen. The correlation between the daily averages at these two stations for the whole simulated period is high ( $r = 0.78$ ,  $p < 0.001$ ), which is representative for the relations between the seven stations. The difference in model performance between the US and the Canadian stations must therefore arise from the measurements.

The difference between the measured concentrations at the US and Canadian stations could be explained if the air passing the stations had completely different origin, which is not very likely for the whole 10 years period. Of the same reason, underestimations of the regional/continental emission estimates used as input in the model is not likely. The closest region with direct usage of Technical HCH is Mexico, where the use was banned in 1993. However, Mexico is characterised as one of the countries with complete information on available production and usage data [Li, 1999], and the emission estimates from this country should thus be one of the most reliable. It is possible to imagine a scenario where the emissions from Mexico are underestimated, but it requires that the air when it has passed the US stations reaches a sink, which could be the Lakes, before it reaches the Canadian stations. It would also require relatively low measured air concentrations at the US stations when the air are coming from the Lakes, which is not the general pattern in the data. This is thus not a very likely scenario. Furthermore, in a correlation analysis of the measured US data for four different compounds (although not  $\alpha$ -HCH), no improved correlation was seen when wind direction or trajectory direction were included as descriptive parameter, with the exception of PAHs [Hafner and Hites, 2005].

Underestimations of the initial water concentration used as input in the model can also be excluded, since this most probably would influence stations on both sides of the lakes. If the difference is to be explained by emissions they must thus be of very local origin, i.e. within the local area of the stations. This is possible, since there are agricultural areas nearby both Sleeping Bear Dunes, Sturgeon Point, and Brule River. Old usage residues may thus be present in the soil in these areas. Indeed there are emissions on both sides of the Lakes (see Figures 5.2 on page 69 and 5.3 on page 70), although they are very small, and not necessarily indicates usage in the local area close to the stations. There are several factors that cast doubt on this possible explanation. The Chicago station display similar results as the other stations, although it is not placed close to an agricultural area. The use of Technical HCH was banned in 1971 in Canada and 1976 in USA [Li, 1999]. Soil residues larger than those from which the emissions are calculated are thus not very likely to be present in the area, even if the usage up to the year of ban is not accurately estimated.

If the local soils surrounding the stations are contaminated with  $\alpha$ -HCH and thus act as source to the measured air concentrations it is questionable if the measured concentrations are representative of the lowermost 50 m in the atmosphere, which approximately constitute the thickness of the lowermost air layer in DEHM-POP. The concentration in air right over a source region is expected to decrease rapidly with height in the lowermost few meters, i.e. within the height of the samplers.

The presence of a strong sink in the model on the US side of the Great Lakes is not very likely, since the land use in the model is similar on both the Canadian and the US side of the Lakes. A possible candidate could be the vegetation compartment, which will be examined in detail in section 7.4.

There is also the possibility of sampling artifacts at the stations and/or in the labo-

ratory analysis. This is also questionable, since the different measurement equipment is tested by applying them at the same site and no differences have been reported from this comparison [IADN, 2005], and since the analysis are made at highly respectable laboratories.

#### 7.2.4 Québec

$\alpha$ -HCH air concentrations were measured at three sites in Québec, Canada [Garmouma and Poissant, 2004; Aulagnier and Poissant, 2005]. Villeroy and St. Anicet are both rural sites surrounded by farms and some wooded areas, while Mingan is a remote site on the north shore of St. Lawrence River [Aulagnier and Poissant, 2005]. The measurements were collected from January 1993 to March 1996 at Villeroy, from March 1994 to March 1996 at St. Anicet, and from June 1994 to June 1995 at Mingan. The measured  $\alpha$ -HCH air concentrations are plotted against the predicted concentrations for the three stations in Figure 7.27. There is a low but statistically significant correlation between measured and modelled concentrations at Villeroy ( $r = 0.24$ ,  $p < 0.002$ ), and the model underestimates the majority of the measured air concentrations. The measured and modelled concentrations do not correlate at St. Anicet, where the model almost consistently underestimates the measured concentrations. The pattern is the same at Mingan, and although the correlation between measured and modelled concentrations is close to the correlation at Villeroy it is not statistically significant.

The data are also plotted as time series. There is generally a good agreement between measured and predicted air concentrations in late autumn and early winter at Villeroy (Figure 7.28). The air concentrations during spring and summer are consistently underestimated by the model, but the difference between measured and predicted results appear to decrease over the summer. The data from St. Anicet (Figure 7.29) display a similar pattern, although not as clear, as the data from Villeroy. A clear pattern is not discernable in the Mingan data (Figure 7.30) due to the relatively few data points.

Similarly to the US IADN stations, the predicted spring and summer concentrations are a factor 2–3 lower than the measured. This could indicate that the stations have the same sources, and if this is the case, most of the discussion about the difference between measured and predicted concentrations from that IADN section can be applied for the Québec stations as well. However, there is a tendency of highest concentrations during spring with slightly decreasing or similar concentrations in summer at the Québec stations. This may be connected to the snowpack season with increasing re-volatilisation towards the end of the winter and into the melting season as discussed by Aulagnier and Poissant [2005]. The measured  $\alpha$ -HCH air concentrations from Québec are hypothesized to mainly be of non-local origin arriving through long-range transport, with re-volatilisation from the nearby North Atlantic Ocean as a possible source for part of the measured concentrations, especially at Mingan [Garmouma and Poissant, 2004; Aulagnier and Poissant, 2005].

#### 7.2.5 European stations

There are data from four European EMEP stations considered not to be part of the Arctic in this study: one in Norway, two in Sweden, and one in the Czech Republic.

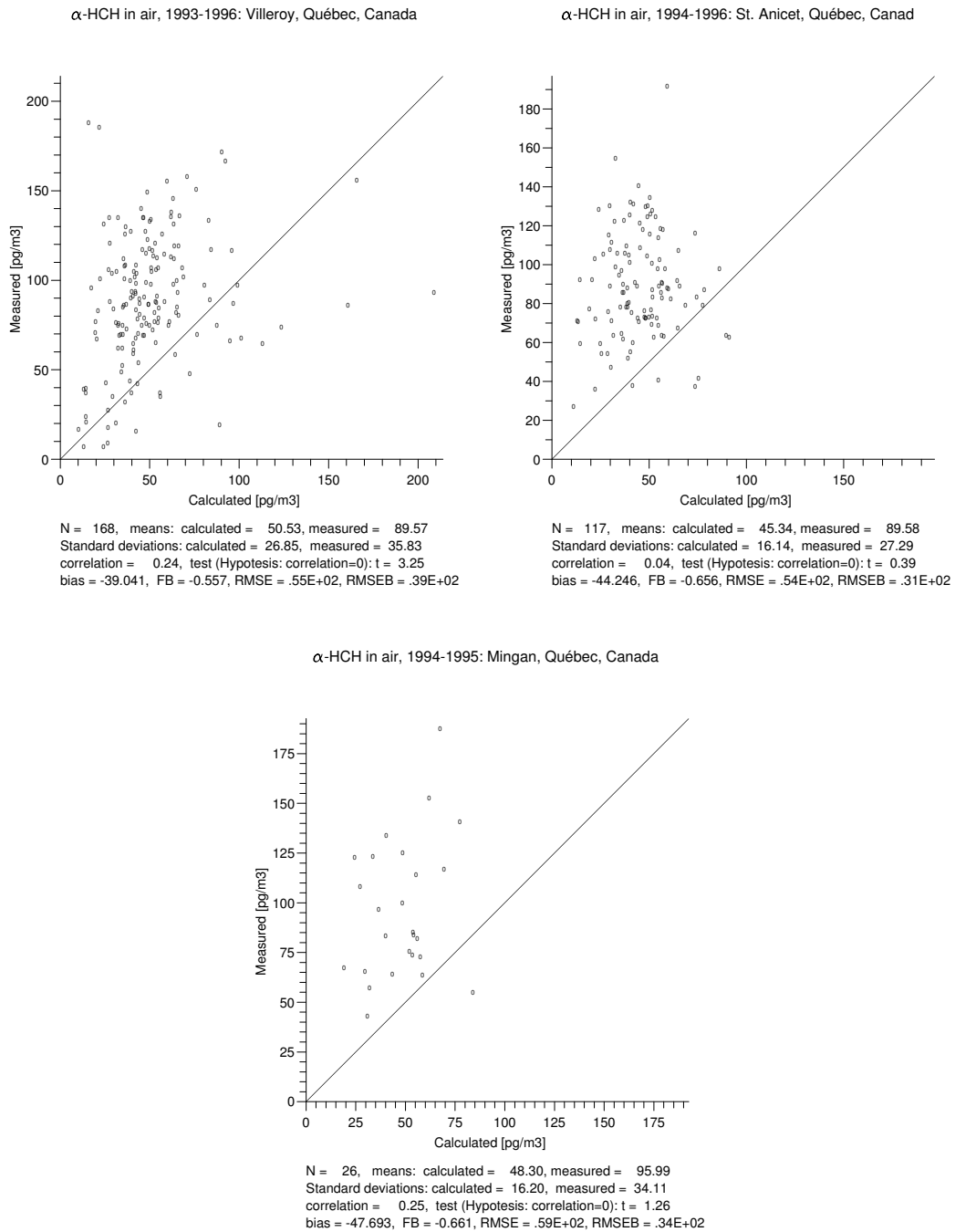


Figure 7.27: Measured  $\alpha$ -HCH air concentrations plotted against predicted concentrations for Villeroy (upper left), St. Anicet (upper right), and Mingan (lower).

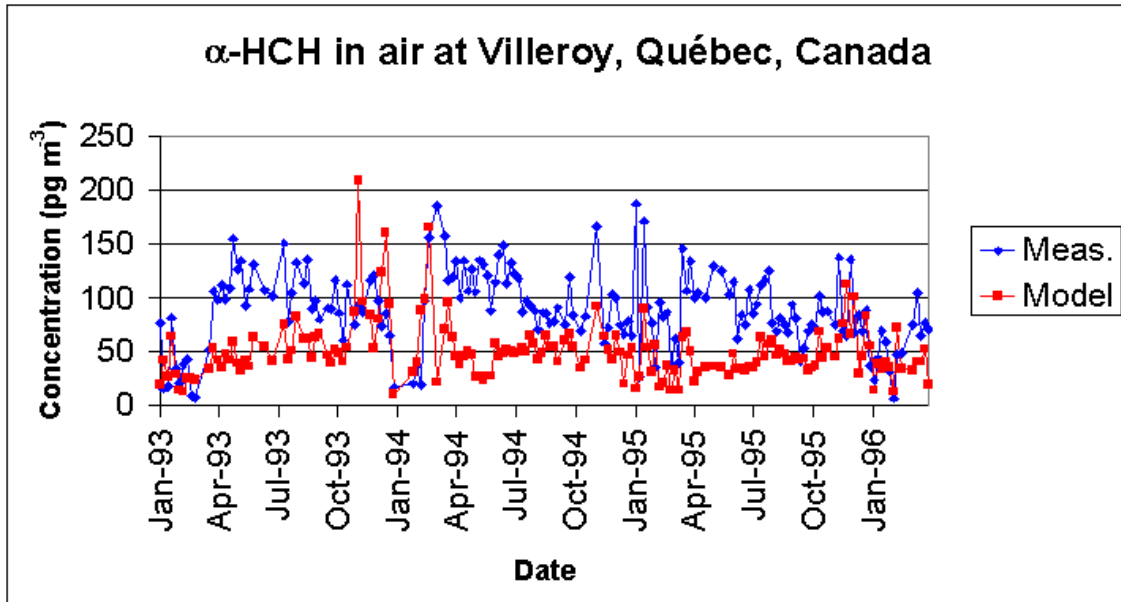


Figure 7.28: Measured and modelled concentrations at Villeroy, Québec, Canada.

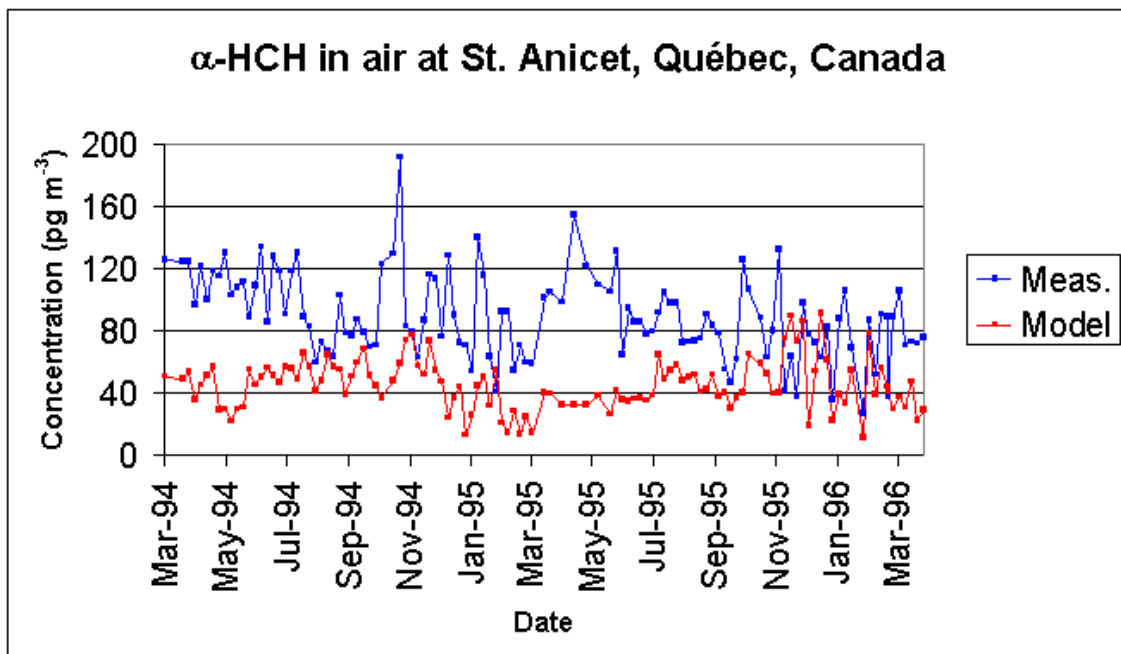


Figure 7.29: Measured and modelled concentrations at St. Anicet, Québec, Canada.

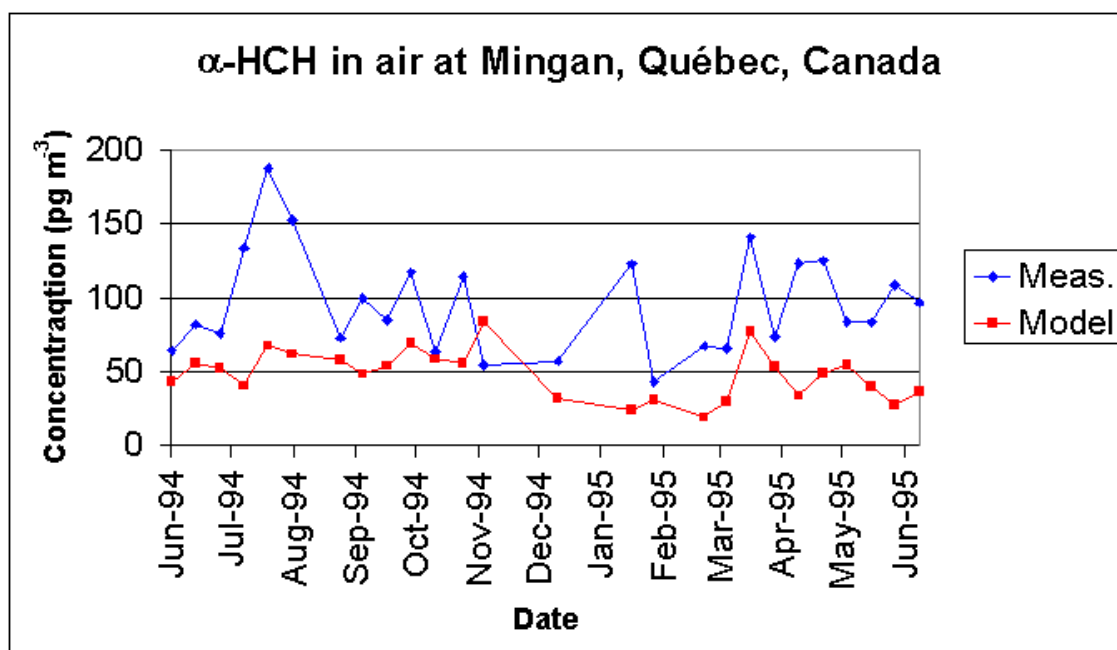


Figure 7.30: Measured and modelled concentrations at Mingan, Québec, Canada.

### Lista, Norway

The sampling station of Lista is placed on a small peninsula on the coast of the North Sea at the southern tip of Norway. The data at this station are sampled over one day with samples taken once a week [Haugen *et al.*, 1998]. Only the data from 1992–1995 and 1999–2000 were directly available for this study. However, the data for the years 1991–1998 were also available as monthly averages, i.e. the 4 or 5 samples per month had been averaged. The available data thus span the whole simulated period, although the temporal resolution is variable. The individual samples that were available are compared to the predicted concentrations as for the other stations. To use the monthly averaged measured concentrations these were compared with the monthly average of the extracted daily average concentrations from the model. This may give a bias to the evaluation, since the few measured concentrations within a month not necessarily are representative of the monthly averaged air concentration at the site.

The measured  $\alpha$ -HCH air concentrations are plotted against predicted concentrations in Figure 7.31. The monthly averaged concentrations are plotted in the left hand side of the figure and the individual measurements in the right hand side of the figure. There is a good agreement between measured and predicted concentrations at Lista with correlation coefficients of ( $r = 0.71$ ,  $p < 0.001$ ) for the monthly averaged and ( $r = 0.69$ ,  $p < 0.001$ ) for the individual measurements. The model tends to underestimate the measured concentrations, and the difference is largest for the monthly averaged values.

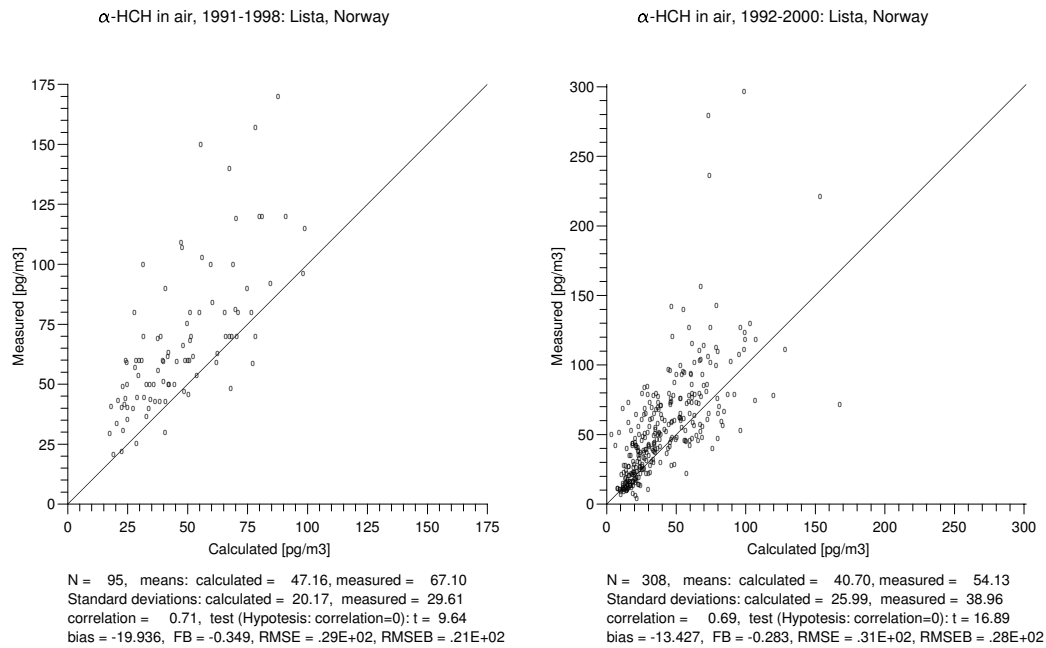


Figure 7.31: Measured  $\alpha$ -HCH air concentrations plotted against predicted concentrations for Lista, Norway (Monthly averages — left, individual measurements — right).

The monthly averaged measured and predicted concentrations are plotted as time series in Figure 7.32. There appear to be a seasonal signal with higher summer than winter concentrations, although the pattern is scattered. The predicted monthly averaged concentrations display similar variability as the measured averages. The difference between predicted and measured averaged concentrations decreases towards the end of the simulated period.

The individual measured and predicted concentrations are plotted as time series in Figure 7.33 for the years 1992–1995 (upper) and the years 1999–2000 (lower). There is a clear seasonal pattern with high concentrations in summer/early autumn and low concentrations in winter/early spring in both measured and predicted concentrations. The predicted variability of the individual measured concentration is generally in good agreement with the measured, which indicates that the model captures the individual transport episodes. The levels of the predicted and measured concentrations are close, and the difference between the two data set decrease towards the end of the simulated period. This shows that the long-term temporal trend is also well captured by the model.

These results indicate that the sources of the measured  $\alpha$ -HCH air concentrations at Lista are well described in the model. As the station is located at the southern tip of Norway, the air concentrations are probably influenced by the nearby North Sea. Indeed, back-trajectory calculations show that about 2/3 of the measured air concentrations at Lista have passed over the North Sea [Haugen *et al.*, 1998]. The good agreement between measured and predicted concentrations indicates that the simple parameterisations in the

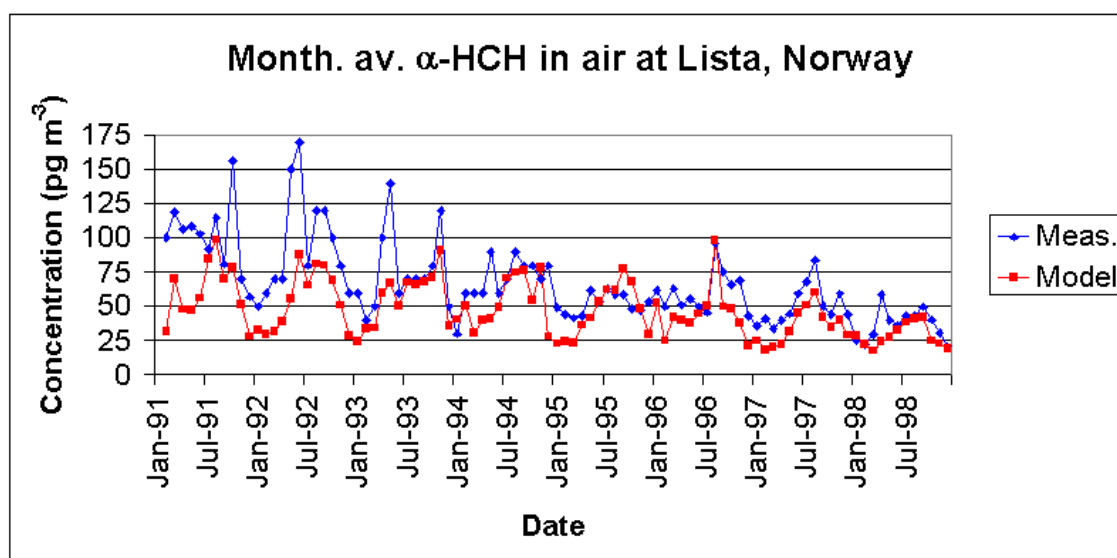


Figure 7.32: Measured and modelled concentrations at Lista, Norway.

surface ocean module is sufficient to capture the dynamics of the air-water exchange in this area.

### Rörvik, Sweden

The Rörvik sampling station is situated on the Swedish west coast in a mainly forested area (30% coniferous, 10% deciduous, and 28% grassland) with some farm land ( $\sim 20\%$ ) [EMEP, 2005]. From this station there are a few data from campaigns conducted in spring 1991 and 1992. Continuous air monitoring was started in winter 1994 with one monthly sample integrated over seven days. The measured  $\alpha$ -HCH air concentrations for Rörvik are plotted against the predicted concentrations in the left part of Figure 7.34. The measured and predicted concentrations correlates ( $r = 0.56$ ,  $p < 0.001$ ), but the model appear to almost consistently overestimate the measured concentrations.

The 11 results from the early measurement campaigns are plotted together with the corresponding predicted concentrations as a bar-plot in Figure 7.35. There are generally good agreement between measured and predicted concentrations for these data. One measured concentration is about a factor two higher than the corresponding predicted concentration, and higher than the other measured values as well, which could be due to a transport episode not captured by the model. For three of the first four samples the model predicts up to a factor of three higher concentrations than measured. As this is in the beginning of the simulated period, it could derive from re-volatilisation from the nearby oceans and thus indicate that the initial ocean concentration used as input is too high in this area. This will be investigated in detail in section 7.3.

The measured and predicted concentrations from 1994 and onwards are plotted as time series in Figure 7.36. The predicted concentrations are in good agreement with the measured concentrations during winter but not during the rest of the year. A clear seasonal

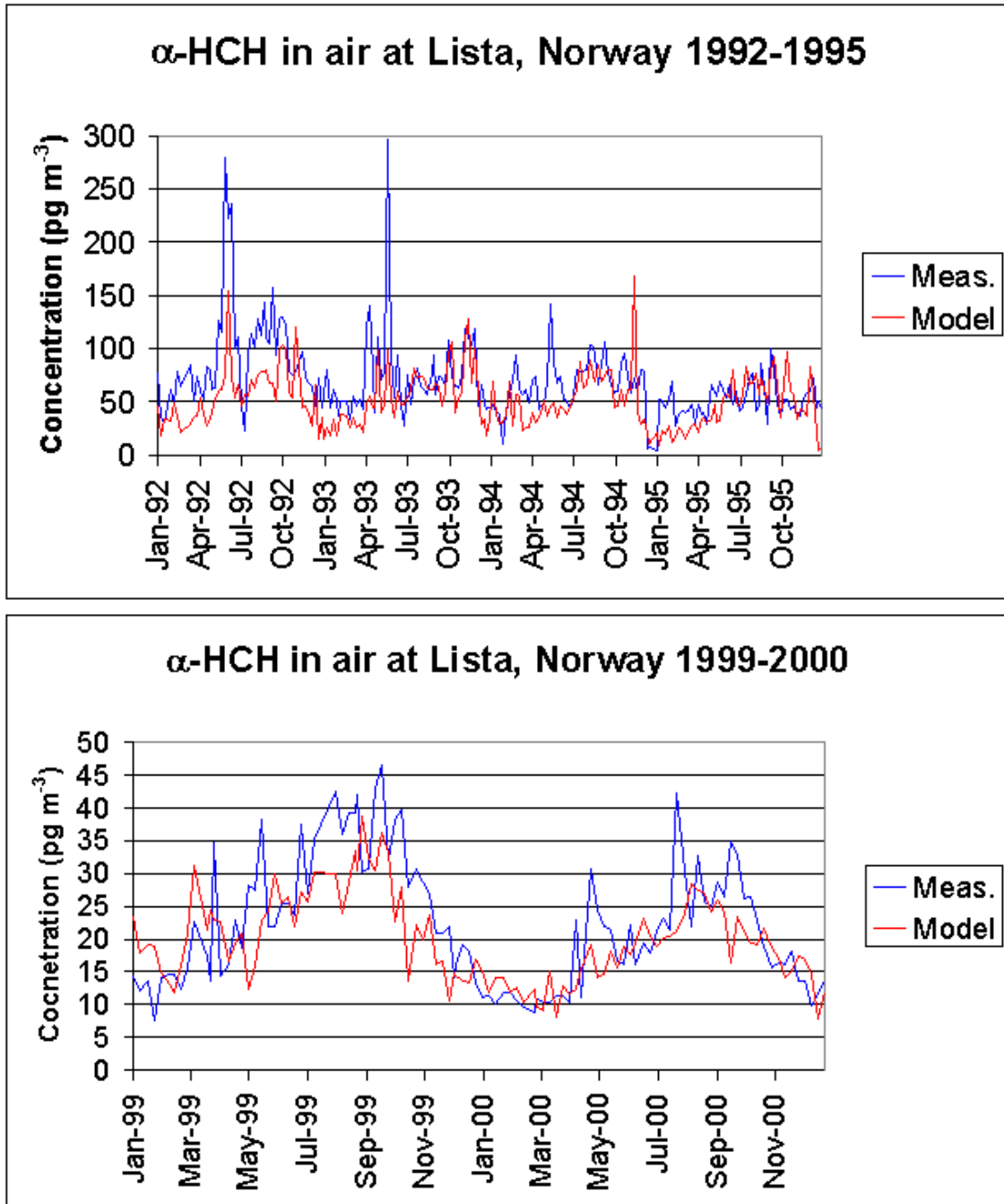


Figure 7.33: Measured and modelled concentrations at Lista, Norway.

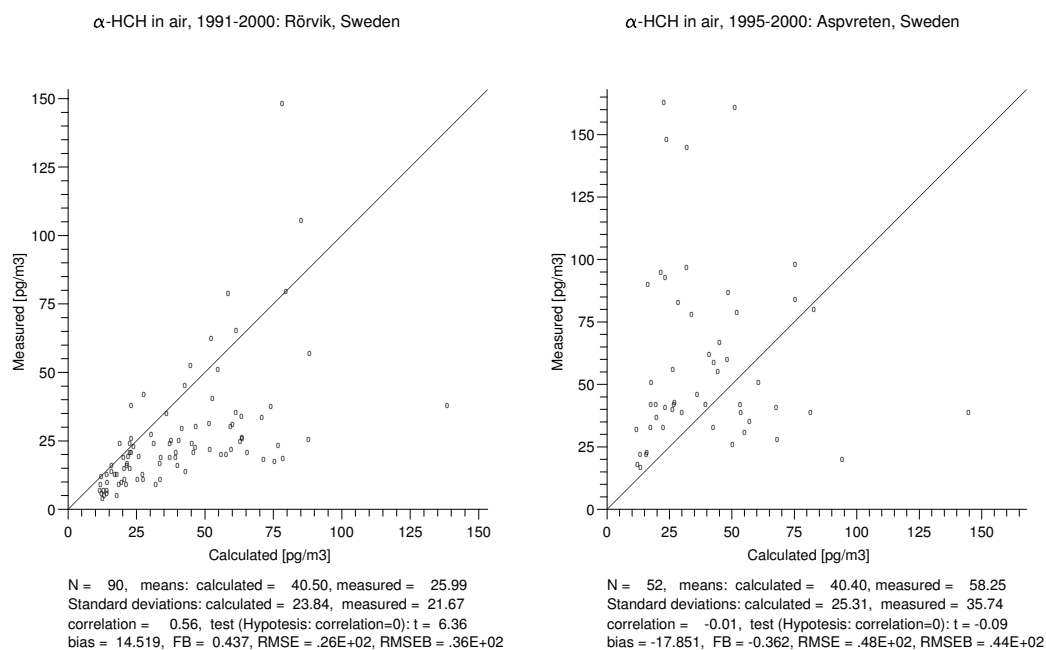


Figure 7.34: Measured  $\alpha$ -HCH air concentrations plotted against predicted concentrations for Rörvik, Sweden (left) and Aspveten, Sweden (right).

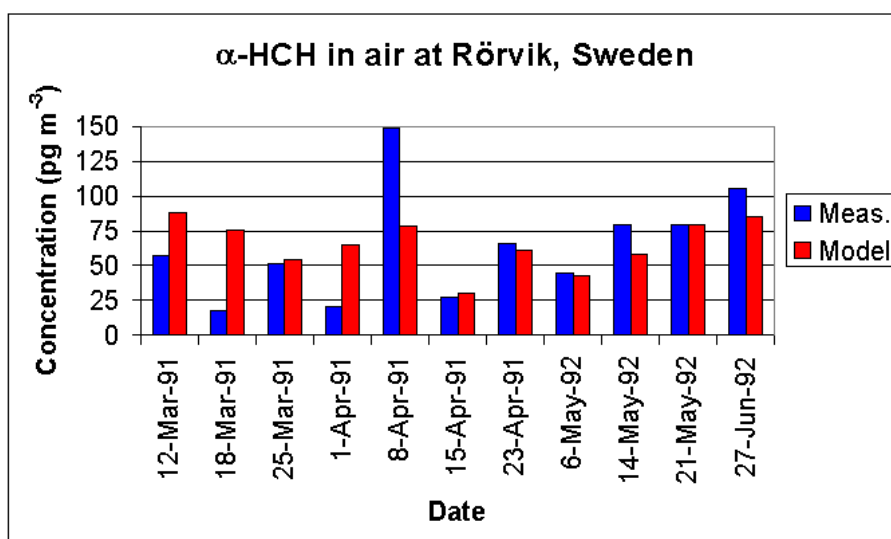


Figure 7.35: Measured and modelled concentrations at Rörvik, Sweden for the years 1991 and 1992.

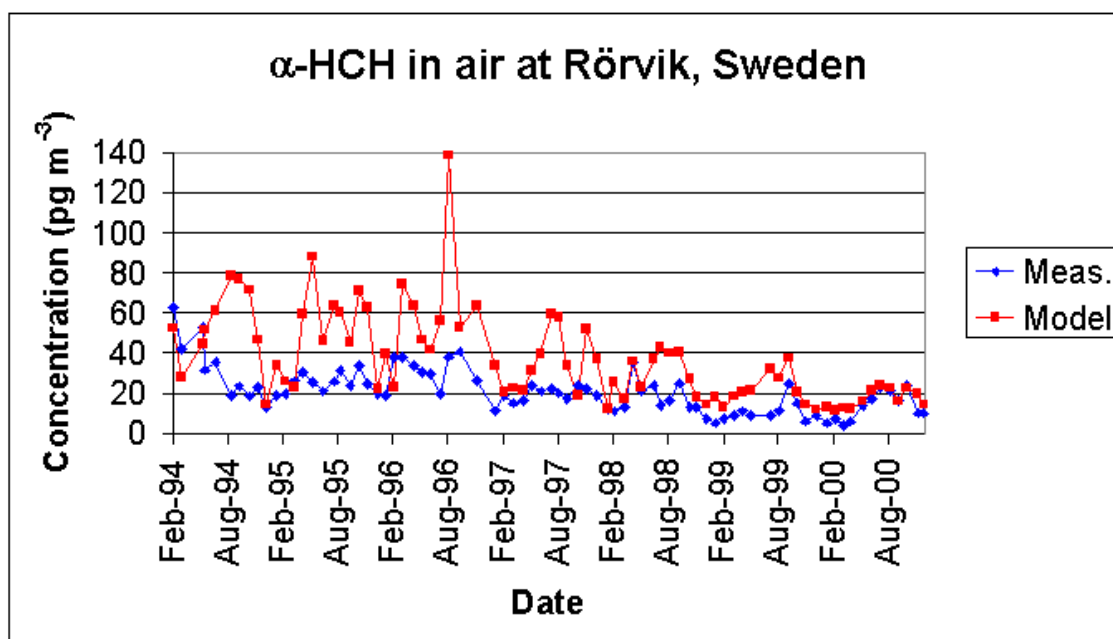


Figure 7.36: Measured and modelled concentrations at Rörvik, Sweden for the year 1994 and onwards.

pattern is seen in the predicted concentrations with higher concentrations during summer than during winter. This pattern is absent in the measured concentrations, that display no or only a weak seasonal patterns. The seasonal pattern in the modelled concentrations become less distinct in the end of the simulated period, and in the last year there is very good agreement between the measured and predicted concentrations. That the agreement between the measured and modelled concentrations improves over the simulated period indicates that the difference arise from a source (direct or indirect) that reduces with time.

The higher predicted than measured concentrations can indicate that the emissions and/or initial ocean concentrations are too high or that there is a strong local sink not accounted for by the model. There are local emissions in Sweden (see Figure 5.2 on page 69), but they are very low and thus not probable to give rise to the predicted results. That more distant but influencing emissions should affect the concentrations consistently are not very probable either, especially when the results from the nearby Lista station is taken into account, which indicates that the fraction of emissions reaching this area are well estimated. The initial ocean concentration in the surrounding oceans may be too large. When studying the initial ocean concentration (Figure 5.4 on page 72) it is seen that the concentration in the Baltic Sea is large compared to the concentration in the surrounding oceans. Furthermore, the concentration in the Baltic Sea is estimated from one measurement only, and it is thus not very certain. This will be investigated in more detail in section 7.3. The vegetated area surrounding the station may act as a sink to the  $\alpha$ -HCH air concentrations. Given the simplicity of the vegetation module included in DEHM-POP it may not account properly for this effect. The effect of the vegetation compartment will be investigated in more detail in section 7.4.

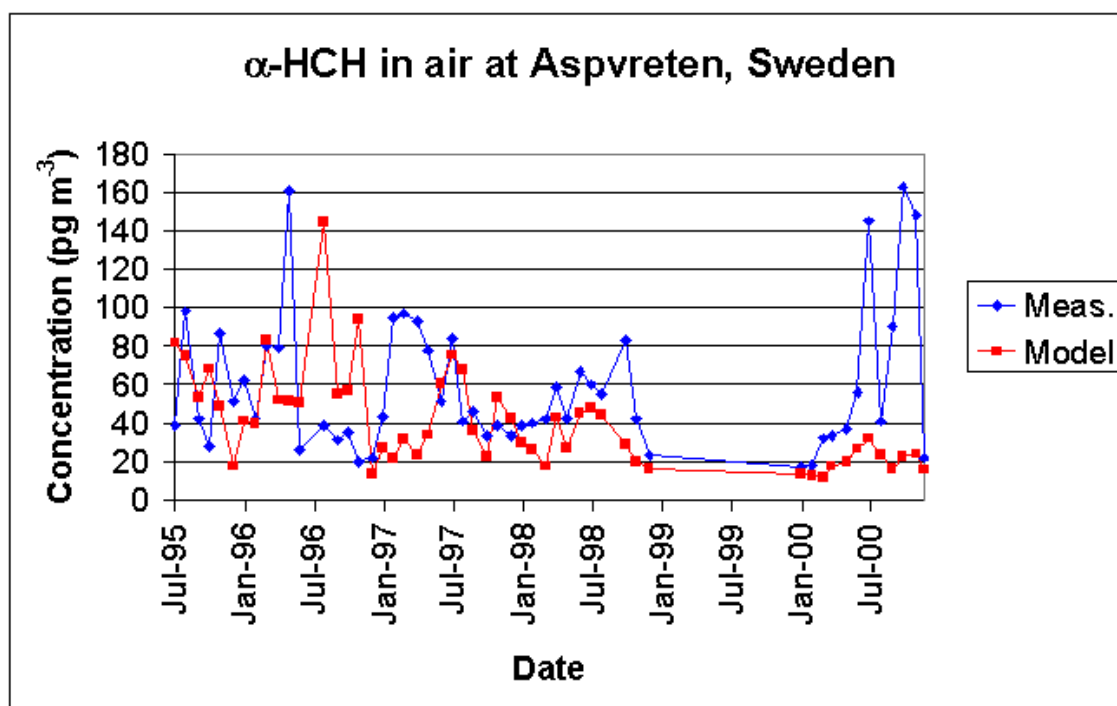


Figure 7.37: Measured and modelled concentrations at Aspvreten, Sweden.

### Aspvreten, Sweden

Aspvreten is situated on the Swedish east coast close to the Baltic Sea, although no information about the surroundings is given [EMEP, 2005]. As for the other Swedish station there is one monthly sample integrated over seven days. The sampling started in the summer of 1995, and there are no data from 1999. The measured  $\alpha$ -HCH air concentrations at Aspvreten are plotted against predicted concentrations in the right side of Figure 7.34. The measured concentrations are on average higher than the predicted, and there is no correlation between measured and predicted concentrations.

The measured and predicted concentrations from Aspvreten are plotted as time series in Figure 7.37. The model generally predicts higher concentrations during summer than winter, whereas there do not appear to be a consistent seasonal pattern in the measured concentrations. In 1996 and 1997, the measured concentrations peak during spring and in 1998 the highest concentrations are found in autumn. Three of the highest four measured concentrations at this station are measured in the summer and autumn of the last simulated year. This is an opposite trend than at all other stations in this study and it could indicate input from fresh usage of local or regional origin, although it is highly unlikely since technical HCH has been banned in the surrounding countries, at least for several years.

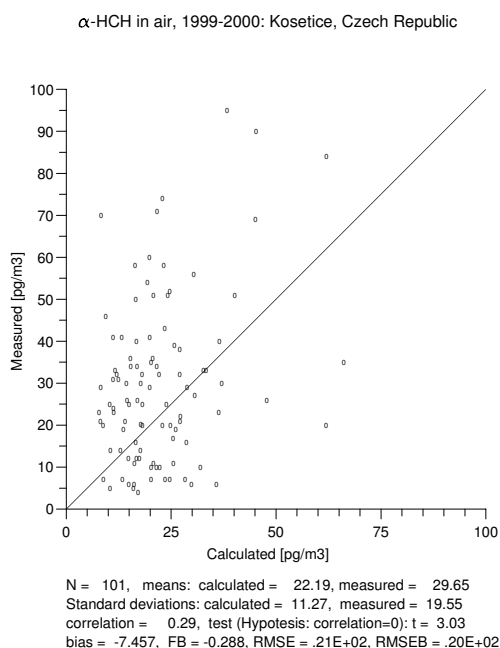


Figure 7.38: Measured  $\alpha$ -HCH air concentrations plotted against predicted concentrations for Košetice, Czech Republic.

### Košetice, Czech Republic

Košetice is situated in an agricultural area in the Czech-Moravian Highlands, about 80 km south-east of Prague, Czech Republic. The main surroundings consist of farmed land ( $\sim 2/3$ ) and forest ( $\sim 1/3$ ) [EMEP, 2005]. Only measurements from the last two years of the simulated period were available for this study. The measured  $\alpha$ -HCH air concentrations for Košetice are plotted against the predicted concentrations in Figure 7.38. There is a low but statistical significant correlation between measured and predicted air concentrations ( $r = 0.29$ ,  $p < 0.01$ ). The model is seen to under-predict most of the measured concentrations. The measured and predicted concentrations from Košetice are plotted as time series in Figure 7.39. The measured and predicted concentrations display two different patterns. The measurements display highest concentrations in spring, whereas the predicted concentrations peak in autumn. The sample-to-sample variability is much larger in the first year than in the second for both measured and predicted air concentrations, and the model is seen to capture most of the variability, although the levels are not of the same magnitude as the measurements. There is a strong decreasing trend in the measured concentrations from 1999 to 2000. The predicted concentrations also decrease, but not to the same extent as the measurements.

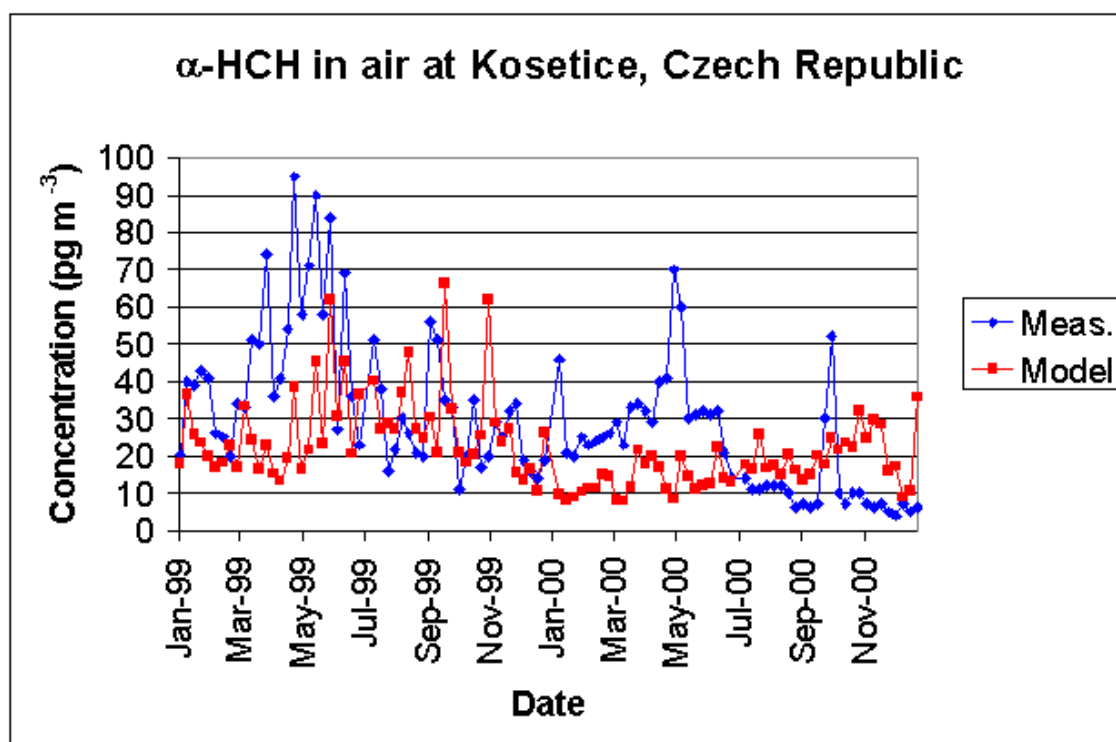


Figure 7.39: Measured and modelled concentrations at Košetice, Czech Republic.

### 7.2.6 Stations in the Arctic

Eight of the measurement stations are considered to belong to the Arctic in this study, one in Iceland, one in northern Finland, one on Svalbard, two stations in northern Russia, and three Canadian stations. The most southerly is the Canadian station Tagish on approximately 60°N.

#### Stórhöfði, Iceland

The Stórhöfði station is placed on a small island south of the main Iceland island. No information on the surroundings of the station is given [EMEP, 2005]. The measured α-HCH air concentrations are plotted against predicted concentrations in Figure 7.40. There is no correlation between measured and modelled α-HCH air concentrations at Stórhöfði, with the model over-predicting most of the measured concentrations. This is confirmed when studying the time series for the station, plotted in Figure 7.41. The predicted concentrations are relatively close to the measured in a short period during winter. However, the modelled concentrations display a clear seasonal cycle with high concentrations during summer and low during winter, whereas the measured concentrations peak in spring and/or autumn.

This pattern could indicate either that the emission data and/or the initial ocean concentrations used as input are too high in the area influencing the Icelandic station. There are local emissions at Iceland (see Figure 5.2 on page 69), but they are very low.

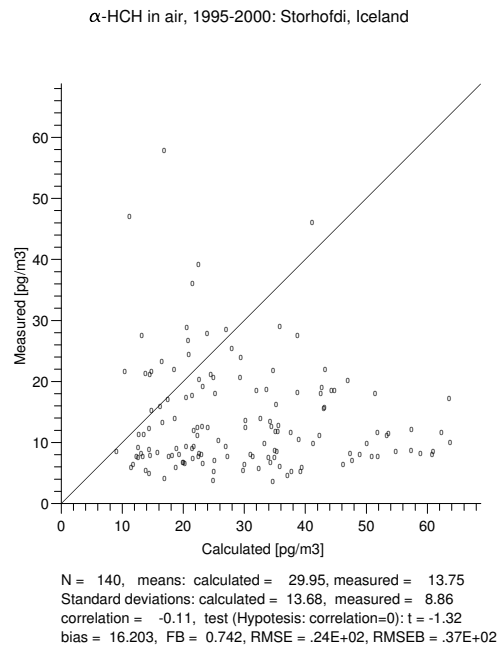


Figure 7.40: Measured α-HCH air concentrations plotted against predicted concentrations for Stórhöfði, Iceland.

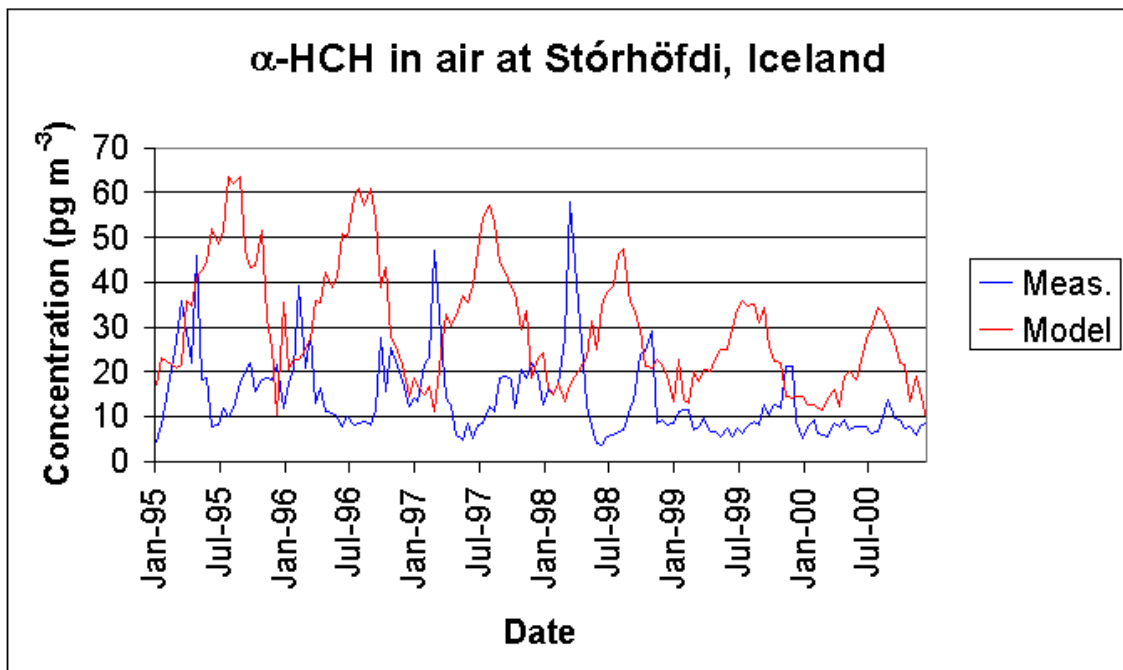


Figure 7.41: Measured and modelled concentrations at Stórhöfði, Iceland.

When studying the monthly averaged air concentrations (Figures 7.3 on page 84 and 7.4 on page 85), it can be seen that the air concentrations over Iceland generally are not higher than the surrounding areas, which suggests that the local primary emissions are not the major source of the air concentrations. Only in October 1998, there appear to be slightly higher concentrations over Iceland than over the surrounding area, but this is not repeated for other years (not shown). The source areas closest to Iceland is Europe and North America. Results from the European stations indicates that the emissions from this area are well estimated (see section 7.2.5), and the results from the North American stations around the Great Lakes and from Québec indicates that the emissions may be underestimated (see sections 7.2.3 and 7.2.4). It is therefore highly unlikely that the emission data are the reason for the higher predicted concentrations than measured. A strong re-volatilisation from the oceans surrounding Iceland could result in elevated predicted concentrations. Re-volatilisation from the surrounding oceans probably supports the air concentrations in the model, however, the water concentrations in the North Atlantic are relatively low in the last half of the modelled period ( $< 2 \text{ ng L}^{-1}$ ), and it is not a likely source for the much higher predicted than measured summer concentrations. However, this will be investigated in more detail in section 7.3. The discrepancy between predicted and measured air concentrations could also be explained by the presence of a strong local sink not included in the model, but it is difficult to suggest what medium it could be and thus not very likely.

There is also a possibility of sampling artifacts at the station. At Stórhöfði the samples are collected over 14 days, which is the longest sampling time for the stations in this study. Recent measurements in Nuuk, Greenland also applied 14 days sampling time [Skov *et al.*, 2005]. Considerable breakthrough (i.e. measurable concentrations on the backup sampling medium) was observed for the more volatile compounds, including  $\alpha$ -HCH, and in some cases higher concentrations were measured at the backup sampling medium than on the first sampling medium, indicating significant loss [Skov *et al.*, 2005]. The breakthrough of  $\alpha$ -HCH was strongly temperature-dependent, with low breakthrough percentage in winter (less than 10%) and so high breakthrough percentage during summer months that it was not possible to estimate [Skov *et al.*, 2005]. If similar conditions are applied at Stórhöfði, the reported measurements from this station may thus be too low. The sampled air mass at Stórhöfði is  $1000 \text{ m}^3$  over the 14 days [EMEP, 2005], which is lower than the  $3500\text{--}4500 \text{ m}^3$  sampled at Nuuk [Skov *et al.*, 2005], and much lower than the  $11400 \text{ m}^3$  typically sampled at Alert [e.g. Halsall *et al.*, 1997]. As the probability of sample breakthrough is expected to be proportional to the sampled air volume, there should thus be a lower probability of sample breakthrough at Stórhöfði than at the other stations. However, the probability of sample breakthrough also depends on other factors, such as air temperature during sampling, the thickness of the sampling medium and the flow velocity [Skov, Personal communication], and the information about the sampling procedure at Stórhöfði are very sparse [see EMEP, 2005]. Possible sampling artifacts due to sample break-through can thus not be excluded from the available information, and until this has been examined in more detail, the results from Stórhöfði are excluded from further evaluation.

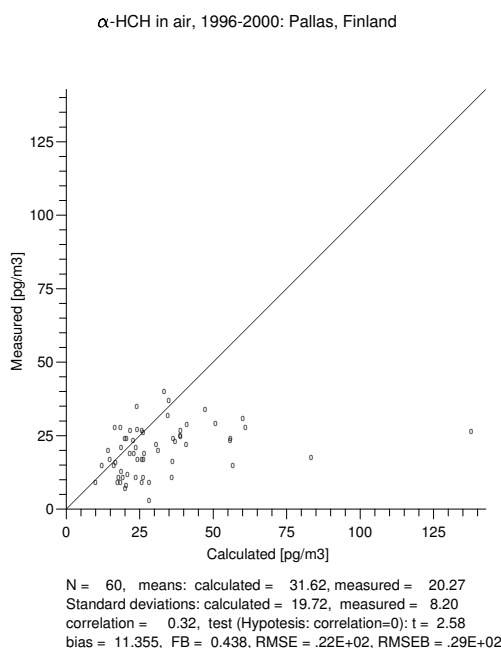


Figure 7.42: Measured  $\alpha$ -HCH air concentrations plotted against predicted concentrations for Pallas, Finland.

### Pallas, Finland

Pallas is situated in the Northern Finland. The measured  $\alpha$ -HCH air concentrations are plotted against predicted concentrations in Figure 7.42. The correlation between measured and predicted concentrations is low, and the statistical significance is also low ( $r = 0.32$ ,  $p < 0.02$ ), with the predicted concentrations generally higher than the measured. The measured and predicted concentrations from Pallas are plotted as time series in Figure 7.43. In the measurements there is a seasonal pattern with highest concentrations generally observed in the summer months, although there is some scatter in the data. The seasonal pattern in the predicted concentrations is less distinct, although the lowest predicted concentrations generally occur during winter, high concentrations are predicted not only in summer, but also in late autumn. The predicted concentrations are much higher than the measured for the first year, whereas the levels are closer for the last four simulated years.

### Russian stations

$\alpha$ -HCH has been sampled in air at two stations in northern Russia, Dunai Island and Amderma on the coast of the Arctic Ocean.

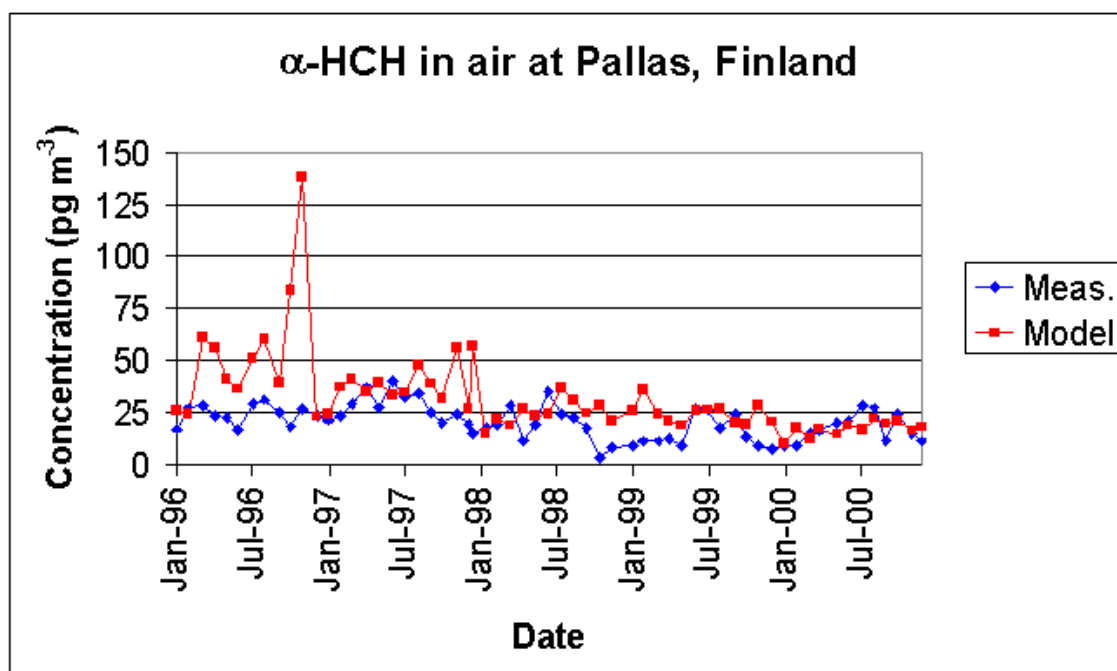


Figure 7.43: Measured and modelled concentrations at Pallas, Finland.

### Dunai Island

The station at Dunai Island was operated from March 1993 to April 1995. The measured  $\alpha$ -HCH air concentrations are plotted against predicted concentrations in the left part of Figure 7.44. There is a low but statistical significant correlation between measured and predicted concentrations ( $r = 0.36$ ,  $p < 0.001$ ), with a tendency of higher predicted concentrations than measured. The measured and predicted concentrations from Dunai Island are plotted as time series in Figure 7.45. Highest concentrations are observed in spring, with lowest concentrations found during summer. The predicted concentrations also peak in spring and decrease in early summer, however, the concentrations increase through the summer to reach a second peak in autumn, after which it decreases again. Good agreement is seen between measured and predicted concentrations during winter and spring, whereas the model predicts higher concentrations than measured during summer and autumn.

The observed spring peak could indicate fresh usage connected to the agricultural season at middle to high latitudes. It could also be the result of release of  $\alpha$ -HCH from a melting snowpack, although the temperature only increase to values above  $0^{\circ}\text{C}$  in June, and thus later in the year [Hung *et al.*, 2005].

### Amderma

The Amderma station was operated from April 1999 to the end of the simulated period. The measured  $\alpha$ -HCH air concentrations are plotted against predicted concentrations in the right side of Figure 7.44. There is no correlation between the measured and predicted

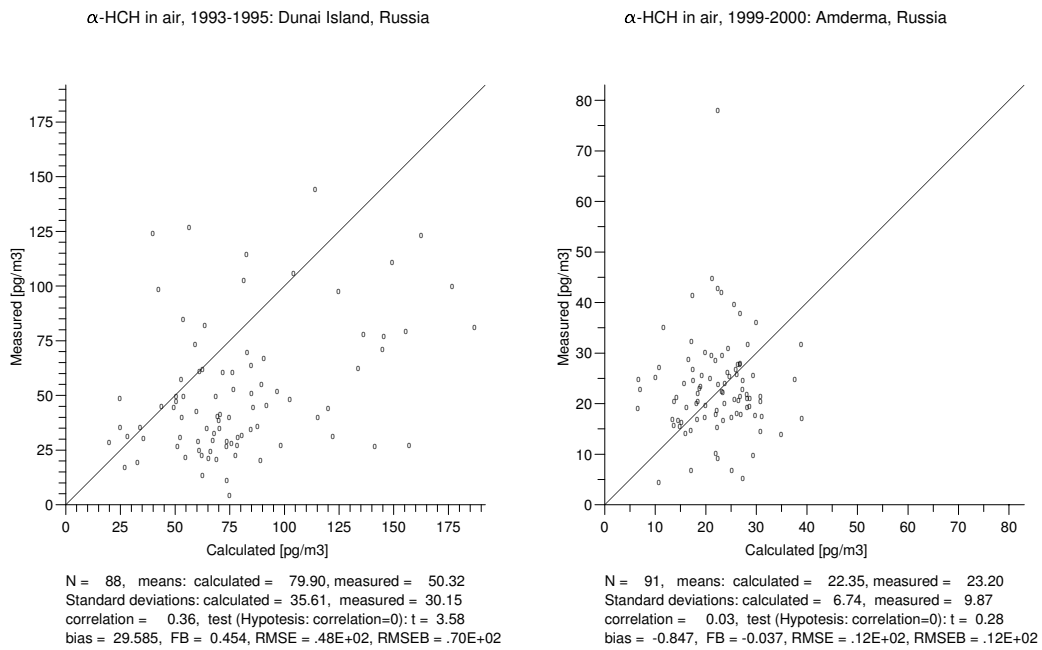


Figure 7.44: Measured  $\alpha$ -HCH air concentrations plotted against predicted concentrations for the Russian stations Dunai Island (left) and Amderma (right).

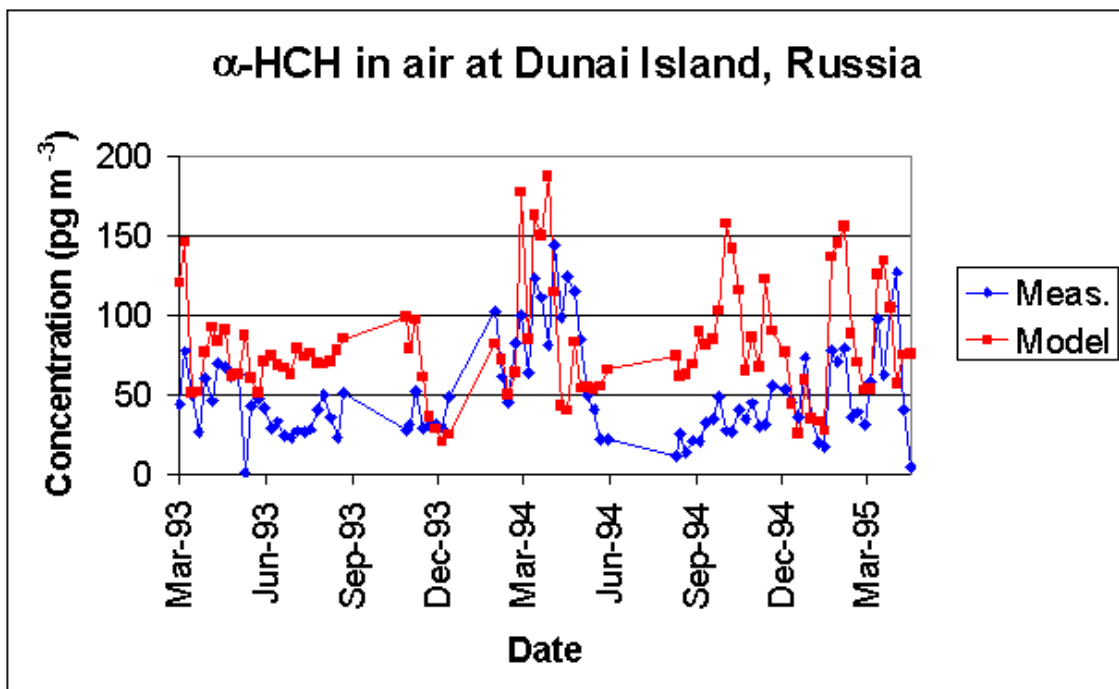


Figure 7.45: Measured and modelled concentrations at Dunai Island, Russia.

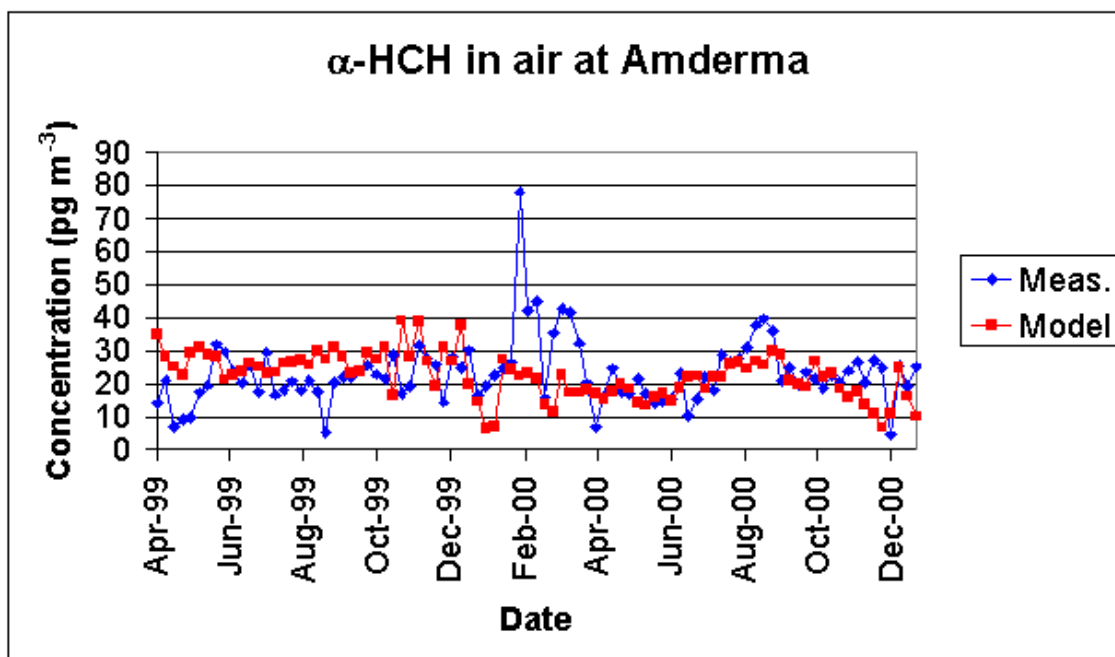


Figure 7.46: Measured and modelled concentrations at Amderma, Russia.

concentrations. The total average concentration is nearly the same, although the variability is higher in the measured than in the predicted concentrations. The measured and predicted concentrations from Amderma are also plotted as time series in Figure 7.46. There is apparently no clear seasonal pattern in either measured or predicted concentrations. The variability is seen to be lower for this station than for Dunai Island for both measured and predicted concentrations. This is probably due to the time of the sampling, where Dunai Island is sampled in the first part of the simulated period and Amderma in the end. It also follows the general pattern in the simulated period with decreasing variability at all stations, which reflects the decreasing primary emissions through the simulation and thus the shift in sources from a few distinct primary sources to the more diffusive secondary source of re-volatilisation from previously deposited chemicals.

### Svalbard

The station at Svalbard is placed on the Zeppelin Mountain, 474 m above sea level, on the northern part of the island Spitsbergen. The surroundings consist of 100% gravel and stone [EMEP, 2005]. The measured α-HCH air concentrations are plotted against predicted concentrations in Figure 7.47. There is a low but statistically significant correlation between measured and predicted concentrations ( $r = 0.35$ ,  $p < 0.001$ ). The model is seen to generally under-predict the measured concentrations. The measured and predicted concentrations from Spitsbergen are plotted as time series in Figure 7.48. There is a large variability in the measured concentrations, especially in the first years, and there is apparently not any seasonal pattern, except towards the end of the simulated period,

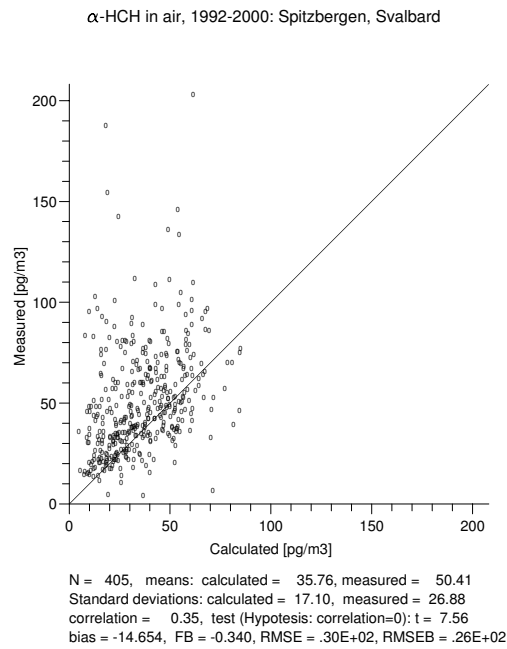


Figure 7.47: Measured  $\alpha$ -HCH air concentrations plotted against predicted concentrations for Spitzbergen, Svalbard.

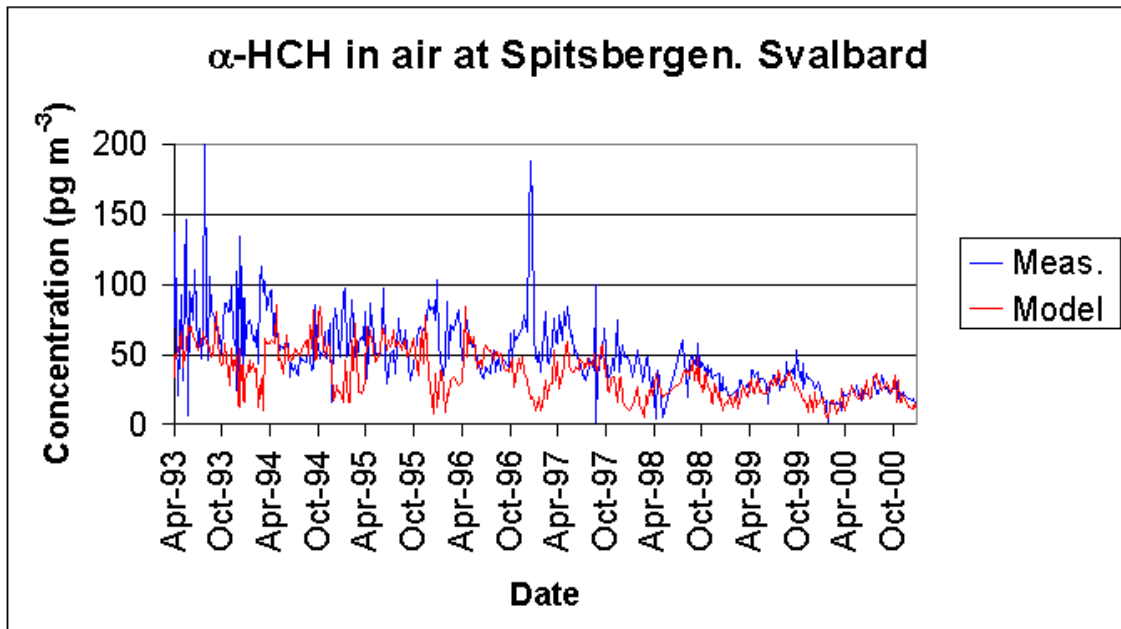


Figure 7.48: Measured and modelled concentrations at Spitzbergen, Svalbard, Norway.

where there are higher concentrations during summer than winter. In the model results, there is a clear seasonal pattern with high concentrations during summer, and low concentrations predicted during winter. The predicted concentrations are in good agreement with the measured concentrations during summer, but too low for the rest of the year. This is opposed to the results from stations at lower latitudes, where the best agreement between measured and predicted concentrations is found during winter. The predicted concentrations approaches the measured towards the end of the simulated period, and good agreement is seen particularly in the last year.

The discrepancy between measured and predicted concentrations indicates either a source not accounted for in the model, or a too strong sink. The emission data used in the model may be too low for the former Soviet Union (see section 5.3 on page 67), and this could influence the predicted concentrations at Svalbard. However, the results from the Russian stations (see section above) do not indicate too low emissions. Furthermore, the eventual missing emissions are expected to occur during summer, where the predicted and modelled concentrations are in good agreement, rather than in winter, where the predicted concentrations are too low. The presented results for the snowpack distribution (see section 7.1.5) indicate that the sea ice coverage is too large. Furthermore, the fraction of open water is kept constant at 5%, which may be under-predicted in the marginal ice zone close to Svalbard. If the predicted sea ice coverage is too high this may reduce an eventual re-volatilisation from the oceans, although this process during winter is doubtful due to the low temperatures.

There is also a possibility that the snowpack module is too efficient in retaining the  $\alpha$ -HCH during winter. The model experiments presented by *Daly and Wania* [2004] resulted in lower  $\alpha$ -HCH air concentrations during winter when including a snowpack module in a multi-compartment mass balance model. The DEHM-POP snowpack module is furthermore seen to efficiently retain  $\alpha$ -HCH in the 'off-line' version [*Hansen et al.*, 2006b]. A too efficient snowpack module would result in lower predicted winter  $\alpha$ -HCH air concentrations than measured. This will be investigated in more detail in section 7.5.

### Canadian stations

Three Canadian stations were established within the framework of the Northern Contaminants Program: Alert, Tagish and Kinngait. Of these stations, Alert has been operated continuously since 1992 and the two other stations were operated for shorter periods.

#### Alert

Alert is the northernmost station in this study, situated on the east part of Ellesmere Island in Nunavut, Canada. Data from the beginning of the sampling in 1992 up to 1998 were available for this study. The data from Alert for 1992 exceed certain quality control criteria, as discussed by *Stern et al.* [1997]. They are however included in the evaluation in this study to increase the number of measurements. There are no correlation between measured and predicted  $\alpha$ -HCH air concentrations (see Figure 7.49). Although the bias is slightly negative, the model do not appear to consistently over- or under-predict the measured concentrations. The measured and predicted concentrations from Alert are plotted as time series in Figure 7.50. There is a clear seasonal pattern in the predicted air concentrations with higher concentrations during summer than during winter.

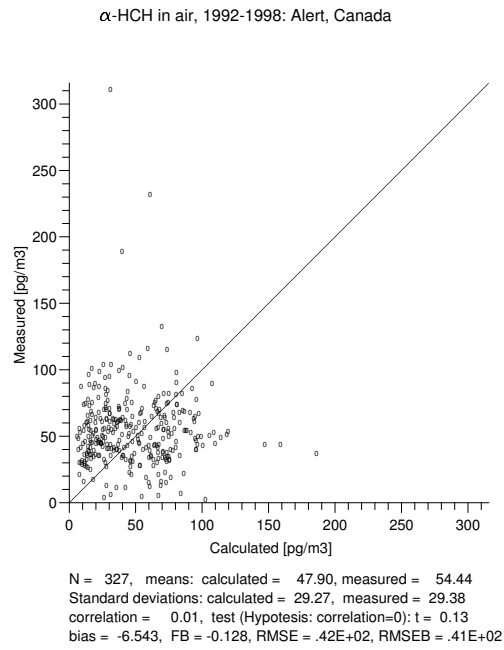


Figure 7.49: Measured α-HCH air concentrations plotted against predicted concentrations for Alert, Canada.

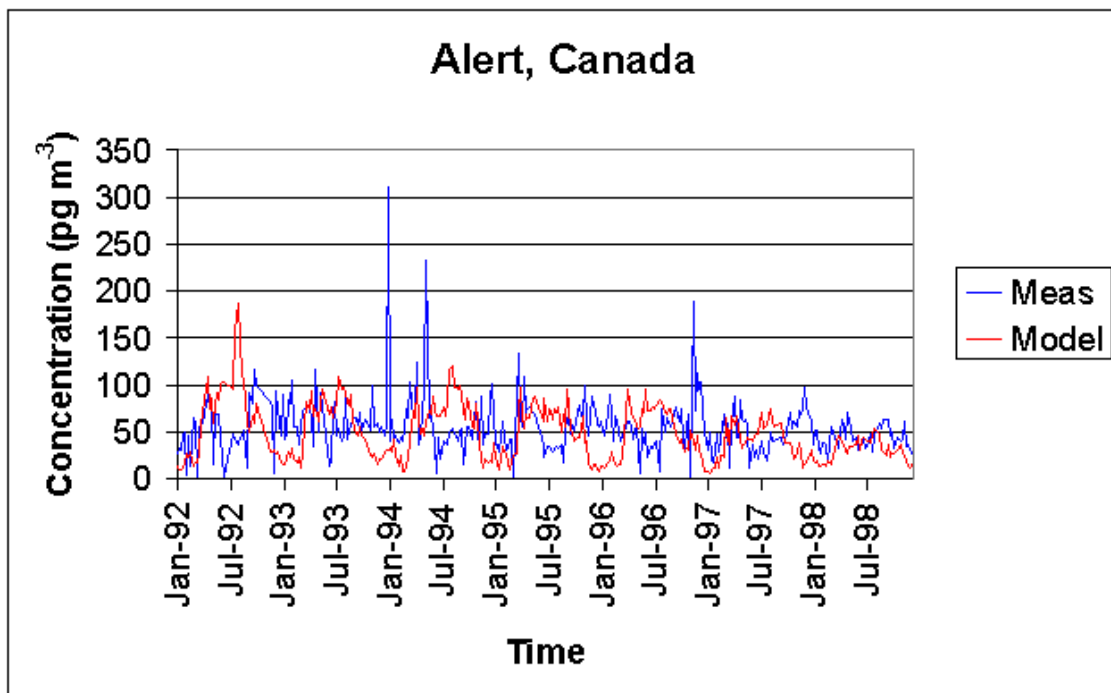


Figure 7.50: Measured and modelled α-HCH air concentrations for Alert, Canada.

This opposes the measured air concentrations, that show a bi-modal pattern with highest concentrations in spring and autumn [Hung *et al.*, 2002, 2005]. The model tend to predict too high concentrations during summer and too low concentrations during winter. But in spring, and to a lesser extent in autumn, there is a better agreement between measured and predicted concentrations for most of the years, and a few distinct features in the measured data series appear to be captured by the model, e.g. in spring in 1992, 1994, 1995, and 1997. The predicted seasonal pattern indicates either that the included emissions are too high during summer, that there is a too strong source in summer and a too strong sink in winter in the model, and/or that there are local features that acts as a sink in summer and as a source in winter.

Several potential factors can give rise to the observed bi-modal seasonal pattern, although mostly the spring peak has been discussed [Hung *et al.*, 2005]. The spring peak has been suggested to arise from fresh usage [Halsall *et al.*, 1998; Hung *et al.*, 2002], however, the peak is also observed for banned pesticides and industrial compounds and this explanation is thus less likely [Hung *et al.*, 2005]. The ‘spring pulse’, i.e. the release of contaminants collected through the winter season by snow melt, may also give rise to higher spring concentrations, but the melt season does not coincides with the elevated concentrations in the Canadian Arctic [Hung *et al.*, 2005]. Snow melt at lower latitudes can though not be ruled out as a possible source for a spring peak [Hung *et al.*, 2005]. Increased atmospheric removal in late spring/summer is also suggested as possible influence of the observed seasonal pattern, but varying patterns at different stations and for different compounds render this less likely [Hung *et al.*, 2005]. It is also suggested that forests along the transport path to the Arctic may scavenge POPs increasingly after leaf burst in spring, and thus reduce the amount transported into the Arctic [Hung *et al.*, 2005]. It is probably not possible to single out one process that can account for the observed seasonal pattern, which may be a result of a combination of the all of the above mentioned processes [Hung *et al.*, 2005].

Several processes in the model may explain the discrepancy between measured and predicted  $\alpha$ -HCH air concentrations, i.e. emissions, initial environmental concentrations, and/or processes. There are no local emissions around Alert in the emission data, and the results from the other stations discussed in previous sections makes it unlikely that the predicted summer peak arise from too high emissions elsewhere. The initial ocean concentration is highest in the Arctic Ocean around Alert. This can lead to re-volatilisation, especially in the relatively warm summer months. If the ocean concentration in the model is too high compared to the actual concentration this can create a summer top. This will be investigated in more detail in section 7.3. As for the results from Svalbard, the lower predicted concentrations than measured during winter, may be explained if the snowpack module retains  $\alpha$ -HCH too efficiently. This will be examined in section 7.5.

### Tagish

Tagish is placed in the western part of Canada, not far from the Pacific Ocean. The station was operated from December 1992 to April 1995. The measured  $\alpha$ -HCH air concentrations are plotted against predicted concentrations in the left side of Figure 7.51. There are no correlation between the measured and predicted air concentrations, and the model tend to over-predict the majority of the measured values. The measured and predicted concentra-

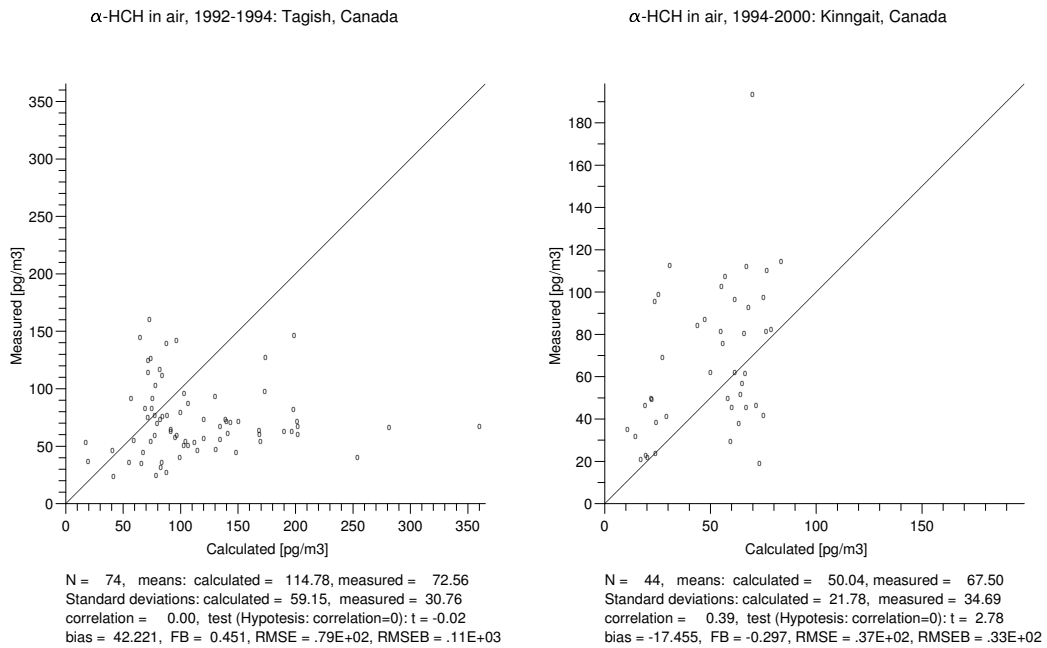


Figure 7.51: Measured  $\alpha$ -HCH air concentrations plotted against predicted concentrations for Tagish (left) and Kinngait (right).

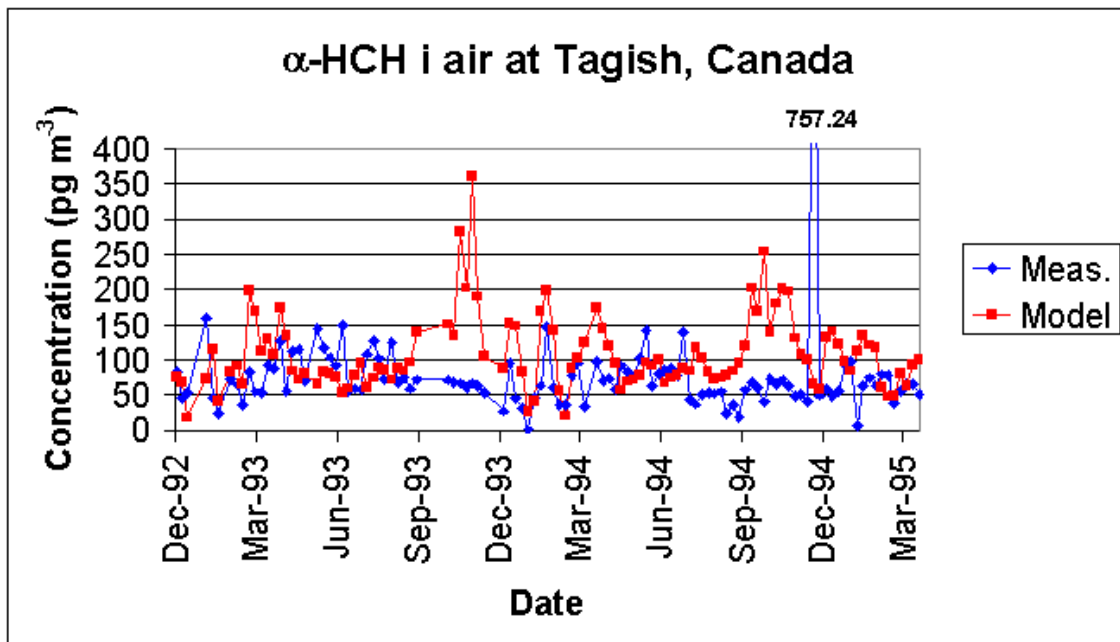


Figure 7.52: Measured and modelled  $\alpha$ -HCH air concentrations for Tagish, Canada.

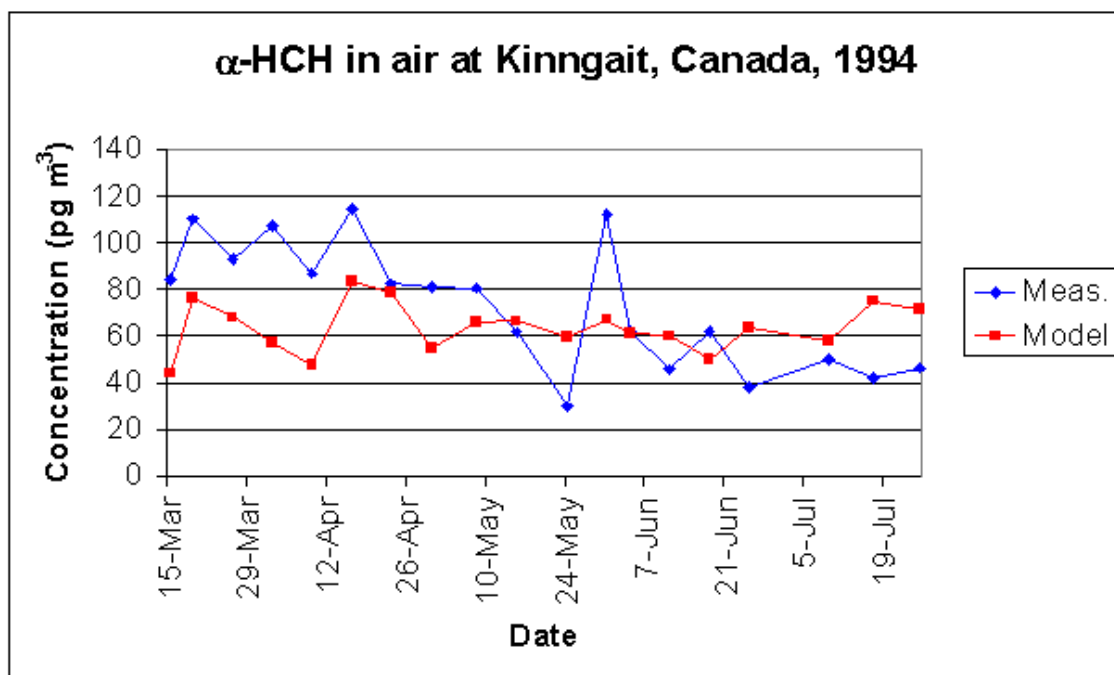


Figure 7.53: Measured and modelled  $\alpha$ -HCH air concentrations for Kinngait, Canada.

tions from Tagish are plotted as time series in Figure 7.52. They are generally of the same levels, except in late autumn (October–November), where the predicted concentrations are up to a factor of 5 higher than the measured. This could indicate re-volatilisation from the close-by Pacific Ocean, which have relatively high concentrations through the simulated period. However, re-volatilisation from the oceans are expected to be highest in summer and early autumn. Another possible explanation is that the high concentrations are associated with the initiation of the snowpack season. This will be investigated in detail in section 7.5.

### Kinngait

The station at Kinngait (Cape Dorset) was operated in two different periods, from March 1994 to February 1996 and again from October 2000 and onwards. The measured  $\alpha$ -HCH air concentrations are plotted against predicted concentrations in the right side of Figure 7.51. The correlation between measured and modelled air concentrations is low and the statistical significance is also low ( $r = 0.39$ ,  $p < 0.01$ ). Most concentrations are under-predicted by the model. The measurements at Kinngait were made once a week. However, 16 of the reported values are from four combined samples. The time series are therefore plotted in three plots. The reported weekly measured and corresponding predicted values from the beginning of the sample period are plotted in Figures 7.53, the combined samples from August 1994 to February 1996 are plotted in Figure 7.54, and the results from year 2000, also weekly samples, are plotted in Figure 7.55. It is difficult to distinguish any seasonal trends in either measured or modelled concentrations or any

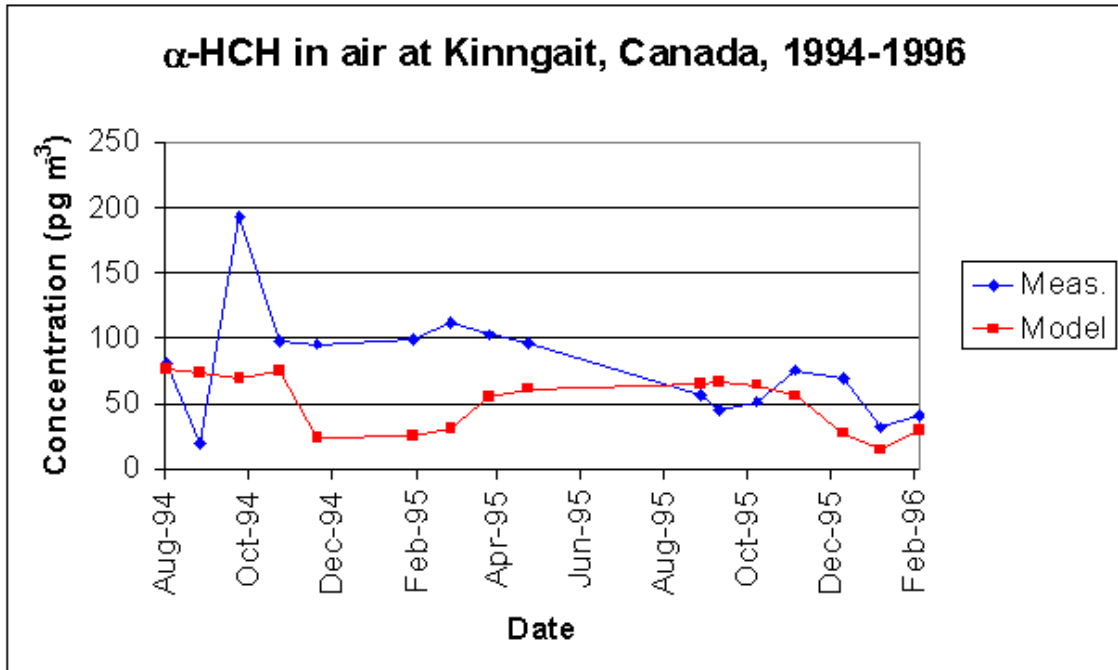


Figure 7.54: Measured and modelled  $\alpha$ -HCH air concentrations for Kinngait, Canada.

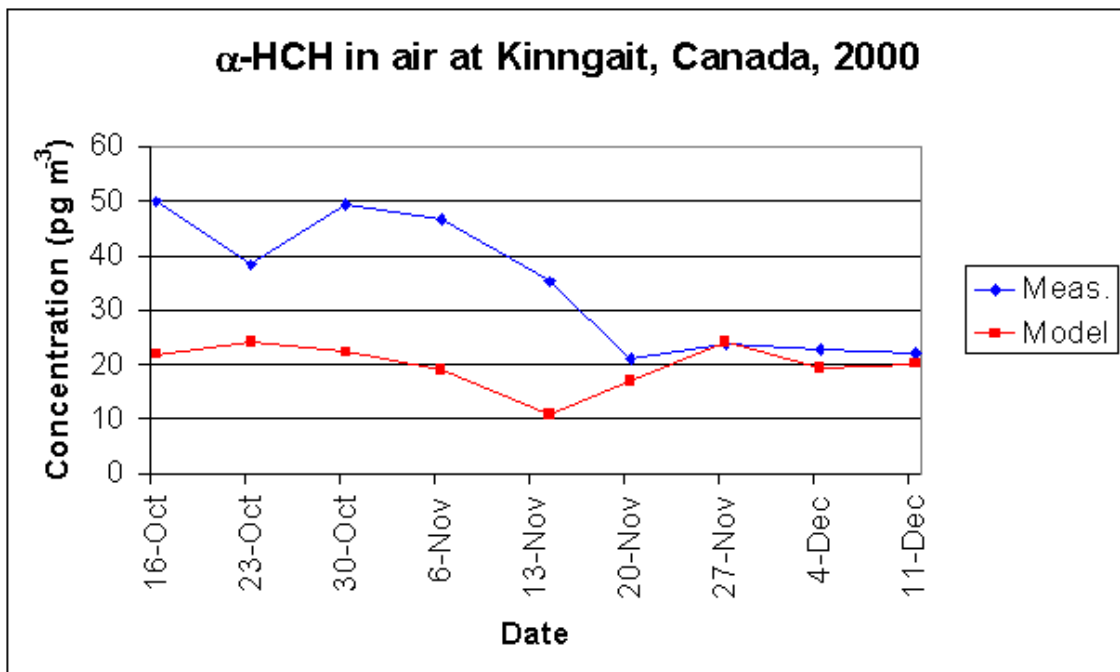


Figure 7.55: Measured and modelled  $\alpha$ -HCH air concentrations for Kinngait, Canada.

patterns in the relationship between the measured and predicted results, e.g. consistently higher concentrations in one period than another due to the low number of results.

### 7.2.7 Vertical distribution

The vertical  $\alpha$ -HCH distribution can not be evaluated directly, since there are only a few studies of the distribution of POPs with height in the atmosphere, and none of these are conducted within the simulated period.

One of the studies of the vertical distribution of POPs is an airplane study, in which air samples were taken from an airplane in different height intervals up to about 3 km over Bermuda, over the western North Atlantic Ocean, and over the Adirondack Mountains (East of Lake Ontario), New York, US in the late 1980s [Knap and Binkley, 1991]. The conclusion from the study is that there is a large variability due to time, meteorological events and location, but that the measured compounds generally appear to be well mixed in the atmosphere and that the ground-level and higher-altitude concentrations were similar in magnitude [Knap and Binkley, 1991]. Increasing  $\alpha$ -HCH concentrations with height are observed in most of the samples from Bermuda [Knap and Binkley, 1991]. This is not seen in the monthly averaged predicted concentrations in that particularly area, but in another remote area over the Pacific Ocean.

In another study, rapidly equilibrating Polymer-coated glass (POG) passive air samplers were deployed at six different heights up to 360 m on the outside of the CN tower in Toronto, Canada in October 2001 to study the vertical distribution of POPs in the urban atmospheric boundary layer [Farrar *et al.*, 2005]. PAHs and PCBs generally displayed decreasing concentrations with height, indicating that the local urban surface is acting as a source to the air concentrations [Farrar *et al.*, 2005]. Unfortunately the vertical distribution pattern of  $\alpha$ -HCH is not evaluated, because the equilibration time of the POG samplers depends on  $K_{oa}$ , and the HCHs having low  $K_{oa}$  values had attained equilibrium so the measured concentrations may have been disturbed by short-term local meteorological events [Farrar *et al.*, 2005].

## 7.3 Importance of the ocean

For several of the studied stations questions about the influence of the  $\alpha$ -HCH residues in ocean for the predicted air concentrations were raised. The importance of the ocean concentrations is examined in this section, by comparing the results of the reference simulation with the results from a simulation in which the re-volatilisation from oceans is excluded, i.e. dry gas deposition (as well as wet deposition) to the water compartment is allowed in the model but an eventual re-volatilisation from the oceans is set to zero.

It should be noted that the air-surface exchange processes as well as the wet gas deposition process in DEHM-POP are non-linear, i.e. they depend on the gradient between the concentration in air and in another medium. The change of one process, resulting in alterations of the environmental concentrations, may thus also affect the behaviour of other processes in the model.

The general effect of excluding re-volatilisation is to decrease air concentrations for all stations in the model domain by more than a factor two. The difference increases towards the end of the simulated period. This highlight the importance of the secondary emissions

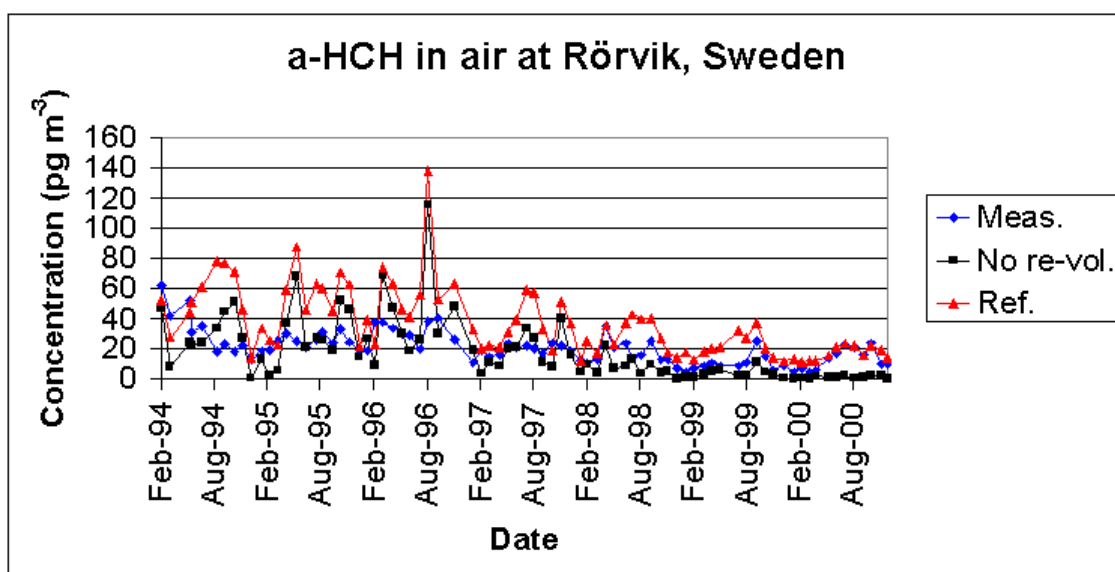


Figure 7.56: Measured  $\alpha$ -HCH air concentrations and predicted concentrations for the reference simulation and the simulation without re-volatilisation from oceans at Rörvik, Sweden.

(i.e. re-volatilisation of previously deposited  $\alpha$ -HCH) to support air concentrations in the simulated period, in which the primary emissions have decreased dramatically compared to previous periods.

### 7.3.1 Rörvik

Regarding the results from Rörvik, Sweden it was speculated that the model predicted too high summer concentrations due to re-volatilisation from the nearby Baltic Sea, for which the initial water concentrations may be estimated to be too high. The measured  $\alpha$ -HCH air concentrations are plotted in Figure 7.56 together with the predicted concentrations for the reference simulation and the simulation without re-volatilisation. The air concentrations at Rörvik are clearly reduced for the simulations without re-volatilisation from the oceans, especially in summer. However, it is difficult to determine if the predicted concentrations for this simulation are in better agreement with the measurements than results from the reference simulation. To investigate this further, the daily averaged concentrations for the years 1991 and 1994 for the three scandinavian stations (Lista, Rörvik, and Aspvreten) are plotted in Figure 7.57. In case re-volatilisation from the Baltic Sea is a strong source in the model, higher concentrations should be predicted at the two Swedish stations than at the Norwegian station. Indeed the predicted summer concentrations at Aspvreten, and to a lesser degree at Rörvik, are higher than at Lista for the first year in the simulation. However, for 1994 there is not a large difference between the predicted concentrations at the three stations, which indicates that local sources are not of high importance. This indicates that an eventual over-estimation of the initial ocean water concentration in the Baltic Sea fairly rapidly re-volatilises in the model simulation

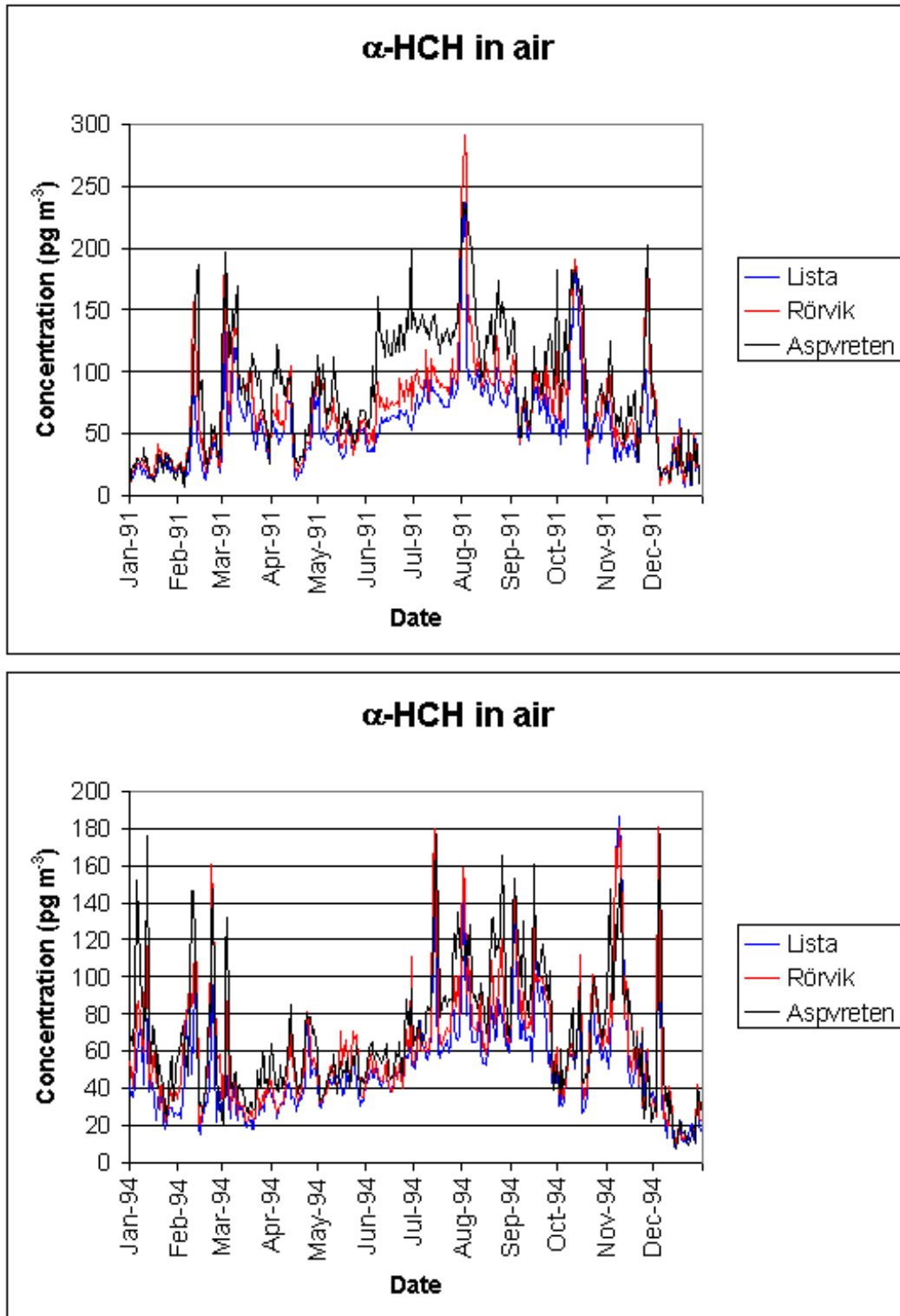


Figure 7.57: Daily averaged  $\alpha$ -HCH air concentrations for the reference simulation at Lista, Norway, as well as Rörvik and Aspövreten, Sweden for the years 1991 (top) and 1994 (bottom).

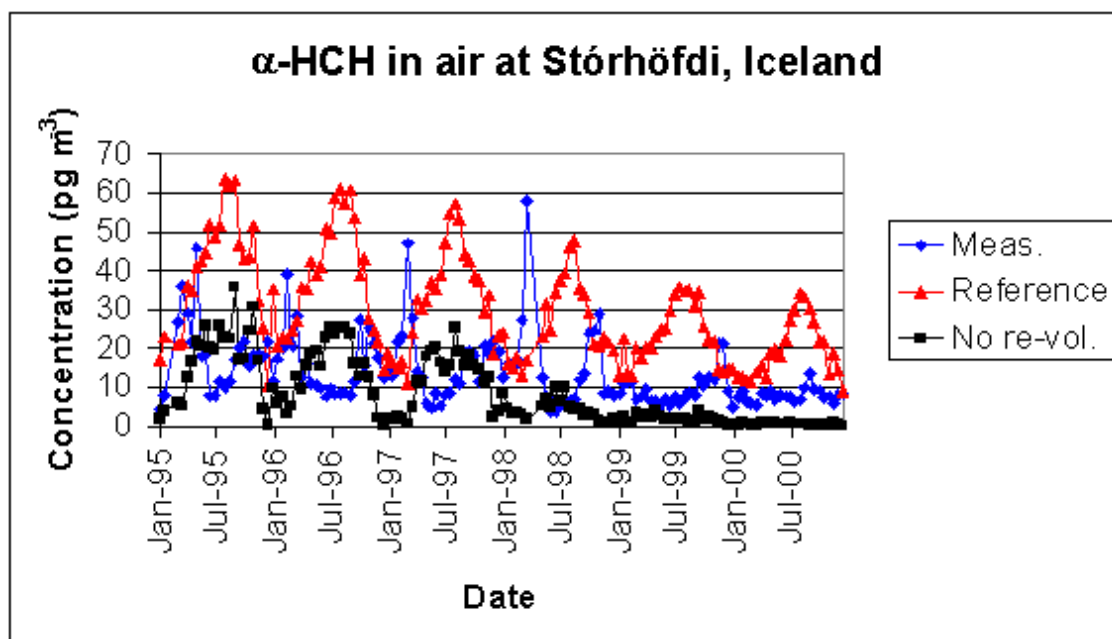


Figure 7.58: Measured  $\alpha$ -HCH air concentrations and predicted concentrations for the reference simulation and the simulation without re-volatilisation from oceans at Stórhöfði, Iceland.

and the ocean concentration approaches a more realistic value, which may be closer to equilibrium with the predicted (and measured) air concentrations. These results indicate that differences between measured and predicted concentrations at Rörvik from 1994 and onwards are less likely to arise due to too high estimated initial ocean concentrations from the Baltic Sea. The higher than measured concentrations predicted in spring 1991 may though be of this origin.

### 7.3.2 Stórhöfði

The measured  $\alpha$ -HCH air concentrations are plotted in Figure 7.58 together with the predicted concentrations for the reference simulation and the simulation without re-volatilisation from Stórhöfði. The predicted air concentrations are about a factor 2–3 lower than for the reference simulation, with increasing differences towards the end of the simulation. This indicates that the Icelandic air concentrations indeed are very influenced by re-volatilisation of  $\alpha$ -HCH from the oceans. However, there is still a strong seasonal pattern in the predicted concentrations with higher summer than winter concentrations and the pattern does not correspond to the measured pattern. It is therefore unlikely that an eventual over-estimation of the ocean concentrations is the reason for the discrepancy between measured and modelled air concentrations at Stórhöfði in Iceland.

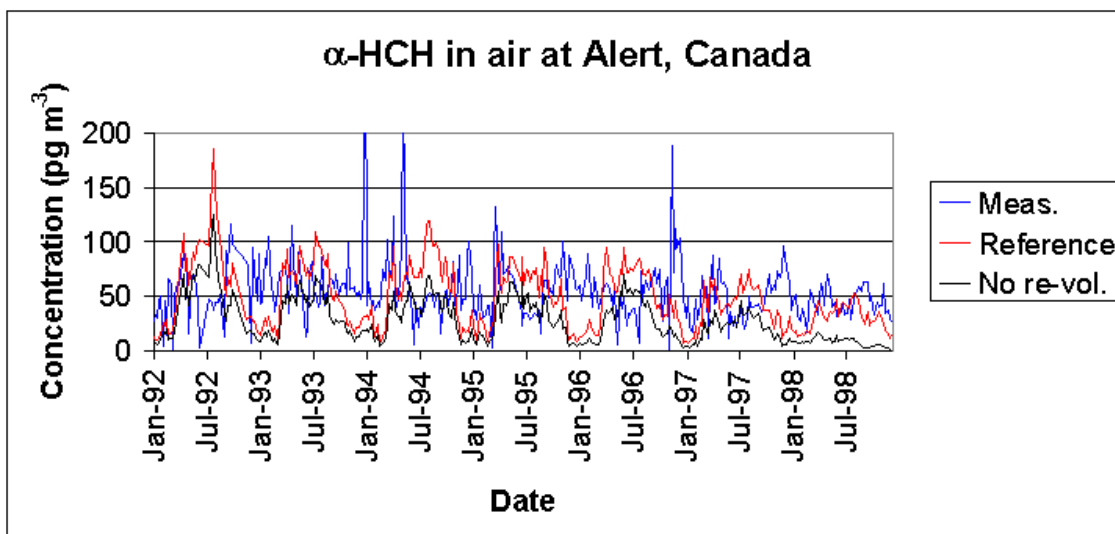


Figure 7.59: Measured  $\alpha$ -HCH air concentrations and predicted concentrations for the reference simulation and the simulation without re-volatilisation from oceans at Alert, Canada.

### 7.3.3 Alert

At Alert, Canada there is a clear summer peak in the predicted air concentrations of the reference simulation, which does not correspond to the measured pattern. An over-estimation of the ocean concentrations in the western Arctic Ocean with a subsequent re-volatilisation in the model may explain this peak. The measured  $\alpha$ -HCH air concentrations are plotted in Figure 7.59 together with the predicted concentrations for the reference simulation and the simulation without re-volatilisation. Shutting off the re-volatilisation from the oceans result in a lower air concentrations, especially during summer, where the predicted concentrations for several years are in better agreement with the measured concentrations. It is thus possible that the higher summer air concentrations predicted by the model may arise due to high estimated ocean concentrations in the western Arctic Ocean.

## 7.4 Importance of the vegetation

The role of vegetation on the predicted environmental fate of  $\alpha$ -HCH in DEHM-POP was examined by making a simulation equivalent to the reference simulation but without the vegetation module. Daily averages for the studied stations are compared, as well as overall changes in correlations for the two simulations. It should be noted that, eventual differences between the two simulations not necessarily arise from the local vegetation close to the station, but from the sum of different processes that the air parcels meet on their way from source areas to the station.

The general effect of vegetation in the model is to decrease the overall average  $\alpha$ -HCH air concentration at all stations except at Svalbard. For the simulation without the

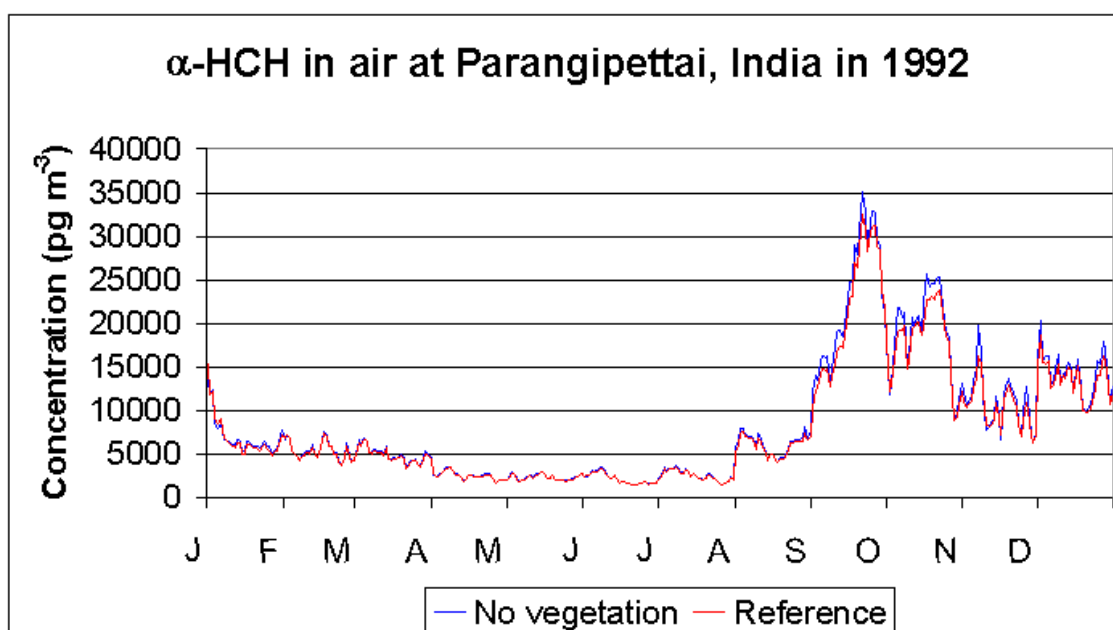


Figure 7.60: The daily averaged predicted  $\alpha$ -HCH air concentration in 1992 for the reference simulation and the simulation without vegetation at Parangipettai, India.

vegetation compartment the correlation between measured and predicted air concentrations is slightly improved at ten stations, unchanged at one and decreases slightly for five, predominantly Arctic, stations (Svalbard, Kinngait and Dunai Island as well as Rörvik and Sleeping Bear Dunes). The only change in statistical significance is for Brule River, Wisconsin where the correlation increase from  $r = 0.15$  to  $r = 0.21$  and the statistical significance increase from  $p < 0.1$  to  $p < 0.02$ . Although a larger number of stations had increased correlation of predicted concentrations with measurements for the simulation without vegetation, indicating that the vegetation module reduces the predictability capacity of DEHM-POP, the average root mean square error bias (*RMSEB*) is lowest for the reference simulation, which indicates the opposite. The vegetation compartment can thus not be said to have a determined influence on the predicted air concentrations of  $\alpha$ -HCH in DEHM-POP.

#### 7.4.1 Source area

The increase in air concentrations for the simulation without vegetation is seasonal variable, depending on the vegetation pattern at the station. At Parangipettai, India the vegetation compartment is largest in autumn and winter (see Figure 4.5 on page 59). The effect of the vegetation module is therefore also largest in this period, which can be seen in Figure 7.60, where the daily averaged air concentrations for the reference simulation and the simulation without vegetation for 1992 is plotted as an example of the difference between the two simulations. The effect of the vegetation in this area is not large, with an average ratio of the no-vegetation-concentration to the reference-concentration:  $R = 1.04$

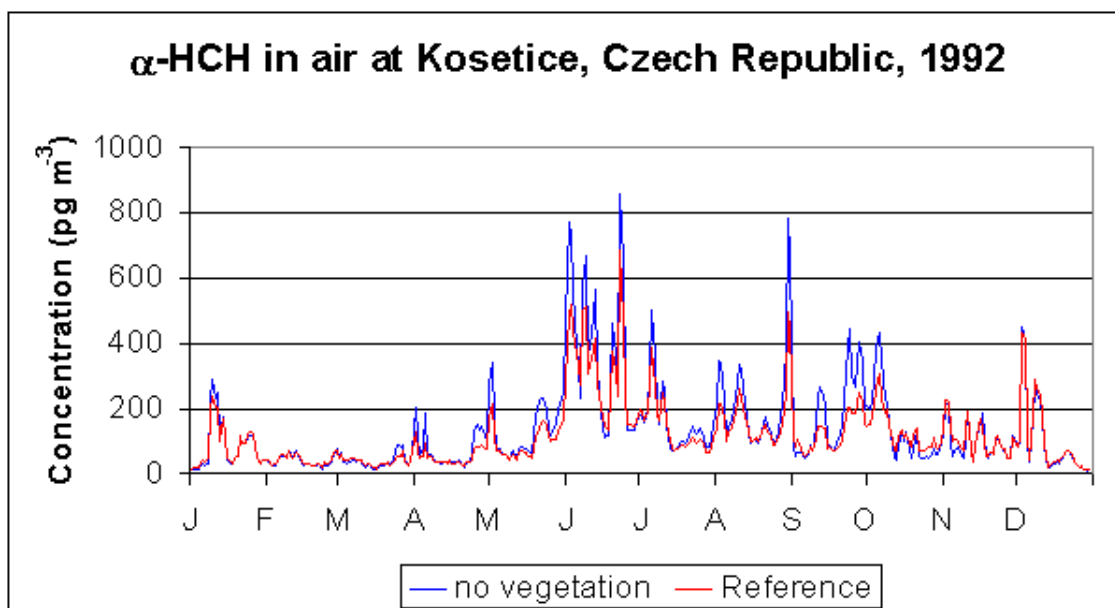


Figure 7.61: The daily averaged predicted  $\alpha$ -HCH air concentration in 1992 for the reference simulation and the simulation without vegetation at Košetice, Czech Republic.

for 1992.

#### 7.4.2 Mid-latitude stations

In Europe and in North America the leaf area index is largest in summer, and the effect of the vegetation on the predicted air concentrations is also largest in the summer months. The daily averaged predicted  $\alpha$ -HCH air concentration in 1992 for the reference simulation and the simulation without vegetation at Košetice, Czech Republic is plotted in Figure 7.61 as an example of the effect in these regions. The average ratio between the two simulations is:  $R = 1.08$  for 1992, but  $R = 1.15$  for the three summer months (June, July and August) only, which shows that the effect of the vegetation is largest in the summer. Up to a factor of 3.17 higher concentrations are predicted for the simulation without vegetation than for the reference simulation. It is also seen that for some periods the simulation without vegetation predicts lower concentrations than the reference simulations, especially in October/November. These are all periods with relatively low air concentrations, and it indicates that the vegetation compartment locally acts as a short-term buffer, which relatively quickly attains equilibrium with the air concentrations. So when air concentrations decrease, e.g. when the wind direction change and air derives from a relatively clean area,  $\alpha$ -HCH re-volatilise from the vegetation which thus acts as a source to the air concentrations.

The effect of the vegetation compartment on the results from the Canadian and the US IADN station is the same (not shown). The difference in behaviour pattern for these stations can thus not be explained by the influence of the vegetation compartment.

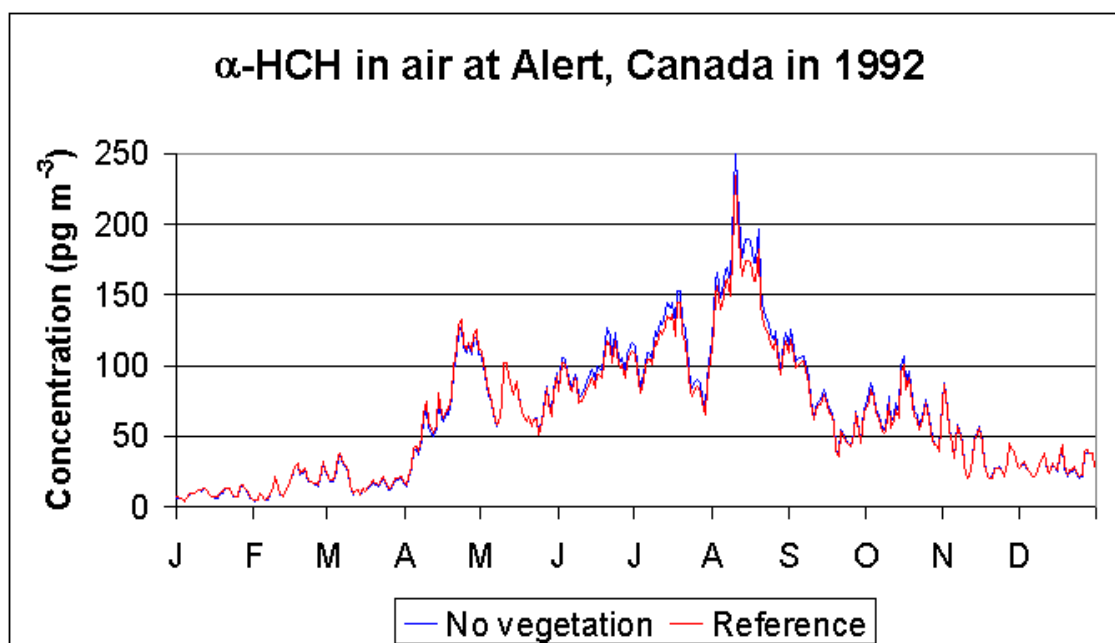


Figure 7.62: The daily averaged predicted  $\alpha$ -HCH air concentration in 1992 for the reference simulation and the simulation without vegetation at Alert, Canada.

### 7.4.3 Arctic stations

At Alert in the high Arctic the effect of the vegetation is limited since there is no vegetation close to the site in the model (see Figure 4.5 on page 59) and the predicted differences between the two simulations are thus only arising from the source regions. The daily averaged predicted  $\alpha$ -HCH air concentration in 1992 for the reference simulation and the simulation without vegetation is plotted for Alert in Figure 7.62. Alert display similar pattern as the stations at lower latitudes, but with lower amplitudes. The difference between the two simulations are only  $R = 1.01$  on average for the whole simulated period and  $R = 1.06$  (with a range of 1.02 – 1.09) for the three summer months in 1992. The smaller effect probably arise because the air interact with several other compartments on the way from the source regions to Alert, so other sources, such as re-volatilisation from water, will increase and thus supply parts of the ‘missing’  $\alpha$ -HCH.

The results from Svalbard display another pattern than the results from the other stations. The predicted air concentrations are on average lower for the simulation without vegetation than for the reference simulation:  $R = 0.95$  for the whole simulated period. The daily averaged predicted  $\alpha$ -HCH air concentration in 1992 for the reference simulation and the simulation without vegetation at Svalbard is plotted in Figure 7.63. As for Alert there is no vegetation compartment in the model close to the station (see Figure 4.5 on page 59), and the difference between the two simulations is thus of non-local origin. It is not evident which process or combination of processes that can account for the observed difference between the two simulations, and it highlights the difficulty of interpreting the results of a dynamic model with non-linear processes.

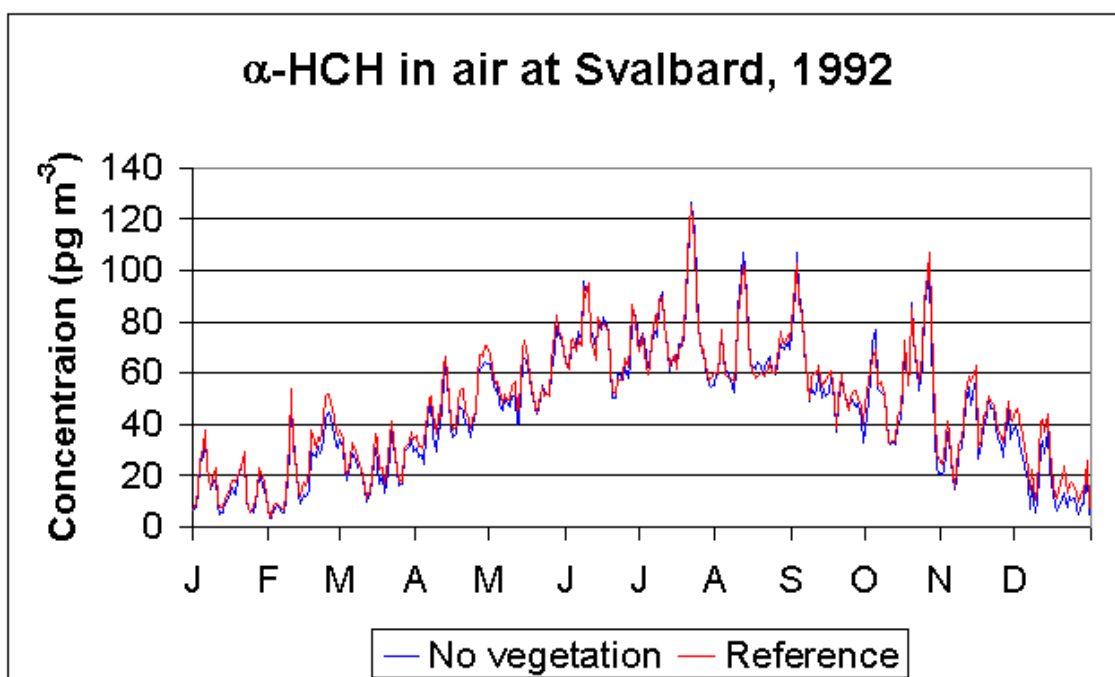


Figure 7.63: The daily averaged predicted  $\alpha$ -HCH air concentration in 1992 for the reference simulation and the simulation without vegetation at Svalbard.

#### 7.4.4 Previous model studies

*Wania and McLachlan* [2001] included a vegetation module in a multi-compartment mass balance model (with settings simulating conditions at Northern Hemisphere mid-latitude) and investigated the effect of the vegetation for the chemical space spanned by  $\log K_{aw} \in [-5; 0]$  and  $\log K_{oa} \in [7; 12]$ . The result was up to a factor 5.5 lower air concentrations during summer for the model including vegetation than without [*Wania and McLachlan*, 2001]. For the physical-chemical properties equivalent to the properties of  $\alpha$ -HCH, the model study predicts a factor 1.0–1.5 lower  $\alpha$ -HCH air concentrations during summer when vegetation is included [*Wania and McLachlan*, 2001]. The results from DEHM-POP are generally within this interval and thus in good agreement with this previous model experiment. The DEHM-POP model results thus indicates that the ‘forest filter effect’ theory, where gas-phase POPs are scavenged from the air by the vegetation as proposed by *McLachlan and Horstmann* [1998], is applicable for  $\alpha$ -HCH. The subsequent transfer of POPs to the soil compartment by leaf litter fall, which would result in increased soil concentrations [*McLachlan and Horstmann*, 1998] is though not investigated here.

## 7.5 Importance of the snowpack

The effect of the snowpack module on the predicted environmental fate of  $\alpha$ -HCH in DEHM-POP was examined by making a simulation equivalent to the reference simulation but without the snowpack module. Precipitation, which is still falling as either rain or

snow, is just entering the vegetation, soil or water compartments instead of forming a snowpack on the ground or on the sea ice.

The effect of the snowpack is evaluated by comparing the measured and modelled concentrations for the reference simulation and for the simulation without snowpack, and by comparing the correlation coefficients with measurements for the two simulations. As for the investigation of the importance of the vegetation module, an eventual difference between the two model simulations at a station can not be interpreted as the contribution of the snowpack at this station only, since the 'detected'  $\alpha$ -HCH air concentrations not only derives from the local interactions of the different media, but is the result of the interactions of all the media that the air passes on its way from a source area to the station.

The overall effect of the snowpack is to increase the average  $\alpha$ -HCH air concentration at all stations in the model, with the largest effect at the Arctic stations. These results will be described separately in section 7.5.1 and the other stations in section 7.5.2. Based on the model results, the role of the snowpack in the environmental cycling of  $\alpha$ -HCH will be proposed in section 7.5.3.

### 7.5.1 The Arctic stations

Of the seven Arctic stations (when Stórhöfði is excluded) there are low but statistical significant correlations between the reference simulation results and the measurements for four: Svalbard, Kinngait, Dunai Island and Pallas. For the simulation without the snowpack module there is only a correlation at Pallas, which has a slightly higher correlation coefficient for this simulation ( $r = 0.37$ ,  $p < 0.01$ ) than for the reference simulation ( $r = 0.32$ ,  $p < 0.02$ ). At Alert, Canada there is a low but statistical significant negative correlation for the simulation without snowpack ( $r = -0.19$ ,  $p < 0.001$ ). The results from the two simulations for Alert are plotted in Figure 7.64 together with the measured concentrations. There is a clear seasonal pattern in the predicted concentrations for the simulation without snowpack with very low concentrations during winter and higher concentrations during summer with the summer peak apparently shorter than the winter trough. The predicted concentrations are lower for the whole season for the simulation without snowpack, but especially for the winter. The predicted summer concentrations are in better agreement with the measured values for the simulation without the snowpack module than with. Similar differences between the two simulations is seen for Spitsbergen, Svalbard (Figure 7.65). The results from the two high Arctic stations indicate that the snowpack module in DEHM-POP acts as a fast-exchanging temporary storage medium for  $\alpha$ -HCH throughout the snowpack season. Deposited  $\alpha$ -HCH concentrations are rapidly re-volatilising back into the atmosphere, which increases the air concentrations.

For the more southerly Arctic stations the predicted air concentrations for the simulation without snowpack have similar seasonal pattern as for the high Arctic stations with lower concentrations during the whole season, especially for the winter, than for the reference simulation. However, the predicted concentrations in autumn for the simulation without snowpack are closer to the measured values at these stations than for the reference simulation. This is seen in the results from Dunai Island (Figure 7.66). These results could indicate that the re-volatilisation of  $\alpha$ -HCH from the snowpack is too large in autumn. This is confirmed by the results from Tagish, Canada, where the concentrations predicted in

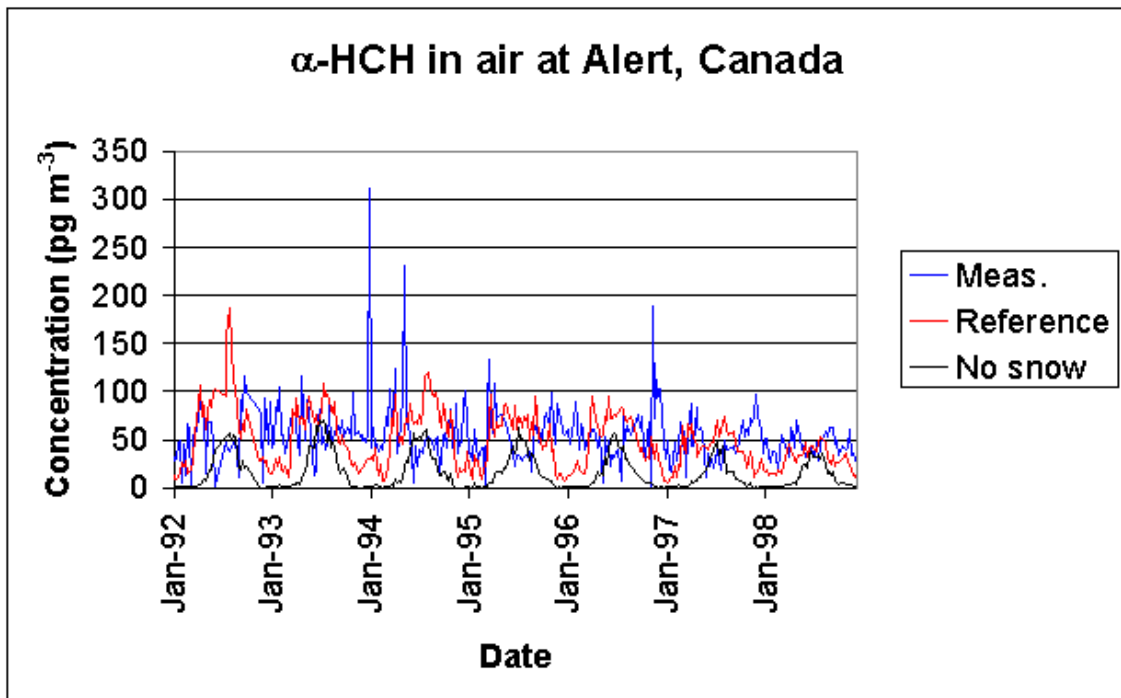


Figure 7.64: Measured  $\alpha$ -HCH air concentrations and predicted concentrations for the reference simulation and the simulation without snowpack at Alert, Canada.

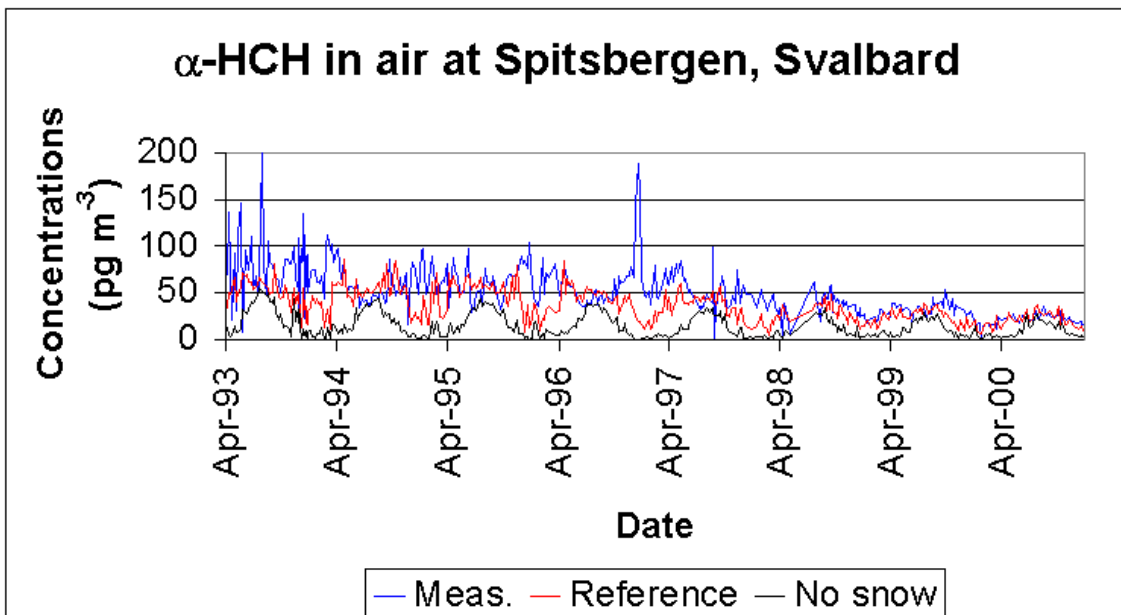


Figure 7.65: Measured  $\alpha$ -HCH air concentrations and predicted concentrations for the reference simulation and the simulation without snowpack at Spitsbergen, Svalbard.

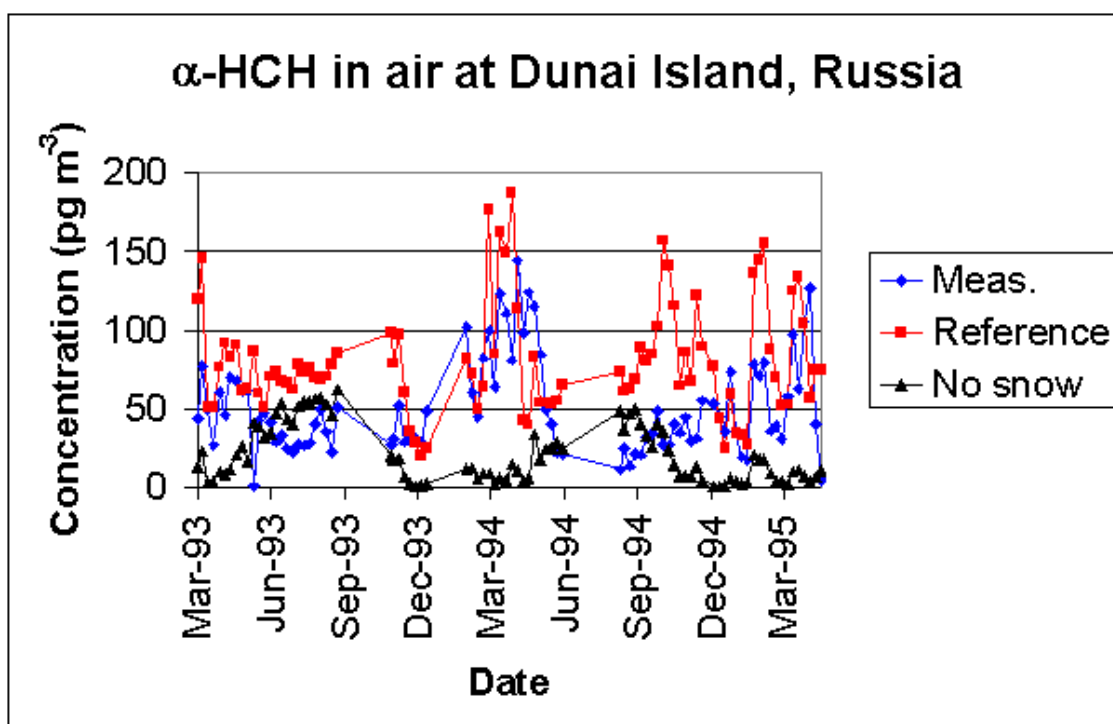


Figure 7.66: Measured  $\alpha$ -HCH air concentrations and predicted concentrations for the reference simulation and the simulation without snowpack at Dunai Island, Russia.

autumn are lower for the simulation without the snowpack module than with, and in better agreement with the measured values (see Figure 7.67). The summer air concentrations for the two simulations are almost the same at this station, whereas the model predicts lower winter concentrations when the snowpack module is not included, than when it is included, which corresponds to the pattern at the other stations.

The results from Pallas, Finland follows mostly the same pattern as the other Arctic stations (see Figure 7.68). The model simulation without snowpack predicts lower concentrations, especially during winter. The predicted winter concentrations for this simulation are also lower than the measured concentrations, except for the year 1999, which are in better agreement with the observed concentrations than the concentrations from the reference simulation. This is probably the reason for the improved correlation for the simulation without the snowpack module together with the lower predicted values in spring and autumn 1996 and 1997.

### 7.5.2 North American and European stations

For four of the North American and European stations the correlation between predicted and measured concentrations decreases for the simulation without the snowpack, but for seven other stations the correlation increases, and several of them have also higher statistical significance. However, when the time series of the results from these stations are inspected, the predicted concentrations are seen not necessarily to be better for the whole

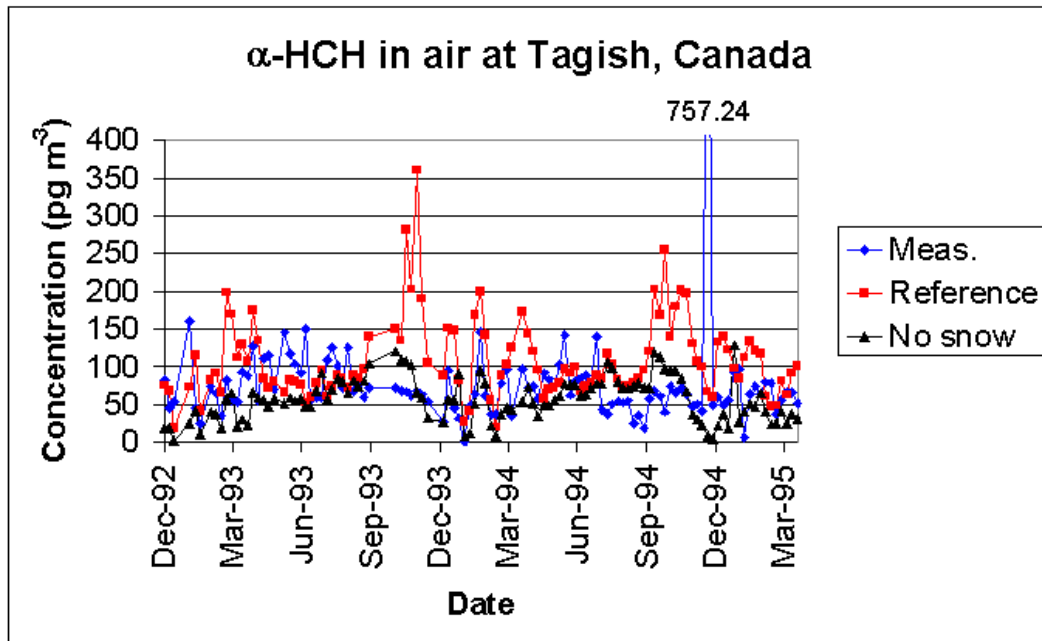


Figure 7.67: Measured  $\alpha$ -HCH air concentrations and predicted concentrations for the reference simulation and the simulation without snowpack at Tagish, Canada.

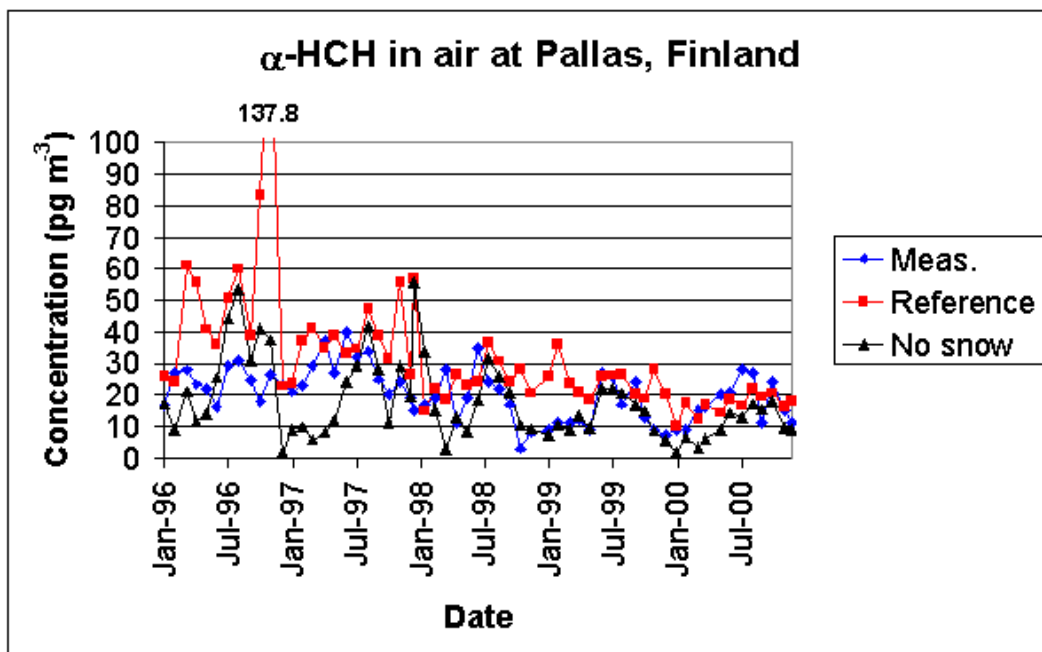


Figure 7.68: Measured  $\alpha$ -HCH air concentrations and predicted concentrations for the reference simulation and the simulation without snowpack at Pallas, Finland.

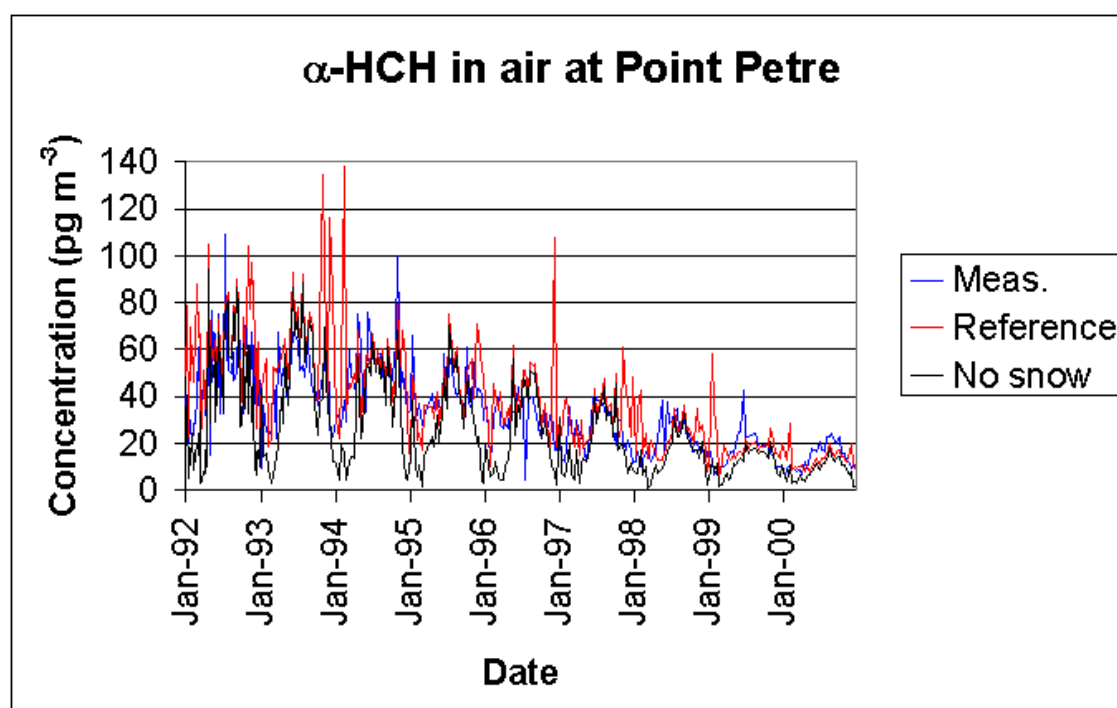


Figure 7.69: Measured  $\alpha$ -HCH air concentrations and predicted concentrations for the reference simulation and the simulation without snowpack at Point Petre, Canada.

season for the simulation without the snowpack module. Measured  $\alpha$ -HCH air concentrations and predicted concentrations for the reference simulation and the simulation without snowpack are plotted for Point Petre, Canada as an example in Figure 7.69. The predicted summer concentrations are almost the same for the two simulations. The predicted concentrations are lower during winter for the simulation without snowpack, similarly to the Arctic stations, but they are also lower than the measurements, with which the reference simulation results are in better agreement. The few very high values predicted in late autumn/early winter for the reference simulation are seen not to be present in the simulation without snowpack. This indicates that these peak concentrations in the reference simulation originates from air-snowpack interactions and supports the finding from the Arctic stations that the re-volatilisation of  $\alpha$ -HCH from the modelled snowpack is too large in autumn. The other stations in North America and the stations in Europe display similar results as Point Petre, with lower air concentrations, especially during winter, for the simulation without snowpack.

### 7.5.3 The role of the snowpack in the environmental cycling of $\alpha$ -HCH

Based on the model results, it is possible to propose how the role of the snowpack for the environmental cycling of  $\alpha$ -HCH is. Snow-precipitation is a very efficient scavenger of  $\alpha$ -HCH; it strips the chemical out of the atmospheric column and as it falls on the ground it forms a snowpack. The capacity of the snowpack to retain  $\alpha$ -HCH depends on

the snow-air partition coefficient, which is highly temperature dependent. Immediately following a precipitation event, the snowpack will be super-saturated with  $\alpha$ -HCH which then re-volatilise and an amount of  $\alpha$ -HCH is thus released to the above lying atmosphere. This correspond to a redistribution of the chemical from the atmospheric column to the lowermost few meters. In the beginning of the snowpack season the temperatures are still relatively high and the retention capacity of the snowpack is thus low, which results in a high degree of re-volatilisation. When the temperature decreases through the season a larger fraction of the incoming  $\alpha$ -HCH is retained in the snowpack, and the air concentrations thus decrease. The re-volatilisation increase again in spring, when the temperature increases and the retention capacity decreases. This leads to a spring peak of  $\alpha$ -HCH, which not necessarily is associated with the melting of the snowpack. If the snowpack behaves according to proposed pattern, the air concentrations will display a bi-modal pattern, with peak concentrations in spring and autumn. This is also the observed pattern at Alert in the high Arctic [Hung *et al.*, 2002, 2005]. The model could also tentatively describe the observed  $\alpha$ -HCH concentrations from Villeroy, Québec, with increasing air concentrations in spring, before the melt season starts [Aulagnier and Poissant, 2005]. There is also an observed peak in November, which is associated with a snowfall period followed by a thawing period [Aulagnier and Poissant, 2005].

A bi-modal pattern is also found in the reference simulation results in some parts of the Arctic, e.g. at Dunai Island. 30-days running average  $\alpha$ -HCH air concentrations for the reference simulation and the simulation without snowpack at Dunai Island, Russia are plotted in figure 7.70. The 30 days running average concentrations are plotted to reduce the scatter. A clear bi-modal pattern is seen in the reference simulation results for all but the first and the last two years of the simulation. The single-modal results from the simulation without snowpack indicates that the bi-modal pattern is associated with the air-snowpack interactions. The bi-modal pattern in the reference simulation may be representative for most of the north Siberia as indicated by the monthly averaged concentrations plotted in Figure 7.3.

In the measured  $\alpha$ -HCH air concentrations at Dunai Island, there is a clear spring peak [Hung *et al.*, 2005]. But there are no clear signs of an autumn peak, although there are holes in the data series and a firm conclusion about this may not be taken on basis of the remaining measurements. The model predicts too high concentrations during autumn. However, as Figure 4.3 on page 53 indicates, the extent of the snowpack in DEHM-POP is over-estimated. This result in the formation of a snowpack too early in the season, which due to the relatively high temperature only retains a small fraction of the deposited chemical. This could be the origin of the too high autumn concentrations predicted at Dunai Island. Indeed the period with predicted snowpack coverage at Dunai Island is long (see Figure 7.71). The predicted snowpack is absent only for a very short period during summer. Measured temperatures at the site are above 0°C from June to September [Hung *et al.*, 2005]. A similar too early initiation of the snowpack season at Tagish may explain the too high predicted air concentrations at this station.

A too long snow-covered period may also explain the lack of correlation between predicted and measured concentrations at Alert, Canada. The predicted snowpack depth for the studied period is plotted in figure 7.72. The snowpack is not melting completely away before the summer of 1995, and even in the last years, the snowpack-free period is only a few days. This may have resulted in a ‘merging’ of the spring and the autumn peak

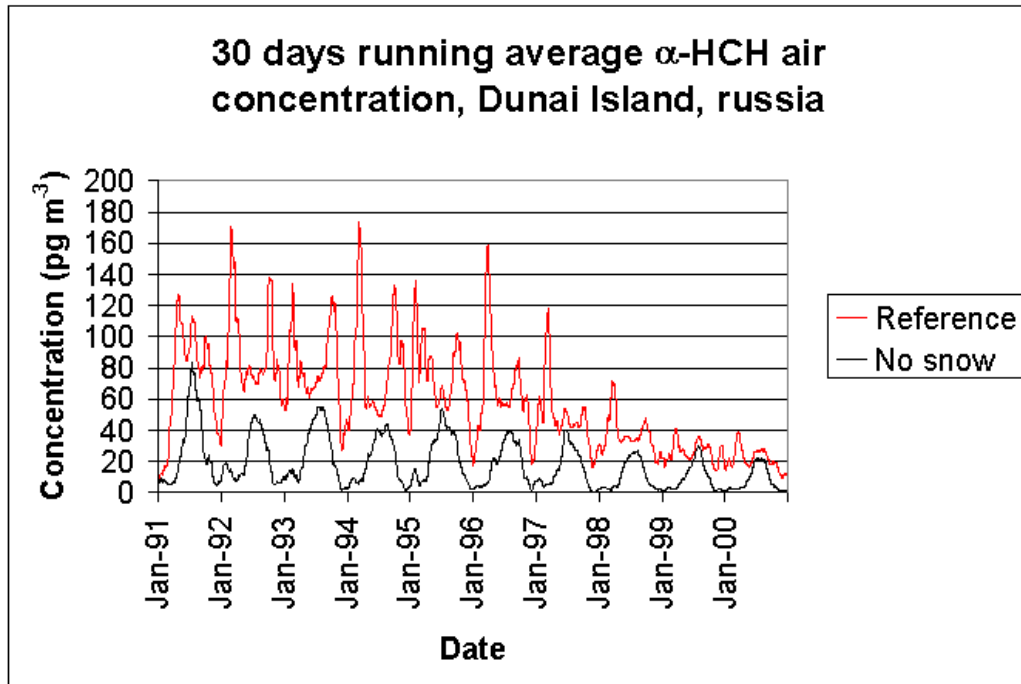


Figure 7.70: 30-days running average  $\alpha$ -HCH air concentrations for the reference simulation and the simulation without snowpack at Dunai Island, Russia.

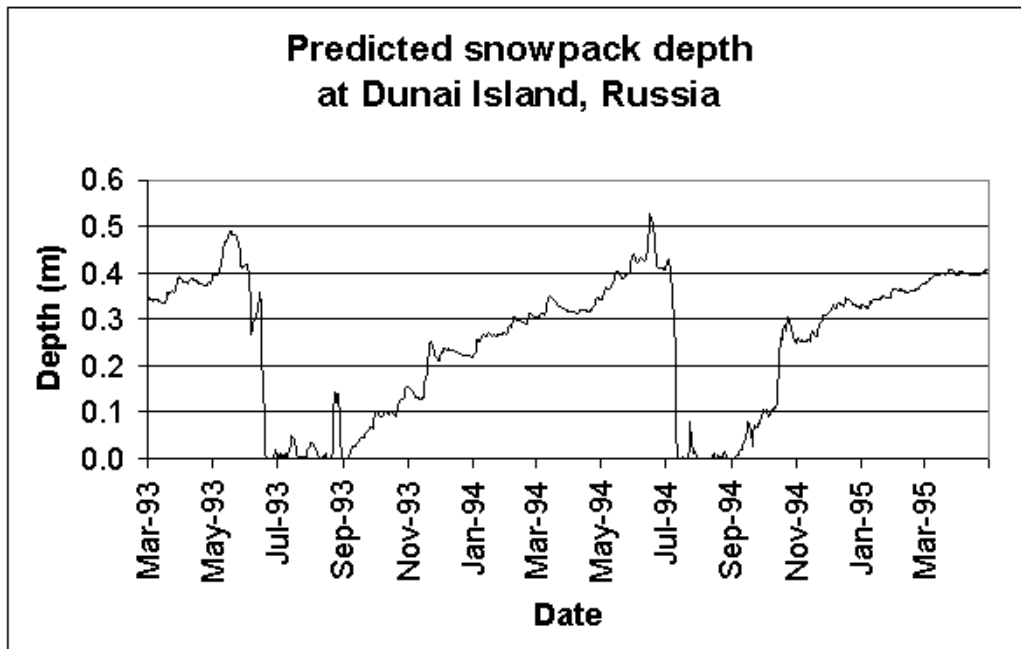


Figure 7.71: The depth of the predicted snowpack at Dunai Island, Russia for the period with measurements.

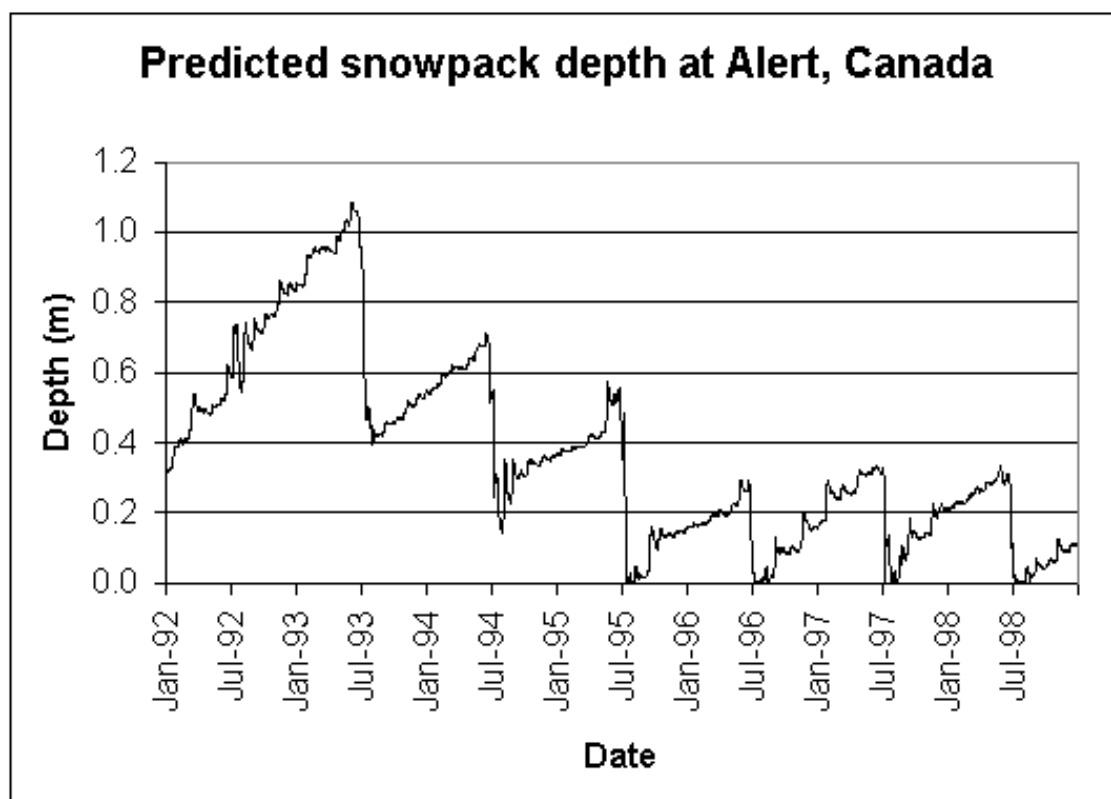


Figure 7.72: The depth of the predicted snowpack at Alert, Canada for the studied period.

air concentrations to a summer top, at least for the first years. The predicted  $\alpha$ -HCH air concentrations at Villeroy, Québec are not in good agreement with the suggested pattern either, which could also be due to a too large extent of the snowpack.

For both high Arctic stations, there is a tendency of too low predicted concentrations during winter, which may indicate that the snowpack is too efficient in retaining the  $\alpha$ -HCH in the snow at low temperatures. This indicates that the  $K_{sa}$  values are too high, which could be due to too high  $K_{ia}$  values, although the values used in this study are expected to be too low [Hoff *et al.*, 1995]. It should be pointed out that the  $K_{ia}$  values, and thus the  $K_{sa}$  values are very uncertain. A snowpack too efficient in retaining  $\alpha$ -HCH could also be due to too large predicted snowpack depths, although the predicted depths at Alert towards the end of the simulated period are comparable with observed depths at the site as made by *Dominé et al.* [2002]. This need to be investigated in more detail.

In a previous model study, a snowpack module was introduced in a multi-compartment mass balance model [Daly and Wania, 2004]. The predicted  $\alpha$ -HCH air concentrations in this model are lower in winter, with a predicted spring peak due to melting and similar summer concentrations for the simulation including a snowpack compared to the model without snowpack [Daly and Wania, 2004].

Although the results from DEHM-POP contradicts previous model experiments the improved agreement of the DEHM-POP model results with measurements when including

a snowpack indicates that the dynamic snowpack module captures the main features of the air-snowpack interaction.

## 7.6 Previous DEHM-POP results

Results from the DEHM-POP model is published in two earlier papers [*Hansen et al.*, 2004, 2006a]. The papers each describe different versions of the model with a variable number of environmental processes included. A comparison of the results presented here with the results from the earlier versions of the model may thus give information about the influence of the environmental processes on the fate of  $\alpha$ -HCH. But it is unfortunately not possible to compare the present results with the results presented in the earlier papers, since several errors were discovered in the model simulations after the papers have been published. Three errors was found and have been corrected, and the model simulations have been repeated to determine the influence of them on the predicted results. The three errors have influence on the predicted concentrations locally, however the large scale pattern remains the same, and although the individual concentrations may have been erroneously predicted and thus the correlation between measured and predicted concentrations not correctly given at each station, the conclusion in the papers are found not to change with the revised model simulation results. The initial ocean concentration was used erroneous in *Hansen et al.* [2004]. This was corrected for the simulation presented in *Hansen et al.* [2006a]. The other two errors are present in both simulations. One error was in the meteorological data, where the soil temperatures (which are not used in DEHM-POP) at certain places were too low, which affected the air temperatures in the lowermost atmospheric layers. But as the results were nudged towards the ECMWF data at a 12 hour interval this error had very limited effect on the predicted  $\alpha$ -HCH concentrations. However, when the air temperatures were used to form the snowpack, this module did not work properly. The third error was in the module calculating the vertical diffusion, where the horizontal and vertical indices were switched so the vertical diffusion was calculated erroneously, being too high in some parts of the domain and too low in others.

## 7.7 Comparison with results from other models

Several models are used to study the environmental fate of  $\alpha$ -HCH (see section 2.5.3 on page 24). However, most of these are low resolution mass balance models, for example the zonally average models of *Strand and Hov* [1996] and *Wania et al.* [1999b]. In these models, each zone consist of a large area, for which an averaged concentration is predicted. It therefore does not make much sense to compare the results from these models with the much higher-resolution results from DEHM-POP. The same is the case with the BETR-World model, in which the world is divided into 25 regions mainly following continental and/or political boundaries [*Toose et al.*, 2004].

Based on the global distribution model of *Wania et al.* [1999b], a regional non-steady-state multi-compartment mass balance model covering the Baltic Sea region was developed (the POPCYCLING-Baltic model) [*Brevik and Wania*, 2002a, 2002b]. The model consist of four atmospheric regions, 10 terrestrial regions, each with five different compartments (agricultural and forest soil, forest canopy, fresh water and sediments) and 16 marine re-

gions and it has been applied to study the environmental fate of  $\alpha$ -HCH for the years 1970–2000 [Breivik and Wania, 2002a, 2002b]. The predicted air concentrations are generally in good agreement with the measured concentrations for the 1980s and 1990s, and the decline in air concentrations over this period, as well as the seasonal variability is well captured by the model. Individual measured air concentrations at Lista, Norway and Rörvik, Sweden are studied in detail for the years 1994 and 1995. At Lista the predicted concentrations are in very good agreement with the measured concentrations during summer, whereas the model predicts lower concentrations during winter than what is measured [Breivik and Wania, 2002a]. At Rörvik the predicted concentrations are higher than measured during summer, with better agreement during winter than for Lista [Breivik and Wania, 2002a]. Except for lower air concentrations during winter, the POPCYCLING-Baltic model predicts similar  $\alpha$ -HCH air concentrations as the results from the DEHM-POP model.

Only one atmospheric chemistry transport model has been applied to study the environmental fate of  $\alpha$ -HCH [Koziol and Pudykiewicz, 2001]. It is a global model with a horizontal resolution of  $2^\circ \times 2^\circ$ , and it has been used to study the atmospheric transport of  $\alpha$ -HCH for the years 1993 – 1994. A clear seasonal pattern with highest predicted concentrations during early summer and lowest during winter is seen in the model results for the four studied stations: Alert, Svalbard, Dunai Island and Tagish [Koziol and Pudykiewicz, 2001]. At Dunai Island and Tagish the model predicts higher spring/summer concentrations than measured, and at Alert and Svalbard the model predicts lower autumn/winter concentrations than measured. The high summer concentrations predicted, especially at Tagish, are attributed to an insufficient scavenging efficiency [Koziol and Pudykiewicz, 2001]. Correlation coefficients between measured and predicted concentrations are not calculated. The annual averaged concentrations are all within a factor of three, where the model predicts lower averaged concentrations at all stations except at Tagish. This model predicts similar seasonal patterns as DEHM-POP for Alert, but not for the other stations. At Alert the predicted concentrations are also of similar magnitude for the two models, whereas it predicts higher concentrations by about a factor of two than DEHM-POP at Svalbard. At Tagish the model also predicts similar concentrations as DEHM-POP, except during summer, where they are a factor 4–5 higher, and for Dunai Island the model predicts higher summer concentrations than DEHM-POP but much lower spring and autumn concentrations. The predicted annual averages are similar to DEHM-POP results for Svalbard and Tagish but a factor 2 lower for Alert and Dunai Island. The two models thus predicts similar concentrations on average, whereas the seasonal pattern generally differs.

## 7.8 Summary of the results and model performance

In general the predicted DEHM-POP model results were in good agreement with the measured concentrations at the studied stations. Annual averages were within a factor of two of the annual measured averages for most of the stations; i.e. all the stations in the Arctic, the European stations and the Canadian stations around the Great Lakes. An exception was five stations in US and three in Québec, Canada where the predicted annual averages were a factor of two to three lower than the annual measured averages. For almost all stations the agreement between the predicted and the measured concentrations were

improving towards the end of the simulated period.

The predicted concentrations in Parangipettai, India, which represents a source area, were not in good agreement with the individual measurements. This is not surprising since the emission data are distributed evenly over one month and over a 150 km × 150 km square, so the timing of usage close to the station can not be captured by the model. However, the predicted range of air concentrations was in good agreement with the range of the measured concentrations within the years of the measurements, and the predicted seasonality was also in good agreement with results from a previous study in the area.

Good agreements were found between the predicted and measured concentrations at the two Canadian Great Lakes stations. A few much higher predicted concentrations than measured during autumn and winter at these stations were seen to derive from the snowpack module. At the corresponding IADN stations on the US side of the Great Lakes the model predicted much lower concentrations during summer than what were measured. The model was seen to predict similar concentrations at both sides of the lakes, but it was not possible to determine any process not accounted for in the model that could give rise to the discrepancy between predicted and measured US concentrations. It is interesting to note that it is two different agencies from two different countries that are running these stations, which may suggest the possibility of a systematic error in the data sets. The stations from Québec, Canada displayed similar pattern as the US IADN stations, with lower predicted summer concentrations than measured. This discrepancy was not possible to explain either.

There was a good agreement between the predicted and measured air concentrations at the Norwegian station Lista. However for the two closely situated Swedish stations the results were in less good agreement at one (Rörvik) and not at all at the other (Aspvreten). This was also not possible to explain by other than effects of local origin, and it may raise the question of the representativeness of these measured concentrations, i.e. whether they are influenced by local features (sources and/or sinks) to a high degree. The predicted results from the Czech Republic station was also in fair agreement with the measured concentrations.

The predicted air concentrations for the Icelandic station were higher than the measured during summer, which possibly could be explained by sampling artifacts, although it can not be determined due to the few information on the sampling procedure. In general the results from the Arctic stations were in fair agreement with the measured concentrations. Low but statistical significant correlations between measured and predicted concentrations were found at four of the seven stations. The snowpack module was seen to give rise to some of the discrepancy between measured and predicted concentrations in autumn at some of the stations (Tagish, Pallas, and Dunai Island). A too long snowpack season probably have led to the discrepancy between measured and predicted concentrations at Alert, although an eventual too high initial ocean concentration in the western Arctic Ocean also may have influenced the predicted concentrations.

The effect of the vegetation compartment was generally to decrease the predicted  $\alpha$ -HCH air concentrations. However, the performance of DEHM-POP with regards to predicting the atmospheric concentrations of  $\alpha$ -HCH was neither seen to improve nor deteriorate with the vegetation compartment included.

The snowpack module clearly improved the agreement between the predicted and measured air concentrations, mainly for the Arctic stations, but also for the stations at lower

latitudes. This clearly indicates that the snowpack module was able to capture some of the variability of the air-snow interactions for  $\alpha$ -HCH. However, some problems with the snowpack module were also displayed. Generally the model predicted too high concentrations during late autumn/early winter at some stations, which indicates that not all of the dynamic air-snow interaction is captured by the snowpack module. The extent of the snowpack cover and the length of the snowpack season were also seen to be too large, probably due to an inefficient melting process in the module.

The simulation excluding re-volatilisation from the oceans showed that the atmospheric concentrations of  $\alpha$ -HCH in the 1990s generally were very influenced by re-volatilisation of previously deposited chemicals. This is also expected, since the primary emissions decrease rapidly through the period following the ban on usage of technical-HCH (see Figure 5.1 on page 68). The improved agreement between measured and predicted concentrations for the reference simulation also reflect this change in source pattern. As the primary emissions decrease, the air concentrations approach equilibrium with the surface media. Although the dynamics of the weather system creates disequilibrium locally, it will generally result in less variability in air concentrations. The air concentration will thus mainly be driven by re-volatilisation from the surface media, and primarily from the medium with the longest residence time, which is water.

## Chapter 8

# Applications of DEHM-POP

In Chapter 7 it is shown that the DEHM-POP model can be used to predict the air concentrations at a specific site or in a region on both short- and long-term averages. There are several other possible applications of the model, and two of these are shortly described in this section.

### 8.1 Transport episodes

DEHM-POP can be used to study individual atmospheric transport episodes. Although the air concentrations of POPs does not reach levels that are acutely harmful, it is interesting to study the origin of eventual elevated measured concentrations. Eventual trans-Pacific transport from Asian sources to the North American west coast has received special focus [e.g. *Bailey et al.*, 2000].

As an example, the atmospheric conditions in the days prior to a particularly high  $\alpha$ -HCH air concentration observed at Tagish, Canada from January 27, 1994 and one week onwards is briefly described here. This sample has the fourth highest measured  $\alpha$ -HCH air concentration at Tagish with  $145.4 \text{ pg m}^{-3}$ , which is more than a factor 2 higher than the measured concentration in the week before and after (approximately  $60 \text{ pg m}^{-3}$ ).

This may not be the best episode to study in the model, since the levels generally are high during these months (see Figure 7.52 on page 131). However, the high levels are probably an artifact arising from the snowpack module as discussed in section 7.5.3 on page 147. Furthermore, the model clearly display an increased concentration for this week with a predicted concentration of  $198.8 \text{ pg m}^{-3}$ , and although it is only slightly higher than the predicted concentrations the week before and after ( $168.3$  and  $141.1 \text{ pg m}^{-3}$ , respectively), it may be possible to trace the origin of the increased concentrations in this period. To do this, a model simulation with similar conditions as the reference simulation was made, but with three hour mean air concentrations extracted instead of daily average concentrations as is done for the reference simulation. From the plotted three hour mean air concentrations it is possible to see that an elevated air concentration reaches the North American coast around 28 January 1994 from the Pacific Ocean. This elevated air concentration can be followed from January 18, where a tongue of contaminated air from southeast Asia is stretching out over the Pacific Ocean (see upper left of Figure 8.1). An air mass associated with a high pressure (see lower left of Figure 8.1) gets separated

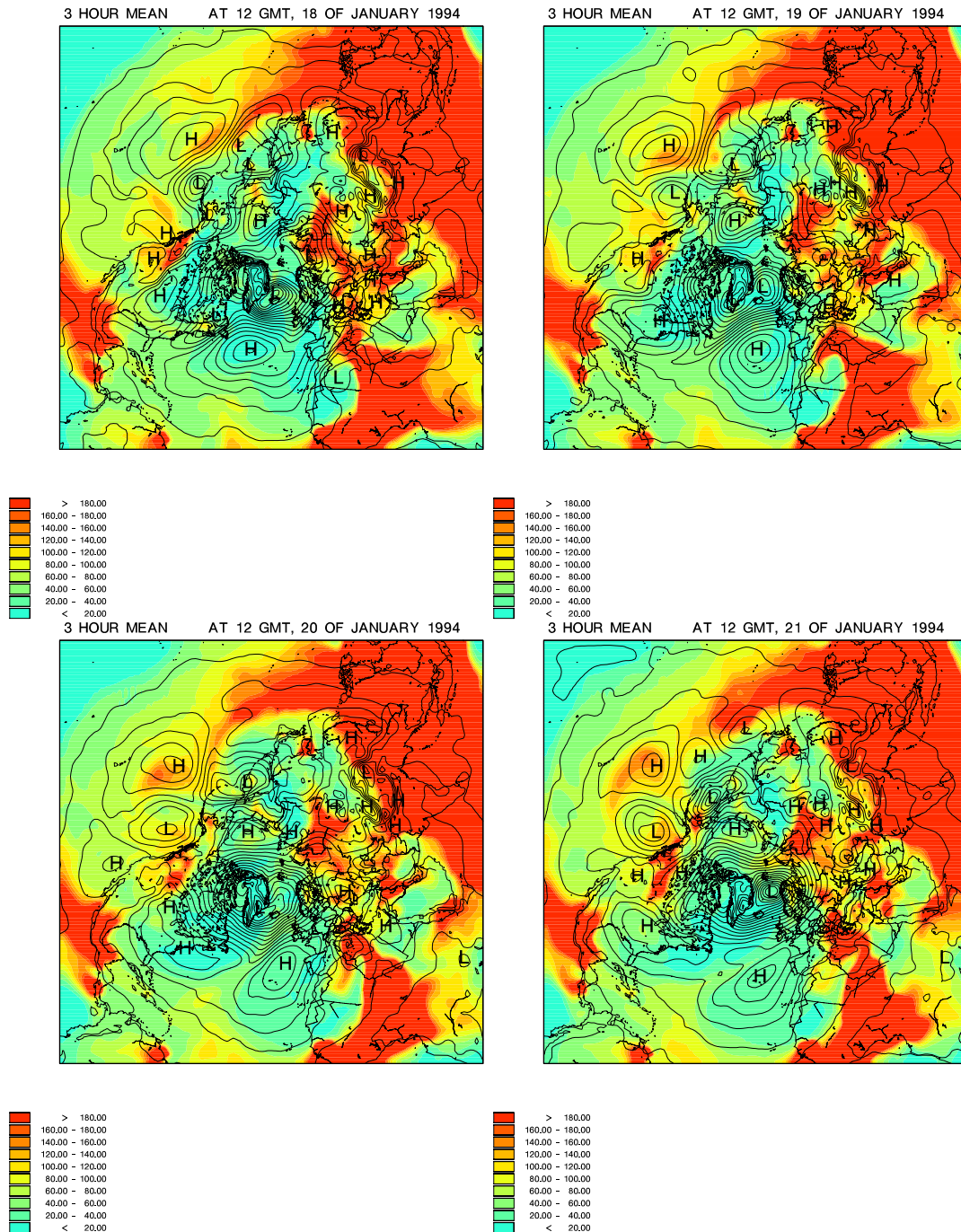


Figure 8.1: The 3 hour mean air concentrations ( $\text{pg m}^{-3}$ ) at 12 GMT for January 18 (upper left), 19 (upper right), 20 (lower left), and 21 (lower right). Black lines denotes isobars.

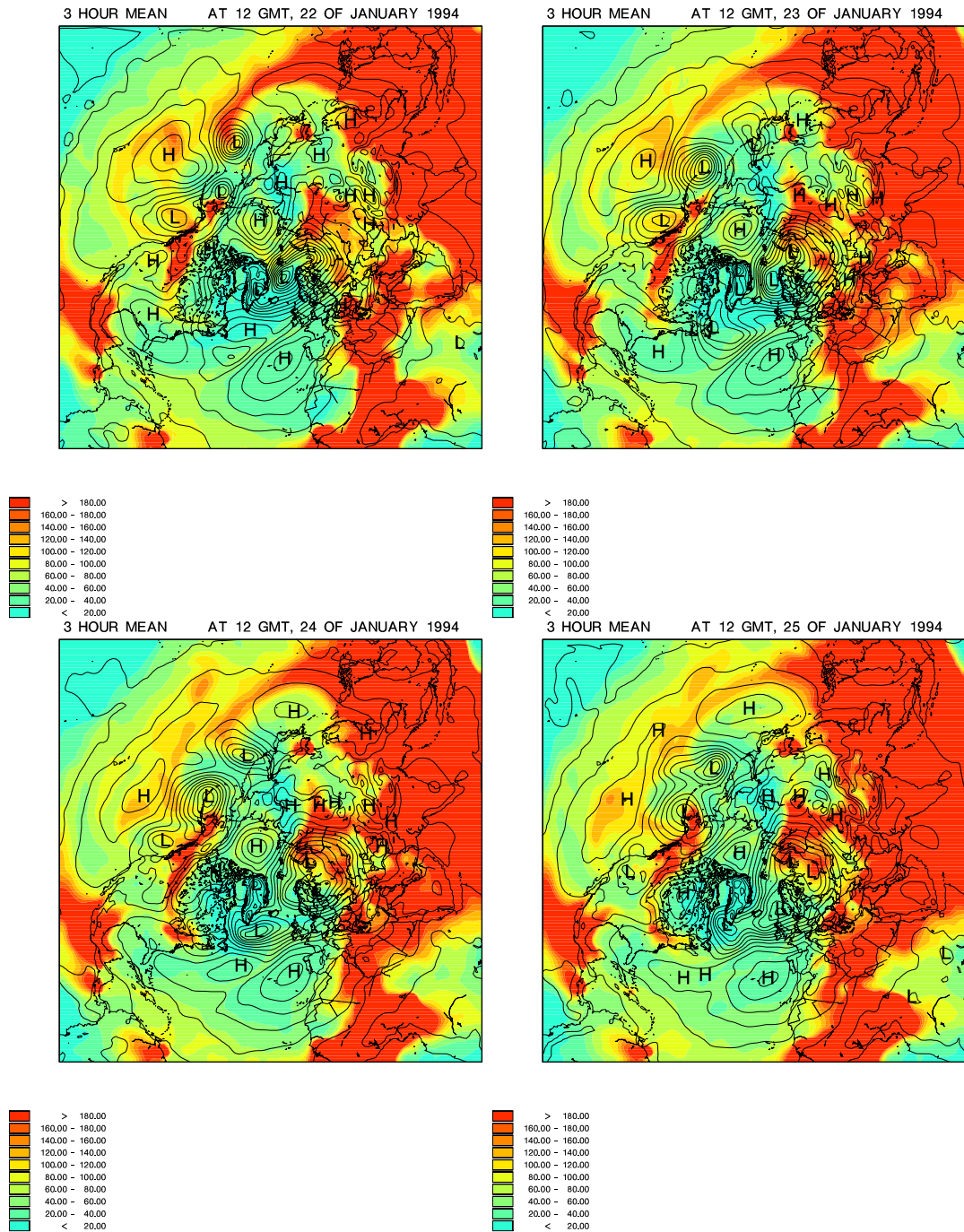


Figure 8.2: The 3 hour mean air concentrations ( $\text{pg m}^{-3}$ ) at 12 GMT for January 22 (upper left), 23 (upper right), 24 (lower left), and 25 (lower right). Black lines denotes isobars.

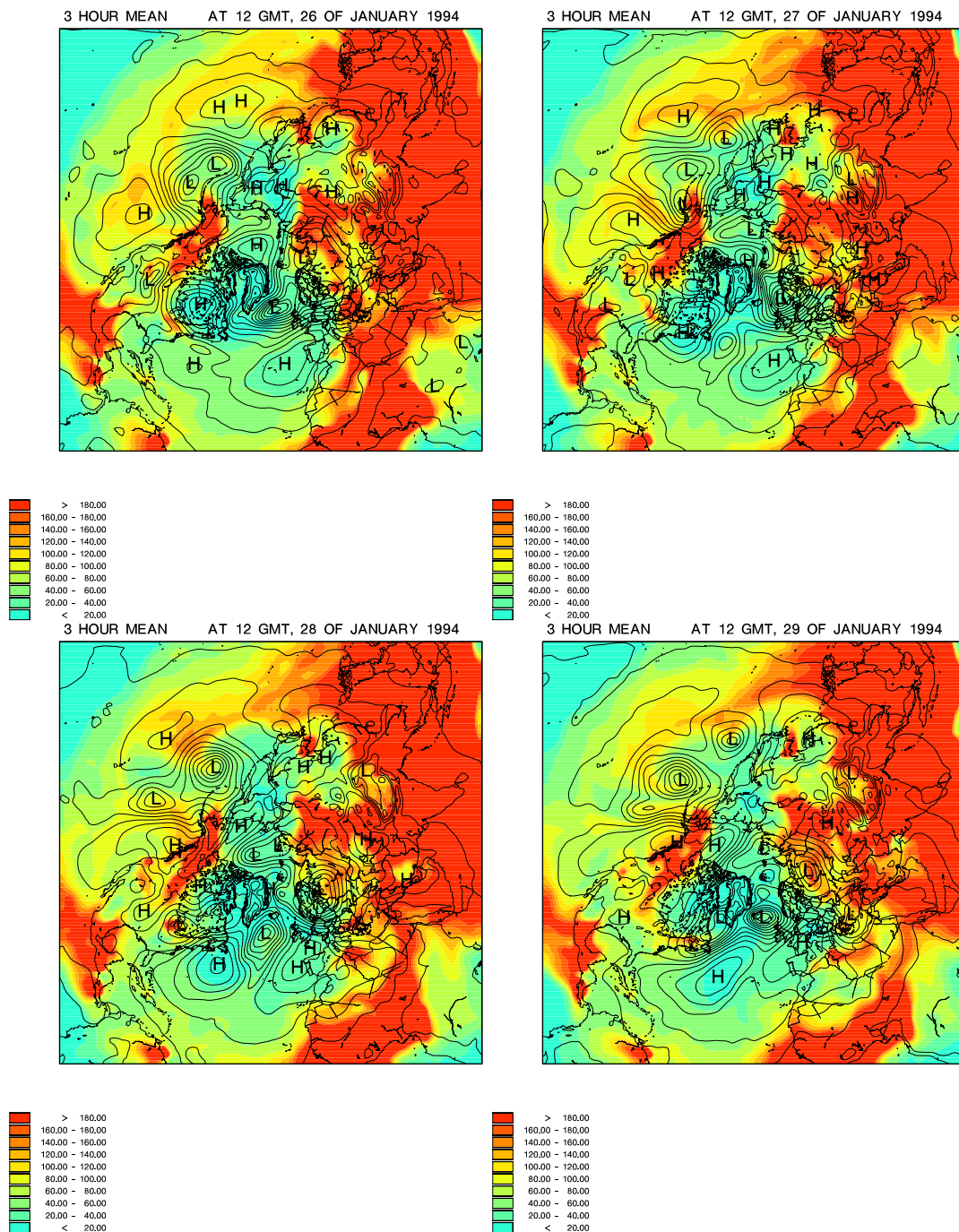


Figure 8.3: The 3 hour mean air concentrations ( $\text{pg m}^{-3}$ ) at 12 GMT for January 26 (upper left), 27 (upper right), 28 (lower left), and 29 (lower right). Black lines denotes isobars.

from the tongue, and moves eastwards over the following 5–6 days (see Figure 8.2). On January 27, the contaminated air mass moves towards the North American coast (see upper right of Figure 8.3), which it reaches on January 28 (see lower left of Figure 8.3), where it moves in over the continent this and the following day, which could have given rise to the elevated measured concentrations at Tagish in that period. It is thus probable that the elevated air concentration measured in this week originates from the southeast Asia. This type of study is also possible to make for the layers higher in the atmosphere within the model, which is not done here.

## 8.2 Long-term simulation: 1945-2000

The emission data used in this study span more than 5 decades, from 1945 to 2000, which makes it possible to simulate the atmospheric transport for this whole period. Unfortunately meteorological data were only available for the period from 1991 to 2000. However, it was attempted to simulate the transport by re-cycling the available meteorological data so the data from 1991 were used as input for the years 1951, 1961, 1971, and 1981, the data from 1992 was used for the years 1952, 1962, 1972, and 1982, and so on. The predicted air concentrations in the period 1945–1990 are not expected to represent the ‘real’ air concentrations on short-term. However, the longer-term average (e.g. annual averages) are probably fairly well estimated, although the 1990s not necessarily are climatic representative for the whole simulated period and the average atmospheric transport pattern for these years may differ.

Two 55 years long simulations were made in this way. The first simulation was made with similar conditions as the reference simulation. However, when reaching 1991 the ocean concentrations for this simulation were much higher than for the reference simulation, which resulted in higher air concentrations by about a factor of 3–4 due to increased re-volatilisation from the oceans. This indicates that the included surface ocean module, although adequately to account for the oceanic processes in the reference simulation, i.e. in a decade with decreasing primary emissions, is too simple to account for the oceanic processes over more than 50 years. Especially the lack of oceanic transport and vertical diffusion may be of importance in this context. To decrease the average residence time in the simple surface ocean module, a vertical diffusion in the ocean was introduced. The diffusion coefficient was set equal to  $3.0 \times 10^{-5} \text{ m}^2 \text{ s}^{-1}$ , which is on the same order of magnitude as the eddy diffusivity included in the ocean module of *Strand and Hov* [1996], and it decreases the average residence time in the surface ocean by about a factor of three. The results for the second 55 years long simulation including the vertical diffusion in the ocean predicted ocean concentrations, and thereby air concentrations, for 1991 closer to the values from the reference simulation, and thus also in better agreement with the measurements, than the first long-term simulation. The results from this simulation will shortly be described in this section.

The annual average air concentrations for the years 1950, 1960, 1970, 1980, 1990, and 2000 are plotted in Figures 8.4 and 8.5. The change in use pattern can be seen, from dominating emissions from North America and Egypt in 1950 and 1960, to eastern Europe and southeast Asia in 1970, with air concentrations reaching highest levels in 1980 and declining towards the end of the simulated period. The averaged predicted concentration

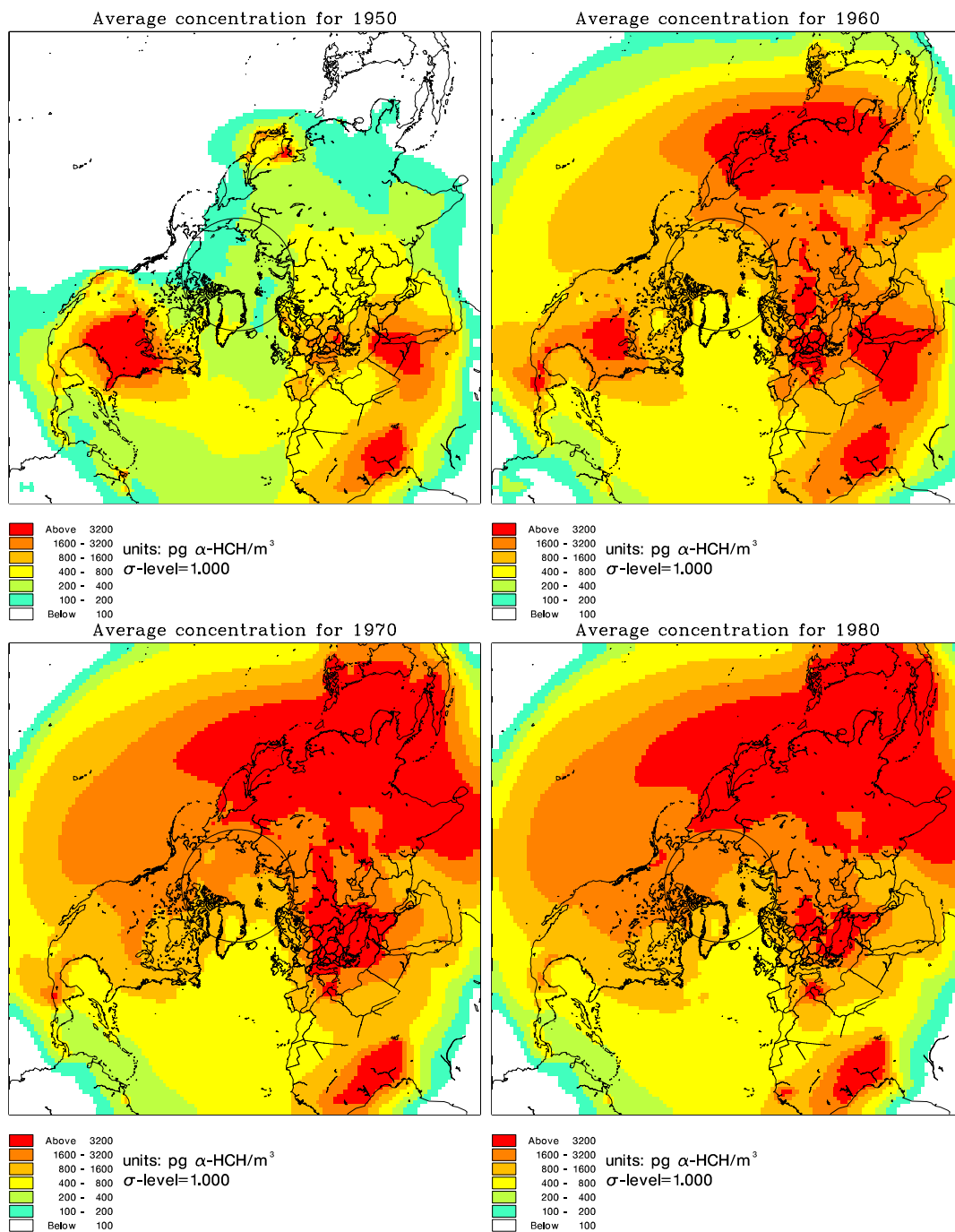


Figure 8.4: Predicted annual average air concentration for the years 1950, 1960, 1970, and 1980.

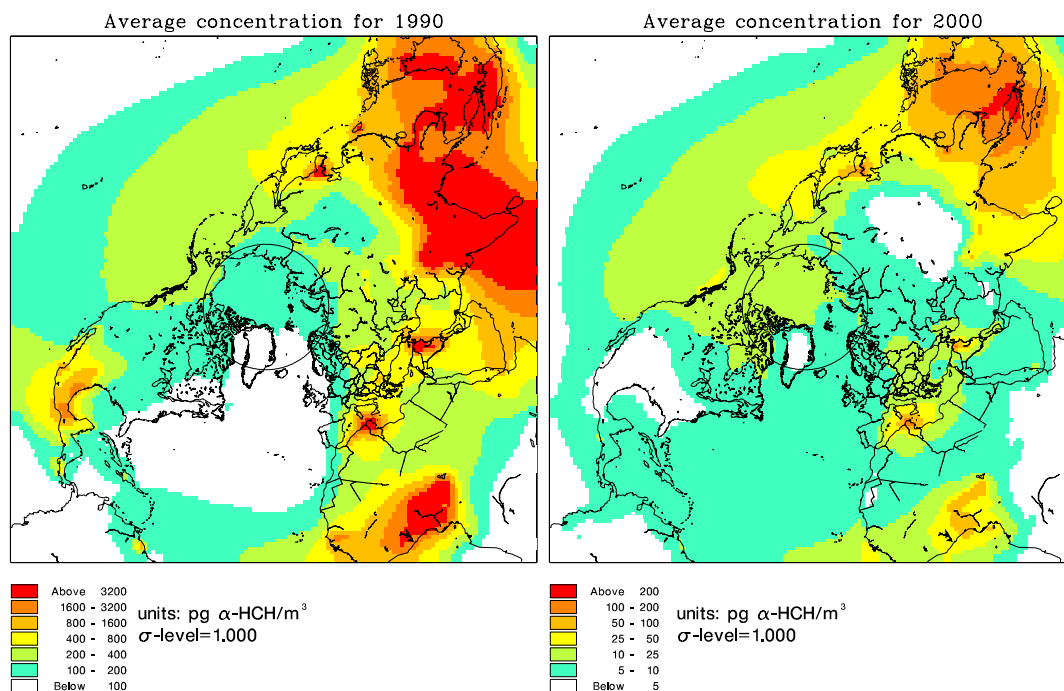


Figure 8.5: Predicted annual average air concentration for the years 1990, and 2000. Note the different colour scale.

for 2000 is seen to be lower than the averaged predicted concentration for the same year from the reference simulation (see 7.2 on page 83, note the different colour scale).

The annual average water concentrations for the years 1950, 1960, 1970, 1980, 1990, and 2000 are plotted in Figures 8.6 and 8.7. Similarly to the air concentrations, the water concentrations are increasing and reaching highest concentration in 1980. Compared to the initial ocean concentration used as input for the reference simulation (Figure 5.4 on page 72) and the annual average ocean concentration for 1991 (upper left part of Figure 7.8 on page 91) the predicted 1990 concentration for this simulation is higher close to the low-latitude source area around India and southeast Asia and in the North Pacific Ocean, whereas it is lower in the Arctic Ocean. This does not correspond to the ‘cold condensation’ pattern as observed (see Figure 2.4 on page 16), and it highlights the importance of the ocean currents in building up high  $\alpha$ -HCH concentrations in the Arctic Ocean. The predicted concentration for the year 2000 from this model simulation is lower than for the reference simulation for the whole domain.

The  $\alpha$ -HCH air concentrations for the whole simulated period are plotted for selected stations in Figure 8.8. One-year running averages are plotted to even out the inter-annual variations so the long-term trends can be studied. The upper part of Figure 8.8 display the concentrations at four stations close to or relatively close to major source areas. The results from these stations reflects the shift in usage pattern from North American and European in the 1950s and 1960s to India, where the usage peak around 1990. In the lower part of Figure 8.8 the predicted concentrations at three Arctic stations as well as one northern European station are plotted. It is interesting to note that the concentrations

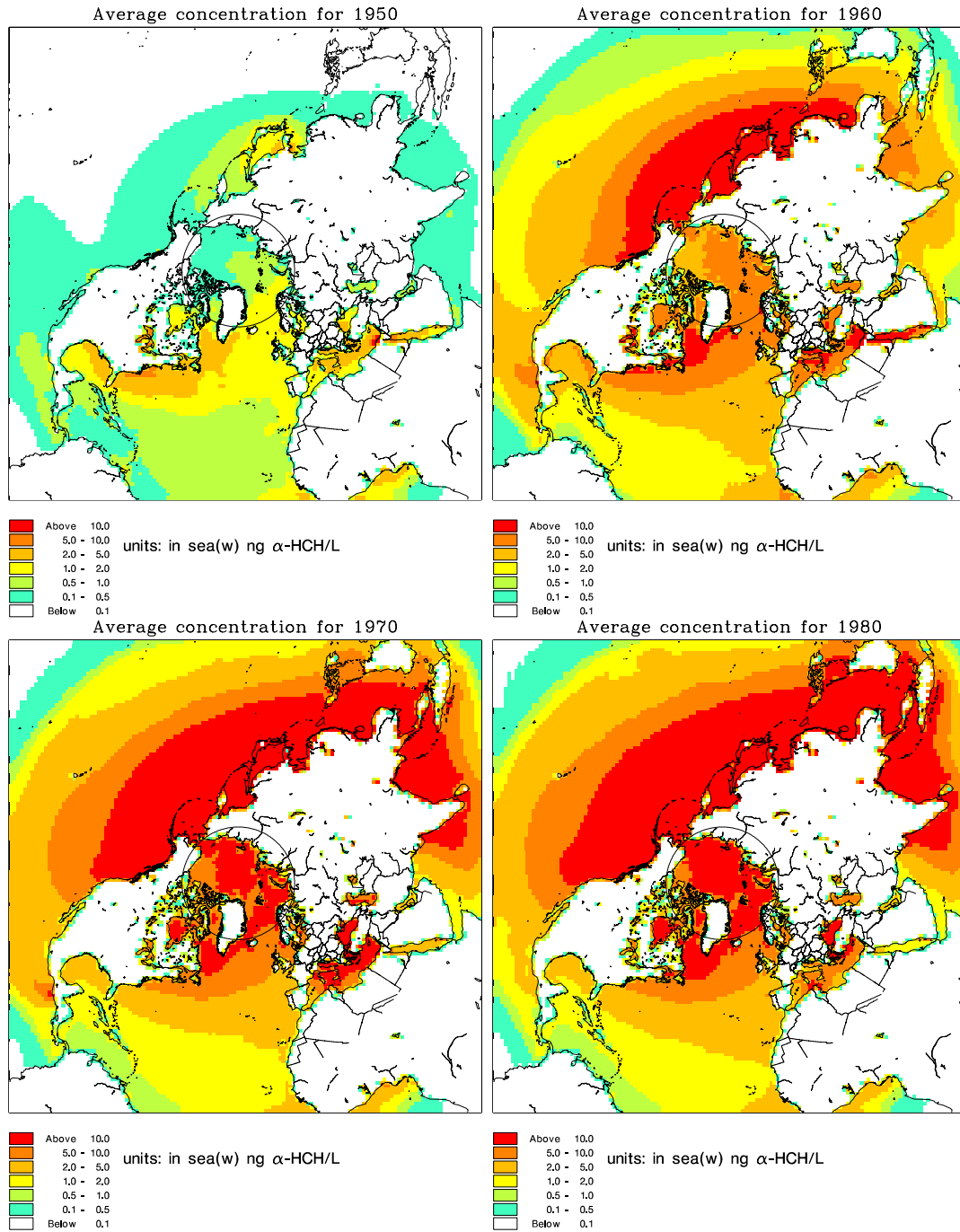


Figure 8.6: Predicted annual average water concentration for the years 1950, 1960, 1970, and 1980.

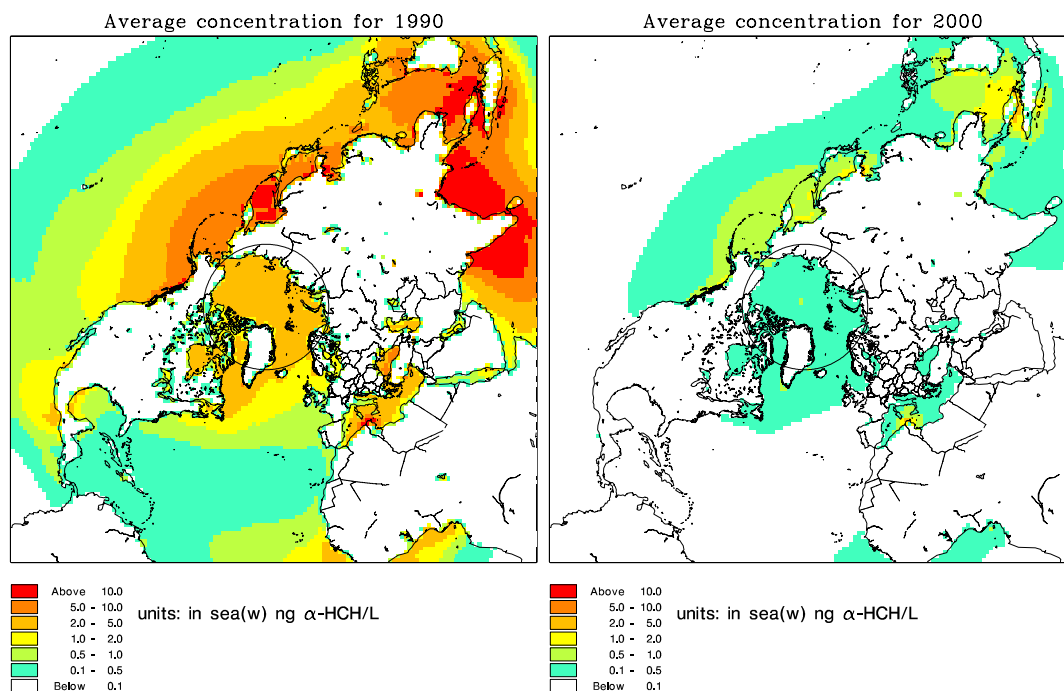


Figure 8.7: Predicted annual average water concentration for the years 1990 and 2000.

in the Arctic are higher than the concentrations in a more southerly non-source area from the 1960s and onwards and that they start to decrease later. This result seem to support the ‘cold condensation’ theory.

Only few environmental concentrations of  $\alpha$ -HCH have been measured before 1991, and it is thus not possible to evaluate the results from the first 45 years thoroughly. However, the predicted air concentrations for the 1990s can be evaluated similarly to the reference simulation. The result of this evaluation shows that the average predicted concentrations at all stations are lower than for the reference simulation. The predicted concentrations at Svalbard for the long-term and the reference simulations and the measured concentrations are plotted as time series in Figure 8.9 as an example. The predicted concentrations for the two simulations are close in the beginning of the simulated period, but the predicted concentrations for the long-term simulation decrease more rapidly than the predicted concentrations from the reference simulation, and also more rapidly than the measured concentrations. This indicates that the included surface ocean module is too simple for a study of the long-term distribution of  $\alpha$ -HCH in the oceans.

At all stations where the predicted concentrations for the reference simulation correlated with the measurements, the correlation between measurements and predicted concentrations from the long-term simulation is higher. For example, the correlation at Lista increases from  $r = 0.69$  to  $r=0.73$ , at Svalbard from  $r=0.35$  to  $r=0.46$  at Košetice it increases from  $r=0.29$  to  $r=0.45$ , and at Kinngait from  $r=0.39$  to  $r=0.54$  (all significant,  $p < 0.001$ ). This indicates that the variability of the air concentrations is better described in the long-term simulation. This is probably because the environmental residues in 1991 and onwards are better distributed for the long-term simulation than for the reference

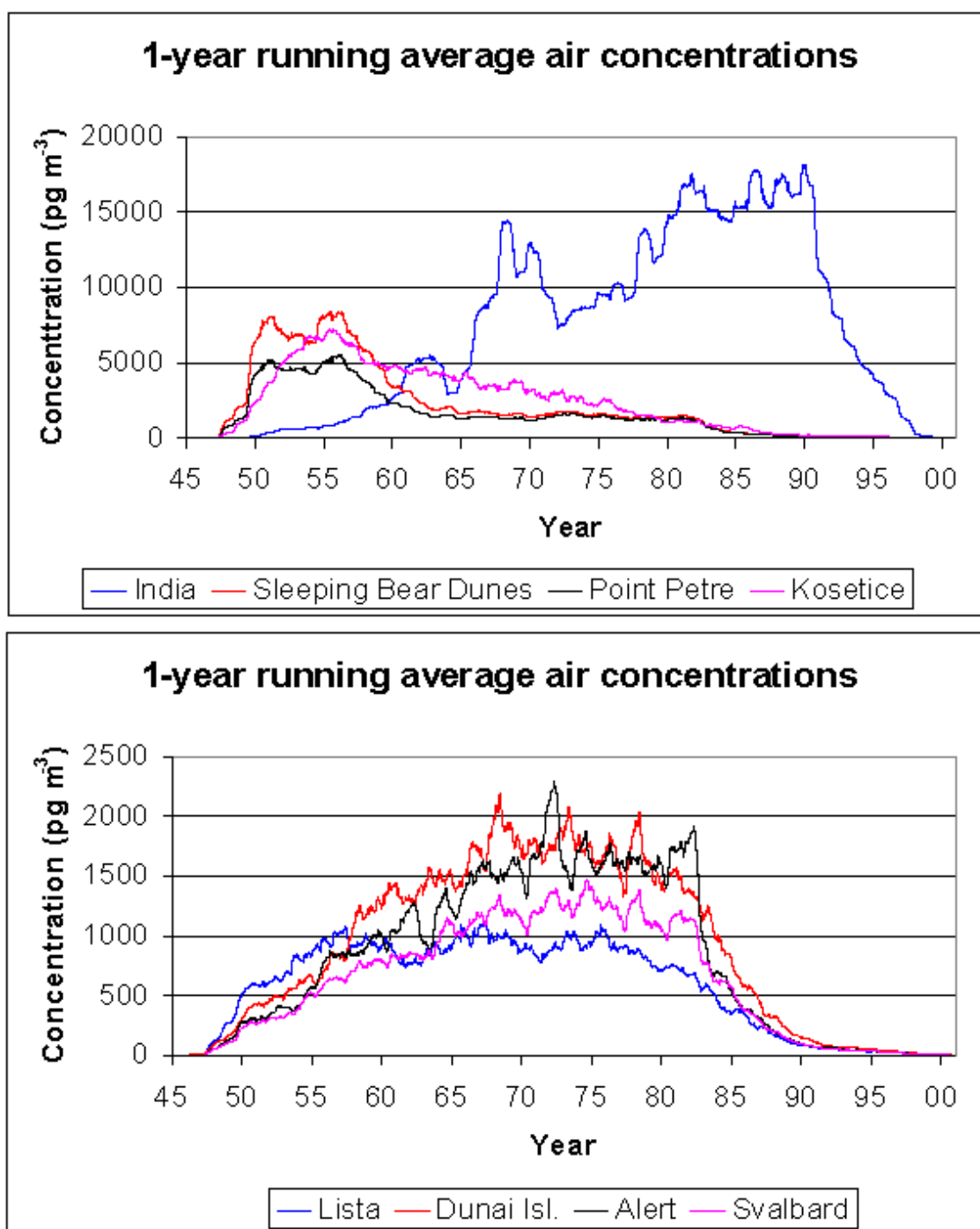


Figure 8.8: One-year running averaged predicted concentrations from Parangipettai, India; Sleeping Bear Dunes, USA; Point Petre, Canada; and Košetice, Czech Republic (upper), and for Lista Norway; Dunai Island, Russia, Alert, Canada; and Spitsbergen, Svalbard (lower).

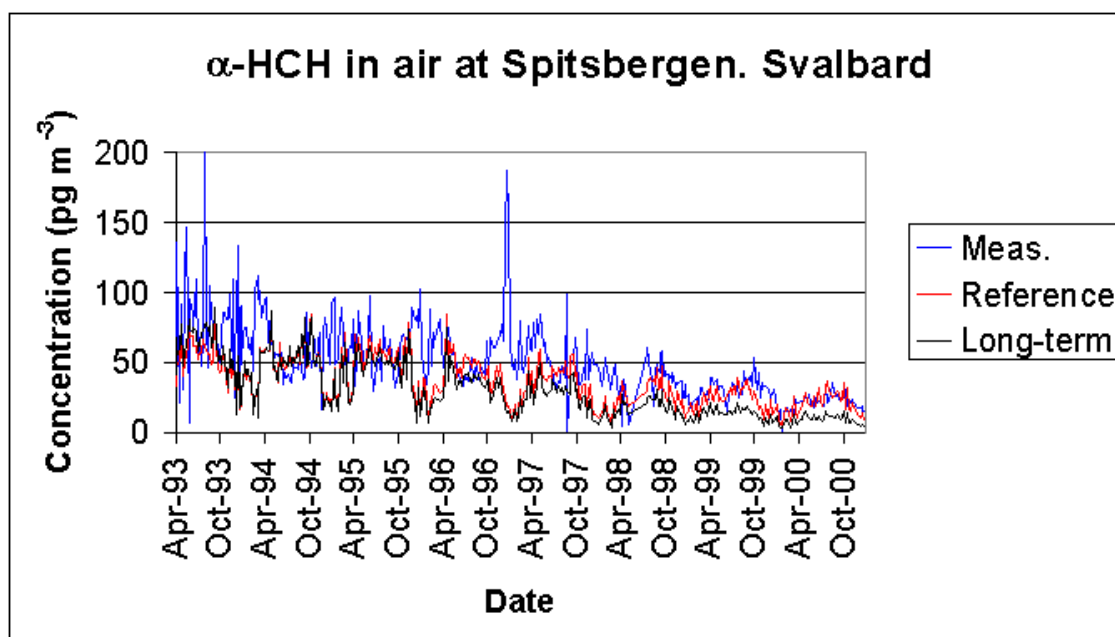


Figure 8.9: Predicted concentrations for the reference and the long-term simulations and measured concentrations at Spitsbergen, Svalbard.

simulation. This indicates that ‘spinning-up’ the model with historical emissions result in a better distribution of the ocean water concentrations than when estimating them from measurements, even though the ‘real’ meteorological data are not used as input for the spin-up period and even though the surface ocean module does not include oceanic transport. Furthermore, that the soil is contaminated with deposited  $\alpha$ -HCH from before 1991 is also more realistic than the zero initial soil concentrations applied in the reference simulation. This apparently does not only affects the results in the beginning of the 1990s, but also towards the end. For example the correlation at Košetice, where the available measurements cover the last two simulated years, is better than for the reference simulation.

For this simulation, the inventory in the different media was not calculated. This is however possible to do, and a mass balance study is thus feasible. It should be kept in mind though, that the model does not include a fresh water compartment and neither fresh water nor oceanic transport is described, so an eventual mass balance estimate will not be complete.



## Chapter 9

# Summary, conclusions and future perspectives

A POP version of the Danish Eulerian Hemispheric Model (DEHM-POP) — a dynamic, high-resolution, 3-D atmospheric chemistry transport model to study the environmental fate of POPs was developed in this study. The model covers the majority of the Northern Hemisphere with a horizontal resolution of  $150 \text{ km} \times 150 \text{ km}$  and it has 20 unevenly distributed vertical layers in terrain-following  $\sigma$ -coordinates. DEHM-POP was based on an atmospheric chemistry transport model which was expanded by including surface modules and atmospheric processes relevant for studying the environmental fate of POPs. The included surface modules were soil, water, snow and sea ice, and in the atmosphere gas-particle partitioning, wet deposition of gas- and particle phase POPs, dry particle deposition, and dry air-surface gas exchange processes were included.

### 9.1 Summary and conclusions

The model was tested for the compound  $\alpha$ -hexachlorocyclohexane ( $\alpha$ -HCH), the major component of the insecticide technical hexachlorocyclohexane.  $\alpha$ -HCH is one of the more volatile POPs with relatively high vapour pressure, and low  $K_{aw}$  and  $K_{oa}$  values. The atmospheric transport of  $\alpha$ -HCH was simulated for a ten year period from 1991 to 2000. Data from the numerical weather prediction model MM5v2 were used as meteorological driver for the model, and monthly averaged emission data for the whole period as well as initial ocean water concentrations based on observations were applied as input to this simulation.

The predicted  $\alpha$ -HCH air concentrations were compared with measurements from 23 different stations within the model domain. In general there was a good agreement between measured and predicted air concentrations. The model was able to predict long-term trends, annual averages as well as shorter-term variability of  $\alpha$ -HCH air concentrations at the studied stations. However, at some stations the discrepancy between measured and predicted concentrations could not be explained.

The most interesting finding from this study is the influence of the snowpack on the environmental fate of  $\alpha$ -HCH. The falling snow is an efficient scavenger of  $\alpha$ -HCH, which transfers large amounts of the chemical to the snowpack, from where it rapidly re-volatilise

into the air. This leads to increasing  $\alpha$ -HCH concentrations in the lowermost air, which may be transported further through the atmosphere by the advection and diffusion processes.

The predicted air concentrations were higher not only during winter, but also during summer when the snowpack was introduced. This is because the snowpack acts as a temporal storage medium, which releases almost all  $\alpha$ -HCH that is deposited more or less rapidly, whereas soil or water will retain a much larger fraction of the deposited  $\alpha$ -HCH in a snow-free area. The effect of the snowpack is thus to increase the transport of  $\alpha$ -HCH into the Arctic, by increasing the number of ‘grasshopper’ transport episodes.

Although the results from this model study concerning the role of the snowpack are not in agreement with previous model predictions, they are supported by the improved agreement with observations. It should be kept in mind that the snowpack not necessarily has the same role in the environmental fate of other POPs than  $\alpha$ -HCH. This depends on the combination of the physical-chemical properties, where the low  $K_{aw}$  of  $\alpha$ -HCH favours deposition by snow and the high vapour pressure leads to readily re-volatilisation.

The oceans were also seen to be important in supporting the atmospheric concentrations of  $\alpha$ -HCH in the simulated period. As the primary emissions decrease, the air concentrations are approaching equilibrium with the surface media, and the levels will be governed by re-volatilisation from the surface, primarily from the medium with the longest residence time, which is the water. This may raise questions about the long-term predictability capacity of the model, since the included ocean module is very simple with neither horizontal nor vertical oceanic transport. The difference between the results from the reference simulation and the two long-term simulations (with and without a reduced averaged residence time in the surface ocean compartment) clearly highlights the importance of a proper description of the oceanic processes for long-term model studies.

When studying persistent compounds with long environmental lifetimes for a period several decades after the initiation of usage of the compound, it becomes important to estimate the environmental concentrations in the beginning of the model simulation. The long-term simulation performed with DEHM-POP showed that the variability of the predicted concentrations were in better agreement with observations when the initial environmental concentrations were estimated by ‘spinning-up’ the model, even without meteorological data covering the whole period. Ideally it should be done for all studied compounds, although it is computationally demanding and requires detailed historical emission estimates for the compounds.

## 9.2 Future perspectives

There are several possible applications of the DEHM-POP model. This model study has shown, that the high spatial and temporal resolution of the model makes it possible to study short-term changes in the atmosphere as well as individual transport episodes. The long-term behaviour of POPs in the environment can also be studied, although these model simulations are computational demanding. The model will also be capable of predicting the contribution from different regions to the contamination at a specific site or in a region.

What this study also has shown is that the application of this model potentially can improve our understanding of the role of the individual environmental processes on the fate

of POPs. The environmental behaviour of POPs are determined by a range of non-linear processes, and when a dynamic model of this type include the most dominant processes, it is possible to study the influence of a single process, such as the snowpack, or the origin of an observed pattern.

The model should also be applicable for studies of the environmental fate of other POPs than  $\alpha$ -HCH. This requires reliable emission estimates and temperature dependent physical-chemical properties as well as reaction rates in the different media for the compound. However, several of the processes included in DEHM-POP are described using first-order approximations, and a review of the importance of the different processes may also be necessary. For example, the gas-particle partitioning process is not very important for  $\alpha$ -HCH and uncertainties in the description of this process may be of little importance. However, for compounds with a higher fraction sorbed to particles it will be of higher importance to describe this process properly. A short discussion of which processes that could be improved in the DEHM-POP model is given in this section.

It needs to be verified whether the *TSP*-concentration is well estimated with the present parameterisation in the model. It would also be interesting to test the dual organic matter absorption and black carbon adsorption gas-particle partitioning model proposed by *Lohmann and Lammel* [2004], although it would require an estimate of the black carbon concentration in the air as well.

The simple surface ocean module has its limitations. Especially for longer-term studies it will be necessary to include horizontal oceanic transport, and vertical movement of contaminants, i.e. by advection, diffusion, and sinking of particles may also be of importance.

Another surface module which at present is very simple is the vegetation module. An improvement of this module would be to introduce several types of vegetation, e.g. coniferous and deciduous forest and grass-land. This may improve the short-term predictability capacity of the model locally. Degradation in vegetation is another process that need to be investigated, however, this is at present not very well understood.

The snowpack module has proved efficient in increasing the predictability of the atmospheric variability. However, the analysis of the simulations with and without the snowpack module has pointed out some shortcomings of the module. The most important is probably the insufficient melting of the snowpack, which prolongs the snowpack season unrealistically. The treatment of the meltwater as well as the particles within the snowpack also needs further investigation. The degradation within the snowpack is also a process that may not be correctly described in the model, however this is not very well understood.

A revised soil module in DEHM-POP could possibly improve the long-term predictability capacity of the model. Such a soil module could include vertical movement of chemicals sorbed to soil particles, by e.g. bioturbation, cryoturbation and erosion into cracks in dry soil as suggested by *McLachlan et al.* [2002], dynamic water balance (i.e. non-constant fractions) and multiple layers and/or soil types (e.g. forest soil and cultivated soil).

Finally, there are several compartments not presently included in the model that possibly would enhance the predictability capacity of the model and enlarge the number of possible applications. One of these is a sea ice module, where an actively accumulating sea ice compartment transported by currents and wind may play a role in the re-distribution of contaminants within the Arctic Ocean. Also the fraction of open water within the sea ice could be better described in DEHM-POP. The lack of fresh water compartments and

transport as well as sediments limits the possible usage of the model for long-term mass balance studies.

## Chapter 10

# Acknowledgements

The work with this thesis started more than three and a half years ago and have been carried out at the Department of Atmospheric Environment, National Environmental Research Institute (NERI/ATMI), Roskilde, Denmark and at the Department of Geophysics (GA), Niels Bohr Institute for Astronomy, Physics and Geophysics, University of Copenhagen. My work was interrupted in November 2004 for a longer period when I lost my new-born daughter Sigrid. I first of all would like to express my gratitude to all the people who helped me and my family through this difficult period of our lives, especially Helle, Lis, Henrik, Susanne and others at The Danish Association for Support in the event of Infant Death (Landsforeningen til støtte ved spædbarnsdød), who have been a great help. Thanks also to family and friends for support and to colleagues at NERI/ATMI in general and Maria Mikkelsen in particular for a good reception upon my return to work.

Numerous people have helped in various ways during the work with this thesis. I would like to thank my two supervisors Jesper H. Christensen (NERI/ATMI) and Aksel Walløe Hansen (GA). Especially Jesper H. Christensen has been invaluable for the help with computer programming and discussions about process parameterisations and interpretation of model results. In addition, I am very grateful to Jørgen Brandt (NERI/ATMI) who has advised me on many aspects of my work that have improved this thesis, and to Crispin Halsall (Lancaster University) with whom I have had many fruitful discussions, especially regarding the development of the snowpack module.

During this project I had the pleasure of a six months long stay at the Environmental Organic Chemistry and Ecotoxicology Research Groups, Lancaster University, UK, arranged by Crispin Halsall. Thanks to Crispin Halsall and to Kevin Jones for letting me into their respective research groups. I would also like to thank Costas Prevedouros, Matteo Dalla Valle, Andy Sweetman, Ben Herbert, Jan Weber and the rest of the group in Lancaster for making the stay enjoyable.

Since the beginning of this project I have had many valuable discussions concerning the project or parts of it. I would like to thank Jesper H. Christensen, Jørgen Brandt, Lise M. Frohn, Camilla Geels, Henrik Skov, Crispin Halsall, Kevin Jones, Costas Prevedouros, Rainer Lohmann, Andy Sweetman, Matteo Dalla Valle, John Barber, Ed Wild, and Jan Weber for useful comments on this project along the way. Jesper H. Christensen, Jørgen Brandt, Aksel Walløe Hansen, Lise M. Frohn, Camilla Geels, Carsten Ambelas Skjøth, Henrik Skov and Costas Prevedouros are greatly acknowledged for their useful comments

to this manuscript.

In general I would like to thank my colleagues at NERI/ATMI for making the working days enjoyable and my family and friends for filling my life with other things than this project. Finally, thanks to my wife Pernille for her never ending support and believe in me, for accepting my preoccupation with this project and for stepping in for me in the family.

Several persons have helped with data for this study. I am very grateful to Dr. Yi-Fan Li for the unique and detailed emission estimates he has made available for me. Thanks also to professor Terry Bidleman for supplying a compilation of data on measurements of  $\alpha$ -HCH in ocean water and to Jrgen Bendtsen for extracting data on ocean currents from the HOPE model. I have also gained access to observational data on  $\alpha$ -HCH air concentrations for model evaluation from several sources. Thanks to Wenche Aas for data from the EMEP monitoring network, to Dr. Eva Brorström-Lundén for 1991 and 1992 data from Rörvik, to Pierette Blanchard for data from the IADN network, to Dr. Hailey Hung and Dr. Yushan Su for data from the Canadian Arctic Contaminants Program, To Dr. Phil Fellin for data from the Amderma station, and to Dr. Laurier Poissant for data from Québec. Meteorological data was provided by the European Center of Medium-range Weather Forecast and the Fifth-Generation NCAR/Penn State Mesoscale Model (MM5v2) was provided by Penn State University and UCAR.

This PhD project was partly funded by the Danish Research Training Council through the Copenhagen Global Change Initiative. I am also very grateful to NERI/ATMI for financial support.

# Bibliography

- Aas, W., S. Solberg, T. Berg, S. Manø, and K. E. Yttri, Monitoring of long range transported air pollutants, Annual report for 2002, technical report, Kjeller, Norwegian Institute for Air Research, SFT Report 877/2003 NILU OR 23/2003, 2003.
- Albert, M. R., and E. F. Shultz, Snow and firn properties and air-snow transport processes at Summit, Greenland, *Atmos. Environ.*, **36**, 2789–2797, 2002.
- AMAP, AMAP Assessment Report: Arctic Pollution Issues, technical report, Arctic Monitoring and Assessment Programme (AMAP), Oslo, Norway, 1998.
- AMAP, AMAP Assessment 2002: Persistent Organic Pollutants in the Arctic, technical report, Arctic Monitoring and Assessment Programme (AMAP), Oslo, Norway, 2004.
- Atkinson, R., R. Guicherit, R. A. Hites, W.-U. Palm, J. N. Seiber, and P. de Voogt, Transformation of pesticides in the atmosphere: a state of the art, *Water Air Soil Poll.*, **115**, 219–243, 1999.
- Aulagnier, F., and L. Poissant, Some pesticides occurrence in air and precipitation in Québec, Canada, *Environ. Sci. Technol.*, **39**, (9), 2960–2967, 2005.
- Bailey, R., L. A. Barrie, C. J. Halsall, P. Fellin, and D. C. G. Muir, Atmospheric organochlorine pesticides in the western Canadian Arctic: Evidence of transpacific transport, *J. Geophys. Res.*, **105**, (D9), 11,805–11,811, 2000.
- Ballschmiter, K., and R. Wittlinger, Interhemisphere exchange of hexachlorocyclohexanes, hexachlorobenzene, polychlorobiphenyls, and 1,1,1-trichloro-2,2-bis(*p*-chlorophenyl)ethane in the lower troposphere, *Environ. Sci. Technol.*, **25**, (6), 1103–1111, 1991.
- Barber, J. L., P. B. Kurt, G. O. Thomas, G. Kerstiens, and K. C. Jones, Investigation into the importance of the stomatal pathway in the exchange of PCBs between air and plants, *Environ. Sci. Technol.*, **36**, (20), 4282–4287, 2002.
- Barber, J. L., G. O. Thomas, G. Kerstiens, and K. C. Jones, Current issues and uncertainties in the measurement and modelling of air-vegetation exchange and within-plant processing of POPs, *Environ. Pollut.*, **128**, 99–138, 2004.
- Barrie, L. A., D. Gregor, B. Hargrave, R. Lake, D. Muir, R. Shearer, B. Tracey, and T. Bidleman, Arctic contaminants: sources, occurrence and pathways, *Sci. Total Environ.*, **122**, (1-2), 1–74, 1992.
- Bartnicki, J. A., A simple filtering procedure for removing negative values from numerical solutions of the advection equation, *Env. Software*, **4**, (4), 187–201, 1989.
- Berg, T., A. G. Hjellbrekke, and R. Larsen, Heavy metals and POPs within the EMEP region 1999, technical report, EMEP/CCC 9/2001, 2001.

- Beyer, A., F. Wania, T. Gouin, D. Mackay, and M. Matthies, Selecting internally consistent physicochemical properties of organic compounds, *Environ. Toxicol. Chem.*, **21**, (5), 941–953, 2002.
- Bidleman, T. F., Atmospheric processes, *Environ. Sci. Technol.*, **22**, (4), 361–367, 1988.
- Blais, J. M., D. W. Schindler, D. C. G. Muir, L. E. Kimpe, D. B. Donald, and B. Rosenberg, Accumulation of persistent organochlorine compounds in mountains of western Canada, *Nature*, **395**, 585–588, 1998.
- Blom, J. G., and J. G. Verwer, A comparison of integration methods for atmospheric transport-chemistry problems, *J. Comput. Appl. Math.*, **126**, 381–396, 2000.
- Borgå, K., M. Poltermann, A. Polder, O. Pavlova, B. Gulliksen, G. W. Gabrielsen, and J. U. Skaare, Influence of diet and sea ice drift on organochlorine bioaccumulation in Arctic ice-associated amphipods, *Environ. Pollut.*, **117**, 47–60, 2002.
- Brandt, J., J. H. Christensen, L. M. Frohn, F. Palmgren, R. Berkowicz, and Z. Zlatev, Operational air pollution forecasts from European to local scale, *Atmos. Environ.*, **35**, (Sup. 1), 91–98, 2001.
- Brandt, J., J. H. Christensen, L. M. Frohn, C. Geels, K. M. Hansen, and C. A. Skjøth, The THOR integrated air pollution forecast system - current status and ongoing developments, *Proceedings from the 2nd GLOREAM/EURASAP Workshop, Modern developments in modelling and chemical data analysis, Copenhagen, September 6-8, 2004*, pp. 10, 2004.
- Brandt, J., J. Christensen, L. M. Frohn, R. Berkowicz, C. A. Skjøth, C. Geels, K. M. Hansen, J. Frydendall, G. B. Hedegaard, O. Hertel, S. S. Jensen, M. Hvidberg, M. Ketzel, H. R. Olesen, P. Løfstrøm, , and Z. Zlatev, THOR - an operational and integrated model system for air pollution forecasting and management from global to local scale, *Proceedings from the First ACCENT Symposium, Urbino, Italy, 12th-16th September 2005*, pp. 10, 2005.
- Brevik, K., and F. Wania, Evaluating a model of the historical behavior of two hexachlorocyclohexanes in the Baltic Sea environment, *Environ. Sci. Technol.*, **36**, (5), 1014–1023, 2002a.
- Brevik, K., and F. Wania, Mass budgets, pathways, and equilibrium states of two hexachlorocyclohexanes in the Baltic Sea environment, *Environ. Sci. Technol.*, **36**, (5), 1024–1032, 2002b.
- Brevik, K., J. M. Pacyna, and J. Münch, Use of  $\alpha$ -,  $\beta$ - and  $\gamma$ -hexachlorocyclohexane in Europe, 1970-1996, *Sci. Total Environ.*, **239**, 151–163, 1999.
- Brevik, K., A. Sweetman, J. M. Pacyna, and K. C. Jones, Towards a global historical emission inventory for selected PCB congeners - a mass balance approach 1. Global production and consumption, *Sci. Total Environ.*, **290**, 181–198, 2002a.
- Brevik, K., A. Sweetman, J. M. Pacyna, and K. C. Jones, Towards a global historical emission inventory for selected PCB congeners - a mass balance approach 2. Emissions, *Sci. Total Environ.*, **290**, 199–224, 2002b.
- Brevik, K., R. Alcock, Y.-F. Li, R. E. Bailey, H. Fiedler, and J. M. Pacyna, Primary sources of selected POPs: regional and global scale emission inventories, *Environ. Pollut.*, **128**, 3–16, 2004.
- Brubaker, W. W., and R. A. Hites, OH reaction kinetics of gas-phase  $\alpha$ - and  $\gamma$ -hexachlorocyclohexane and hexachlorobenzene, *Environ. Sci. Technol.*, **32**, (6), 766–769, 1998.
- Buehler, S. S., and R. A. Hites, The Great Lakes integrated atmospheric deposition network, *Environ. Sci. Technol.*, **36**, (17), 354A–359A, 2002.
- Buehler, S. S., I. Basu, and R. A. Hites, Gas-phase polychlorinated biphenyl and hexachlorocyclohexane concentrations near the Great Lakes: A historical perspective, *Environ. Sci. Technol.*, **36**, (23), 5051–5056, 2002.

- Buehler, S. S., I. Basu, and R. A. Hites, Causes of variability in pesticide and PCB concentrations in air near the Great Lakes, *Environ. Sci. Technol.*, **38**, (2), 414–422, 2004.
- Cabanes, A., L. Legagneux, and F. Dominé, Rate of evolution of the specific surface area of surface snow layers, *Environ. Sci. Technol.*, **37**, (4), 661–666, 2003.
- Carson, R., *Silent Spring*, Houghton Mifflin, Boston, MA, USA, 1962.
- Chen, J. W., T. Harner, K.-W. Schramm, X. Quan, X. Y. Xue, W. Z. Wu, and A. Kettrup, Quantitative relationships between molecular structures, environmental temperatures and octanol-air partition coefficients of PCDD/Fs, *Sci. Total Environ.*, **300**, 155–166, 2002.
- Christensen, J. H., Testing advection schemes in a three-dimensional air pollution model, *Math. Comp. Model.*, **18**, (2), 75–88, 1993.
- Christensen, J. H., *Transport of Air Pollution in the Troposphere to the Arctic*, Ph.D. thesis, National Environmental Research Institute, Roskilde, Denmark, pp. 377, 1995.
- Christensen, J. H., The Danish Eulerian Hemispheric Model - A three-dimensional air pollution model used for the Arctic, *Atmos. Environ.*, **31**, (24), 4169–4191, 1997.
- Christensen, J. H., *An overview of modelling the Arctic mass budget of metals and sulphur: Emphasis on source apportionment of atmospheric burden and deposition*, In: Modelling and sources: A workshop on techniques and associated uncertainties in quantifying the origin and long-range transport of contaminants to the Arctic, Report and extended abstracts of the workshop, Bergen, 1416 June 1999, AMAP report 99:4. see also <http://www.amap.no/>, 1999.
- Christensen, J. H., J. Brandt, L. M. Frohn, and H. Skov, Modelling of mercury in the Arctic with the Danish Eulerian Hemispheric Model, *Atmos. Chem. Phys.*, **4**, 2251–2257, 2004.
- Cohen, M. D., R. R. Draxler, R. Artz, B. Commoner, P. Bartlett, P. Cooney, K. Couchot, A. Dickar, H. Eisl, C. Hill, J. Quigley, J. E. Rosenthal, D. Niemi, D. Ratté, M. Deslauriers, R. Laurin, L. Mathewson-Brake, and J. McDonald, Modeling the atmospheric transport and deposition of PCDD/F to the Great Lakes, *Environ. Sci. Technol.*, **36**, (22), 4831–4845, 2002.
- Cousins, I. T., and D. Mackay, Strategies for including vegetation compartments in multimedia models, *Chemosphere*, **44**, 643–654, 2001.
- Cousins, I. T., A. J. Beck, and K. C. Jones, A review of the processes involved in the exchange of semi-volatile organic compounds (SVOC) across the air-soil interface, *Sci. Total Environ.*, **228**, 5–24, 1999.
- Dachs, J., R. Lohmann, W. A. Ockenden, L. Méjanelle, S. J. Eisenreich, and K. C. Jones, Oceanic biogeochemical controls on global dynamics of persistent organic pollutants, *Environ. Sci. Technol.*, **36**, (20), 4229–4237, 2002.
- Dalla Valle, M., A. Marcomini, A. Sfriso, A. J. Sweetman, and K. C. Jones, Estimation of PCDD/F distribution and fluxes in the Venice Lagoon, Italy: combining measurement and modelling approaches, *Chemosphere*, **51**, 603–616, 2003.
- Daly, G. L., and F. Wania, Simulating the influence of snow on the fate of organic compounds, *Environ. Sci. Technol.*, **38**, (15), 4176–4186, 2004.
- Diamond, M. L., S. E. Gingrich, K. Fertuck, B. E. McCarty, G. A. Stern, B. Billeck, B. Grift, D. Brooker, and T. D. Yager, Evidence for organic film on an impervious urban surface: characterization and potential teratogenic effects, *Environ. Sci. Technol.*, **34**, (14), 2900–2908, 2000.
- Diamond, M. L., D. A. Priemer, and N. L. Law, Developing a multimedia model of chemical dynamics in an urban area, *Chemosphere*, **44**, 1655–1667, 2001.

- Dominé, F., and P. B. Shepson, Air-snow interactions and atmospheric chemistry, *Science*, **297**, 1506–1510, 2002.
- Dominé, F., A. Cabanes, and L. Legagneux, Structure, microphysics, and surface area of the Arctic snowpack near Alert during the ALERT 2000 campaign, *Atmos. Environ.*, **36**, 2753–2765, 2002.
- Dudhia, J., D. Gill, Y.-R. Guo, K. Manning, W. Wang, and V. Collin, PSU/NCAR Mesoscale Modeling System. Tutorial Class Notes and User's Guide: MM5 Modeling System Version 2, technical report, Mesoscale and Microscale Meteorology Division, Natl. Cent. for Atmos. Res., Boulder, Colo., 1999.
- Elliott, S., C.-Y. J. Kao, F. Gifford, S. Barr, M. Shen, R. P. Turco, and M. Jacobson, Free tropospheric ozone production after deep convection of dispersing tropical urban plumes, *Atmos. Environ.*, **30**, (24), 4263–4274, 1996.
- EMEP, EMEP measurement data online, Internet: <http://www.nilu.no/projects/ccc/emepdata.html>, 2005.
- Falconer, R. L., T. F. Bidleman, D. J. Gregor, R. Semkin, and C. Teixeira, Enantioselective breakdown of  $\alpha$ -hexachlorocyclohexane in a small Arctic lake and its watershed, *Environ. Sci. Technol.*, **29**, (5), 1297–1302, 1995.
- Farrar, N. J., T. Harner, M. Shoeib, A. Sweetman, and K. C. Jones, Field deployment of thin film passive air samplers for persistent organic pollutants: A Study in the urban atmospheric boundary layer, *Environ. Sci. Technol.*, **39**, (1), 42–48, 2005.
- Fellin, P., L. A. Barrie, D. Dougherty, D. Toom, D. Muir, N. Grift, L. Lockhart, and B. Billeck, Air monitoring in the Arctic: Results for selected persistent organic pollutants for 1992, *Environ. Toxicol. Chem.*, **15**, (3), 253–261, 1996.
- Finizio, A., D. Mackay, T. F. Bidleman, and T. Harner, Octanol-air partition coefficient as a predictor of partitioning of semi-volatile organic chemicals to aerosols, *Atmos. Environ.*, **31**, (15), 2289–2296, 1997.
- Forester, C. K., Higher order monotonic convective difference schemes, *J. Comput. Phys.*, **23**, 1–22, 1977.
- Franz, T. P., and S. J. Eisenreich, Snow scavenging of polychlorinated biphenyls and polycyclic aromatic hydrocarbons in Minnesota, *Environ. Sci. Technol.*, **32**, (12), 1771–1778, 1998.
- Frohn, L. M., *A Study of Long-term High-resolution Air Pollution Modelling*, Ph.D. thesis, National Environmental Research Institute, Roskilde, Denmark, pp. 444, 2004.
- Frohn, L. M., J. H. Christensen, and J. Brandt, Development of a high-resolution nested air pollution model - The numerical approach, *J. Comput. Phys.*, **179**, (1), 68–94, 2002.
- Frohn, L. M., J. H. Christensen, J. Brandt, C. Geels, and K. M. Hansen, Validation of a 3-D hemispheric nested air pollution model, *Atmos. Chem. Phys. Discuss.*, **3**, 3543–3588, 2003.
- Garmouma, M., and L. Poissant, Occurrence, temperature and seasonal trends of  $\alpha$ - and  $\gamma$ -HCH in air (Québec, Canada), *Atmos. Environ.*, **38**, 369–382, 2004.
- Geels, C., *Simulating the Current CO<sub>2</sub> Content of the Atmosphere: Including Surface Fluxes and Transport Across the Northern Hemisphere*, Ph.D. thesis, National Environmental Research Institute, Roskilde, Denmark, pp. 238, 2003.
- Geels, C., J. H. Christensen, A. W. Hansen, S. Kiilsholm, N. W. Larsen, S. E. Larsen, T. Pedersen, and L. L. Sørensen, Modeling concentrations and fluxes of atmospheric CO<sub>2</sub> in the North East Atlantic region, *Phys. Chem. Earth*, **26**, (10), 763–768, 2001.

- Geels, C., J. H. Christensen, L. M. Frohn, and J. Brandt, Simulating spatiotemporal variations of atmospheric CO<sub>2</sub> using a nested hemispheric model, *Phys. Chem. Earth*, **27**, (35), 1495–1505, 2002.
- Geels, C., J. H. Christensen, J. Brandt, L. M. Frohn, and K. M. Hansen, *A nested hemispheric model for simulations of atmospheric CO<sub>2</sub>* In: Air Pollution Modelling and Its Application XXVI, Kluwer Academic/Plenum Publishers, New York, Borrego and Incecik (eds.), pp. 215–223, 2004a.
- Geels, C., S. C. Doney, R. Dargaville, J. Brandt, and J. H. Christensen, Investigating the sources of synoptic variability in atmospheric CO<sub>2</sub> measurements over the Northern Hemisphere continents: a regional model study, *Tellus*, **56B**, 35–50, 2004b.
- Geels, C., J. Brandt, J. H. Christensen, L. M. Frohn, K. M. Hansen, and C. A. Skjøth, *Long-term calculations with a comprehensive nested hemispheric air pollution transport model* In: Advances in Air Pollution Modeling for Environmental Security, Springer, Netherlands, Farago et al. (eds.), pp. 11, 2005.
- Gifford, F., Horizontal diffusion in the atmosphere: A Lagrangian-dynamical theory, *Atmos. Environ.*, **16**, (3), 505–512, 1982.
- Goldberg, E. D., Synthetic organohalides in the sea, *P. Roy. Soc. B-Biol. Sci.*, **189**, 277–289, 1975.
- Granberg, H. D., *Snow cover on sea ice*, In: Physics of Ice-Covered Seas, Vol. 2, 605–649, Helsinki University Printing house, M. Leppäranta (ed.), 1998.
- Grell, G. A., J. Dudhia, and D. R. Stauffer, A description of the fifth-generation Penn State/NCAR Mesoscale Model (MM5), technical report, Mesoscale and Microscale Meteorology Division, Natl. Cent. for Atmos. Res., Boulder, Colo., NCAR Tech. Note, NCAR/TN-398+STR, 1995.
- Gusev, A., E. Mantseva, V. Shatalov, and B. Strukov, Regional Multicompartment Model MSCE-POP, technical report, MSC-E Technical Report 5/2005., 2005.
- Gustafsson, Ö., P. Andersson, J. Axelman, T. D. Bucheli, P. Kömp, M. S. McLachlan, A. Sobek, and J.-O. Thörngren, Observations of the PCB distribution within and in-between ice, snow, ice-rafted debris, ice-interstitial water, and seawater in the Barents Sea marginal ice zone and the North Pole area, *Sci. Total Environ.*, **342**, 261–279, 2005.
- Hafner, W. D., and R. A. Hites, Effects of wind and air trajectory directions on atmospheric concentrations of persistent organic pollutants near the Great Lakes, *Environ. Sci. Technol.*, **39**, (20), 7817–7825, 2005.
- Halsall, C. J., Investigating the occurrence of persistent organic pollutants (POPs) in the Arctic: their atmospheric behaviour and interaction with the seasonal snow pack, *Environ. Pollut.*, **128**, (1-2), 163–175, 2004.
- Halsall, C. J., L. A. Barrie, P. Fellin, D. C. G. Muir, B. N. Billeck, L. Lockhart, F. Ya. Rovinsky, E. Ya. Kononov, and B. Pastukhov, Spatial and temporal variation of polycyclic aromatic hydrocarbons in the Arctic atmosphere, *Environ. Sci. Technol.*, **31**, (12), 3593–3599, 1997.
- Halsall, C. J., R. Bailey, G. A. Stern, L. A. Barrie, P. Fellin, D. C. G. Muir, B. Rosenberg, F. Ya. Rovinsky, E. Ya. Kononov, and B. Pastukhov, Multi-year observations of organohalogen pesticides in the Arctic atmosphere, *Environ. Pollut.*, **102**, 51–62, 1998.
- Hanna, S. R., *Mesoscale meteorological model evaluation techniques with emphasis on needs of air quality models*, In: Mesoscale modeling of the atmosphere, vol. 25, chapter 6, 47–58, American Meteorological Society, R. A. Pielke and R. P. Pearce (ed.), 1994.

- Hansen, K. M., J. H. Christensen, J. Brandt, L. M. Frohn, and C. Geels, Modelling atmospheric transport of  $\alpha$ -hexachlorocyclohexane in the Northern Hemisphere with a 3-D dynamical model: DEHM-POP, *Atmos. Chem. Phys.*, **4**, 1125–1137, included in appendix 1, 2004.
- Hansen, K. M., J. H. Christensen, J. Brandt, L. M. Frohn, and C. Geels, *Modelling the atmospheric transport and environmental fate of persistent organic pollutants in the Northern Hemisphere using a 3-d dynamical model* In: Air Pollution Modelling and Its Application XXVII, Kluwer Academic/Plenum Publishers, New York, Borrego and Norman (eds.), *in press*, included in appendix 3, 2006a.
- Hansen, K. M., C. J. Halsall, and J. H. Christensen, A dynamic model to study the exchange of gas-phase persistent organic pollutants between air and a seasonal snowpack, *Environ. Sci. Technol.*, **40**, (8), 2644–2652, included in appendix 2, 2006b.
- Hansen, K. M., K. Prevedouros, A. J. Sweetman, K. C. Jones, and J. H. Christensen, A process-oriented inter-comparison of a box model and an atmospheric chemistry transport model: Insights into model structure using  $\alpha$ -HCH as the modelled substance, *Atmos. Environ.*, **40**, (12), 2089–2104, included in appendix 4, 2006c.
- Hargrave, B. T., W. P. Vass, P. E. Erikson, and B. R. Fowler, Atmospheric transport of organochlorines to the Arctic Ocean, *Tellus*, **40B**, 480–493, 1988.
- Harner, T., and T. F. Bidleman, Octanol-air partition coefficient for describing particle/gas partitioning of aromatic compounds in urban air, *Environ. Sci. Technol.*, **32**, (10), 1494–1502, 1998.
- Harner, T., H. Kylin, T. F. Bidleman, and W. M. J. Strachan, Removal of  $\alpha$ - and  $\gamma$ -hexachlorocyclohexane and enantiomers of  $\alpha$ -hexachlorocyclohexane in the eastern Arctic Ocean, *Environ. Sci. Technol.*, **33**, (8), 1157–1164, 1999.
- Haugen, J.-E., F. Wania, N. Ritter, and M. Schlabach, Hexachlorocyclohexanes in air in Southern Norway. Temporal variation, source allocation, and temperature dependence, *Environ. Sci. Technol.*, **32**, (2), 217–224, 1998.
- Heidam, N. Z., J. H. Christensen, P. Wählin, and H. Skov, Arctic atmospheric contaminants in NE Greenland: levels, variations, origins, transport, transformations and trends 1990 - 2001, *Sci. Total Environ.*, **331**, (1-3), 5–28, 2004.
- Hippelein, M., and M. S. McLachlan, Soil/air partitioning of semivolatile organic compounds. 1. method development and influence of physical-chemical properties, *Environ. Sci. Technol.*, **32**, (2), 310–316, 1998.
- Hippelein, M., and M. S. McLachlan, Soil/air partitioning of semivolatile organic compounds. 2. influence of temperature and relative humidity, *Environ. Sci. Technol.*, **34**, (16), 3521–3526, 2000.
- Hoff, J. T., D. Mackay, R. Gillham, and W. Y. Shiu, Partitioning of organic chemicals at the air-water interface in environmental systems, *Environ. Sci. Technol.*, **27**, (10), 2174–2180, 1993.
- Hoff, J. T., F. Wania, D. Mackay, and R. Gillham, Sorption of nonpolar organic vapors by ice and snow, *Environ. Sci. Technol.*, **29**, (8), 1982–1989, 1995.
- Holden, A. V., *Monitoring organochlorine contamination of the marine environment by the analysis of residues in seals*, In: Marine Pollution and Sea Life, 266–272, Fishing News Books Ltd., England, M. Ruivo (ed.), 1972.
- Hühnerfuss, H., J. Faller, W. A. König, and P. Ludwig, Gas chromatographic separation of the enantiomers of marine pollutants. 4. fate of hexachlorocyclohexane isomers in the Baltic and North Sea, *Environ. Sci. Technol.*, **26**, (11), 2127–2133, 1992.

- Hung, H., C. J. Halsall, P. Blanchard, H. H. Li, P. Fellin, G. A. Stern, and B. Rosenberg, Are PCBs in the Canadian Arctic atmosphere declining? Evidence from 5 years of monitoring, *Environ. Sci. Technol.*, **35**, (7), 1303–1311, 2001.
- Hung, H., C. J. Halsall, P. Blanchard, H. H. Li, P. Fellin, G. A. Stern, and B. Rosenberg, Temporal trends of organochlorine pesticides in the Canadian Arctic atmosphere, *Environ. Sci. Technol.*, **36**, (5), 862–868, 2002.
- Hung, H., P. Blanchard, C. J. Halsall, T. F. Bidleman, G. A. Stern, P. Fellin, D. C. G. Muir, L. A. Barrie, L. M. Jantunen, P. A. Helm, J. Ma, and A. Konoplev, Temporal and spatial variabilities of atmospheric polychlorinated biphenyls (PCBs), organochlorine (OC) pesticides and polycyclic aromatic hydrocarbons (PAHs) in the Canadian Arctic: Results from a decade of monitoring, *Sci. Total Environ.*, **342**, 119–144, 2005.
- IADN, Integrated Atmospheric Deposition Network, Internet: [http://www.msc-smc.ec.gc.ca/iadn/index\\_e.html](http://www.msc-smc.ec.gc.ca/iadn/index_e.html), 2005.
- Iversen, T., Numerical modelling of the long range atmospheric transport of sulphur dioxide and particulate sulphate to the Arctic, *Atmos. Environ.*, **23**, (11), 2571–2595, 1989.
- Iwata, H., S. Tanabe, N. Sakal, and R. Tatsukawa, Distribution of persistent organochlorines in the oceanic air and surface seawater and the role of ocean on their global transport and fate, *Environ. Sci. Technol.*, **27**, (6), 1080–1098, 1993.
- Jantunen, L. M., and T. F. Bidleman, Reversal of the air-water gas exchange direction of hexachlorocyclohexanes in the Bering and Chukchi Seas: 1993 versus 1988, *Environ. Sci. Technol.*, **29**, (4), 1081–1089, 1995.
- Jantunen, L. M., and T. F. Bidleman, Air-water gas exchange of hexachlorocyclohexanes (HCHs) and the enantiomers of  $\alpha$ -HCH in arctic regions, *J. Geophys. Res.*, **101**, (D22), 28,837–28,846, 1996.
- Jantunen, L. M., and T. F. Bidleman, Correction to “Air-water gas exchange of hexachlorocyclohexanes (HCHs) and the enantiomers of  $\alpha$ -HCH in arctic regions”, *J. Geophys. Res.*, **102**, (D15), 19,279–19,282, 1997.
- Jaward, F. M., N. J. Farrar, T. Harner, A. J. Sweetman, and K. C. Jones, Passive air sampling of PCBs, PBDEs, and organochlorine pesticides across Europe, *Environ. Sci. Technol.*, **38**, (1), 34–41, 2004.
- Jones, K. C., and P. de Voogt, Persistent organic pollutants (POPs): state of the science, *Environ. Pollut.*, **100**, 209–221, 1999.
- Jönsson, A., Ö. Gustafsson, J. Axelman, and H. Sundberg, Global accounting of PCBs in the continental shelf sediments, *Environ. Sci. Technol.*, **37**, (2), 245–255, 2003.
- Junge, C., *Basic considerations about trace constituents in the atmosphere as related to the fate of global pollutants*, In: *Fate of Pollutants in the Air and Water Environments, Part 1*, 7–26, John Wiley, New York, Suffett I.H. (Ed.), 1977.
- Jury, W. A., W. F. Spencer, and W. J. Farmer, Behavior assessment model for trace organics in soil: I. Model description, *J. Env. Qual.*, **12**, (4), 558–564, 1983.
- Jury, W. A., W. J. Farmer, and W. F. Spencer, Behavior assessment model for trace organics in soil: II. Chemical classification and parameter sensitivity, *J. Env. Qual.*, **13**, (4), 567–572, 1984a.
- Jury, W. A., W. F. Spencer, and W. J. Farmer, Behavior assessment model for trace organics in soil: III. Application of screening model, *J. Env. Qual.*, **13**, (4), 573–579, 1984b.
- Jury, W. A., W. F. Spencer, and W. J. Farmer, Behavior assessment model for trace organics in soil: IV. Review of experimental evidence, *J. Env. Qual.*, **13**, (4), 580–586, 1984c.

- Jury, W. A., W. F. Spencer, and W. J. Farmer, Behavior assessment model for trace organics in soil: I. Model description Erratum, *J. Env. Qual.*, **16**, (4), 448, 1987.
- Klán, P., and I. Holoubek, Ice (photo)chemistry. Ice as a medium for long-term (photo)chemical transformations — environmental implications, *Chemosphere*, **46**, 1201–1210, 2002.
- Klán, P., J. Klánová, I. Holoubek, and P. Čupr, Photochemical activity of organic compounds in ice induced by sunlight irradiation: The Svalbard project, *Geophys. Res. Lett.*, **30**, (6), 1313, doi:10.1029/2002GL016385, 2003.
- Klánová, J., P. Klán, J. Nosek, and I. Holoubek, Environmental ice photochemistry: Monochlorophenols, *Environ. Sci. Technol.*, **37**, (8), 1568–1574, 2003.
- Knap, A. H., and K. S. Binkley, Chlorinated organic compounds in the troposphere over the western North Atlantic Ocean measured by aircraft, *Atmos. Environ.*, **25A**, (8), 1507–1516, 1991.
- Korsnes, R., O. Pavlova, and F. Godtlielsen, Assessment of potential transport of pollutants into the Barents Sea via sea ice – an observational approach, *Mar. Pollut. Bull.*, **44**, 861–869, 2002.
- Koziol, A. S., and J. A. Pudykiewicz, Global-scale environmental transport of persistent organic pollutants, *Chemosphere*, **45**, 1181–1200, 2001.
- Kucklick, J. R., D. A. Hinckley, and T. F. Bidleman, Determination of Henry's law constants for hexachlorocyclohexanes in distilled water and artificial seawater as a function of temperature, *Marine Chemistry*, **34**, 197–209, 1991.
- Lam, B., M. L. Diamond, A. J. Simpson, P. A. Makar, J. Truong, and N. A. Hernandez-Martinez, Chemical composition of surface films on glass windows and implications for atmospheric chemistry, *Atmos. Environ.*, **39**, 6578–6586, 2005.
- Lammel, G., J. Feichter, and A. Leip, Long-range transport and multimedia partitioning of semivolatile organic compounds: a case study on two modern agrochemicals, technical report, Report Max Planck Institute for Meteorology No. 324, 2001.
- Lanser, D., and J. G. Verwer, Analysis of operator splitting for advection-diffusion-reaction problems from air pollution modelling, *J. Comput. Appl. Math.*, **111**, 201–216, 1999.
- Law, N. L., and M. L. Diamond, The role of organic films and the effect on hydrophobic organic compounds in urban areas: An hypothesis, *Chemosphere*, **36**, (12), 2607–2620, 1998.
- Legagneux, L., A. Cabanes, and F. Dominé, Measurement of the specific surface area of 176 snow samples using methane adsorption at 77 K, *J. Geophys. Res.*, **107**, (D17), 4335, doi:10.1029/2001JD001016, 2002.
- Lei, Y. D., and F. Wania, Is rain or snow a more efficient scavenger of organic chemicals?, *Atmos. Environ.*, **38**, 3557–3571, 2004.
- Lerche, D., E. van de Plassche, A. Schwegler, and F. Balk, Selecting chemical substances for the UN-ECE POP Protocol, *Chemosphere*, **47**, 617–630, 2002.
- Li, Y.-F., Global technical hexachlorocyclohexane usage and its contamination consequences in the environment: from 1948 to 1997, *Sci. Total Environ.*, **232**, 121–158, 1999.
- Li, Y.-F., and R. W. Macdonald, Sources and pathways of selected organochlorine pesticides to the Arctic and the effect of pathway divergence on HCH trends in biota: a review, *Sci. Total Environ.*, **342**, (1-3), 87–106, 2005.
- Li, Y.-F., T. F. Bidleman, L. A. Barrie, and L. L. McConnell, Global hexachlorocyclohexane use trends and their impact on the Arctic atmospheric environment, *Geophys. Res. Lett.*, **25**, (1), 39–41, 1998.

- Li, Y.-F., M. T. Scholtz, and B. J. van Heyst, Global gridded emission inventories of  $\alpha$ -hexachlorocyclohexane, *J. Geophys. Res.*, **105**, (D5), 6621–6632, 2000.
- Li, Y.-F., R. W. Macdonald, L. M. M. Jantunen, T. Harner, T. F. Bidleman, and W. M. J. Strachan, The transport of  $\beta$ -hexachlorocyclohexane to the western Arctic Ocean: a contrast to  $\alpha$ -HCH, *Sci. Total Environ.*, **291**, 229–246, 2002.
- Li, N., F. Wania, Y. D. Lei, and G. Daly, A comprehensive and critical compilation, evaluation, and selection of physical-chemical property data for selected polychlorinated biphenyls, *J. Phys. Chem. Ref. Data.*, **32**, (4), 1545–1590, 2003a.
- Li, Y.-F., M. T. Scholtz, and B. J. van Heyst, Global gridded emission inventories of  $\beta$ -hexachlorocyclohexane, *Environ. Sci. Technol.*, **37**, (16), 3493–3498, 2003b.
- Li, Y.-F., R. W. Macdonald, J. M. Ma, H. Hung, and S. Venkatesh, Historical  $\alpha$ -HCH budget in the Arctic Ocean: the Arctic Mass Balance Box Model (AMBBM), *Sci. Total Environ.*, **324**, (1-3), 115–139, 2004a.
- Li, Y.-F., S. Venkatesh, and D. Li, Modeling global emissions and residues of pesticides, *Environ. Mon. Assess.*, **9**, 237–243, 2004b.
- Ligocki, M. J., C. Leuenberger, and J. F. Pankow, Trace organic compounds in rain - II. Gas scavenging of neutral organic compounds, *Atmos. Environ.*, **19**, (10), 1609–1617, 1985a.
- Ligocki, M. J., C. Leuenberger, and J. F. Pankow, Trace organic compounds in rain - II. Particle scavenging of neutral organic compounds, *Atmos. Environ.*, **19**, (10), 1619–1626, 1985b.
- Lohmann, R., and G. Lammel, Adsorptive and absorptive contributions to the gas-particle partitioning of Polycyclic Aromatic Hydrocarbons: state of knowledge and recommended parametrization for modeling, *Environ. Sci. Technol.*, **38**, (14), 3793–3803, 2004.
- Macdonald, R. W., L. A. Barrie, T. F. Bidleman, M. L. Diamond, D. J. Gregor, R. G. Semkin, W. M. J. Strachan, Y.-F. Li, F. Wania, M. Alaee, L. B. Alexeeva, S. M. Backus, R. Bailey, J. M. Bewers, C. Gobeil, C. J. Halsall, T. Harner, J. T. Hoff, L. M. M. Jantunen, W. L. Lockhart, D. Mackay, D. C. G. Muir, J. Pudykiewicz, K. J. Reimer, J. N. Smith, G. A. Stern, W. H. Schroeder, R. Wagemann, and M. B. Yunker, Contaminants in the Canadian Arctic: 5 years of progress in understanding sources, occurrence and pathways, *Sci. Total Environ.*, **254**, (2-3), 93–234, 2000.
- Mackay, D., *Multimedia Environmental Models: The Fugacity Approach, second ed.*, Lewis Publishers, 2001.
- MacLeod, M., D. G. Woodfine, D. Mackay, T. McKone, D. Bennett, and R. Maddalena, BETR North America: A regionally segmented multimedia contaminant fate model for North America, *Environ. Sci. Pollut. R.*, **8**, (3), 156–163, 2001.
- MacLeod, M., W. J. Riley, and T. E. McKone, Assessing the influence of climate variability on atmospheric concentrations of polychlorinated biphenyls using a global-scale mass balance model (BETR Global), *Environ. Sci. Technol.*, **39**, (17), 6749–6756, 2005.
- Ma, J., S. Daggupati, T. Harner, and Y.-F. Li, Impacts of Lindane usage in the Canadian prairies on the Great Lakes ecosystem, 1. Coupled atmospheric transport model and modeled concentrations in air and soil, *Environ. Sci. Technol.*, **37**, (17), 3774–3781, 2003a.
- Ma, J., S. Venkatesh, and L. M. Jantunen, Evidence of the impact of ENSO events on temporal trends of hexachlorobenzene air concentrations over the Great Lakes, *Sci. Total Environ.*, **313**, 177–184, 2003b.

- Ma, J., Z. Cao, and H. Hung, North Atlantic Oscillation signatures in the atmospheric concentrations of persistent organic pollutants: An analysis using Integrated Atmospheric Deposition Network-Great Lakes monitoring data, *J. Geophys. Res.*, **109**, D12305, doi:10.1029/2003JD004435, 2004a.
- Ma, J., S. Daggupati, T. Harner, P. Blanchard, and D. Waite, Impacts of Lindane usage in the Canadian prairies on the Great Lakes ecosystem, 2. Modeled fluxes and loadings to the Great Lakes, *Environ. Sci. Technol.*, **38**, (4), 984–990, 2004b.
- Ma, J., H. Hung, and P. Blanchard, How do climate fluctuations affect persistent organic pollutant distribution in North America? Evidence from a decade of air monitoring, *Environ. Sci. Technol.*, **38**, (9), 2538–2543, 2004c.
- Malanichev, A., E. Mantseva, V. Shatalov, B. Strukov, and N. Vulykh, Numerical evaluation of the PCBs transport over the Northern Hemisphere, *Environ. Pollut.*, **128**, (1-2), 279–289, 2004.
- Marsland, S. J., H. Haak, J. H. Jungclaus, M. Latif, and F. Röske, The Max-Planck-Institute global ocean/sea ice model with orthogonal curvilinear coordinates, *Ocean Model.*, **5**, 91–127, 2003.
- McLachlan, M. S., and M. Horstmann, Forests as filters of airborne organic pollutants: a model, *Environ. Sci. Technol.*, **32**, (3), 413–420, 1998.
- McLachlan, M. S., G. Czub, and F. Wania, The influence of vertical sorbed phase transport on the fate of organic chemicals in surface soils, *Environ. Sci. Technol.*, **36**, (22), 4860–4867, 2002.
- Meijer, S. N., W. A. Ockenden, A. Sweetman, K. Breivik, J. O. Grimalt, and K. C. Jones, Global distribution and budget of PCBs and HCB in background surface soils: implications for sources and environmental processes, *Environ. Sci. Technol.*, **37**, (4), 667–672, 2003a.
- Meijer, S. N., M. Shoeib, L. M. M. Jantunen, K. C. Jones, and T. Harner, Air-soil exchange of organochlorine pesticides in agricultural soils. 1. field measurements using a novel in situ sampling device, *Environ. Sci. Technol.*, **37**, (7), 1292–1299, 2003b.
- Meijer, S. N., M. Shoeib, K. C. Jones, and T. Harner, Air-soil exchange of organochlorine pesticides in agricultural soils. 2. laboratory measurements of the soil-air partition coefficient, *Environ. Sci. Technol.*, **37**, (7), 1300–1305, 2003c.
- Miguel, A. H., A. Eiguren-Fernandez, P. A. Jaques, J. R. Froines, B. L. Grant, P. R. Mayo, and C. Sioutas, Seasonal variation of the particle size distribution of polycyclic aromatic hydrocarbons and of major aerosol species in Claremont, California, *Atmos. Environ.*, **38**, 3241–3251, 2004.
- Muir, D. C. G., B. Hargrave, R. Wagemann, B. T. Hargrave, D. J. Thomas, D. B. Peakall, and R. J. Norstrom, Arctic marine ecosystem contamination, *Sci. Total Environ.*, **122**, (1-2), 75–134, 1992.
- Myneni, R. B., R. R. Nemani, and S. W. Running, Algorithm for the estimation of global land cover, LAI and FPAR based on radiative transfer models, *IEEE Trans. Geosc. Remote Sens.*, **35**, 1380–1393, 1997.
- Ngabe, B., T. F. Bidleman, and R. L. Falconer, Base hydrolysis of  $\alpha$ - and  $\gamma$ -hexachlorocyclohexanes, *Environ. Sci. Technol.*, **27**, (9), 1930–1933, 1993.
- Oehme, M., Further evidence for long range air transport of polychlorinated aromates and pesticides: North America and Eurasia to the Arctic, *Ambio*, **20**, 293–297, 1991.
- Oehme, M., J.-E. Haugen, and M. Schlabach, Seasonal changes and relations between levels of organochlorines in arctic ambient air: First results of an all-year-round monitoring program at Ny-Ålesund, Svalbard, Norway, *Environ. Sci. Technol.*, **30**, (7), 2294–2304, 1996.

- Paasivirta, J., S. Sinkkonen, P. Mikkelsen, T. Rantio, and F. Wania, Estimation of vapor pressures, solubilities and Henry's law constants of selected persistent organic pollutants as functions of temperature, *Chemosphere*, **39**, (5), 811–832, 1999.
- Pacyna, J. M., and M. Oehme, Long-range transport of some organic compounds to the Norwegian Arctic, *Atmos. Environ.*, **22**, (2), 243–257, 1988.
- Pankow, J. F., Review and comparative analysis of the theories on partitioning between the gas and aerosol particulate phases in the atmosphere, *Atmos. Environ.*, **21**, (11), 2275–2283, 1987.
- Pankow, J. F., The calculated effect of non-exchangeable material on the gas particle distribution of organic compounds, *Atmos. Environ.*, **22**, (7), 1405–1409, 1988.
- Pankow, J. F., An absorption model of gas/aerosol partitioning involved in the formation of secondary organic aerosol, *Atmos. Environ.*, **28**, (2), 189–193, 1994a.
- Pankow, J. F., An absorption model of gas/particle partitioning of organic compounds in the atmosphere, *Atmos. Environ.*, **28**, (2), 185–188, 1994b.
- Pankow, J. F., Further discussion of the octanol/air partition coefficient  $K_{oa}$  as a correlating parameter for gas/particle partitioning coefficients, *Atmos. Environ.*, **32**, (9), 1493–1497, 1998.
- Paterson, W. S. B., *The Physics of Glaciers*, 3rd ed., Pergamon: New York, 1994.
- Patton, G. W., M. D. Walla, T. F. Bidleman, and L. A. Barrie, Polycyclic aromatic and organochlorine compounds in the atmosphere of northern Ellesmere-Island, Canada, *J. Geophys. Res.*, **96**, (D6), 10867–10877, 1991.
- Pfirman, S. L., H. Eicken, D. Bauch, and W. F. Weeks, The potential transport of pollutants by Arctic sea ice, *Sci. Total Environ.*, **159**, 129–146, 1995.
- Poissant, L., and J.-F. Koprivnjak, Fate and atmospheric concentrations of  $\alpha$ - and  $\gamma$ -hexachlorocyclohexane in Québec, Canada, *Environ. Sci. Technol.*, **30**, (3), 845–851, 1996.
- Prevedouros, K., K. C. Jones, and A. J. Sweetman, European-scale Modeling of concentrations and distribution of polybrominated diphenyl ethers in the pentabromodiphenyl ether product, *Environ. Sci. Technol.*, **38**, (22), 5993–6001, 2004a.
- Prevedouros, K., M. MacLeod, K. C. Jones, and A. J. Sweetman, Modelling the fate of persistent organic pollutants in Europe: parameterisation of a gridded distribution model, *Environ. Pollut.*, **128**, (1-2), 251–261, 2004b.
- Priemer, D. A., and M. L. Diamond, Application of the multimedia urban model to compare the fate of SOCs in an urban and forested watershed, *Environ. Sci. Technol.*, **36**, (5), 1004–1013, 2002.
- Raja, S., and K. T. Valsaraj, Adsorption and transport of gas-phase naphthalene on micron-size fog droplets in air, *Environ. Sci. Technol.*, **38**, (3), 763–768, 2004.
- Rajendran, R. B., V. K. Venugopalan, and R. Ramesh, Pesticide residues in air from coastal environment, South India, *Chemosphere*, **39**, (10), 1699–1706, 1999.
- Ramesh, R., S. Tanabe, R. Tatsukawa, A. N. Subramanian, S. Palanichamy, D. Mohan, and V. K. Venugopalan, Seasonal variations of organochlorine insecticide residues in air from Porto Novo, South India, *Environ. Pollut.*, **62**, 213–222, 1989.
- Roth, C. M., K.-U. Goss, and R. P. Schwarzenbach, Adsorption of a diverse set of organic vapors on the bulk water surface, *J. Colloid. Interf. Sci.*, **252**, 21–30, 2002.
- Roth, C. M., K.-U. Goss, and R. P. Schwarzenbach, Sorption of diverse organic vapors to snow, *Environ. Sci. Technol.*, **38**, (15), 4078–4084, 2004.

- Roth, C. M., K.-U. Goss, and R. P. Schwarzenbach, Sorption of a diverse set of organic vapors to diesel soot and road tunnel aerosols, *Environ. Sci. Technol.*, **39**, (17), 6632–6637, 2005.
- Russell, A., and R. Dennis, NARSTO critical review of photochemical models and modeling, *Atmos. Environ.*, **34**, (12-14), 2283–2324, 2000.
- Sahsuvar, L., P. A. Helm, L. M. Jantunen, and T. F. Bidleman, Henry's law constants for  $\alpha$ -,  $\beta$ -, and  $\gamma$ -hexachlorocyclohexanes (HCHs) as a function of temperature and revised estimates of gas exchange in Arctic regions, *Atmos. Environ.*, **37**, 983–992, 2003.
- Scheringer, M., Characterization of the environmental distribution behavior of organic chemicals by means of persistence and spatial range, *Environ. Sci. Technol.*, **31**, (10), 2891–2897, 1997.
- Scheringer, M., F. Wegmann, K. Fenner, and K. Hungerbühler, Investigation of the cold condensation of persistent organic pollutants with a global multimedia fate model, *Environ. Sci. Technol.*, **34**, (9), 1842–1850, 2000.
- Scheringer, M., M. Stroebe, F. Wania, F. Wegmann, and K. Hungerbühler, The effect of export to the deep sea on the long-range transport potential of persistent organic pollutants, *Environ. Sci. Pollut. R.*, **11**, (1), 41–48, 2004.
- Schreitmüller, J., and K. Ballschmiter, Air-water equilibrium of hexachlorocyclohexanes and chloromethoxybenzenes in the North and South Atlantic, *Environ. Sci. Technol.*, **29**, (1), 207–215, 1995.
- Schwarzenbach, R. P., P. M. Gschwend, and D. M. Imboden, *Environmental Organic Chemistry*, John Wiley & Sons, Inc.: New York, 1993.
- Seinfeld, J. H., and S. N. Pandis, *Atmospheric chemistry and physics: From air pollution to climate change*, John Wiley & Sons, Inc., 1998.
- Semeena, V. S., and G. Lammel, Effects of various scenarios of entry of DDT and  $\gamma$ -HCH on the global environmental fate as predicted by a multicompartiment chemistry-transport model, *Fresenius Environ. Bull.*, **12**, (8), 925–939, 2003.
- Semeena, V. S., and G. Lammel, The significance of the grasshopper effect on the atmospheric distribution of persistent organic substances, *Geophys. Res. Lett.*, **32**, L07804, doi:10.1029/2004GL022229, 2005.
- Seth, R., D. Mackay, and J. Muncke, Estimating the organic carbon partition coefficient and its variability for hydrophobic chemicals, *Environ. Sci. Technol.*, **33**, (14), 2390–2394, 1999.
- Severinsen, M., and T. Jager, Modelling the influence of terrestrial vegetation on the environmental fate of xenobiotics, *Chemosphere*, **37**, (1), 41–62, 1998.
- Shatalov, V., E. Mantseva, A. Baart, P. Bartlett, K. Breivik, J. H. Christensen, S. Dutchak, D. Kallweit, R. Farret, M. Fedyunin, S. Gong, K. M. Hansen, I. Holoubek, P. Huang, K. C. Jones, M. Matthies, G. Petersen, K. Prevedouros, J. Pudykiewicz, M. Roemer, M. Salzmänn, M. Sheringer, J. Stocker, B. Strukov, N. Suzuki, A. J. Sweetman, D. van de Meent, and F. Wegmann, POP Model Intercomparison Study, Stage I. Comparison of descriptions of main processes determining POP behaviour in various environmental compartments., technical report, MSC-E Technical Report 1/2004., 2004.
- Shatalov, V., E. Mantseva, A. Baart, P. Bartlett, K. Breivik, J. H. Christensen, S. Dutchak, S. Gong, A. Gusev, K. M. Hansen, A. Hollander, P. Huang, K. Hungerbühler, K. C. Jones, G. Petersen, M. Roemer, M. Sheringer, J. Stocker, N. Suzuki, A. J. Sweetman, D. van de Meent, and F. Wegmann, POP Model Intercomparison Study, Stage II. Comparison of mass balance estimates and sensitivity studies, technical report, MSC-E Technical Report 4/2005., 2005.

- Shen, L., F. Wania, Y. D. Lei, C. Teixeira, D. C. G. Muir, and T. F. Bidleman, Hexachlorocyclohexanes in the North American atmosphere, *Environ. Sci. Technol.*, **38**, (4), 965–975, 2004.
- Shen, L., F. Wania, Y. D. Lei, C. Teixeira, D. C. G. Muir, and T. F. Bidleman, Atmospheric distribution and long-range transport behavior of organochlorine pesticides in North America, *Environ. Sci. Technol.*, **39**, (2), 409–420, 2005.
- Shimmo, M., K. Saarnio, P. Aalto, K. Hartonen, T. Hyötyläinen, M. Kulmala, and M.-L. Riekkola, Particle Size Distribution and Gas-Particle Partition of Polycyclic Aromatic Hydrocarbons in Helsinki Urban Area, *J. Atmos. Chem.*, **47**, 223–241, 2004.
- Shiu, W.-Y., and K.-C. Ma, Temperature dependence of physical-chemical properties of selected chemicals of environmental interest. I. mononuclear and polynuclear aromatic hydrocarbons, *J. Phys. Chem. Ref. Data*, **29**, (1), 41–130, 2000a.
- Shiu, W.-Y., and K.-C. Ma, Temperature dependence of physical-chemical properties of selected chemicals of environmental interest. II. chlorobenzenes, polychlorinated biphenyls, polychlorinated dibenzo-p-dioxins, and dibenzofurans, *J. Phys. Chem. Ref. Data*, **29**, (3), 387–462, 2000b.
- Simcik, M. F., The importance of surface adsorption on the washout of semivolatile organic compounds by rain, *Atmos. Environ.*, **38**, 491–501, 2004.
- Simonich, S. L., and R. A. Hites, Organic pollutant accumulation in vegetation, *Environ. Sci. Technol.*, **29**, (12), 2905–2914, 1995.
- Skov, H., J. H. Christensen, M. E. Goodsite, N. Z. Heidam, B. Jensen, P. Wåhlin, and G. Geernaert, Fate of elemental mercury in the Arctic during atmospheric mercury depletion episodes and the load of atmospheric mercury to the Arctic, *Environ. Sci. Technol.*, **38**, (8), 2373–2382, 2004.
- Skov, H., R. Bossi, P. Wåhlin, J. Vikelsøe, J. Christensen, A. H. Egeløv, B. J. N. Z. Heidam, H. P. Ahleson, L. Stausgård, I. Jensen, and D. Petersen, Contaminants in the atmosphere: AMAP-Nuuk, Westgreenland 2002-2004, technical report, National Environmental Research Institute. - NERI Technical Report 547, 45 pp., 2005.
- Smith, A. G., *Chlorinated hydrocarbon insecticides. Classes of pesticides*, In: Handbook of pesticide toxicology, 731–915, Academic Press: San Diego, CA, Hayes, W. J., Laws, E. R. (eds.), 1991.
- Sobek, A., Ö. Gustafsson, S. Hajdu, and U. Larsson, Particle-water partitioning of PCBs in the photic zone: A 25-month study in the open Baltic Sea, *Environ. Sci. Technol.*, **38**, (5), 1375–1382, 2004.
- Sportisse, B., An analysis of operator splitting techniques in the stiff case, *J. Comp. Phys.*, **161**, 140–168, 2000.
- Stern, G. A., C. J. Halsall, L. A. Barrie, D. C. G. Muir, P. Fellin, B. Rosenberg, F. Ya. Rovinsky, E. Ya. Kononov, and B. Pastuhov, Polychlorinated biphenyls in Arctic air. 1. Temporal and spatial trends: 1992-1994, *Environ. Sci. Technol.*, **31**, (12), 3619–3628, 1997.
- Strand, A., and Ø. Hov, A model strategy for the simulation of chlorinated hydrocarbon distributions in the global environment, *Water Air Soil Poll.*, **86**, 283–316, 1996.
- Su, Y., and F. Wania, Does the forest filter effect prevent semivolatile organic compounds from reaching the Arctic?, *Environ. Sci. Technol.*, **39**, (18), 7185–7193, 2005.
- Suzuki, N., K. Murasawa, T. Sakurai, K. Nansai, K. Matsuhashi, Y. Moriguchi, K. Tanabe, O. Nakasugi, and M. Morita, Geo-referenced multimedia environmental fate model (G-CIEMS): model formulation and comparison to the generic model and monitoring approaches, *Environ. Sci. Technol.*, **38**, (21), 5682–5693, 2004.

- Tanabe, K., and R. Tatsukawa, Chlorinated hydrocarbons in the North Pacific and Indian Oceans, *J. Oceanogr. Soc. Jpn.*, **36**, 217–226, 1980.
- Toose, L., D. G. Woodfine, M. MacLeod, D. Mackay, and J. Gouin, BETR-World: A geographically explicit model of chemical fate: application to transport of  $\alpha$ -HCH to the Arctic, *Environ. Pollut.*, **128**, (1-2), 223–240, 2004.
- UNECE, The 1998 Aarhus Protocol on Persistent Organic Pollutants (POPs), United Nations Economic Commission for Europe. Internet: [http://www.unece.org/env/lrtap/pops\\_h1.htm](http://www.unece.org/env/lrtap/pops_h1.htm), 1998.
- UNEP, Stockholm Convention on Persistent Organic Pollutants (POPs), Internet: <http://www.pops.int>, 2005a.
- UNEP, Stockholm Convention on Persistent Organic Pollutants (POPs). List of signatories and ratifications to the Stockholm Convention on POPs, <http://www.pops.int/documents/signature/signstatus.htm>, 2005b.
- Vallack, H. W., D. J. Bakker, I. Brandt, E. Broström-Lundén, A. Brouwer, K. R. Bull, C. Gough, R. Guardans, I. Holoubek, B. Jansson, R. Koch, J. Kuylenstierna, A. Lecloux, D. Mackay, P. McCutcheon, P. Mocarelli, and R. D. F. Taalman, Controlling persistent organic pollutants - what next?, *Environ. Toxicol. Phar.*, **6**, 143–175, 1998.
- van Jaarsveld, J. A., W. A. J. van Pul, and F. A. A. M. de Leeuw, Modelling transport and deposition of persistent organic pollutants in the European region, *Atmos. Environ.*, **31**, (7), 1011–1024, 1997.
- Voldner, E. C., and W. H. Schroeder, Modelling of atmospheric transport and deposition of toxaphene into the Great Lakes ecosystem, *Atmos. Environ.*, **23**, (9), 1949–1961, 1989.
- Voldner, E. C., L. A. Barrie, and A. Sirois, A literature review of dry deposition of oxides of sulphur and nitrogen with emphasis on long-range transport modelling in North America, *Atmos. Environ.*, **20**, (11), 2101–2123, 1986.
- Waddington, E. D., J. Cunningham, and S. L. Harder, *The effects of snow ventilation on chemical concentrations*, In: Chemical Exchange Between the Atmosphere and Polar Snow, 403–452, Springer-Verlag: Berlin, E. W. Wolff, R. C. Bales (Eds.), 1996.
- Wadhams, P., *Sea ice morphology*, In: Physics of Ice-Covered Seas, Vol. 1, 231–287, Helsinki University Printing house, M. Leppäranta (ed.), 1998.
- Wania, F., Modelling the fate of non-polar organic chemicals in an ageing snow pack, *Chemosphere*, **35**, (10), 2345–2363, 1997.
- Wania, F., *Differences, Similarities, and Complementarity of Various Approaches to Modelling Persistent Organic Pollutant Distribution in the Environment*, In: Proceedings of the WMO/EMEP/UNEP Workshop on Modelling of Atmospheric Transport and Deposition of Persistent Organic Pollutants and Heavy Metals, 1, pp. 115–140, 1999.
- Wania, F., and G. L. Daly, Estimating the contribution of degradation in air and deposition to the deep sea to the global loss of PCBs, *Atmos. Environ.*, **36**, 5581–5593, 2002.
- Wania, F., and J.-E. Haugen, Long term measurements of wet deposition and precipitation scavenging of hexachlorocyclohexanes in Southern Norway, *Environ. Pollut.*, **105**, 381–386, 1999.
- Wania, F., and D. Mackay, Global fractionation and cold condensation of low volatility organochlorine compounds in polar regions, *Ambio*, **21**, (1), 10–18, 1993.
- Wania, F., and D. Mackay, A global distribution model for persistent organic chemicals, *Sci. Total Environ.*, **160/161**, 211–232, 1995.

- Wania, F., and D. Mackay, Tracking the distribution of persistent organic pollutants, *Environ. Sci. Technol.*, **30**, (9), 390A–396A, 1996.
- Wania, F., and D. Mackay, The evolution of mass balance models of persistent organic pollutant fate in the environment, *Environ. Pollut.*, **100**, 223–240, 1999a.
- Wania, F., and D. Mackay, Global chemical fate of  $\alpha$ -hexachlorocyclohexane. 2. use of a global distribution model for mass balancing, source apportionment and trend prediction, *Environ. Toxicol. Chem.*, **18**, (7), 1400–1407, 1999b.
- Wania, F., and M. S. McLachlan, Estimating the influence of forests on the overall fate of semivolatile organic compounds using a multimedia fate model, *Environ. Sci. Technol.*, **35**, (3), 582–590, 2001.
- Wania, F., and Y. Su, Quantifying the global fractionation of polychlorinated biphenyls, *Ambio*, **33**, (3), 161–168, 2004.
- Wania, F., J. Axelman, and D. Broman, A review of processes involved in the exchange of persistent organic pollutants across the air-sea interface, *Environ. Pollut.*, **102**, 3–23, 1998a.
- Wania, F., J. T. Hoff, C. Q. Jia, and D. Mackay, The effects of snow and ice on the environmental behaviour of hydrophobic organic chemicals, *Environ. Pollut.*, **102**, 25–41, 1998b.
- Wania, F., D. Mackay, and J. T. Hoff, The importance of snow scavenging of polychlorinated biphenyl and polycyclic aromatic hydrocarbon vapors, *Environ. Sci. Technol.*, **33**, (1), 195–197, 1999a.
- Wania, F., D. Mackay, Y.-F. Li, T. F. Bidleman, and A. Strand, Global chemical fate of  $\alpha$ -hexachlorocyclohexane, 1. Evaluation of a global distribution model, *Environ. Toxicol. Chem.*, **18**, (7), 1390–1399, 1999b.
- Wania, F., R. Semkin, J. T. Hoff, and D. Mackay, Modelling the fate of non-polar organic chemicals during the melting of an Arctic snowpack, *Hydrol. Process.*, **13**, 2245–2256, 1999c.
- Wegmann, F., M. Scheringer, M. Möller, and K. Hungerbühler, Influence of vegetation on the environmental partitioning of DDT in two global models, *Environ. Sci. Technol.*, **38**, (5), 1505–1512, 2004.
- Wild, E., J. Dent, G. O. Thomas, and K. C. Jones, Real-time visualization and quantification of PAH photodegradation on and within plant leaves, *Environ. Sci. Technol.*, **39**, (1), 268–273, 2005.
- Willett, K. L., E. M. Ulrich, and R. A. Hites, Differential toxicity and environmental fates of hexachlorocyclohexane isomers, *Environ. Sci. Technol.*, **32**, (15), 2197–2207, 1998.
- Wilson, M. F., and A. Henderson-Sellers, A global archive of land cover and soils data for use in general circulation models, *J. Climatol.*, **5**, 119–143, 1985.
- Woodfine, D. G., M. MacLeod, D. Mackay, and D. Brimacombe, Development of continental scale multimedia contaminant fate models: integrating GIS, *Environ. Sci. Pollut. R.*, **8**, (3), 164–172, 2001.
- Xiao, H., and F. Wania, Is vapor pressure or the octanol-air partition coefficient a better descriptor of the partitioning between gas phase and organic matter?, *Atmos. Environ.*, **37**, 2867–2878, 2003.
- Xiao, H., N. Li, and F. Wania, Compilation, evaluation, and selection of physical-chemical property data for  $\alpha$ -,  $\beta$ -, and  $\gamma$ -Hexachlorocyclohexane, *J. Chem. Eng. Data*, **49**, 173–185, 2004.
- Xie, W.-H., W.-Y. Shiu, and D. Mackay, A review of the effect of salts on the solubility of organic compounds in seawater, *Mar. Environ. Res.*, **44**, (4), 429–444, 1997.

Yamasaki, H., K. Kuwata, and H. Miyamoto, Effects of ambient temperature on aspects of airborne polycyclic aromatic hydrocarbons, *Environ. Sci. Technol.*, **16**, (4), 189–194, 1982.

Zetsch, C., UWSF-Z, *Umweltchem. Ökotox.*, **3**, 59–64, 1991.

Zhao, H., Q. Zhang, J. Chen, X. Xue, and X. Liang, Prediction of octanol-air partition coefficients of semivolatile organic compounds based on molecular connectivity index, *Chemosphere*, **59**, 1421–1426, 2005.

# Appendix A

## Paper I

Hansen, K. M., J. H. Christensen, J. Brandt, L. M. Frohn, C. Geels, 2004, Modelling atmospheric transport of  $\alpha$ -hexachlorocyclohexane in the Northern Hemisphere using a 3-D dynamical model: DEHM-POP, *Atmospheric Chemistry and Physics*, 4, 1125-1137.



# Modelling atmospheric transport of $\alpha$ -hexachlorocyclohexane in the Northern Hemisphere with a 3-D dynamical model: DEHM-POP

K. M. Hansen, J. H. Christensen, J. Brandt, L. M. Frohn, and C. Geels

Department of Atmospheric Environment, National Environmental Research Institute, Roskilde, Denmark

Received: 5 February 2004 – Published in Atmos. Chem. Phys. Discuss.: 8 March 2004

Revised: 30 June 2004 – Accepted: 2 July 2004 – Published: 13 July 2004

**Abstract.** The Danish Eulerian Hemispheric Model (DEHM) is a 3-D dynamical atmospheric transport model originally developed to describe the atmospheric transport of sulphur into the Arctic. A new version of the model, DEHM-POP, developed to study the atmospheric transport and environmental fate of persistent organic pollutants (POPs) is presented. During environmental cycling, POPs can be deposited and re-emitted several times before reaching a final destination. A description of the exchange processes between the land/ocean surfaces and the atmosphere is included in the model to account for this multi-hop transport. The  $\alpha$ -isomer of the pesticide hexachlorocyclohexane ( $\alpha$ -HCH) is used as tracer in the model development. The structure of the model and processes included are described in detail. The results from a model simulation showing the atmospheric transport for the years 1991 to 1998 are presented and evaluated against measurements. The annual averaged atmospheric concentration of  $\alpha$ -HCH for the 1990s is well described by the model; however, the shorter-term average concentration for most of the stations is not well captured. This indicates that the present simple surface description needs to be refined to get a better description of the air-surface exchange processes of POPs.

## 1 Introduction

The term persistent organic pollutants (POPs) is used to describe a group of chemical compounds with different origins but common characteristics: semi-volatility, hydrophobicity, bioaccumulation, toxicity and great persistence in the environment (Jones and de Voogt, 1999). POPs are measured in all environmental media and in remote areas with no usage or direct emissions of the compounds (AMAP, 1998).

Correspondence to: K. M. Hansen  
(kmh@dmu.dk)

The environmental fate of POPs is determined by environmental conditions such as temperature and soil organic carbon content and by key physical-chemical properties of the compounds, such as the aqueous solubility, the vapour pressure, and the partitioning coefficient between air and water (the Henry's law constant), octanol and water, and octanol and air, where octanol is used as a surrogate for the solid state (Jones and de Voogt, 1999).

POPs have a potential for long-range transport through the atmosphere because they are semi-volatile. The volatility is temperature dependent and POPs show a tendency to accumulate in cold regions, a process named cold condensation (Wania and Mackay, 1993). POPs can also be re-emitted to the atmosphere after deposition to the surface due to the temperature dependent volatility. In this way POPs can undergo several cycles of deposition and re-emission before reaching their final destination, a process named grasshopper or multi-hop transport (Wania and Mackay, 1996).

POPs may have adverse health effects on humans and wildlife: harmful effects on the immune and reproductive systems, and carcinogenic effects (Jones and de Voogt, 1999). POPs are hydrophobic; they bioaccumulate and magnify through the food chain (Jones and de Voogt, 1999). This raises concern especially for the top-predator species due to the harmful effects.

Several of the POPs are now banned or regulated through international treaties but they are still found in the Arctic environment (AMAP, 1998). The most important pathways of POPs to the Arctic environment are the atmosphere, the ocean and the fresh water system (AMAP, 1998). The atmosphere constitutes the most rapid of these pathways; therefore the atmospheric concentration and transport are key factors in the study of the Arctic environmental fate of POPs.

Concentrations of POPs in the environment are generally small and large samples are required to quantify them. The result is a low spatial and temporal resolution of the available measurements. Beside measurements, the environmental

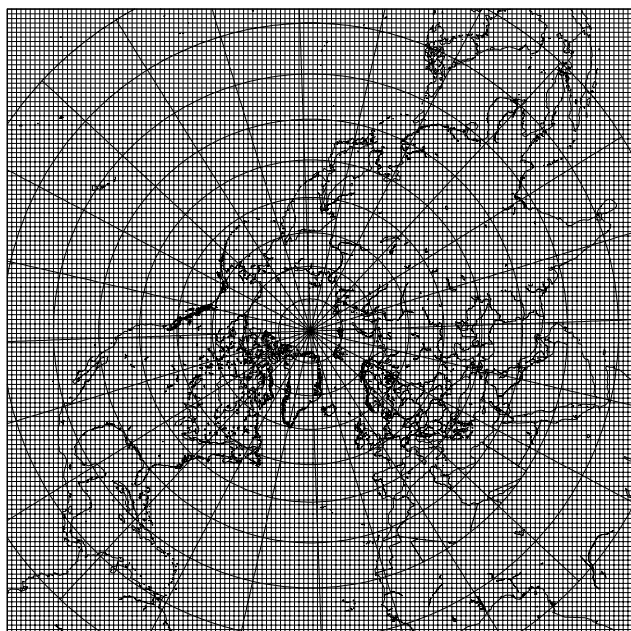


**Fig. 1.** The DEHM-POP model domain and horizontal grid: A polar stereographic projection with a resolution of  $150\text{ km} \times 150\text{ km}$  at  $60^\circ\text{ N}$ .

fate of POPs can be estimated using different types of models. Multimedia compartment models have been used to evaluate the environmental fate of POPs on different scales with good results (e.g. Strand and Hov, 1996; Wania et al., 1999; Scheringer et al., 2000; MacLoed et al., 2001; Breivik and Wainia, 2002; Prevedouros et al., 2004; Toose et al., 2004). These models have generally very low spatial resolution with the whole globe or a confined region divided into few climate zones with a compartment for each of the environmental compartments described in each zone of the model. Information on size and extension of each compartment and exchange between climate zones and between environmental compartments is inferred from geographical reference databases and climatic averages of meteorological data. This type of model can be run in steady state mode to evaluate the environmental partitioning of POPs, or in dynamic mode to simulate the environmental fate of a compound over a longer period. However, to evaluate the spatial and temporal distribution of a compound in a certain area in detail, dynamical 3-D models must be used. Several models have been developed to describe the atmospheric transport of POPs on both regional (e.g. van Jaarsveld et al., 1997; Ma et al., 2003), hemispheric (Malanichev et al., 2004) and global scales (Koziol and Pudykiewicz, 2001).

The aim of this study is to present a high-resolution 3-D dynamical model, DEHM-POP, describing the atmospheric transport and environmental fate of POPs within the Northern Hemisphere with special focus on the transport into the Arctic. DEHM-POP has a higher spatial resolution and is

used to simulate the atmospheric transport of POPs over a longer period than previous models with comparable domain size.

## 2 Model description

DEHM-POP is developed based on the Danish Eulerian Hemispheric Model (DEHM): a 3-D Eulerian dynamical atmospheric transport model. DEHM was originally developed to study the atmospheric transport of sulphur into the Arctic (Christensen, 1997). DEHM has also been expanded to study the atmospheric transport of lead (Christensen, 1999),  $\text{CO}_2$  (Geels et al., 2004) and a chemical scheme with 60 components (Frohn et al., 2002); it has been validated thoroughly for these compounds. In the horizontal the model is defined on a regular grid using a polar-stereographic projection with a resolution of  $150\text{ km} \times 150\text{ km}$  at  $60^\circ\text{ N}$ . The DEHM-POP domain was enlarged from  $96 \times 96$  grid cells in the horizontal in the earlier versions of DEHM to  $135 \times 135$  grid cells and it now extends into the Southern Hemisphere (Fig. 1). There are 20 unevenly distributed vertical layers discretized using terrain-following  $\sigma$ -coordinates extending to a height of approximately 18 km with the highest resolution near the surface.

The model is based on the continuity equation:

$$\begin{aligned} \frac{\partial q}{\partial t} = & - \left( u \frac{\partial q}{\partial x} + v \frac{\partial q}{\partial y} + \dot{\sigma} \frac{\partial q}{\partial \sigma} \right) \\ & + K_x \frac{\partial^2 q}{\partial x^2} + K_y \frac{\partial^2 q}{\partial y^2} + \frac{\partial}{\partial \sigma} \left( K_\sigma \frac{\partial q}{\partial \sigma} \right) \\ & + P(t, x, y, \sigma, q) - Q(t, x, y, \sigma, q), \end{aligned} \quad (1)$$

where  $q$  is the mixing ratio of the modelled compound,  $t$  is time,  $x$ ,  $y$ , and  $\sigma$  are the horizontal and vertical coordinates,  $u$  and  $v$  are the components of the horizontal wind field and  $\dot{\sigma}$  is the generalised vertical velocity,  $K_x$ ,  $K_y$ , and  $K_\sigma$  are the horizontal and vertical diffusion coefficients, and  $P$  and  $Q$  are sources and sinks.

Time integration of the continuity equation is done by splitting it into five sub-models, which are then solved successively in each time step. The first sub-model is the three-dimensional advection, sub-models two to four are diffusion in the three dimensions and the fifth sub-model is sources and sinks including the special air-surface exchange processes for POPs. The first four sub-models are unchanged from previous versions of DEHM and they are thoroughly described by Christensen (1997) and Frohn et al. (2002). The fifth sub-model is described in detail in the following subsections.

The time step is calculated using a Courant-Friedrich-Levy stability criterion on the basis of the horizontal and vertical wind fields and the horizontal boundary conditions are non-periodic (Frohn et al., 2002). The boundary conditions are free at the top of the domain (Christensen, 1997), and are given by the air-surface exchange fluxes at the ground.

## 2.1 The modelled compound

DEHM-POP is developed using the  $\alpha$ -isomer of the insecticide hexachlorocyclohexane (HCH) as tracer.  $\alpha$ -HCH is the most abundant POP measured in air, water and snow in the Arctic (AMAP, 1998). HCH is used worldwide in two different formulations: Technical HCH and Lindane. Technical HCH contains five stable isomers. Percentages of isomers in the mixture are typically:  $\alpha$ : 60–70%,  $\beta$ : 10–12%,  $\gamma$ : 6–10%,  $\delta$ : 3–4%,  $\epsilon$ : 3–4% depending on the manufacturer (Willett et al., 1998). Lindane is a refined product containing almost pure  $\gamma$ -HCH, the isomer that exhibits the highest insecticidal activity (Willett et al., 1998).

Technical HCH is historically the most used insecticide worldwide (Li et al., 2000). A total usage of 9.4 million tonnes between 1948 and 1997 with maximum usage around 1980 has been estimated (Li et al., 2003). Technical HCH is banned in most countries and only small amounts are used worldwide, primarily for vector control. Lindane is still in use as seed treatment in some countries, but is banned in others (Li, 1999).  $\alpha$ -HCH primarily affects the central nervous system and also promotes tumours (Willett et al., 1998).

$\alpha$ -HCH is one of the most volatile POPs with a high vapour pressure. It also partitions more readily into water than into solid phase (particles and soil) with high water-air partitioning coefficient and low octanol-air partitioning coefficient. Measurements at the Canadian station Alert in the high Arctic have shown that even at temperatures of  $-40^\circ\text{C}$  the average fraction sorbed on particles is less than 1% of the measured gas-phase fraction (Halsall et al., 1998). Therefore the particle-bound fraction of  $\alpha$ -HCH can be disregarded and  $\alpha$ -HCH is modelled as a pure gas-phase chemical in DEHM-POP.

## 2.2 Atmospheric sources and sinks

The change in  $\alpha$ -HCH concentration,  $C_a$ , in the atmospheric layers with time is described in the model by:

$$\frac{\partial C_a}{\partial t} = \frac{1}{z_a}(F_{\text{emis}} - F_{\text{exc},s}) - \lambda C_a - k_{\text{air}} C_a, \quad (2)$$

where  $z_a$  is the thickness of the layer,  $F_{\text{emis}}$  is the emission, described in Sect. 2.4.2,  $F_{\text{exc},s}$  is the air-surface gas exchange flux, which is zero for all layers but the lowermost, described in Sects. 2.3.1 and 2.3.2,  $\lambda$  is the wet deposition scavenging coefficient, described in Sect. 2.2.1, and  $k_{\text{air}}$  is the chemical transformation rate in air, described in Sect. 2.2.2.

### 2.2.1 Wet deposition

Wet deposition of  $\alpha$ -HCH is calculated in DEHM-POP using a simple parameterisation based on a scavenging coefficient formulation as in earlier versions of DEHM (Christensen, 1997). The scavenging coefficients used in the model

**Table 1.** Values of soil and chemical properties used in DEHM-POP, as suggested by Jury et al. (1983).

Parameter	Symbol	Units	Value
Soil depth	$z_s$	m	0.15
Water content	$l$	$\text{m}^3\text{m}^{-3}$	0.3
Air content	$a$	$\text{m}^3\text{m}^{-3}$	0.2
Bulk density	$\rho_s$	$\text{kgm}^{-3}$	1350
Organic carbon fraction	$f_{\text{oc}}$	$\text{kgkg}^{-1}$	0.0125
Air diffusion coefficient	$D_g^{\text{air}}$	$\text{m}^2\text{s}^{-1}$	$5.0 \times 10^{-6}$
Water diffusion coefficient	$D_L^{\text{water}}$	$\text{m}^2\text{s}^{-1}$	$5.0 \times 10^{-10}$

are  $7.0 \times 10^5$  and  $1.0 \times 10^5$  for in-cloud and below-cloud scavenging, respectively. In-cloud scavenging is more efficient due to the higher density of water droplets in clouds than below clouds.

### 2.2.2 Chemical reactions in the atmosphere

Reaction with OH radicals is assumed to be the most important degradation of  $\alpha$ -HCH in the atmosphere (Atkinson et al., 1999). The degradation rate depends on temperature and OH concentration in air as studied by Brubaker and Hites (1998). However, as an approximation a first order degradation rate is calculated in the model using an estimated mean residence time in the atmosphere due to reactions with OH radicals of  $k_{\text{air}}=1/(118 \text{ days})$  (Mackay et al., 2000). This value is in agreement with an average atmospheric lifetime of 120 days calculated from the reaction rates measured by Brubaker and Hites (1998). The degradation rate is applied for the whole model domain and is not seasonal dependent. A transformation of  $\gamma$ -HCH into  $\alpha$ -HCH by UV radiation has been speculated (Pacyna and Oehme, 1988), but is not taken into account in the model since no direct observation has been made of this reaction in the environment.

## 2.3 Surface compartments and air-surface exchange

A description of the air-surface exchange processes is important when modelling the environmental fate of POPs to account for the multi-hop transport. A soil module and an ocean module are therefore included in DEHM-POP. The parameterisation of the exchange processes between air and surface compartments is based on a zonally averaged multi-compartment model (Strand and Hov, 1996).

### 2.3.1 The soil module

The land covered surface in the model consists of a 0.15 m thick soil layer containing a mixture of soil, air and water in fractions kept constant with time. The soil layer is assumed to have the standard properties suggested by Jury et

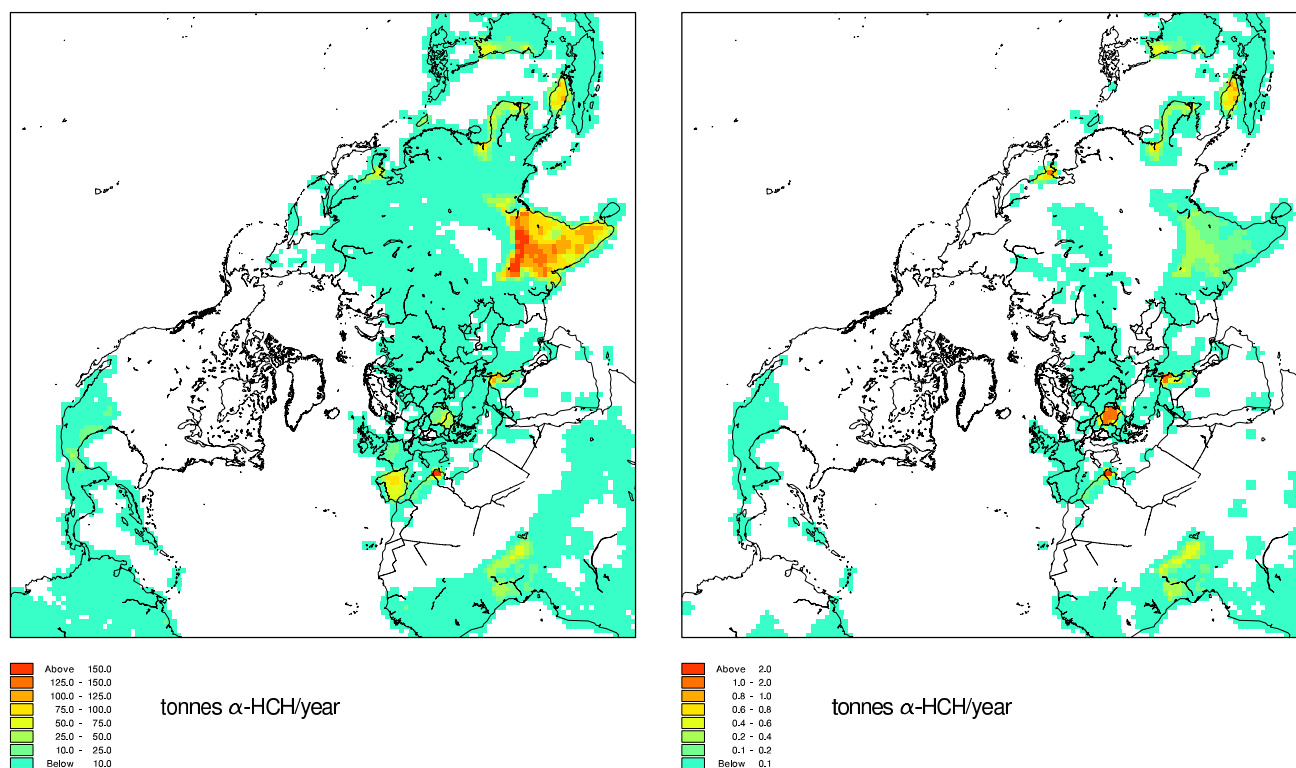


**Fig. 2.** Emissions of  $\alpha$ -HCH for 1990 (left) and 2000 (right) (Li et al., 2000). The data are redistributed to the DEHM-POP model grid. Note the different colour scales.

al. (1983) that are listed in Table 1. The change in  $\alpha$ -HCH concentration in soil,  $C_s$ , with time is expressed by:

$$\frac{\partial C_s}{\partial t} = \frac{1}{z_s} (F_{\text{exc,soil}} + F_{\text{wet}} - F_{\text{run-through}}) - k_{\text{soil}} C_s, \quad (3)$$

where  $z_s$  is the soil depth,  $F_{\text{exc,soil}}$  is the air-soil gas exchange flux,  $F_{\text{wet}}$  is the wet deposition,  $F_{\text{run-through}}$  is the amount of chemical running out with the excess water through the bottom of the soil layer, and  $k_{\text{soil}}$  is the degradation rate in soil.

Two additional fluxes are included in the original air-soil exchange process description: Application input and flux out of the soil due to evaporation of water (Strand and Hov, 1996). The amount of  $\alpha$ -HCH applied to the soil is taken into account when emissions to air are calculated and it is therefore disregarded in this context. The evaporation of water is omitted since data on the latent heat flux were not extracted from the meteorological model driving DEHM-POP.

The air-soil gas exchange flux is given by:

$$F_{\text{exc,soil}} = \nu_s \left( C_a - \frac{C_s}{K_{\text{sa}}} \right), \quad (4)$$

where  $\nu_s$  is the exchange velocity, and  $K_{\text{sa}}$  is the partitioning coefficient between soil and air in the soil. The exchange velocity is given by (Strand and Hov, 1996):

$$\nu_s = \frac{(D_G^{\text{air}} a^{10/3} + D_L^{\text{water}} l^{10/3} H) (1 - l - a)^{-2}}{z_s/2}, \quad (5)$$

where  $D_G^{\text{air}}$  is the air diffusion coefficient,  $D_L^{\text{water}}$  is the liquid diffusion coefficient,  $l$  and  $a$  is the water and air fractions in soil, respectively, and  $H$  is the dimensionless Henry's law constant (Strand and Hov, 1996). Partitioning between soil and air in the soil is given by:

$$K_{\text{sa}} = \rho_s f_{\text{oc}} K_{\text{oc}} H + l + a, \quad (6)$$

where  $\rho_s$  is the soil density,  $f_{\text{oc}}$  is the organic carbon fraction, and  $K_{\text{oc}}$  is the organic carbon partitioning coefficient taken to be:  $K_{\text{oc}} = 1.3 \text{ m}^3 \text{ kg}^{-1}$  (Strand and Hov, 1996). The dimensionless Henry's law constant,  $H$ , is temperature dependent and calculated using the equation:

$$H = RT \exp \left( \frac{2.303m}{T} - 2.303b \right), \quad (7)$$

where  $R$  is the molar gas constant,  $T$  is the temperature and  $m=2810$  and  $b=9.31$  are empirical constants determined for distilled water (Kucklick et al., 1991).

The excess run-through is calculated by:

$$F_{\text{run-through}} = F_{\text{excess}} C_s \frac{H}{K_{\text{sa}}}, \quad (8)$$

where  $F_{\text{excess}}$  is the flux of excess water, which in the model is equal to the precipitation rate because the water content in the soil layer is kept constant and water evaporation is omitted.

$\alpha$ -HCH is subject to biodegradation in soil. This process is not well quantified and the degradation rate in soil is estimated to be:  $k_{\text{soil}}=1/(1 \text{ year})$  (Strand and Hov, 1996). This value is generally higher than degradation rates used in other models. A half-life in soil of 120 days at 20°C, increasing with decreasing temperatures, is used by Wania et al. (1999) and Breivik and Wainia (2002). Degradation rates of 1/(3 months)–1/(4 months) are used for the temperature range 270–301 K by Scheringer et al. (2000).

### 2.3.2 The ocean water module

The ocean is assumed to be a 75 m deep well mixed surface ocean compartment. The deep ocean, sediments and sea ice are not taken into account in the model.

The  $\alpha$ -HCH concentration in the ocean,  $C_o$ , changes with time:

$$\frac{\partial C_o}{\partial t} = \frac{1}{z_o} (F_{\text{exc, ocean}} + F_{\text{wet}}) - k_{\text{ocean}} C_o, \quad (9)$$

where  $z_o$  is the depth of the ocean compartment,  $k_{\text{ocean}}$  is the loss rate in the surface ocean compartment, and  $F_{\text{exc, ocean}}$  is the air-ocean gas exchange flux given by:

$$F_{\text{exc, ocean}} = v_o (C_a - \frac{C_o}{H}), \quad (10)$$

where  $v_o$  is the exchange velocity calculated using the two layer resistance method.  $v_o$  is increasing with increasing wind speed.

The Henry's law constant is determined as in Eq. (7) but with values for the empirical constants:  $m=2969$  and  $b=9.88$  determined for artificial ocean water (Kucklick et al., 1991).

Apart from re-volatilisation,  $\alpha$ -HCH is lost from the surface compartment by hydrolysis, biological degradation and particle settling. None of these processes is well quantified, and a simple degradation rate of  $k_{\text{ocean}}=1/(10 \text{ years})$  is used (Strand and Hov, 1996). This value is generally higher than estimates used in other models. A half-life of 4 months for ocean water and 3 years for fresh water is used by Wania et al. (1999). Breivik and Wainia (2002) use a half-life of 1 year for both ocean and fresh water. Degradation rates of 1/(5.4 years) to 1/(1.8 months) is used for the temperature range 270–301 K by Scheringer et al. (2000).

## 2.4 Model input

Meteorological data and emissions are used as input to the model simulations. Initial concentrations in the three me-

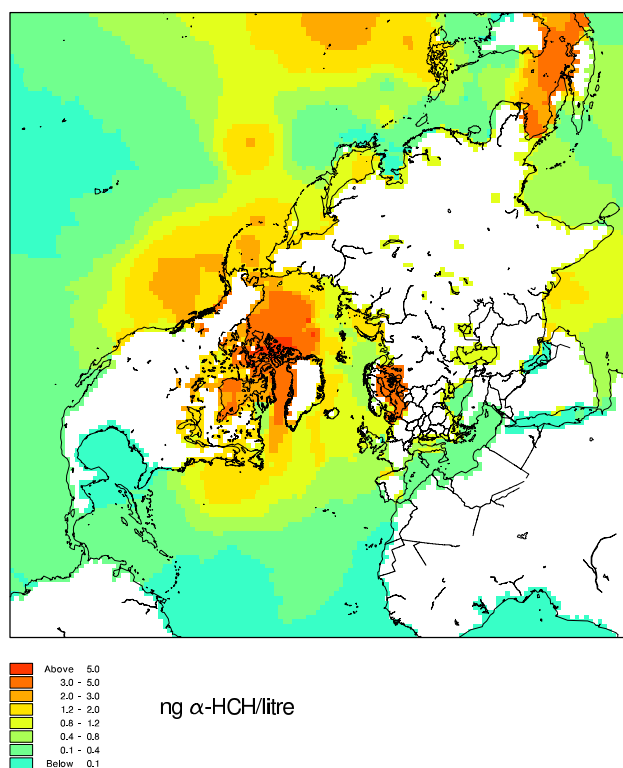


**Fig. 3.** Initial  $\alpha$ -HCH concentration in ocean water derived from an inter- and extra-polarization of measurements from the late 1980s and early 1990s.

dia are also considered as input, since the usage of  $\alpha$ -HCH started more than 40 years before the modelling period.

### 2.4.1 Meteorological data

DEHM-POP is driven by meteorological data from the numerical weather prediction model MM5v2 (Grell et al., 1995). This model supplies temperature, wind velocity, and humidity data in each DEHM-POP grid cell for the years 1991–1998 with a time resolution of 3 h. It uses the global meteorological TOGA data set from the European Centre for Medium Range Weather Forecasts on a  $2.5^\circ \times 2.5^\circ$  grid with a time resolution of 12 h as input.

### 2.4.2 Emission data

As emission input we use data on global  $\alpha$ -HCH emissions in 1990 and 2000 distributed on a  $1^\circ \times 1^\circ$  grid (Li et al., 2000). The emissions for each year are calculated by taking usage from that year as well as volatilisation from previous years usage into account (Li et al., 2000). The emissions have been redistributed to the DEHM-POP model grid (Fig. 2).

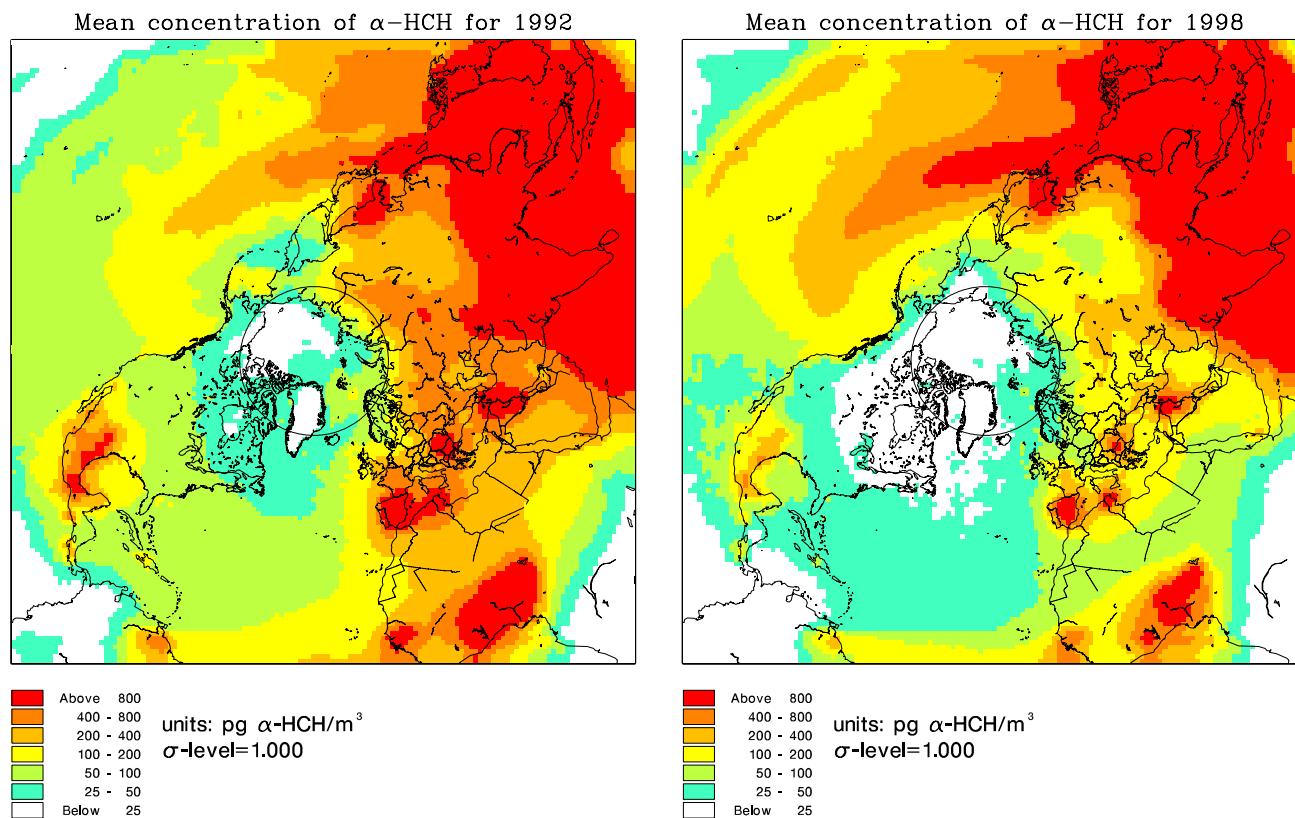


**Fig. 4.** Mean concentrations of  $\alpha$ -HCH in the lowermost atmospheric layer for the years 1992 (left) and 1998 (right).

Emissions for the years 1991–1998 have been obtained by assuming a linear development of the emissions between 1990 and 2000 in each grid cell. The emissions for each year have been distributed evenly throughout the year. Emissions are mixed up to a height of 800 m, a typical extension of the planetary boundary layer.

#### 2.4.3 Initial concentrations

Most of the estimated 9.4 million tonnes Technical HCH was used before the start of the modelled period. Due to the great persistence of the compound some of it is still found in the environment, especially in the ocean since  $\alpha$ -HCH is one of the most water soluble POPs. This can act as a source to the atmosphere by re-volatilisation, which has been observed in the Bering and Chukchi Seas (Jantunen and Bidleman, 1995). A set of  $\alpha$ -HCH measurements from the late 1980s and early 1990s collected from the literature (Terry Bidleman, personal communication) was plotted in the DEHM-POP grid. Values in all DEHM-POP grid cells were inter- and extrapolated from these (Fig. 3). This is used as initial condition for the model simulation. Measurements from between 1987 and 1996 are used to ensure a reasonable coverage of the world's oceans and as large a number of points for the interpolation as possible. In grid points with more than one measurement, the average value of the measurements was used.

No initial concentration in soil is used in the model simulation. Since emissions from residues in agricultural soil from previous years usage is taken into account in the emission data, only the re-emission from previous deposition of chemicals to the soil is not accounted for.

The mixing time in the atmosphere is short and atmospheric concentrations rapidly disperse through the model domain. No initial concentration in the atmosphere is therefore used in the model simulation. To minimise the effect of this assumption, data from January 1991 is omitted in the model evaluation.

### 3 Results

The model was run for the years 1991–1998. The mean concentration in the lowermost atmospheric layer for the years 1992 and 1998 is seen in Fig. 4. Air concentrations are generally high over areas with emissions such as India, Southeast Asia, Southern Europe and Mexico, but significant concentrations are also seen in air over areas without primary emissions such as the Atlantic and Pacific Oceans and the Arctic. There is generally a decrease in air concentrations from 1992 to 1998. However, in some areas over the Pacific Ocean the air concentrations increase.

**Table 2.** Years of sampling, number, typical deployment time and sampling frequency of the measurements, and mean and range of measurements and model results for each of the studied stations (Aas et al., 2003; Berg et al., 2001). <sup>1</sup>Measurements at Lista have been made once a week but only monthly mean values were available for this study.

Station	Years of sampling	Number of measurements	Average deployment time (days)	Average sampling frequency	Measurements Mean and range ( $\text{pgm}^{-3}$ )	Model results Mean and range ( $\text{pgm}^{-3}$ )
Alert	1992–1998	303	7	1/week	54.4 (0.1–310.7)	28.8 (2.6–84.2)
Tagish	1992–1994	80	7	1/week	70.4 (23.6–160.0)	42.1 (16.9–86.3)
Spitzbergen	1993–1998	303	2	1/week	58.9 (0.1–203.1)	49.5 (5.5–153.8)
Dunai Island	1993	33	7	1/week	40.0 (0.6–77)	60.5 (9.8–124.9)
Lista <sup>1</sup>	1991–1998	95	1	1/week	66.6 (20.8–170)	96.1 (39.6–197.4)
Rörvik	1994–1998	56	7	1/month	24.2 (2–63)	65.4 (15.8–191.4)
Aspvreten	1995–1998	40	7	1/month	55.7 (20–161)	73.1 (18.6–190.3)
Pallas	1996–1998	36	7	1/month	23.2 (3–40)	37.6 (8.4–88.1)
Storhófdi	1995–1998	103	14	2/month	16.7 (3.7–55.9)	30.4 (11.7–57.8)

### 3.1 Model evaluation

Monitoring programs with regular measurements of atmospheric POPs concentrations have been established since the beginning of the 1990s by deployment of active air samplers at different sites. The time span and the temporal resolution of the measurements are very variable at the different stations (Table 2). To evaluate the model results, measurements from 9 stations in the Northern Hemisphere are obtained from EMEP (Aas et al., 2003; Berg et al., 2001). The location of the stations is plotted in Fig. 5. Only four stations conduct continuous measurements: Alert, Tagish, Dunai Island, and Storhófdi. At the other stations measurements are made only 20–30% of the time.

Daily averaged concentrations from the lowermost atmospheric layer of the model are extracted at each measurement site. A clear seasonal pattern with higher concentrations during summer than winter is found in the daily averaged  $\alpha$ -HCH concentrations in the model at all stations and most clearly for the two high Arctic stations at Alert and Spitzbergen (not shown). At the more southerly stations the amplitude of the seasonal signal is lower and the seasonal pattern is perturbed by short-term spikes mainly during summer (not shown). When air samples are taken over several days, the model results are averaged over the deployment time of the air sampler to make a direct comparison of the model results with individual measurements possible. Measurements at Lista are made once a week but only monthly averaged values were available for this study. These were compared to the average concentration for the whole month from the model, because the date of the individual measurements were not known. Concentrations in soil and ocean water are not evaluated.

#### Stations placements

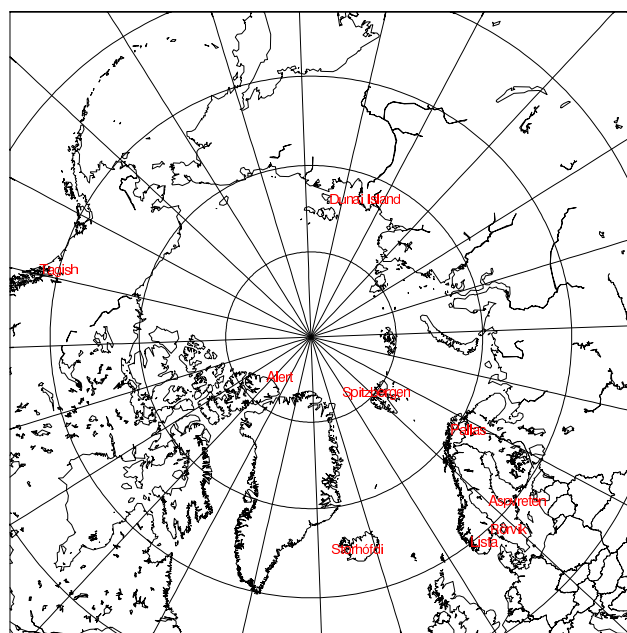


**Fig. 5.** Location of the 9 measurement stations used in the model evaluation.

#### 3.1.1 Annual averaged air concentrations

The average and range for all measurements and corresponding model results are calculated for each station (Table 2). Annual averages are also calculated and compared (Fig. 6). The predicted averaged concentrations are within a factor 3 of the measurements at all stations and for most stations within a factor 2 or less. The averaged concentrations are consistently underestimated by the model at the three stations

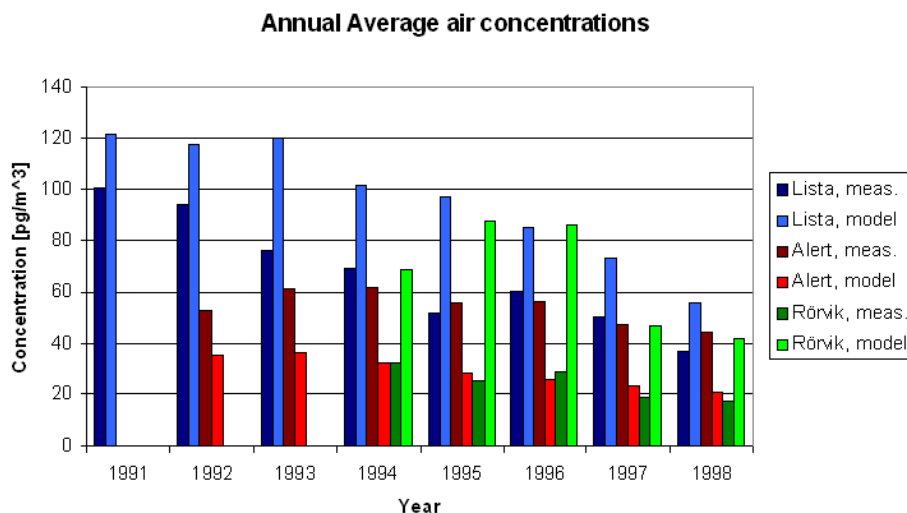


**Fig. 6.** Three examples of the annual averaged concentration of  $\alpha$ -HCH in the lowermost atmospheric layer: Lista (blue) Alert (red) and Rörvik (green). Measurements are shown in dark colours and model results in light colours.

Alert, Spitzbergen and Tagish but consistently overestimated at all other stations. Except for some very low measured values, the range of the model predictions is within a factor 4 of the range of measurements (Table 2).

### 3.1.2 Evaluation against individual measurements

The model results are also compared directly with individual measurements. When the model results are averaged over the days of each individual measurement, the seasonal pattern seen in the daily averaged model concentrations is averaged out at all stations but Alert, Spitzbergen and Lista (not shown). Measured  $\alpha$ -HCH concentrations are plotted against model calculations in scatter plots and correlation is tested with a t-test. No statistically significant correlation is found except at Rörvik, significant within a 1% significance level, and at Lista, significant within a 0.1% significance level (Fig. 7).

There are negative trends in both measured and modelled concentrations over the years 1991–1998 at Lista that are very similar; the measurements decrease with  $8.4 \text{ pgm}^{-3}$  per year, while the model results decrease by  $9.1 \text{ pgm}^{-3}$  per year on average (Fig. 8).

## 4 Discussion

The decreased air concentrations from 1992 to 1998 predicted by the model (see Fig. 4) reflect the reduced emissions in this period. Higher  $\alpha$ -HCH concentrations over the Bering Sea than over the surrounding seas in the beginning of the model simulation indicate a re-volatilisation from the ocean to the air, which has also been observed in the beginning of the 1990s (Jantunen and Bidleman, 1995). In 1998 there is a higher  $\alpha$ -HCH concentrations in air over some parts

of the Pacific Ocean than in 1992. This can be interpreted as a closer equilibrium between air and ocean water towards the end of the model simulation, which will lead to a decreased deposition to the ocean and hence a potential for higher concentrations in the air.

The spikes found in the daily averaged model data can be interpreted as individual transport episodes from areas with primary emissions. More spikes are therefore found at the low latitude stations closer to source areas than at the high latitude stations.

The seasonal pattern, with higher concentrations during summer than during winter found in the daily averaged model results, indicates that temperature dependent re-volatilisation from the surface contributes significantly to the atmospheric concentrations. Another indication of this is the trend in air concentrations seen at Lista (see Fig. 8), which decrease much less than the emissions over the modelled period (see Fig. 2). Higher amplitudes in the seasonal pattern at the high Arctic stations are probably due to higher temperature amplitudes here. Another factor influencing the air concentrations at the high Arctic sites is the omission of sea ice in the model, which leads to higher re-volatilisation from the oceans. Sea ice acts as a lid on the Arctic Ocean reducing the air-ocean exchange greatly.

Observations of  $\alpha$ -HCH in air at the high Arctic stations indicate a bi-modal pattern with peak concentrations in spring and autumn (Hung et al., 2002). Different mechanisms have been suggested to explain this pattern, e.g. a filter effect of the vegetation, removing the chemicals in air from contaminated areas before it reaches the Arctic (Hung et al., 2002). Other factors influencing the air concentration pattern could be re-volatilisation from the snowpack and a change in type of precipitation (Halsall, 2004). Neither of these processes is, at present, taken into account in the model

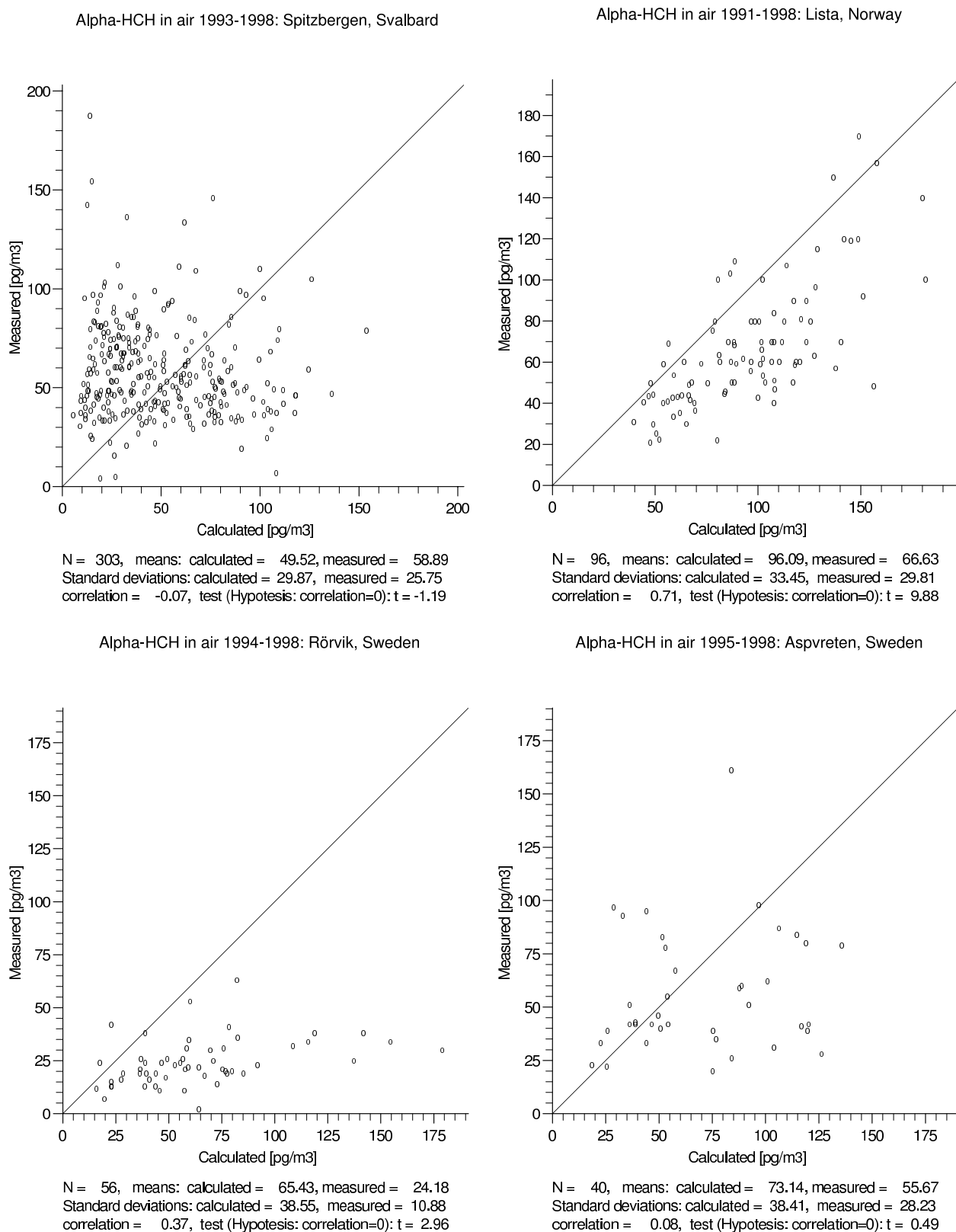


**Fig. 7.** Four examples of the measured  $\alpha$ -HCH concentrations in the lowermost atmospheric layer plotted against predicted concentrations: Spitzbergen (upper left), Lista (upper right), Rörvik (lower left) and Aspveten (lower right). The results from all other stations are similar to Spitzbergen and Aspveten.

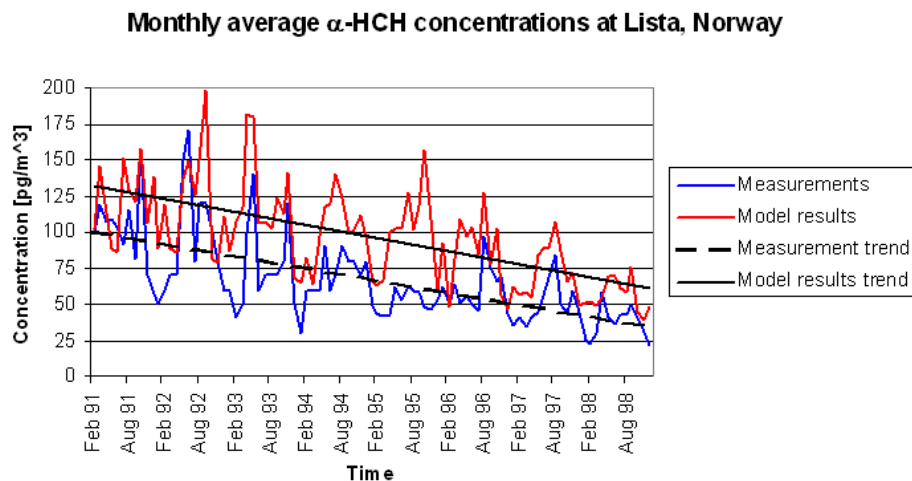


**Fig. 8.** Monthly averaged  $\alpha$ -HCH concentrations at Lista for measurements (blue) and model results (red). Black lines show the decreasing trend in concentrations for the measurements (dashed) and model results (solid).

with the very simple surface parameterisation. This offers an explanation of the deviation of the model results from the observed pattern. There are further indications that surface characteristics not described with the simple surface parameterisation in the model, e.g. vegetation, influence the observed values but not the model results. The lack of correlation between individual measurements and model results is one indication (see Fig. 7). Another indication of this is the difference between the two Swedish stations Rörvik and Aspvreten, which are separated by only a few grid cells. There is a high correlation of the daily averaged air concentrations in the model between the two stations, but the similar evaluation against measurements is very different. Almost all measured concentrations are underestimated at Rörvik and there is a low but statistically significant correlation between measurements and model results, while the data show more scatter at Aspvreten (Fig. 7).

Contrary to the other stations, the correlation between measurements and model results at Lista is evident (see Figs. 7 and 8). Although the model results are not compared directly with measurements at Lista but with average values of 4–5 measurements for each month, the correlation is not believed to be an artifact of the data treatment. The location of the station, at the southern tip of Norway, probably influences the correlation between measurements and model results. Back-trajectory calculations indicate that the air measured at Lista originate from the nearby North Sea about 2/3 of the time (Haugen et al., 1998). In this case, the simple surface parameterisation used in the model apparently is sufficient to capture the air-surface exchange processes.

A seasonal pattern is not noticed in  $\alpha$ -HCH measurements from Lista, and the concentrations measured between 1991 and 1995 are suggested to arise from advection into the area (Haugen et al., 1998). However, seasonal patterns may not be captured by the measurements due to non-continuous de-

ployment periods at most stations. An indication of this is found for the model results where the seasonal pattern is no longer apparent for most stations when the results are averaged over the periods of the individual measurements (not shown). Furthermore, when the monthly averaged measurements from 1991–1998 at Lista are averaged for each month there do appear to be higher concentrations in the summer months than in the winter months as is found in the model results (Fig. 9).

The emission data is also a source of uncertainty in the model results. The assumption of evenly distributed emissions throughout the year can also contribute to the deviations between measurements and model results. The usage of HCH is closely linked to the crop season since it is an insecticide. However, different usage patterns in different parts of the world complicate estimation of emission factors, and, at present, emission data with higher temporal resolution are not available. Another uncertainty induced by the emission input arises from the estimation of the annual emissions for the years 1991–1998 by linear interpolation of the 1990 and 2000 emissions. This approach fails to account for sudden decrease in emissions from one year to another due to a ban on usage of the compound. We chose to use this approach, since no emission estimates for the years were available.

#### 4.1 Comparison with other model results

Three different box models were used previously to study the global fate of  $\alpha$ -HCH. Two models are zonally averaged models with 6 and 10 zonally averaged regions, respectively (Strand and Hov, 1996; Wania et al., 1999). The third model is divided into 25 zones following both climatic and continental or political borders (Toose et al., 2004). It is difficult to compare the results from these models directly with the DEHM-POP results because of their low spatial resolution.

### Average concentration for each month for the years 1991–1998

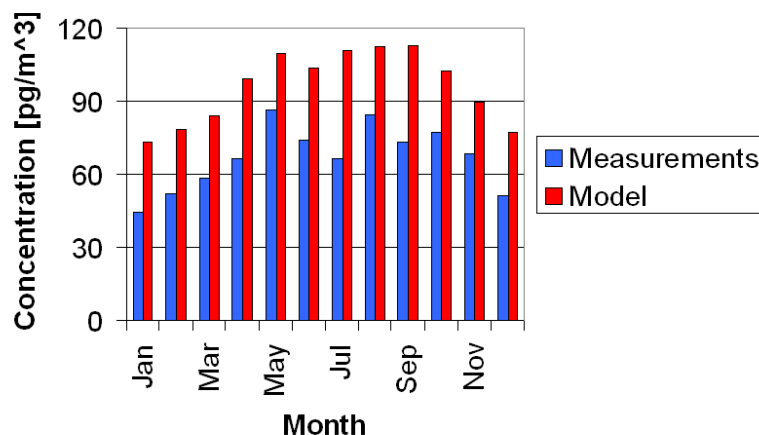


**Fig. 9.** Average  $\alpha$ -HCH concentration for each month for the years 1991–1998 at Lista, Norway. Measurements are shown in blue and model results in red.

The results from the Strand and Hov model are given as annual average concentrations for the year 1985 and the air concentrations are higher than predicted by DEHM-POP (Strand and Hov, 1996). This can be explained by higher emissions for the years before 1990.

The other two models were run for a 50 year period. The Wania et al. model predicts generally a factor 2–3 higher concentrations than DEHM-POP in the 1990s (Wania et al., 1999). Results from the Toose et al. model agree well with DEHM-POP model results for the European and Arctic regions, but are approximately a factor 10 lower for Arctic Canada (Toose et al., 2004).

A regional scale model covering the Baltic Sea region based on the global distribution model of Wania et al. (1999) was used to study the environmental fate of  $\alpha$ -HCH for the years 1970–2000 (Breivik and Wainia, 2002). This model obtains very good predictions of both seasonal averaged and individual measured air concentrations at Lista and Rörvik for the 1980s and 1990s (Breivik and Wainia, 2002).

Overall, there is a fairly good agreement between DEHM-POP and the four box models despite the differences in spatial resolution and process description. However, it is important to note that the two types of models should not be seen as competitors but rather as complementing each other, as discussed by Wania (1999).

Only one atmospheric transport model using dynamical meteorological data as input was used to study the environmental fate of  $\alpha$ -HCH (Koziol and Pudykiewicz, 2001). The model is a global atmospheric transport model with a horizontal resolution of  $2^\circ \times 2^\circ$  and 11 vertical layers, and it has been used to study the atmospheric transport of  $\alpha$ -HCH for the years 1993–1994 (Koziol and Pudykiewicz, 2001). A clear seasonal pattern with higher values during summer

than winter is also seen in the model results for the four studied stations: Alert, Spitzbergen, Dunai Island and Tagish (Koziol and Pudykiewicz, 2001). For the first three stations the concentrations predicted by the two models are of comparable magnitude, whereas for Tagish the Koziol and Pudykiewicz model predicts a factor 5–6 higher concentrations than DEHM-POP.

## 5 Conclusions

The Danish Eulerian Hemispheric Model was further developed to describe the atmospheric transport and environmental fate of persistent organic pollutants in the Northern Hemisphere. Two surface compartments and exchange processes between air and the surfaces were introduced in the model to account for the multi-hop transport of POPs.

The model was used to study the atmospheric transport and environmental fate of the insecticide  $\alpha$ -hexachlorocyclohexane for the years 1991–1998, and the results were evaluated against measurements. The model results are promising. The annual averaged air concentration of  $\alpha$ -HCH is predicted within a factor 2–3 of measured concentrations in the model domain. These results are of equal or higher accuracy than results from previous models describing the environmental fate of  $\alpha$ -HCH. The shorter-term averaged air concentration of  $\alpha$ -HCH is well predicted at two of the stations, however, at the other stations there is no correlation between individual measurements and model results. This is probably due to the simple description of the surface characteristics, where only two types of surfaces are included: soil and ocean water. There is thus a need for investigating the role of the omitted surface

characteristics such as vegetation, snow, ocean currents, and sea ice on the fate of POPs. To study POPs in general there is also a need for describing the partitioning between the gas phase and the aerosol phase. We are currently developing the model further by considering these issues.

*Acknowledgements.* This project is partly funded by the Danish Research Training Council through the Copenhagen Global Change Initiative. Thanks to professor Terry Bidleman for supplying a collection of data on measured  $\alpha$ -HCH concentrations in ocean water and to Mr. Carsten Ambelas Skjøth for comments on the manuscript.

Edited by: O. Hertel

## References

- Aas, W., Solberg, S., Berg, T., Manø, S., and Yttri, K. E.: Monitoring of long range transported air pollutants, Annual report for 2002. Kjeller, Norwegian Institute for Air Research, SFT Report 877/2003 NILU OR 23/2003, 2003.
- AMAP, AMAP Assessment Report: Arctic Pollution Issues. Arctic Monitoring and Assessment Programme (AMAP), Oslo, Norway, xii+859, 1998.
- Atkinson, R., Guicherit, R., Hites, R. A., Palm, W.-U., Seiber, J. N., and De Voogt, P.: Transformation of pesticides in the atmosphere: A state of the art, *Water Air Soil Poll.*, 115, 219–243, 1999.
- Berg, T., Hjellbrekke, A. G., and Larsen R.: Heavy metals and POPs within the EMEP region 1999, EMEP/CCC 9/2001, 2001.
- Brevik, K. and Wania, F.: Evaluating a model of the historical behaviour of two hexachlorocyclohexanes in the Baltic Sea environment, *Env. Sc. Techn.*, 36, 5, 1014–1023, 2002.
- Brubaker, W. W. and Hites, R. A.: OH reaction kinetics of gas-phase  $\alpha$ - and  $\gamma$ -hexachlorocyclohexane and hexachlorobenzene, *Env. Sc. Techn.*, 32, 6, 766–769, 1998.
- Christensen, J. H.: The Danish Eulerian Hemispheric Model – a three-dimensional air pollution model used for the Arctic, *Atmos. Env.*, 31, 4169–4191, 1997.
- Christensen, J. H.: An overview of Modelling the Arctic mass budget of metals and sulphur: Emphasis on source apportionment of atmospheric burden and deposition, In: *Modelling and sources: A workshop on Techniques and associated uncertainties in quantifying the origin and long-range transport of contaminants to the Arctic*, Report and extended abstracts of the workshop, Bergen, 14–16 June 1999, AMAP report 99:4. see also [urlhttp://www.amap.no/](http://www.amap.no/), 1999.
- Frohn, L. M., Christensen, J. H., and Brandt, J.: Development of a high-resolution nested air pollution model – the numerical approach, *J. Comp. Phys.*, 179, 68–94, 2002.
- Geels C., Doney, S., Dargaville, R., Brandt, J., and Christensen, J. H.: Investigating the sources of synoptic variability in atmospheric CO<sub>2</sub> measurements over the Northern Hemisphere continents – a regional model study, *Tellus B*, 56B, 35–50, 2004.
- Grell, G. A., Dudhia, J., and Stauffer, D. R.: A description of the fifth-generation Penn State NCAR Mesoscale Model (MM5), NCAR/TN-398+STR, NCAR Technical Note, Mesoscale and Microscale Meteorology Division, National Center for Atmospheric Research, Boulder, Colorado, 122, 1995.
- Halsall, C. J., Bailey, R., Stern, G. A., Barrie, L. A., Fellin, P., Muir, D. C. G., Rosenberg, B., Rovinsky, F. Ya., Kononov, E. Ya., and Pastukhov, B.: Multi-year observations of organohalogen pesticides in the Arctic atmosphere, *Env. Poll.*, 102, 51–62, 1998.
- Halsall, C. J.: Investigating the occurrence of persistent organic pollutants (POPs) in the Arctic: Their atmospheric behaviour and interaction with the seasonal snow pack, *Env. Poll.*, 128, 1–2, 163–175, 2004.
- Haugen, J.-E., Wania, F., Ritter, N., and Schlabach, M.: Hexachlorocyclohexanes in air in Southern Norway. Temporal variation, source allocation, and temperature dependence, *Env. Sc. Techn.*, 32, 2, 217–224, 1998.
- Hung, H., Halsall, C. J., Blanchard, P., Li, H. H., Fellin, P., Stern, G., and Rosenberg, B.: Temporal trends of organochlorine pesticides in the Canadian Arctic atmosphere, *Env. Sc. Techn.*, 36, 5, 862–868, 2002.
- Jantunen, L. M. and Bidleman, T. F.: Reversal of the air-water gas exchange direction of hexachlorocyclohexanes in the Bering and Chukchi Seas: 1993 versus 1988, *Env. Sc. Techn.*, 29, 4, 1081–1089, 1995.
- Jones, K. C. and de Voogt, P.: Persistent organic pollutants (POPs): State of the science, *Env. Poll.*, 100, 209–221, 1999.
- Jury, W. A., Spencer, W. F., and Farmer, W. J.: Behaviour assessment model for trace organics in soil: I. Model description, *J. Env. Qual.*, 12, 558–564, 1983.
- Koziol, A. S. and Pudykiewicz, J. A.: Global-scale environmental transport of persistent organic pollutants, *Chemosphere*, 45, 1181–1200, 2001.
- Kucklick, J. R., Hinckley, D. A., and Bidleman, T. F.: Determination of Henry's law constants for hexachlorocyclohexanes in distilled water and artificial seawater as a function of temperature, *Mar. Chem.*, 34, 197–209, 1991.
- Li, Y.-F.: Global technical hexachlorocyclohexane usage and its contamination consequences in the environment: From 1948 to 1997, *Sci. Total Environ.*, 232, 121–158, 1999.
- Li, Y.-F., Scholtz, M. T., and van Heyst, B. J.: Global gridded emission inventories of  $\alpha$ -hexachlorocyclohexane, *J. Geophys. Res.*, 102, D5, 6621–6632, 2000.
- Li, Y.-F., Scholtz, M. T., and van Heyst, B. J.: Global gridded emission inventories of  $\beta$ -hexachlorocyclohexane, *Env. Sc. Techn.*, 37, 16, 3493–3498, 2003.
- Ma, J., Daggupati, S., Harner, T., and Li, Y.-F.: Impacts of Lindane usage in the Canadian prairies on the Great Lakes ecosystem, 1. Coupled atmospheric transport model and modeled concentrations in air and soil, *Env. Sc. Techn.*, 37, 17, 3774–3781, 2003.
- Mackay, D., Shiu, W.-Y., and Ma, K.-C.: *Physical-Chemical Properties and Environmental Fate Handbook*. CD-ROM, Chapman & Hall/CRnetBASE, London, 2000.
- MacLeod, M., Woodfine, D. G., Mackay, D., McKone, T., Bennett, D., and Maddalena, R.: BETR North America: A regionally segmented multimedia contaminant fate model for North America, *Env. Sc. Poll. Res.*, 8, 3, 156–163, 2001.
- Malanichev, A., Mantseva, E., Shatalov, V., Strukov, B., and Vulykh, N.: Numerical evaluation of the PCB transport over the Northern Hemisphere, *Env. Poll.*, 128, 1–2, 279–289, 2004.
- Pacyna, J. M. and Oehme, M.: Long-range transport of some organic compounds to the Norwegian Arctic, *Atmos. Env.*, 22, 2, 243–257, 1988.

- Prevedouros, K., MacLeod, M., Jones, K. C., and Sweetman, A. J.: Modelling the fate of persistent organic pollutants in Europe: parameterisation of a gridded distribution model, *Env. Poll.*, 128, 1–2, 251–261, 2004
- Scheringer, M., Wegmann, F., Fenner, K., and Hungerbühler, K.: Investigation of the cold condensation of persistent organic pollutants with a global multimedia fate model, *Env. Sc. Techn.*, 34, 9, 1842–1850, 2000.
- Strand, A. and Hov, Ø.: A model strategy for the simulation of chlorinated hydrocarbon distributions in the global environment, *Water Air Soil Poll.*, 86, 283–316, 1996.
- Toose, L., Woodfine, M., MacLeod, M., Mackay, D., and Gouin, J.: BETR-World: A geographically explicit model of chemical fate: Application to transport of  $\alpha$ -HCH to the Arctic, *Env. Poll.*, 128, 1–2, 223–240, 2004.
- van Jaarsveld, J. A., van Pul, W. A. J., and de Leeuw, F. A. A. M.: Modelling transport and deposition of persistent organic pollutants in the European region, *Atmos. Env.*, 31, 7, 1011–1024, 1997.
- Wania, F. and Mackay, D.: Global fractionation and cold condensation of low volatility organochlorine compounds in polar regions, *Ambio*, 22, 1, 10–18, 1993.
- Wania, F. and Mackay, D.: Tracking the distribution of persistent organic pollutants, *Env. Sc. Techn.*, 30, 9, 390A–396A, 1996.
- Wania, F.: Differences, Similarities, and Complementarity of Various Approaches to Modelling Persistent Organic Pollutant Distribution in the Environment, In: *Proceedings of the WMO/EMEP/UNEP Workshop on Modelling of Atmospheric Transport and Deposition of Persistent Organic Pollutants and Heavy Metals*, 1, pp. 115–140, 1999.
- Wania, F., Mackay, D., Li, Y.-F., Bidleman, T. F., and Strand, A.: Global chemical fate of  $\alpha$ -hexachlorocyclohexane, 1. Evaluation of a global distribution model, *Env. Toxi. Chem.*, 18, 7, 1390–1399, 1999.
- Willett, K. L., Ulrich, E. M., and Hites, R. A.: Differential toxicity and environmental fates of hexachlorocyclohexane isomers, *Env. Sc. Techn.*, 32, 15, 2197–2207, 1998.

*[Blank page]*

## Appendix B

### Paper II

Hansen, K. M., C. J. Halsall, and J. H. Christensen, 2006, A dynamic model to study the exchange of gas-phase POPs between air and a seasonal snowpack, *Environ. Sci. Technol.*, 40(8), 2644-2652.



# A Dynamic Model To Study the Exchange of Gas-Phase Persistent Organic Pollutants between Air and a Seasonal Snowpack

KAJ M. HANSEN,<sup>\*,†</sup>  
CRISPIN J. HALSALL,<sup>‡</sup> AND  
JESPER H. CHRISTENSEN<sup>†</sup>

*Department of Atmospheric Environment, National Environmental Research Institute, P.O. Box 358, Frederiksborgvej 399, 4000 Roskilde, Denmark, and Environmental Science Department, Lancaster University, Lancaster LA1 4YQ, United Kingdom*

An arctic snow model was developed to predict the exchange of vapor-phase persistent organic pollutants between the atmosphere and the snowpack over a winter season. Using modeled meteorological data simulating conditions in the Canadian High Arctic, a single-layer snowpack was created on the basis of the precipitation rate, with the snow depth, snow specific surface area, density, and total surface area (TSA) evolving throughout the annual time series. TSA, an important parameter affecting the vapor-sorbed quantity of chemicals in snow, was within a factor of 5 of measured values. Net fluxes for fluorene, phenanthrene, PCB-28 and -52, and  $\alpha$ - and  $\gamma$ -HCH (hexachlorocyclohexane) were predicted on the basis of their wet deposition (snowfall) and vapor exchange between the snow and atmosphere. Chemical fluxes were found to be highly dynamic, whereby deposition was rapidly offset by evaporative loss due to snow settling (i.e., changes in TSA). Differences in chemical behavior over the course of the season (i.e., fluxes, snow concentrations) were largely dependent on the snow/air partition coefficients ( $K_{sa}$ ). Chemicals with relatively higher  $K_{sa}$  values such as  $\alpha$ - and  $\gamma$ -HCH were efficiently retained within the snowpack until later in the season compared to fluorene, phenanthrene, and PCB-28 and -52. Average snow and air concentrations predicted by the model were within a factor of 5–10 of values measured from arctic field studies, but tended to be overpredicted for those chemicals with higher  $K_{sa}$  values (i.e., HCHs). Sensitivity analysis revealed that snow concentrations were more strongly influenced by  $K_{sa}$  than either inclusion of wind ventilation of the snowpack or other changes in physical parameters. Importantly, the model highlighted the relevance of the arctic snowpack in influencing atmospheric concentrations. For the HCHs, evaporative fluxes from snow were more pronounced in April and May, toward the end of the winter, providing evidence that the snowpack plays an important role in influencing the seasonal increase in air concentrations for these compounds at this time of year.

\* Corresponding author phone: +45 46 30 18 72; fax: +45 46 30 12 14; e-mail: kmh@dmu.dk.

<sup>†</sup> National Environmental Research Institute.

<sup>‡</sup> Lancaster University.

## Introduction

The role of snow in providing airborne organic contaminants such as persistent organic pollutants (POPs) to regions of high altitude and latitude has received growing attention (1–4). Falling snow has a high efficiency at scavenging both vapor- and particle-bound semivolatile organic compounds (SVOCs) from the atmosphere, essentially due to the large surface area presented by snow crystals and the subzero temperatures which promote surface sorption (5). Understanding the fate of these contaminants in cold environments is complicated by the presence of snow and ice. Chemical accumulation in the seasonal snowpack and subsequent release into meltwater is confounded by the dynamic nature of snow, whereby snow metamorphosis and aging results in revolatilization of previously deposited chemicals to the overlying atmosphere (4). In the Arctic, the size and extent of terrestrial and sea-ice snowfields ensures that snow plays a major role in influencing atmospheric chemistry and ultimately the composition of the polar boundary layer (e.g., ref 6). Snow as a porous substrate provides a large surface area for both heterogeneous chemistry and the sorption/release of trace gases (7), and it is plausible that such extensive snowfields would also influence the atmospheric behavior of POPs in polar regions.

Recently, Daly and Wania (8) incorporated a seasonal snowpack into a dynamic multimedia fugacity model (CoZMo-POP) to assess the role of snow on the environmental fate of a number of SVOCs. This model incorporated a dynamic water balance based on the typical seasonal cycle for south/central Canada, with three seasons defined as “snow accumulation”, “snowmelt”, and “summer” (no snow). The inclusion of the snowpack in the model had a notable effect on the predicted seasonal air concentrations for some compounds; more volatile compounds such as the lighter PCBs displayed an increase in atmospheric levels during the spring due to volatilization from the melting snowpack. However, subsequent comparison of these modeled data to observed air concentrations from the Great Lakes (9) revealed a discrepancy with no evidence of an observed spring increase for several PCB congeners. Results from the model however indicate that the occurrence and intensity of these springtime peaks would increase with the length of the snow accumulation period (10). In other words, the longer the duration of snow cover (especially regions at higher latitudes) the stronger the influence of snow on the seasonal fluctuations in air concentrations. Tentative evidence to support this comes from the Canadian High Arctic, where many OC pesticides show an increase in air concentrations during April/May (2, 11, 12). While these months do not represent significant snowmelt in the High Arctic, this may be the case further south in the large sub-Arctic regions, and the role of extensive snowpacks in influencing air concentrations and air/surface interactions needs investigating.

In this study, a dynamic model to study the exchange of gas-phase POPs between air and a seasonal snowpack is presented. The model is used to simulate conditions in the Canadian High Arctic, with respect to snow accumulation, precipitation, and meteorological inputs, and describes both the evolution of a single-layer snowpack over a winter season and the exchange of SVOCs with the overlying atmosphere. The purpose of this model is for inclusion in the POP version of the Danish Eulerian Hemispheric Model (DEHM-POP), an atmospheric chemistry transport model developed to study the environmental fate of POPs in the northern hemisphere (13). The goal is to simulate a seasonal snowpack and the chemical fluxes into and out of snow as well as to examine

the effect of these processes on atmospheric concentrations for a number of POPs in the northern hemisphere.

## Model Description

The model describes the physical evolution of a single-layer snowpack over a year and comprises the three components of snow accumulation, settling, and melting. The chemistry within the model details the interaction of a vapor-phase SVOC with snow, and describes fluxes into and out of the snowpack, on the basis of changes in snow physical parameters, the partitioning of the chemical to snow surfaces, and the chemical concentration. Both wet deposition and dry gaseous exchange fluxes between air and the snow determine the chemical mass balance between the boundary layer and the snowpack. In essence, the model consists of an air compartment, a snowpack compartment (on a nonspecified surface), and a meltwater compartment and is driven by dynamic data on the temperature, precipitation rate, and wind speed for a given location. Air is continuously exchanged by inflow/outflow through the air compartment, which is dependent on the wind speed. The snowpack is formed by snowfall, determined from the precipitation rate and the ambient temperature. For example, when the air temperature ( $T$ ) falls below  $0\text{ }^{\circ}\text{C}$ , precipitation is assumed to be snowfall; similarly, temperature is also used to determine periods of melting ( $T > 0\text{ }^{\circ}\text{C}$ ) as well as refreezing ( $T < 0\text{ }^{\circ}\text{C}$ ).

The snowpack is considered to be homogeneous and is characterized by the following physical parameters: depth ( $d$ , m), specific mass ( $m$ ,  $\text{kg m}^{-3}$ ), density ( $\rho$ ,  $\text{kg m}^{-3}$ ), specific surface area (SSA,  $\text{m}^2 \text{kg}^{-1}$ ), and total surface area (TSA,  $\text{m}^2 \text{m}^{-2}$ ). Three different processes determine the development of the snowpack through the season, accumulation, settling, and melting, and are described below.

**Snow Accumulation.** The snowpack accumulates by consecutive snowfall events, whereby for each time step including a precipitation event a low-density snow layer is formed, which is assumed to mix instantaneously with the existing snowpack. Mass and TSA are conserved in this process, and the other physical parameters are then calculated from the following equations:

$$\text{SSA} = (\text{TSA})/m \quad (1)$$

$$\rho = 350.29 \exp(-0.0162(\text{SSA})) \quad (2)$$

$$d = m/\rho \quad (3)$$

The relationship between the density and SSA (eq 2) has been empirically derived from snow observations and measurements (14). In this case, simultaneous measurements of density and SSA from 131 samples of different snow types, combined with grain observations, were made from a number of locations including Svalbard (Norwegian Arctic), Arctic Canada, and the Alps. A number of linear SSA–density relationships were derived for the different snow types by Legagneux et al. (14). As the model in this study operates with only one homogeneous snow layer, these data were pooled, resulting in a “best-fit” exponential relationship given by eq 2. Subsequent values for the total surface area, density, and depth were calculated from eqs 1–3 in each time step. An SSA value of  $120 \text{ m}^2 \text{kg}^{-1}$  was selected as an initial value for freshly fallen snow, yielding a density of  $50.1 \text{ kg m}^{-3}$  (eq 2), which corresponds to observed values for freshly fallen snow in calm weather conditions (14, 15). It is important to note that the snowpack depth may also be influenced by wind-blown snow, resulting in uneven accumulation. However, this process was disregarded due to the homogeneous (single-layer) structure of the snowpack in the model and its simulation of the arctic sea-ice snowpack, with its relatively

homogeneous topography compared to terrestrial mountain regions for example.

**Settling.** Changes to the snow crystal structure, or snow metamorphosis, is brought about through the action of wind, changes in temperature, and general snow aging (7). This continuous “settling” following snowfall results in increases in snow density and decreases in SSA. The settling process in the model is described using an empirically derived expression in which the SSA decreases with time,  $t$  (7):

$$\text{SSA}(t) = \text{SSA}(0) \exp(-at) \quad (4)$$

where the settling rate  $a = 8.87 \times 10^{-4} \exp(-1708/T)$  and  $T$  is the temperature of the snowpack, which is considered to be the same as the boundary layer air temperature. New values for the total surface area, density, and depth are then calculated from eqs 1–3 in each time step.

**Melting.** The snow melts when  $T > 0\text{ }^{\circ}\text{C}$  at a rate of  $5 \text{ cm day}^{-1} T^{-1}$ . The meltwater is assumed to be lost from the snowpack as runoff, with the amount of meltwater within the snowpack reduced to  $1/e$  after 24 h. The meltwater refreezes if the temperature decreases to  $< 0\text{ }^{\circ}\text{C}$ , and the refreeze rate is determined by the amount of heat supplied by the temperature difference between the meltwater ( $0\text{ }^{\circ}\text{C}$ ) and the snowpack. Instantaneous mixing is again enforced, where the refrozen melt layer is assumed to have a TSA = 0. Importantly, during melt, the meltwater rapidly fills the pore spaces in the snowpack, thereby “shutting off” chemical exchange between air and the snow surface. In this case, it is assumed that air–snow gas exchange is zero during periods of melting.

**Chemical Fate.** Deposition and exchange of vapor-phase POPs between the snowpack and the atmosphere are described by the following equations. The wet deposition flux,  $F_{\text{wet}}$ , from the atmosphere was determined for each time step according to

$$F_{\text{wet}}(t) = W_g P C_a \quad (5)$$

where  $P$  is the precipitation rate,  $C_a$  is the air concentration, and  $W_g$  is the scavenging coefficient given by  $W_g = K_{\text{ia}}(\text{SSA}_{\text{initial}})\rho_w$ , where  $K_{\text{ia}}$  is the snow interface–air partition coefficient and  $\rho_w$  is the density of water ( $1000 \text{ kg m}^{-3}$ ). Values for  $K_{\text{ia}}$  were taken from Lei and Wania (5), as calculated from the polyparameter linear free energy relationship empirically derived by Roth et al. (16). Initial values of  $C_a$  were selected from observations conducted as part of the long-term air monitoring program at Alert (11, 12, 17). The partitioning between the snow surface and air within the snowpack can be expressed by the snow–air partition coefficient ( $K_{\text{sa}}$ ) (5):

$$K_{\text{sa}} = K_{\text{ia}}(\text{SSA})\rho \quad (6)$$

The dry gas exchange flux at the surface was derived as the gradient between the boundary layer air concentration and the concentration in the snow pore space multiplied by an exchange velocity,  $v$ :

$$F_{\text{gas}} = v(C_s/K_{\text{sa}} - C_a) \quad (7)$$

$v$  was calculated using the Whitman two-layer resistance method equivalent to the expression for the air–water interface (18):

$$v^{-1} = (v_{\text{air}})^{-1} + (v_{\text{snow}}K_{\text{sa}})^{-1} \quad (8)$$

The air side exchange velocity ( $v_{\text{air}}$ ) was calculated as (19)

$$v_{\text{air}} = k^2 U (\ln(z_w/z_0) \ln(z_{\text{ref}}/z_0))^{-1} \quad (9)$$

where  $k$  is von Karman's constant ( $k = 0.4$ ),  $U$  is the wind speed,  $z_w$  is the height of the wind ( $z_w = 10$  m),  $z_{ref}$  is the reference height ( $z_{ref} = 2$  m), and  $z_0$  is the surface roughness for snow ( $z_0 = 0.001$  m) (19).  $\nu_{snow}$  is given by the snow diffusion coefficient,  $D_{snow}$ , divided by half the thickness of the snowpack, which represents the average diffusion path given the evolution of the snowpack depth over the course of a winter season.  $D_{snow}$  depends on the air diffusion coefficient ( $D_{air}$ ) and the density of the snow and was determined according to

$$D_{snow} = D_{air}(1 - \rho_{snow}/\rho_{ice})^n \quad (10)$$

where  $n = 1.5$  and was empirically determined for a volatile tracer, sulfur hexafluoride ( $SF_6$ ), from field experiments conducted at Summit, Greenland (20). Temperature-dependent  $D_{air}$  values were calculated according to Schwarzenbach et al. (21).

## Results and Discussion

The model was run for one season between July 1, 1999, and June 30, 2000, with environmental conditions based on the High Arctic site of Alert, Canada ( $82^\circ 30' N$ ,  $62^\circ 20' W$ ). Temperatures, precipitation rates, and wind speeds were extracted from the numerical weather prediction model MM5v2 (22), which uses analyzed data as input. The temperature over the 1999–2000 period ranged between  $-39.4$  and  $+3.1$  °C, wind speed between  $0.03$  and  $9.53$  m  $s^{-1}$ , and precipitation between  $0$  and  $0.5$  mm of water/h with a total of  $197$  mm of water equivalent during the whole season. This compares well with the observed meteorology at Alert during the 1999/2000 season (23), although the air temperatures from MM5v2 were generally lower than the measured temperatures during the melting season due to the presence of the snowpack cooling the overlying atmosphere. This may have led to an underestimation of the melt rate of the snowpack in the model. As the MM5v2 model has been successfully utilized in a number of atmospheric chemistry transport model studies using DEHM (13, 24–26) with a spatial resolution of  $150$  km  $\times$   $150$  km, the snowpack model described here was also run with a horizontal resolution of  $150$  km with the height of the air compartment set to  $1000$  m.

**Snow Physics.** At the beginning of the season (July/August 1999), the air temperature oscillated around  $0$  °C and shallow snow layers often formed due to precipitation events. These frequently melted away due to increases in ambient temperature. A permanent snow layer was present by the end of August, and continued to grow in depth with the onset of winter to reach a maximum of  $\sim 50$  cm. Figure 1 presents the 1999/2000 time series of snow depth (a), SSA (b), and TSA (c) starting from July 1999 to June 2000. The snow depth decreased from about the middle of June (the following year) onward and had completely melted away by the end of June. SSA decreased rapidly from its initial value of  $120$  m<sup>2</sup> kg<sup>-1</sup>, typically ranging between  $5$  and  $25$  m<sup>2</sup> kg<sup>-1</sup> throughout most of the winter season (Figure 1b). TSA increased to a maximum value of about  $2000$  m<sup>2</sup> m<sup>-2</sup> by the end of November and decreased thereafter to around  $500$  m<sup>2</sup> m<sup>-2</sup>, remaining relatively constant throughout the rest of the season. To compare the physical development of the model snowpack with actual snow observations, Figure 1 incorporates physical measurements ( $d$ , SSA, and TSA) made at Alert during early February and mid-April 2000 (23). For example, the range of observed snow depths during these February/April campaigns spans the modeled snow depths derived for these periods. In addition, SSA and TSA observations were conducted of the snowpack during the respective February and April field campaigns. However, these parameters were measured for each recognizable snow layer/band that

comprised the snowpacks (23), and therefore, the weighted average SSA and the calculated TSA for these two campaigns are included in Figure 1b,c. While the average depth and density of the modeled snowpack are in good agreement with these field observations, SSA and hence TSA are underestimated by a factor of  $\sim 5$ . The reason for this discrepancy is probably due to the modeled snowpack consisting of one homogeneous layer, rather than comprising a series of heterogeneous snow layers. The effect of SSA and hence TSA underestimation on POP fate is discussed further below.

**Snow–POP Interactions.** The model was run with  $\alpha$ - and  $\gamma$ -hexachlorocyclohexane ( $\alpha$ - and  $\gamma$ -HCH), PCB-28 and -52, fluorene (FLU), and phenanthrene (PHEN) as trace chemical species. These compounds were considered to be present in the atmosphere solely in the vapor phase, a reasonable assumption based on limited gas/particle partitioning data for the Arctic (27–29), although significant particle-bound fractions ( $>40\%$ ) have been observed for PHEN at the extremely cold temperatures encountered during the arctic winter (30). The atmospheric concentrations for these compounds in the in-flowing air were kept constant at  $50$  pg m<sup>-3</sup> ( $\alpha$ -HCH,  $\gamma$ -HCH, FLU, PHEN) and  $1$  pg m<sup>-3</sup> (PCB-28, PCB-52) in the model simulations.

Figure 2 displays the predicted net fluxes for both PHEN and FLU (a), PCB-28 and -52 (b), and  $\alpha$ -HCH (c) over the time series, whereby negative values represent net deposition into the snow and positive fluxes are net evaporative fluxes into the atmosphere (the net  $\gamma$ -HCH flux is presented in Figure S1 of the Supporting Information). These fluxes illustrate the dynamic nature of the snow throughout the winter, whereby chemical fluxes into the snow appear to be rapidly offset by fluxes back to the atmosphere, the latter brought about by snow metamorphosis and a concomitant decrease in TSA. For example, the wet depositional and gaseous exchange fluxes of PHEN both averaged  $\sim 0.52$  pg m<sup>-2</sup> s<sup>-1</sup> throughout the season and were anticorrelated for each compound, e.g., (PHEN)  $r^2 = 0.61$  and ( $\alpha$ -HCH)  $r^2 = 0.64$  ( $p < 0.01$ ), indicating that revolatilization from the snowpack occurs rapidly following deposition. To support this finding, rapid loss of SVOCs from snow has been observed in the Norwegian Arctic, with PCB and OC pesticide half-lives in fresh snow averaging  $65$  h (4). Differences between PHEN and  $\alpha$ -HCH were apparent (Figure 2), with the most pronounced fluxes of  $\alpha$ -HCH (and  $\gamma$ -HCH; see Figure S1) occurring later in the season compared to those of PHEN. This can be attributed to varying  $K_{sa}$  values and hence the capacity of the snow to retain these chemicals and is subject to further discussion below (depositional and evaporative fluxes for PHEN, PCB-52, and  $\alpha$ -HCH are presented in Figure S2 of the Supporting Information).

Figure 3 presents the time series of modeled snow concentrations for PHEN (a), FLU, PCB-28 and -52 (b), and  $\alpha$ - and  $\gamma$ -HCH (c). Snow concentrations generally increased from October onward, attaining a maximum concentration between December and March before declining toward final snowmelt in June. A high degree of variability was evident, notably for PHEN, FLU, and PCB-28 and -52 (Figure 3a,b) and marked by erratic changes in snow concentrations during the coldest months. Again, these fluctuations were concurrent with the evolution of the  $K_{sa}$  values throughout the time series as illustrated in Figure 3a for PHEN. As these compounds possessed relatively lower values of  $K_{sa}$  compared to the HCHs, their snow concentrations were sensitive to small changes in temperature and SSA, with concentrations in the snow often in equilibrium with the air. On the other hand,  $\alpha$ -HCH and  $\gamma$ -HCH did not display the same variability, and this can be attributed to their relatively higher  $K_{ia}$  values (and hence higher  $K_{sa}$ ) and subsequent retention within the snowpack. A significant rise in temperature toward the end

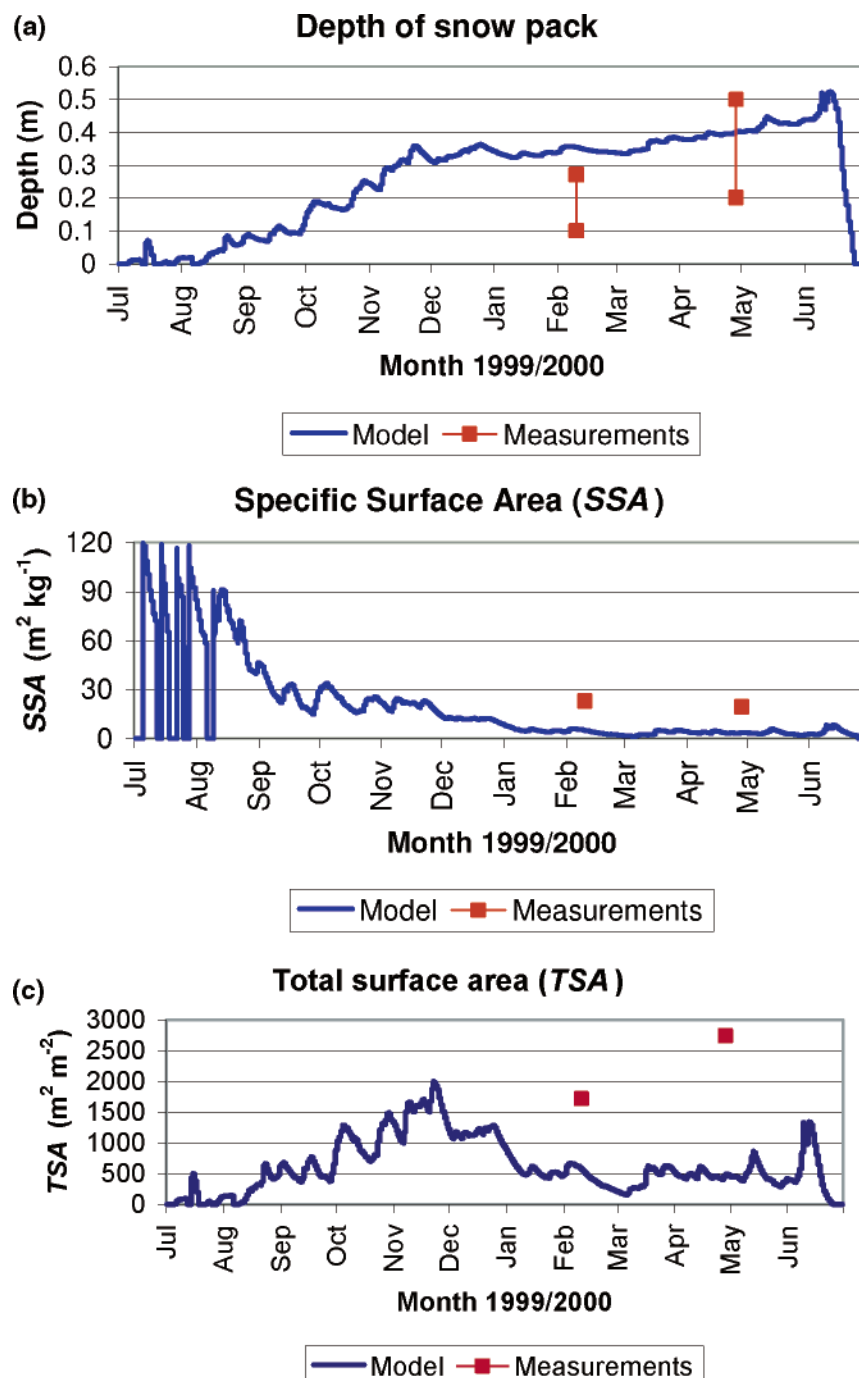


FIGURE 1. Predicted depth (a), SSA (b), and TSA (c) of the snowpack during the season (solid lines). Red dots mark the range of observed snowpack depths (a), weighted averaged measured SSA values (b), and total measured TSA values at Alert (c) (23).

of the winter, however, increased desorption and resulted in net evaporative fluxes out of the snow. The decreasing  $K_{sa}$  values at the end of the season are mainly driven by decreases in  $K_{ia}$  as temperatures increased, rather than through changes in SSA, as this parameter remained relatively constant throughout the late winter/spring (see Figure 1). The HCH snow concentrations increased almost uniformly, throughout the early winter, attaining peak values of  $11850 \text{ pg L}^{-1}$  ( $\alpha$ -HCH) by mid-February. This is concurrent with net deposition into the snow until mid-February (Figure 2c), followed by large evaporative fluxes out of the snow in the late winter. During this period the  $K_{sa}$  values had decreased, resulting in a large snowpack concentration that was out of equilibrium with the atmosphere.

The importance of the partition coefficients and their variation among the test chemicals is illustrated by examining their values at the coldest temperatures, when values of  $K_{ia}$  were at their highest. For example, the lowest temperatures occurred toward the end of January, when  $K_{ia}$  reached a maximum of 16 for PHEN, 80 for PCB-52, and 733 for  $\alpha$ -HCH. However, temperature fluctuations resulted in large variations in  $K_{ia}$ , particularly at colder temperatures, when, for example, a 7-fold increase in  $K_{ia}$  was found over a two week period in February, when temperatures decreased from  $-27$  to  $-38$  °C. As a result,  $K_{sa}$  values showed a similar variability, although SSA also played a significant role by increasing  $K_{sa}$ , particularly in the early part of the season (December) when  $K_{sa}$  reached a maximum of  $35 \times 10^3$  for PHEN,  $160 \times 10^3$  for PCB-52, and

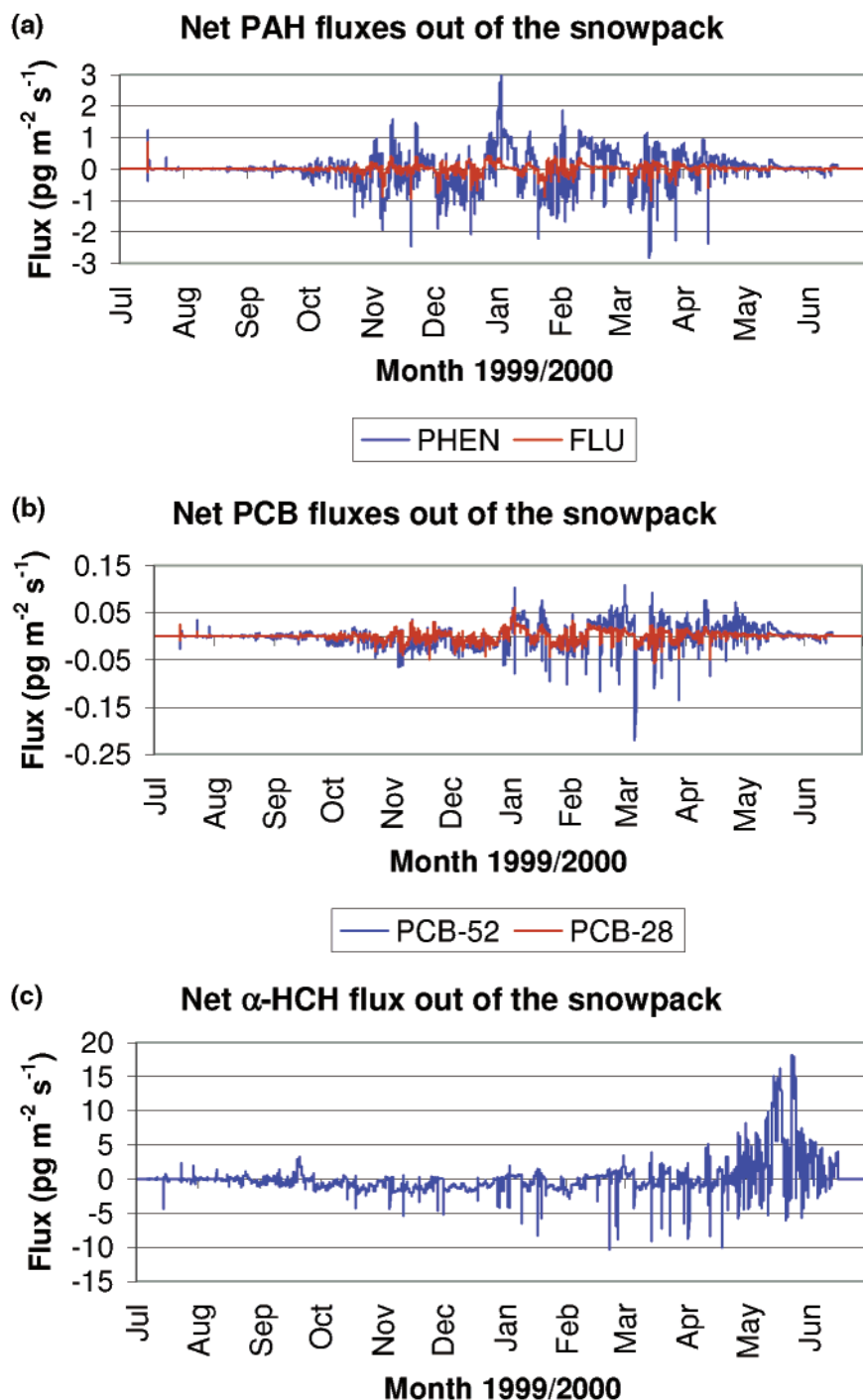


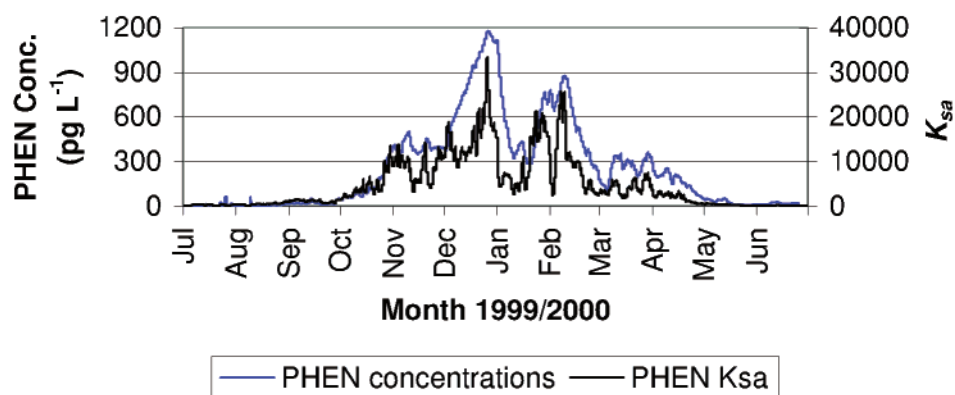
FIGURE 2. Predicted net fluxes out of the snowpack for phenanthrene and fluorene (a), PCB-28 and -52 (b), and  $\alpha$ -HCH (c).

$1.4 \times 10^6$  for  $\alpha$ -HCH (the time series of both  $K_{ia}$  and  $K_{sa}$  for PHEN are presented in Figure S3 of the Supporting Information as an example).

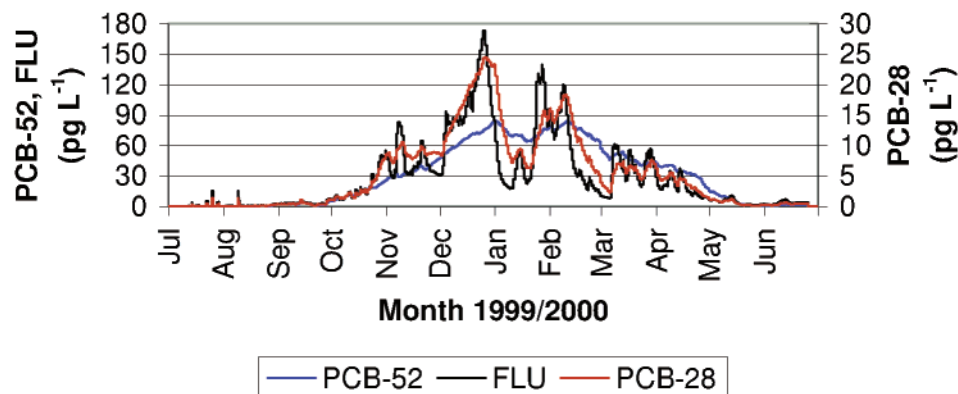
Table 1 compares the range of modeled snow concentrations to measured values determined from a number of field studies, although it should be kept in mind that the conditions at these sites are not necessarily comparable to the conditions in the model simulations. Measurements of POPs in arctic snow are sparse and are typically made only once during a season, making it difficult to evaluate the model thoroughly. Nevertheless, in comparison to these observations, data from the model show reasonable agreement, with values falling within a factor of 10 of measured concentrations. The model tends to underpredict the snow concentrations of PCB-28. This is probably due to the selection of lower air concentra-

tions than those observed at sites such as Svalbard in the Norwegian Arctic (4). Modeled PCB-52 concentrations are in good agreement with the observed values. The predicted HCH concentrations are in good agreement with measurements from the late 1980s, although  $\alpha$ -HCH concentrations are up to a factor of 100 higher than those from recent studies. Arctic HCH air concentrations have generally declined through the past decade (11, 12), and the concentrations used as input in the model are higher than those recently measured at Tromsø in northern Norway (4). In addition, the use of theoretically derived  $K_{ia}$  values may have served to overbias air to snow partitioning, effectively overemphasizing the “stickiness” of snow for some of the chemicals. Additional laboratory studies are required, however, to fully test the appropriateness of the derived  $K_{ia}$  values (using the

(a) Concentrations and  $K_{sa}$  for PHEN in the snowpack



(b) PCB-28, -52 & FLU concentrations in the snowpack



(c)  $\alpha$ -,  $\gamma$ -HCH concentrations in the snowpack

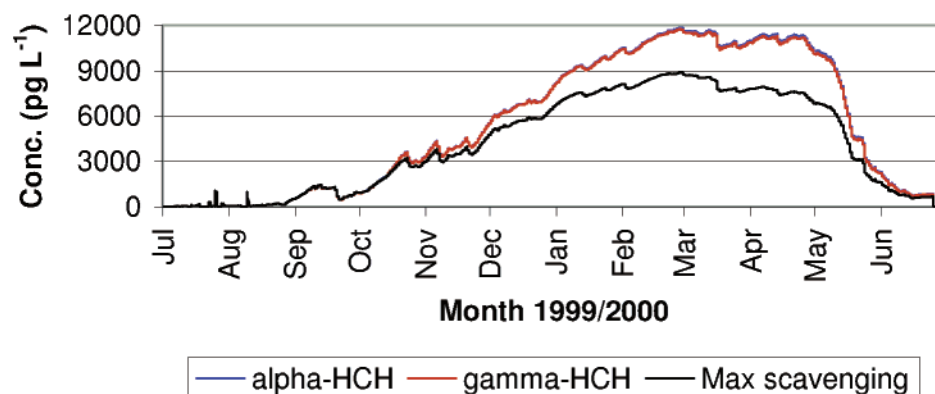


FIGURE 3. Predicted  $K_{sa}$  for phenanthrene (a) and predicted snowpack concentrations ( $\text{pg L}^{-1}$ ) of phenanthrene (a), fluorene and PCB-28 and -52 (b), and  $\alpha$ - and  $\gamma$ -HCH (c). Note: The black line in (c) illustrates snow concentrations when  $W_g$  is limited to  $10^6$ . This value was considered to be a maximum value for SVOCs by Lei and Wania (5).

polyparameter linear free energy approach (8)) for describing snow-air partitioning.

**Air Concentrations.** The influence of the snowpack on atmospheric concentrations of PHEN and  $\alpha$ -HCH can be observed in Figure 4, which presents the modeled air concentrations over the winter period. The variability in air concentrations follows the variability of the snow fluxes, whereby atmospheric concentrations respond to net evaporative fluxes from the snowpack. The air concentrations of PHEN range between 2.9 and  $144 \text{ pg m}^{-3}$ , with the maximum air concentration occurring during early January. This "spike" coincides with a net evaporative flux from the snow and a

marked decrease in snow concentrations (see Figure 3). The range of predicted air concentrations for each chemical is also included within Table 1. For  $\alpha$ -HCH, the increase in the net flux to the atmosphere during May results in elevated air concentrations over this period, in contrast to those of the studied PAHs and PCBs. The average concentrations of  $\alpha$ -HCH and  $\gamma$ -HCH over this month were 331 and  $328 \text{ pg m}^{-3}$ , respectively, and, although greater than observed concentrations ( $\sim 10$ -fold), highlight the influence of the snowpack on seasonal changes in air concentrations.

Changing the size of the model domain from the length of a small valley (1 km) to the length of the Arctic Ocean

**TABLE 1. Model Air ( $\text{pg m}^{-3}$ ) and Snow ( $\text{pg L}^{-1}$ ) Concentrations for the Arctic Including POP Field Observations for Snow**

	predicted air concn range	predicted av snow concn	predicted max snow concn	Tromsø (4), spring 2003	Ny-Ålesund (32), spring 2001	Canadian Arctic (33), winter 1987	Agassiz ice cap (33), 1987	Amituk Lake (34), 1994
FLU	22.3–67.3	28.2	173					
PHEN	2.9–143.7	245.7	1179					
PCB-28	0.06–2.8	5.3	24.6	13.2–340	ND to 110			
PCB-52	0.01–3.9	29.3	84.6	2.6–68.9	2.9–56			
ΣPCB				160–2540	116–2000	257–1770	972 ± 344	118–1317
α-HCH	0.03–911.3	5372.3	11850	17.0–382	ND to 47.6	143–42700	6576 ± 1441	
γ-HCH	0.03–897.1	5314.4	11750	265–4390	186–3090	83–10050	4080 ± 909	ΣHCH, 651–1943

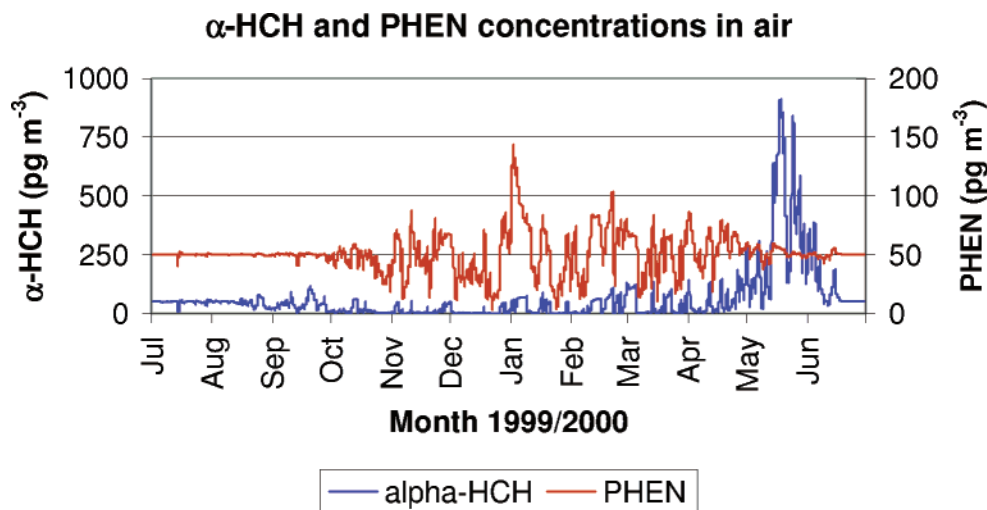


**FIGURE 4. Predicted air concentrations of phenanthrene and α-HCH.**

**TABLE 2. Seasonal Average Concentrations of α-HCH Predicted for Different Model Domain Sizes**

model domain length (km)	snow ( $\text{pg L}^{-1}$ )	air ( $\text{pg m}^{-3}$ )	model domain length (km)	snow ( $\text{pg L}^{-1}$ )	air ( $\text{pg m}^{-3}$ )
1	106971	51.7	1000	1298	46.1
10	35630	56.2	2000	744	35.3
150	5372	61.8	4000	416	24.5
500	2202	55.1			

(4000 km) results in changes to the model output, affecting average concentrations and chemical profiles in both snow and air, with the results shown in Table 2. The larger model domains resulted in the inflow of contaminated air having less influence on the model results, with the snow and air concentrations controlled more by the dynamics of the model rather than by fresh contaminant loadings. Using a small model domain, the air compartment was soon “refilled” with in-flowing contaminated air, and a larger net air-to-snow transfer was seen, resulting in higher concentrations in the snow. As the domain size was increased, the inflow became less important and the air-to-snow transfer decreased, resulting in lower snow concentrations and a shift in the peak air concentrations toward the end of the modeled period (most notably for α- and γ-HCH). Importantly, the average air concentrations of α-HCH dropped to  $25 \text{ pg m}^{-3}$  (closer to measured values) when the model dimensions were increased to include an area approximating the entire Arctic Ocean.

**Sensitivity Analysis.** The sensitivity of the physical parameters in influencing the evolution of the snowpack was investigated. The effect on snow depth and TSA with changes in the settling rate as well as the initial value of SSA was examined. The settling rate was varied by a factor of 2

and the initial SSA value by a factor of 0.25, i.e., from 90 to 150. The depth of the snowpack appeared to be insensitive to changes in these parameters, whereby a 15% increase in the average depth throughout the season was observed by halving the settling rate. TSA responded linearly to changes in the initial SSA and the settling rate, whereby a 2-fold increase/decrease in the average TSA was found for a 2-fold decrease/increase in the settling rate. Furthermore, changing the initial SSA value to 90 and 150 resulted in a 25% decrease/increase of TSA, respectively.

The sensitivity of the snow concentrations to changes in the chemical and physical input parameters was tested for α-HCH.  $K_{ia}$ ,  $K_{sa}$ ,  $W_g$ , the settling rate, the height of the air compartment, and the air diffusion coefficient were changed by a factor of 2, and the exchange velocity as well as the air and snow side resistances was changed by a factor of 10. The average snow concentration was generally sensitive to changes in the input parameters, whereby changes to the chemical parameters yielded snow concentrations that changed by >10% (see Table 3). Aside from altering the physical dimensions of the model domain (i.e., the height of the air compartment and the size of the model domain), the model was most sensitive to changes in  $K_{ia}$  and  $K_{sa}$ . For example, 26% and 16% increases in the average snowpack concentration were observed, when a 2-fold increase in  $K_{ia}$  and  $K_{sa}$  was applied, respectively.

In an attempt to assess the impact of wind ventilation on the chemical behavior in the snow, a “wind pumping” effect was incorporated into the model. When wind blows across the snow surface, it gives rise to pressure variations in the snowpack, which can result in the movement of interstitial air within the snow. This ventilation process can lead to enhanced chemical exchange between the air and the snowpack (20, 31). The ventilation was described in the model by calculating an effective snow diffusion coefficient de-

**TABLE 3. Sensitivity of the Seasonal Average  $\alpha$ -HCH Snowpack Concentration to Varying Input Parameters**

param <sup>a</sup>	change in		change in		change in	
	percent	param <sup>a</sup>	percent	param <sup>a</sup>	percent	param <sup>a</sup>
2a	-14	2K <sub>sa</sub>	16	2D <sub>air</sub>	-1	
a/2	-7	K <sub>sa</sub> /2	-17	D <sub>air</sub> /2	2	
SSA <sub>initial</sub> = 150	8	2W <sub>g</sub>	9	10v <sub>air</sub>	-32	
SSA <sub>initial</sub> = 90	-13	W <sub>g</sub> /2	-10	v <sub>air</sub> /10	40	
2K <sub>ia</sub>	26	2H <sub>a</sub>	72	10v <sub>snow</sub>	-3	
K <sub>ia</sub> /2	-27	H <sub>a</sub> /2	-42	v <sub>snow</sub> /10	13	

<sup>a</sup> a = settling rate, SSA<sub>initial</sub> = specific snow surface area at the start of the model run, K<sub>ia</sub> = snow interface–air partition coefficient, K<sub>sa</sub> = snow air partition coefficient, W<sub>g</sub> = gas-phase scavenging coefficient, H<sub>a</sub> = height of the air compartment, D<sub>air</sub> = air diffusion coefficient, v<sub>air</sub> = air side gas exchange velocity, and v<sub>snow</sub> = snow side gas exchange velocity.

**TABLE 4. WPE on Snow Concentrations (pg L<sup>-1</sup>)**

	av concn, no WPE	av concn, WPE	decrease in seasonal av snow concn (%)	max difference through season, (no WPE)/(WPE) × 100 (%)
$\alpha$ -HCH	5372	5346	-0.5	131
$\gamma$ -HCH	5315	5288	-0.5	131
PCB-28	5.3	4.7	-11	185
PCB-52	29.3	28.2	-4	158
FLU	28.2	23.4	-17	341
PHEN	245.7	219.3	-11	192

pending on the wind speed. The description is based on measurements from central Greenland where SF<sub>6</sub> diffusion in snow was examined at different wind speeds (20). The diffusion coefficient was measured for calm (3 m s<sup>-1</sup>) and windy (9 m s<sup>-1</sup>) conditions, with an observed increase of the SF<sub>6</sub> diffusion coefficient of about a factor of 6 for the higher wind speed (20). Therefore, for wind speeds at or below 3 m s<sup>-1</sup> the diffusion coefficients for the SVOCs were assumed to be constant, with a linear increase between 3 and 9 m s<sup>-1</sup>, with D<sub>snow</sub> derived according to eq 10. The wind pumping effect (WPE) on snow concentrations is given in Table 4. For FLU, the snowpack concentration was up to 341% lower, with a seasonal average of 17% when the wind pumping effect was included (see Figure S4 of the Supporting Information), with PCB-28 and PHEN displaying similar results. The snow concentration of the HCHs however decreased by <1%, and the concentration did not differ by more than a factor of 1.3 during the season. Therefore, wind ventilation did not appear to have a large influence on the average snow concentrations, particularly for those compounds with higher K<sub>ia</sub> values (hence higher sorptive capacity of snow) although the effect of wind on reducing (or radically altering) SSA and hence TSA was not investigated.

### Acknowledgments

K.M.H. was partly funded by the Danish Research Training Council through the Copenhagen Global Change Initiative (COGCI). This work was also supported by UK NERC Grant GR3/12930.

### Supporting Information Available

Figures of the net  $\gamma$ -HCH flux, wet deposition and dry gas exchange fluxes for PHEN, PCB-28, and  $\alpha$ -HCH, K<sub>ia</sub> and K<sub>sa</sub> for PHEN, and FLU snowpack concentrations for simulations with and without the wind pumping effect. This material is available free of charge via the Internet at <http://pubs.acs.org>.

### Literature Cited

- Blais, J. M.; Schindler, D. W.; Muir, D. C. G.; Kimpe, L. E.; Donald, D. B.; Rosenberg, B. Accumulation of persistent organochlorine compounds in mountains of western Canada. *Nature* **1998**, *395*, 585–588.
- Halsall, C. J. Investigating the occurrence of persistent organic pollutants (POPs) in the Arctic: Their atmospheric behaviour and interaction with the seasonal snowpack. *Environ. Pollut.* **2004**, *128*, 163–175.
- Daly, G. L.; Wania, F. Organic contaminants in mountains. *Environ. Sci. Technol.* **2005**, *39*, 385–398.
- Herbert, B. M. J.; Halsall, C. J.; Villa, S.; Jones, K. C.; Kallenborn, R. Rapid changes in PCB and OC pesticide concentrations in Arctic snow. *Environ. Sci. Technol.* **2005**, *39*, 2998–3005.
- Lei, Y. D.; Wania, F. Is rain or snow a more efficient scavenger of organic chemicals? *Atmos. Environ.* **2004**, *38*, 3557–3571.
- Domine, F.; Shepson, P. B. Air–snow interactions and atmospheric chemistry. *Science* **2002**, *297*, 1506–1510.
- Cabanes, A.; Legagneux, L.; Dominé, F. Rate of evolution of the specific surface area of surface snow layers. *Environ. Sci. Technol.* **2003**, *37*, 661–666.
- Daly, G. L.; Wania, F. Simulating the influence of snow on the fate of organic compounds. *Environ. Sci. Technol.* **2004**, *38*, 4176–4186.
- Carlson, D. L.; Hites, R. A. Comment on “Simulating the influence of snow on the fate of organic compounds”. *Environ. Sci. Technol.* **2004**, *38*, 6904–6904.
- Daly, G. L.; Wania, F. Response to comment on “Simulating the influence of snow on the fate of organic compounds”. *Environ. Sci. Technol.* **2004**, *38*, 6905–6906.
- Hung, H.; Halsall, C. J.; Blanchard, P.; Li, H. H.; Fellin, P.; Stern, G. A.; Rosenberg, B. Temporal trends of organochlorine pesticides in the Canadian Arctic atmosphere. *Environ. Sci. Technol.* **2002**, *36*, 862–868.
- Hung, H.; Blanchard, P.; Halsall, C. J.; Bidleman, T. F.; Stern, G. A.; Fellin, P.; Muir, D. C. G.; Barrie, L. A.; Jantunen, L. M.; Helm, P. A.; Ma, J.; Konoplev, A. Temporal and spatial variabilities of atmospheric polychlorinated biphenyls (PCBs), organochlorine (OC) pesticides and polycyclic aromatic hydrocarbons (PAHs) in the Canadian Arctic: Results from a decade of monitoring. *Sci. Total Environ.* **2005**, *342*, 119–144.
- Hansen, K. M.; Christensen, J. H.; Brandt, J.; Frohn, L. M.; Geels, C. Modelling atmospheric transport of  $\alpha$ -hexachlorocyclohexane in the Northern Hemisphere with a 3-D dynamical model: DEHM-POP. *Atmos. Chem. Phys.* **2004**, *4*, 1125–1137.
- Legagneux, L.; Cabanes, A.; Dominé, F. Measurement of the specific surface area of 176 snow samples using methane adsorption at 77 K. *J. Geophys. Res.* **2002**, *107*, No. 4335.
- Paterson, W. S. B. *The Physics of Glaciers*, 3rd ed.; Pergamon: New York, 1994.
- Roth, C. M.; Goss, K. U.; Schwarzenbach, R. P. Sorption of diverse organic vapors to snow. *Environ. Sci. Technol.* **2004**, *38*, 4078–4084.
- Hung, H.; Halsall, C. J.; Blanchard, P.; Li, H. H.; Fellin, P.; Stern, G. A.; Rosenberg, B. Are PCBs in the Canadian Arctic atmosphere declining? Evidence from 5 years of monitoring. *Environ. Sci. Technol.* **2001**, *35*, 1303–1311.
- Wania, F.; Axelman, J.; Broman, D. A review of processes involved in the exchange of persistent organic pollutants across the air–sea interface. *Environ. Pollut.* **1998**, *102*, 3–23.
- Seinfeld, J. H.; Pandis, S. N. *Atmospheric chemistry and physics: From air pollution to climate change*; John Wiley & Sons: New York, 1998.
- Albert, M. R.; Shultz, E. F. Snow and firn properties and air–snow transport processes at Summit, Greenland. *Atmos. Environ.* **2002**, *36*, 2789–2797.
- Schwarzenbach, R. P.; Gschwend, P. M.; Imboden, D. M. *Environmental Organic Chemistry*; John Wiley & Sons: New York, 1993.
- Grell, G. A.; Dudhia, J.; Stauffer, D. R. *A description of the fifth-generation Penn State NCAR Mesoscale Model (MM5)*; NCAR/TN-398+STR, NCAR Technical Note; Mesoscale and Microscale Meteorology Division, National Center for Atmospheric Research: Boulder, CO, 1995; 122 pp.
- Dominé, F.; Cabanes, A.; Legagneux, L. Structure, microphysics, and surface area of the Arctic snowpack near Alert during the ALERT 2000 campaign. *Atmos. Environ.* **2002**, *36*, 2753–2765.
- Frohn, L. M.; Christensen, J. H.; Brandt, J. Development of a high-resolution nested air pollution model. The numerical approach. *J. Comput. Phys.* **2002**, *179*, 68–94.
- Geels, C.; Doney, S. C.; Dargaville, R.; Brandt, J.; Christensen, J. H. Investigating the sources of synoptic variability in

- atmospheric CO<sub>2</sub> measurements over the Northern Hemisphere continents: a regional model study. *Tellus* **2004**, *56B*, 35–50.
- (26) Skov, H.; Christensen, J. H.; Goodsite, M. E.; Heidam, N. Z.; Jensen B.; Wählín, P.; Geernaert, G. Fate of elemental mercury in the Arctic during atmospheric mercury depletion episodes and the load of atmospheric mercury to the Arctic. *Environ. Sci. Technol.* **2004**, *38*, 2373–2382.
- (27) Patton, G. W.; Walla, M. D.; Bidleman, T. F.; Barrie, L. A. *J. Geophys. Res., [Atmos.]* **1991**, *96* (D6), 10867–10877.
- (28) Stern, G. A.; Halsall, C. J.; Barrie, L. A.; Muir, D. C. G.; Fellin, P.; Rosenberg, B.; Rovinsky, F. Ya.; Kononov, E. Ya.; Pastukhov, P. *Environ. Sci. Technol.* **1997**, *31*, 3619–3628.
- (29) Halsall, C. J.; Bailey, R.; Stern, G. A.; Barrie, L. A.; Fellin, P.; Muir, D. C. G.; Rosenberg, B.; Rovinsky, F. Y.; Kononov, E. Y.; Pastuhov, B. Multi-year observations of organohalogen pesticides in the Arctic atmosphere. *Environ. Pollut.* **1998**, *102*, 51–62.
- (30) Halsall, C. J.; Barrie, L. A.; Fellin, P.; Muir, D. C. G.; Billeck, B. N.; Lockhart, L.; Rovinsky, F. Y.; Kononov, E. Y.; Pastuhov, B. Spatial and temporal variation of polycyclic aromatic hydrocarbons in the Arctic atmosphere. *Environ. Sci. Technol.* **1997**, *31*, 3593–3599.
- (31) Waddington, E. D.; Cunningham, J.; Harder, S. L. The effects of snow ventilation on chemical concentrations. In *Chemical Exchange Between the Atmosphere and Polar Snow*; Wolff, E. W., Bales, R. C., Eds.; Springer-Verlag: Berlin, 1996; pp 403–452.
- (32) Herbert, B. M. J.; Halsall, C. J.; Domine, F.; Legagneux, L.; Fitzpatrick, L.; Jones, K. C.; Thomas, G. O.; Kallenborn, R. The use of specific surface area and Henry's Law constants to predict PCB and OC pesticide concentrations in surface snow. *Environ. Sci. Technol.*, in preparation.
- (33) Gregor, D. J.; Gummer, W. D. Evidence of atmospheric transport and deposition of organochlorine pesticides and polychlorinated biphenyls in Canadian Arctic snow. *Environ. Sci. Technol.* **1989**, *23*, 561–565.
- (34) Semkin, R. Processes and fluxes of contaminants in aquatic systems—1994/95. In *Synopsis of research conducted under the 1994/95 Northern Contaminants Program*; Environmental Studies Report No. 73; Murray, J. L., Shearer, R. G., Han, Indian, S. L., Eds.; Northern Affairs Canada: Ottawa, Ontario, Canada, 1996; pp 105–118.

*Received for review August 25, 2005. Revised manuscript received January 17, 2006. Accepted January 20, 2006.*

ES051685B

*[Blank page]*

# A dynamic model to study the exchange of gas-phase POPs between air and a seasonal snowpack

*Kaj M. Hansen,<sup>1,\*</sup> Crispin J. Halsall,<sup>2</sup> and Jesper H. Christensen<sup>1</sup>*

**Department of Atmospheric Environment, National Environmental Research Institute,  
P.O. box 358, Frederiksborgvej 399, 4000 Roskilde, Denmark, and Environmental  
Science Department, Lancaster University, Lancaster, LA1 4YQ, UK.**

\*CORRESPONDING AUTHOR phone: +45 46 30 18 72; fax: +45 46 30 12 14; e-mail: [kmh@dmu.dk](mailto:kmh@dmu.dk). <sup>1</sup> National Environmental Research Institute. <sup>2</sup> Lancaster University.

FIGURE S1

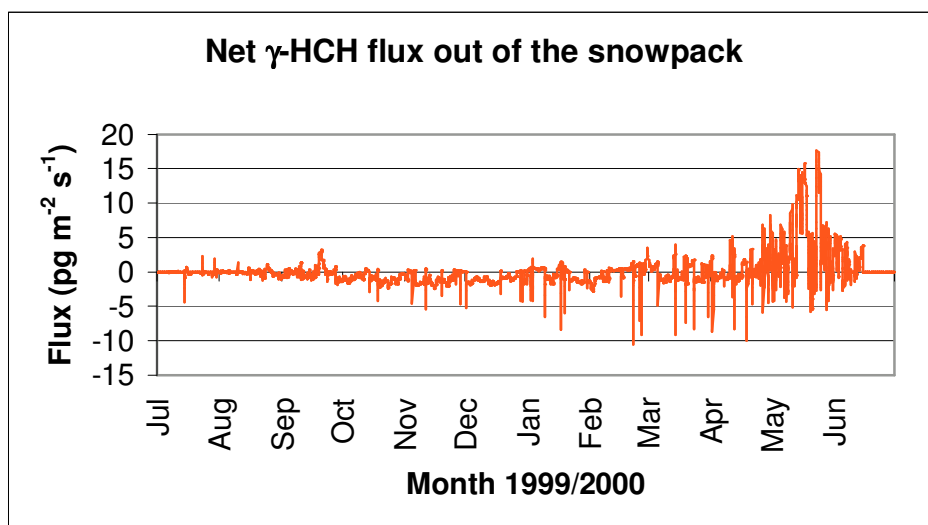


FIGURE S1. Net  $\gamma$ -HCH fluxes out of the snowpack.

FIGURE S2

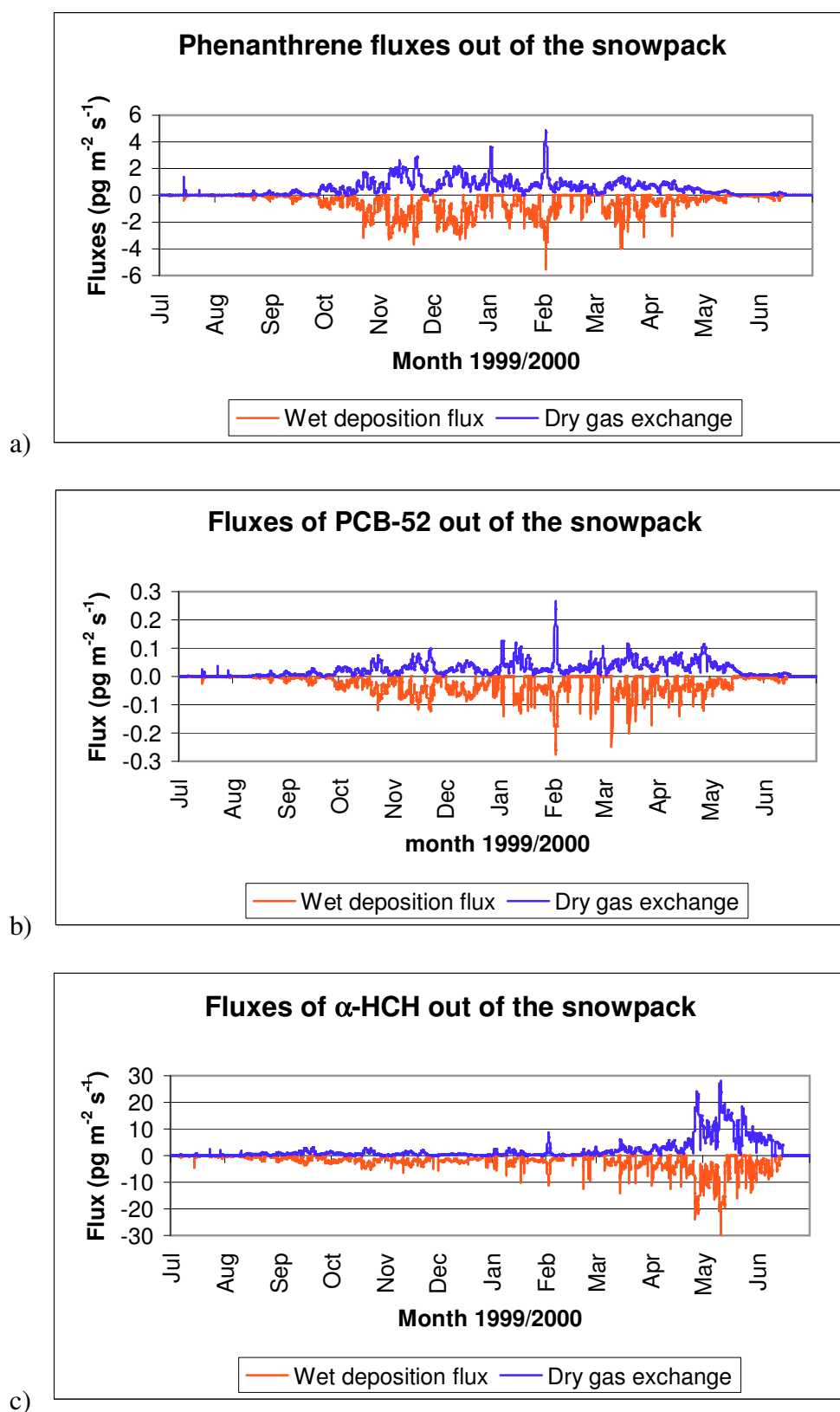
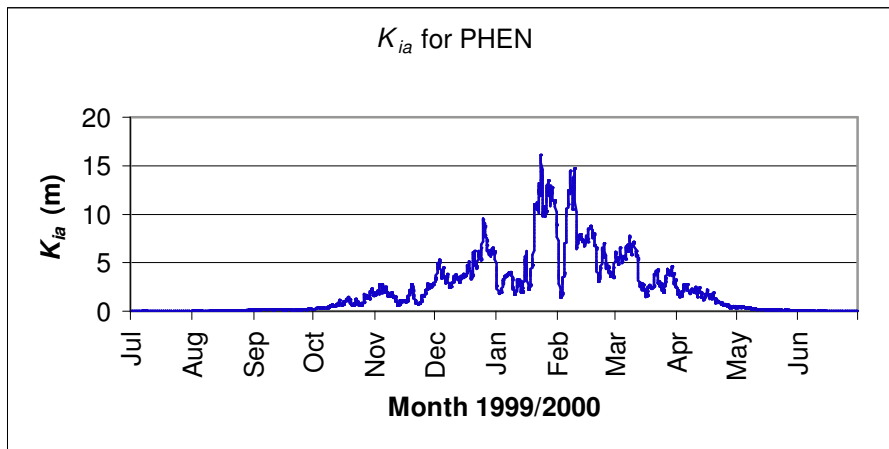


FIGURE S2. Wet deposition (red) and gas exchange (blue) fluxes out of the snowpack for phenanthrene (a), PCB-52 (b), and  $\alpha$ -HCH (c).

FIGURE S3

a)



b)

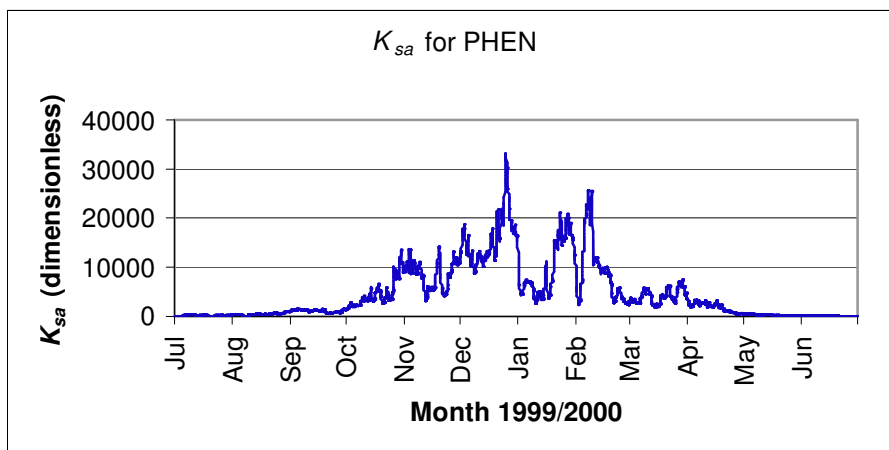


FIGURE S3.  $K_{ia}$  and  $K_{sa}$  values for phenanthrene.

FIGURE S4

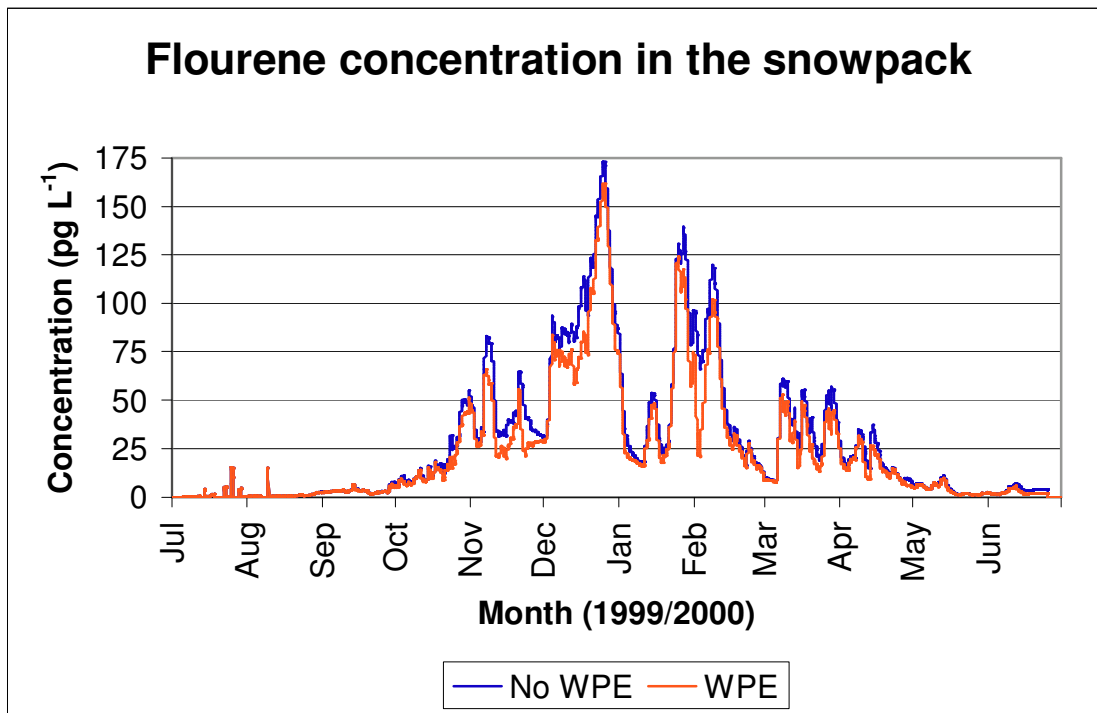


FIGURE S4. Predicted flourene concentration in the snowpack when including the wind pumping effect (WPE) and without (No WPE).

*[Blank page]*

## Appendix C

### Paper III

Hansen, K. M., J. H. Christensen, J. Brandt, L. M. Frohn, and C. Geels, 2006, *Modelling the atmospheric transport and environmental fate of persistent organic pollutants in the Northern Hemisphere using a 3-d dynamical model*, In: Air Pollution Modelling and Its Application XXVII, Kluwer Academic/Plenum Publishers, New York, Borrego and Norman (eds.), in press.



# **MODELLING THE ATMOSPHERIC TRANSPORT AND ENVIRONMENTAL FATE OF PERSISTENT ORGANIC POLLUTANTS IN THE NORTHERN HEMISPHERE USING A 3-D DYNAMICAL MODEL**

Kaj M. Hansen, Jesper H. Christensen, Jørgen Brandt, Lise M. Frohn and Camilla Geels \*

## **1. INTRODUCTION**

Persistent organic pollutants (POPs) are a group of chemical compounds with mainly anthropogenic origin; they are semi-volatile, hydrophobic, they bioaccumulate, they have toxic effects on human and wildlife and they display low degradation rates in the environment (Jones and de Voogt, 1999). POPs are emitted to the atmosphere either from industrial production, as by-products from combustion, or intentionally as pesticides used on crops or for insect control. A number of POPs are banned or subject to regulation, e.g. under the UNEP Stockholm convention for POPs and emissions of them have decreased during the last decades (Jones and de Voogt, 1999). However, due to the great persistence large amounts are still cycling in the environment. The volatility of POPs is temperature dependent, which can lead to several consecutive deposition and re-emission events named multi-hop or grasshopper transport (Wania and Mackay, 1996). To contribute to the understanding of these processes several models are developed. Environmental fate of POPs is traditionally studied with box models (e.g. Wania et al., 1999). Recently, atmospheric transport models with high spatiotemporal resolution are also developed to address these issues (e.g. Koziol and Pudykiewicz, 2001; Hansen et al., 2004).

The latest development of the Danish Eulerian Hemispheric Model (DEHM) at the National Environmental Research Institute now includes a description of the air-surface gas-exchange processes of soil, water and snow to study the environmental fate of POPs. The original version of the DEHM model was developed for studying the long-range transport of SO<sub>2</sub> and SO<sub>4</sub> to the Arctic (Christensen, 1997). It has been further developed to study transport, transformation and deposition of reactive and elemental mercury (Christensen et al., 2002), concentrations and depositions of various pollutants (Frohn et al., 2002a,b) through the inclusion of an extensive chemistry scheme, and transport and exchange of atmospheric CO<sub>2</sub> (Geels et al., 2001, 2002).

---

\* National Environmental Research Institute, Department of Atmospheric Environment, Frederiksborgvej 399, P. O. Box 358, DK-4000, Roskilde, Denmark.

This paper describes the POP version: DEHM-POP with the focus on the air-surface gas-exchange processes that are special for this model version. A general description of the DEHM-POP model system and the included air-surface exchange processes is given in the following. Thereafter a few examples from the simulations and model evaluation are discussed.

## 2. THE MODEL SYSTEM

The DEHM-POP model domain is centred at the North Pole and covers the majority of the Northern Hemisphere with a horizontal resolution of  $150 \text{ km} \times 150 \text{ km}$  at  $60^\circ\text{N}$ . The horizontal model grid extends into the Southern Hemisphere, an expansion of the grid to  $135 \times 135$  cells compared to the  $96 \times 96$  grid cells in previous DEHM model versions (Figure 1). The model is divided into 20 unevenly distributed vertical layers defined on terrain following  $\sigma$ -levels. The finest resolution is within the lowest few kilometres and the uppermost level is at a height of approximately 15 km. The applied numerical schemes have all been carefully tested for the previous versions of the model (Christensen, 1997; Frohn et al., 2002a). In order to obtain the required high-resolution meteorological data field the MM5 modelling subsystem (Grell et al., 1995), has been implemented as a meteorological driver between the data from ECMWF ( $2.5^\circ \times 2.5^\circ$  spatial and 12 h temporal resolution) and the DEHM model. In this study the domains and resolutions are the same in MM5 and DEHM and the meteorological data are archived at a 3 h interval.

The model is developed using  $\alpha$ -hexachlorocyclohexane ( $\alpha$ -HCH), the major component of the historically most used insecticide, as a tracer. This is one of the most abundant POPs in air, water and snow. Extensive monitoring data as well as reliable emission estimates exist for this compound. Being one of the most volatile POPs  $\alpha$ -HCH is found almost exclusively in the gas-phase, so the particle bound fraction is omitted in this study. Emission input used in this study is adapted from Li et al. (2000). A large amount of  $\alpha$ -HCH is found in the world oceans deposited through the historical emissions. This is taken into account by introducing an initial ocean concentration estimated from measurements.

### 2.1. Parameterisations of air-surface gas-exchange fluxes

The special characteristics of POPs necessitate a description of air-surface exchange processes, since the compounds not only are deposited to the surface but also can be re-emitted to the air. Therefore the model is expanded with surface compartments representing soil, ocean water, sea ice and snow. The air-soil and air-water exchange processes are adapted from a zonally averaged global multimedia box model (Strand and Hov, 1996). Details of this implementation can be found in Hansen et al. (2004) together with an evaluation of the model including these two surface compartments only. The sea ice is considered to be a passive media without accumulation of contaminants. It acts as a lid on oceans preventing the air-ocean gas exchange. Data on sea-ice extension within the model domain is obtained from the MM5 model together with the meteorological data. The snow module is adapted from a newly developed dynamical model describing the exchange between air and a homogeneous snow pack (Hansen et al., in prep.).

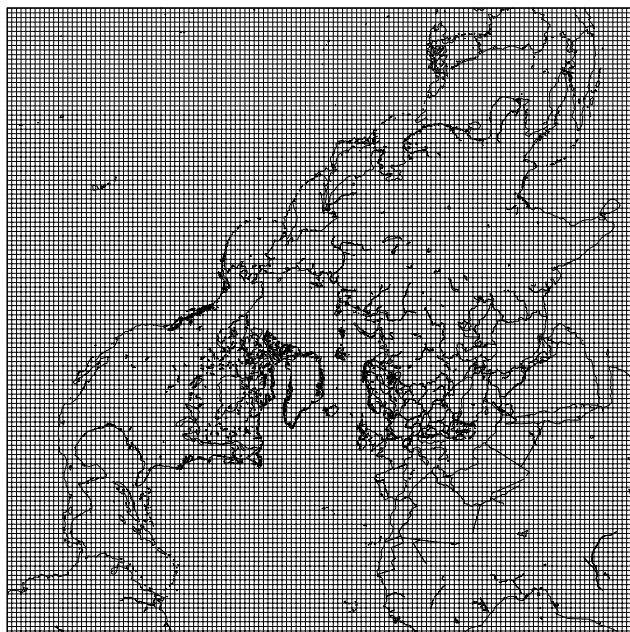


**Figure 1.** The model domain and horizontal grid.

### 3. MODEL EVALUATION

The model was run for the period 1991 – 1998. High  $\alpha$ -HCH concentrations are found in air over source areas such as India, Southeast Asia, and Mexico, but contaminated air is also found over regions without primary emissions such as the Atlantic and Pacific Oceans, and the Arctic, indicating long-range transport (Figure 2). Observations from several monitoring sites are available for model evaluation. Data used in this paper are from: Dunai Island in northern Russia, Spitzbergen at Svalbard, Alert and Tagish in Northern and Western Canada, respectively, Stórhöfði in Iceland, Pallas in northern Finland, Lista at the Southern tip of Norway and Rörvik and Aspveten in Sweden (Berg et al., 2001; Aas et al., 2003). The time span and the temporal resolution of the measurements are variable at the sites. As the air concentrations are very low, samples are often integrated over a long time period. The deployment time of the samplers vary from between 1 and 14 days with a frequency of between 1 sample per week to 1 per month. The monitoring stations have been operated between 1 and 8 years within the simulated period. Daily averaged air concentrations from the lowermost atmospheric layer are extracted from the model at each of the monitoring sites. These data are averaged over the deployment time of the individual measurements to enable a direct comparison between measurements and model results.

Annual averages of measured and modelled air concentrations are compared for each of the stations (Figure 3). Air concentrations during the simulated period are generally declining within the model domain reflecting the reduced emissions during the period. Averaged modelled air concentrations are generally within a factor 2 of the averaged

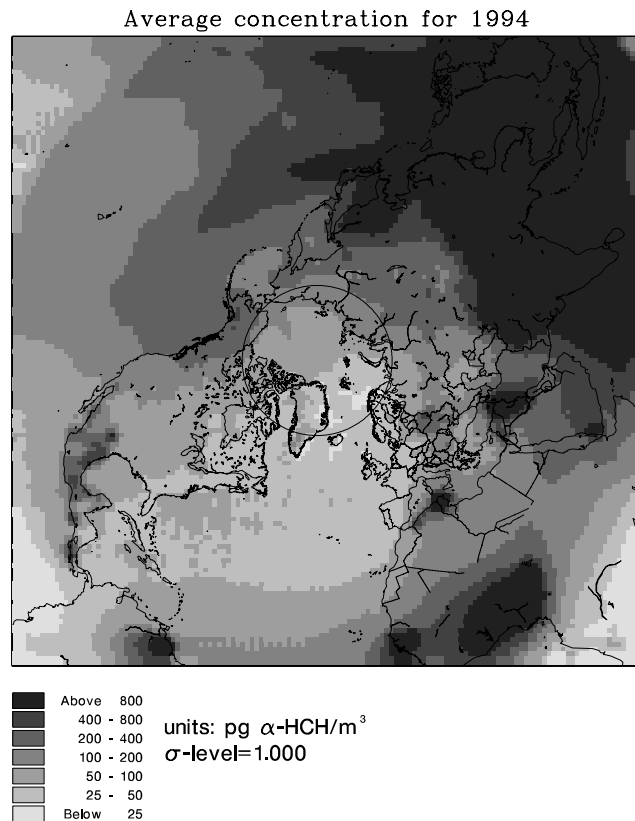


**Figure 2.** Annual average  $\alpha$ -HCH concentrations in the lowermost atmospheric model layer for 1994.

measured concentrations. Exceptions are at Lista and Aspvreten where the modelled concentrations are up to a factor 2.5 and 3 lower than measured, respectively, and at Tagish and Dunai Island where the modelled concentrations are up to a factor 6 and 4 higher than measured, respectively (not shown). It is interesting to note that the predicted annual averaged air concentrations at Lista, Rörvik, and Aspvreten, which in the model are separated by only a few grid cells, are very close, whereas the measured concentrations are up to a factor 3 higher at Aspvreten and Lista than at Rörvik (Figure 3). This indicates that local surface exchange processes not described in the model, e.g. between vegetation and air have a great influence on the observed values.

#### 4. EVALUATION AGAINST INDIVIDUAL MEASUREMENTS

To evaluate the short-term average prediction capacity of the model measured  $\alpha$ -HCH concentrations are plotted against model calculations in scatter plots. Four examples of the comparison between model results and observations are given in Figure 4. Various statistical parameters are given below the scatter plots. These include the number of data samples, (N), mean values, standard deviation, correlation coefficients

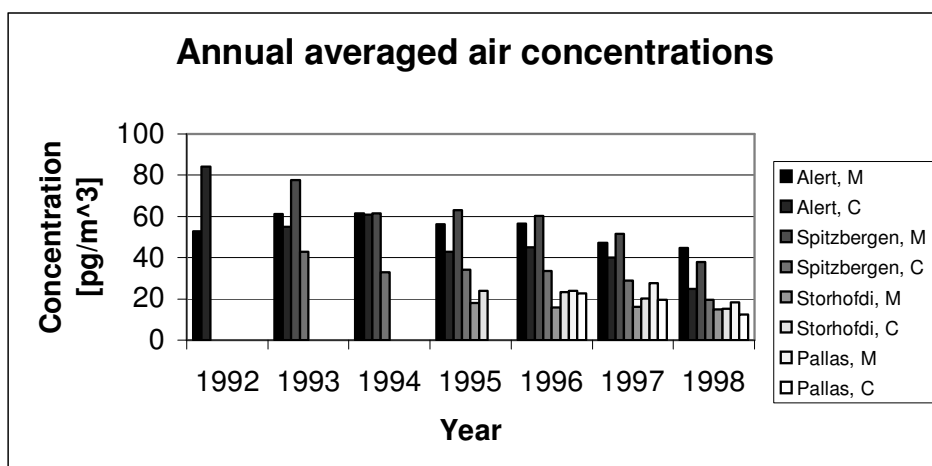
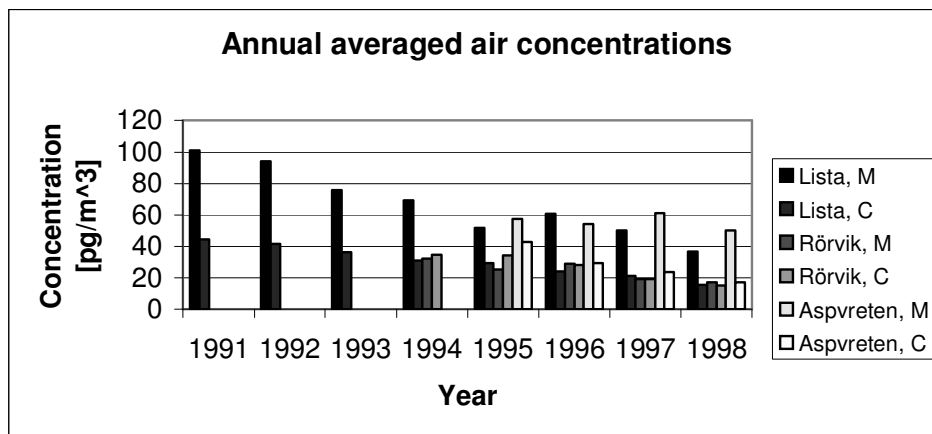
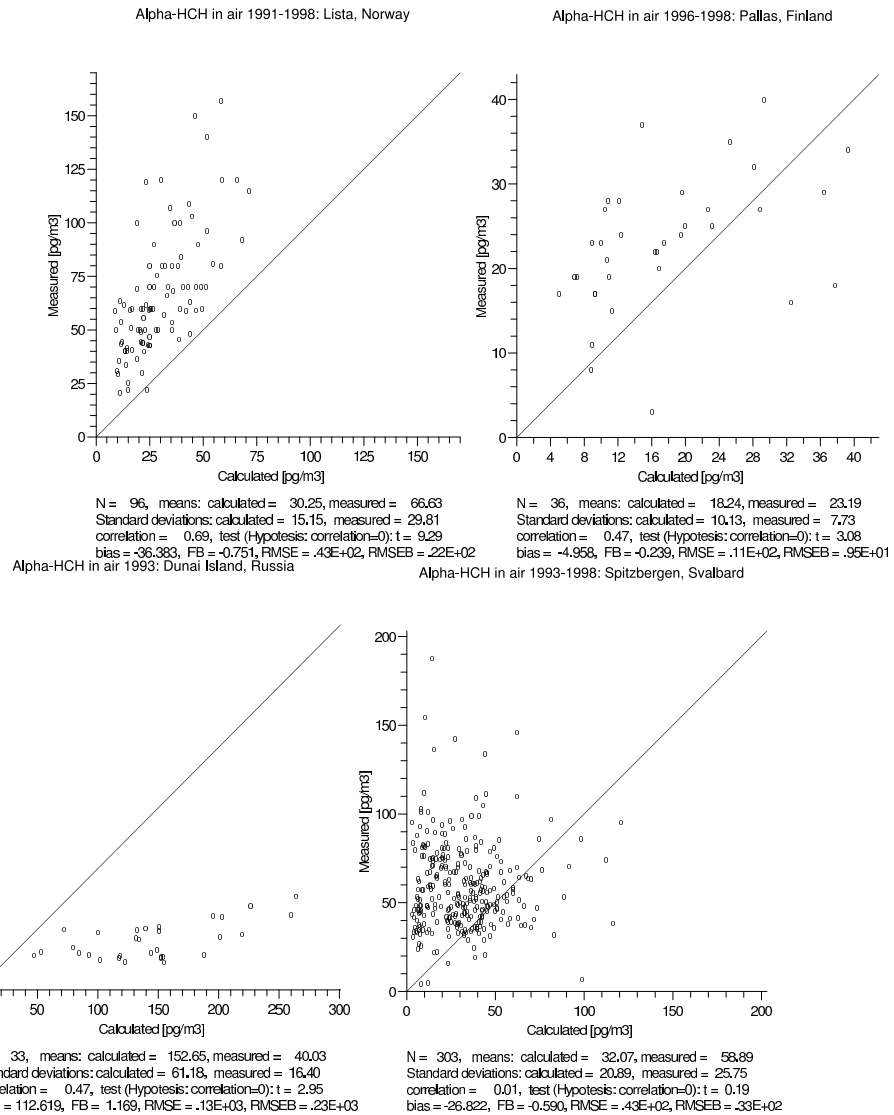


Figure 3. Annual averaged measured (M) and calculated (C) air concentrations in  $\text{pg/m}^3$  for Lista, Rörvik and Aspvreten (upper figure) and Alert, Spitzbergen, Storhofdi, and Pallas (lower figure).

with test for significance, bias, fractional bias (FB), root mean square error (RMSE) and RMSE based on values where the bias has been subtracted (RMSEB). The latter parameters are mostly helpful for comparing results from different model simulations. The correlation found at Lista, Pallas and Dunai Island is significant within a 0.1%, 1% and 1% significance level, respectively (Figure 4). A low correlation (0.24) significant within a 10% significance level is also found for Rörvik (not shown). No correlation is found at the other stations as illustrated by the example from Spitzbergen (Figure 4). The lack of correlation between measured and calculated air concentrations at some stations but not at others and the variation in bias from strong negative to strong positive is a further indication that the surface exchange is not well enough parameterised, i.e. there are surface characteristics not described in the model, which possibly influence observed values.



**Figure 4.** Four examples of the measured  $\alpha$ -HCH concentrations plotted against calculated concentrations in the lowermost atmospheric model layer: Lista (upper left), Pallas (upper right), Dunai Island (lower left), and Spitzbergen (lower right). The results from the other stations except Rörvik are similar to Spitzbergen.

A time series of the measured and calculated concentrations at Pallas, Finland is shown in Figure 5. It is seen that the model at this site captures a large part of the variability in measurements; an apparent annual variation with higher values during summer than during winter is found in both measurements and model results. The variability is not equally well described at all station, as also indicated in Figure 4.

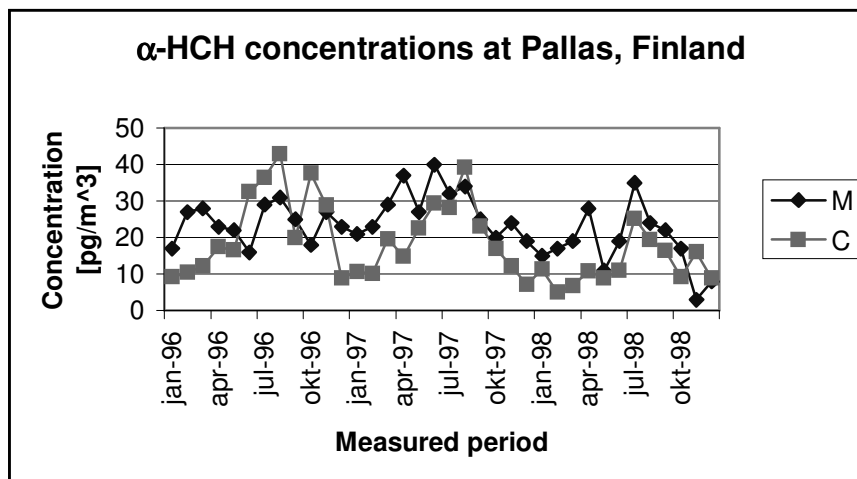


**Figure 5.** Measured (M) and calculated (C) air concentrations in  $\text{pg/m}^3$  for Pallas, Finland from 1996 – 1998. The measurements are one-week integrated samples taken once a month.

## 5. CONCLUSIONS AND FUTURE WORK

A hemispheric model for simulations of atmospheric transport and environmental fate of persistent organic pollutants (POPs) has been developed with  $\alpha$ -HCH as a model tracer. This model includes modules representing the surface compartments: soil, water, sea ice and snow pack, and the air-surface exchange processes characteristic for POPs are thereby included in the model. Here the model simulations of atmospheric transport of  $\alpha$ -HCH for the period 1991 – 1998 have been described and validated against observations. By comparing the annual averaged model results and measurements it has been shown that the model captures the long-term atmospheric concentrations. However shorter-term averaged concentrations are not well resolved by the model in the whole model domain. This indicates that the air-surface exchange is not well enough characterised by the present surface compartments, where e.g. exchange of air with vegetation and fresh water is not accounted for. A further expansion of the surface compartments is therefore needed. Furthermore, the inclusion of a description of the partitioning between gas-phase and particle-phase compounds is necessary to study POPs in general. These issues are part of the ongoing model development.

## 6. ACKNOWLEDGMENTS

This study is partly funded by the Danish Research Training Council through the Copenhagen Global Change Initiative.

## 7. REFERENCES

- Aas, W., Solberg, S., Berg, T., Manø, S., and Yttri, K. E., 2003, Monitoring of long rang transported air pollutants, Annual report for 2002. Kjeller, Norwegian Institute for Air Research, SFT Report 877/2003 NILU OR 23/2003.
- Berg, T., Hjellbrekke, A. G., and Larsen R., 2001, Heavy metals and POPs within the EMEP region 1999, EMEP/CCC 9/2001.
- Christensen, J. H., 1997, The Danish Eulerian Hemispheric Model - a three-dimensional air pollution model used for the Arctic, *Atmos. Environ.*, **31** (24), pp. 4169-4191.
- Christensen, J. H., Brandt, J., Frohn, L. M., and Skov, H., Modelling of mercury with the Danish Eulerian Hemispheric Model. *Atmos. Chem. Phys.* Submitted December 19, 2002.
- Frohn, L. M., Christensen, J. H., and Brandt, J., 2002a, Development of a high resolution nested air pollution model – the numerical approach, *J. Comp. Phys.*, **179** (1), pp. 68-94.
- Frohn, L. M., Christensen, J. H., and Brandt, J., 2002b, Development and testing of numerical methods for two-way nested air pollution modelling, *Phys. Chem. Earth*, **27** (35), pp. 1487-1494.
- Geels, C., Christensen, J. H., Hansen, A. W., Kiilsholm, S., Larsen, N. W., Larsen, S. E., Pedersen, T., and Sørensen, L. L., 2001, Modelling concentrations and fluxes of atmospheric CO<sub>2</sub> in the North East Atlantic region, *Phys. Chem. Earth*, **106** (10), pp. 763-768.
- Geels, C., Christensen, J. H., Frohn, L. M., and Brandt, J., 2002, Simulating spatiotemporal variations of atmospheric CO<sub>2</sub> using a nested hemispheric model, *Phys. Chem. Earth*, **27** (35), pp. 1495-1505.
- Grell, G. A., Dudhia, J., and Stauffer, D. R., 1995, A description of the Fifth-Generation Penn State/NCAR Mesoscale Model (MM5), NCAR/TN-398+STR, NCAR Technical Note, June 1995, p. 122, Mesoscale and Microscale Meteorology Division, National Center for Atmospheric Research, Boulder, Colorado.
- Hansen, K. M., Christense, J. H., Brandt, J., Frohn, L. M., and Geels, C., 2004, Modelling atmospheric transport of  $\alpha$ -hexachlorocyclohexane in the Northern Hemisphere with a 3-D dynamical model: DEHM-POP, *Atmos. Chem. Phys.*, **4**, pp. 1125-1137.
- Hansen, K. M., Halsall, C. J., and Christensen, J. H., in prep., A dynamic model to study the exchange of gas-phase POPs between air and a seasonal snow pack, in prep. for *Environ. Sci. Technol.*
- Jones, K. C. and de Voogt, P. 1999, Persistent organic pollutants (POPs): State of the science, *Environ. Pollut.*, **100**, pp. 209–221.
- Koziol, A. S. and Pudykiewicz, J. A., 2001, Global-scale environmental transport of persistent organic pollutants, *Chemosphere*, **45**, pp. 1181–1200.
- Li, Y.-F., Scholtz, M. T., and van Heyst, B. J., 2000, Global gridded emission inventories of  $\alpha$ -hexachlorocyclohexane, *J. Geophys. Res.*, **102**, D5, pp. 6621–6632.
- Strand, A. and Hov, Ø., 1996, A model strategy for the simulation of chlorinated hydrocarbon distributions in the global environment, *Water Air Soil Poll.*, **86**, pp. 283–316.
- Wania, F. and Mackay, D., 1996, Tracking the distribution of persistent organic pollutants, *Environ. Sci. Technol.*, **30**, 9, pp. 390A–396A.
- Wania, F., Mackay, D., Li, Y.-F., Bidleman, T. F., and Strand, A., 1999, Global chemical fate of  $\alpha$ -hexachlorocyclohexane. I. Evaluation of a global distribution model. *Environ. Toxicol. Chem.*, **18**, 7, pp 1390–1399.

## Appendix D

### Paper IV

Hansen, K. M., K. Prevedouros, A. J. Sweetman, K. C. Jones, and J. H. Christensen, 2006, A process-oriented inter-comparison of a box model and an atmospheric chemistry transport model: insights into model structure using  $\alpha$ -HCH as the modelled substance, *Atmos. Environ.*, 40(12), 2089-2104.

*[Blank page]*

# A process-oriented inter-comparison of a box model and an atmospheric chemistry transport model: Insights into model structure using $\alpha$ -HCH as the modelled substance

Kaj M. Hansen<sup>a,\*</sup>, Konstantinos Prevedouros<sup>b,1</sup>, Andrew J. Sweetman<sup>b</sup>,  
Kevin C. Jones<sup>b</sup>, Jesper H. Christensen<sup>a</sup>

<sup>a</sup>*Department of Atmospheric Environment, National Environmental Research Institute, P.O. box 358, Frederiksborgvej 399, DK-4000 Roskilde, Denmark*

<sup>b</sup>*Environmental Science Department, Institute of Environmental and Natural Sciences, Lancaster University, Lancaster, LA1 4YQ, UK*

Received 20 June 2005; received in revised form 5 November 2005; accepted 14 November 2005

## Abstract

Two models that use different approaches to model the environmental distribution and fate of persistent organic pollutants (POPs) and feature different approaches to the description of environmental processes are compared. The European Variant Berkeley–Trent model (EVn-BETR) is a fugacity based box model using long-term averaged environmental input to drive inter-compartmental and inter-regional exchange processes. The POP version of the Danish Eulerian Hemispheric Model (DEHM-POP) is a 3-D atmospheric chemistry transport model using dynamic meteorological input to drive atmospheric transport and deposition to the surface. It is expanded with surface modules to describe the post-depositional re-emission processes of POPs. Seasonally averaged air, soil and water  $\alpha$ -hexachlorocyclohexane ( $\alpha$ -HCH) concentrations and distribution patterns within the European region are compared for a number of emissions scenarios. There is generally a good agreement between the predicted distribution patterns of the two models. Discrepancies in environmental concentrations are attributed to the difference in efficiency of atmospheric removal processes arising from the differences in model parameterisation.

© 2005 Elsevier Ltd. All rights reserved.

*Keywords:* Model inter-comparison; Dynamic models; Fugacity models; Atmospheric chemistry transport models;  $\alpha$ -hexachlorocyclohexane

## 1. Introduction

Mathematical models are increasingly used to simulate the environmental fate of persistent

organic pollutants (POPs) to increase the knowledge of the involved physical processes, particularly in the absence of available monitoring data. Models of varying complexity in the description of the environmental matrices of interest are being developed to investigate the environmental partitioning and chemical exchange between mobile and immobile media. Recently there has also been a shift of focus from regional to global modelling studies as

\*Corresponding author. Tel.: +45 46 30 18 72;

fax: +45 46 30 12 14.

E-mail address: [kmh@dmu.dk](mailto:kmh@dmu.dk) (K.M. Hansen).

<sup>1</sup>Present address: Department of Applied Environmental Science (ITM), Stockholm University, 10691 Stockholm, Sweden.

POPs disregard political boundaries during their journey from their point of release to repositories or sinks. There have been a number of model approaches that broadly fall into two categories, box and chemistry transport models. An example of the former class is the global distribution model of Wania and Mackay (1995) that divided the world into nine climatic zones, each having six environmental compartments connected by advective and intermedia transport processes. The BETR North America model has followed similar approaches where the regional environment of North America was divided into 24 ecological regions (MacLeod et al., 2001). The CliMoChem model consists of 20–30 two-dimensional latitudinal zones with different annual temperature regimes, vegetation types, compartmental volumes, etc. (Scheringer et al., 2000). A common feature of these models is that the description of fluxes between regions and environmental compartments is based on averaged values of air and water flow and precipitation.

Concurrent to these so-called box models, several high-resolution atmospheric chemistry transport models have also been developed to address similar issues and modelling challenges. These fully dynamic models use dynamic meteorology to drive advective atmospheric transport; they are generally able to predict environmental concentrations with a higher spatial resolution and on shorter time scales, but have the drawback of requiring very high-resolution input on emissions and other environmental parameters. These models have been used to study the environmental fate of POPs in both regional (van Jaarsveld et al., 1997; Ma et al., 2003), hemispheric (Malanichev et al., 2004; Hansen et al., 2004), and global scale studies (Kozioł and Pudykiewicz, 2001; Lammel et al., 2001).

The two types of models should not be seen as competitors but rather as supplementing each other; box models are well suited to study long-term environmental fate on large scales, whereas atmospheric chemistry transport models focus on short-term fluctuations and individual transport episodes (Wania, 1999).

With an increasing number of models using different parameterisation of environmental processes at different resolution, there is a clear need for inter-comparison of model results from different types of models. A number of studies have already been published, for example, using box models to estimate atmospheric long-range transport potential and persistence and to rank different POPs

according to these criteria (Wania and Mackay, 2000; Bennett et al., 2001; Beyer et al., 2001; Wania and Dugani, 2003; Stroebe et al., 2004a). The Cooperative Programme for Monitoring and Evaluation of the Long-Range Transmission of Air Pollutants in Europe (EMEP), in line with the recommendation of the Executive Body for the Convention on Long-Range Transboundary Air Pollution, recently initiated a multimedia model inter-comparison study (Shatalov et al., 2004).

This paper presents the results of an inter-comparison study between a fugacity-based box model (EVn-BETR) and a fully dynamic 3-D atmospheric chemistry transport model (DEHM-POP). The influence of different modelling approaches on the model output is discussed, with respect to the environmental fate of  $\alpha$ -hexachlorocyclohexane ( $\alpha$ -HCH). The two models have been “homogenised” in order to apply similar environmental and chemical input and a series of testing scenarios have been assessed.

## 2. Models and input

### 2.1. EVn-BETR

The European Variant Berkeley–Trent model (EVn-BETR) follows the fugacity approach (Mackay, 2001) and comprises 50 regions, with 4 regions in the periphery to describe the outside Europe world (Fig. 1). Each region represents an area of approximately 500 km  $\times$  500 km ( $5^\circ \times 5^\circ$ ), with the whole model domain covering an area from 38.7°N to 61.1°N latitude and 10.1°W to 39.4°E longitude (Prevedouros et al., 2004b). All landcover and environmental data were projected using a polar stereographic projection. Each region consists of 7 environmental compartments: lower (0–1000 m) and upper air (1000–2000 m), soil, vegetation, ocean water, fresh water and sediment. The model regions are linked in terms of air, fresh/coastal water and water runoff exchange between adjacent segments. For further details of the compartmental construction, the reader is directed to MacLeod et al. (2001) and Woodfine et al. (2001). The model was utilised to quantify the environmental (air and soil) distribution of  $\gamma$ -HCH (lindane) in Europe (Prevedouros et al., 2004b) and has also been applied to polybrominated diphenyl ethers (PBDEs) on the European scale (Prevedouros et al., 2004a).

The atmospheric transport of chemicals within the EVn-BETR model framework is described by

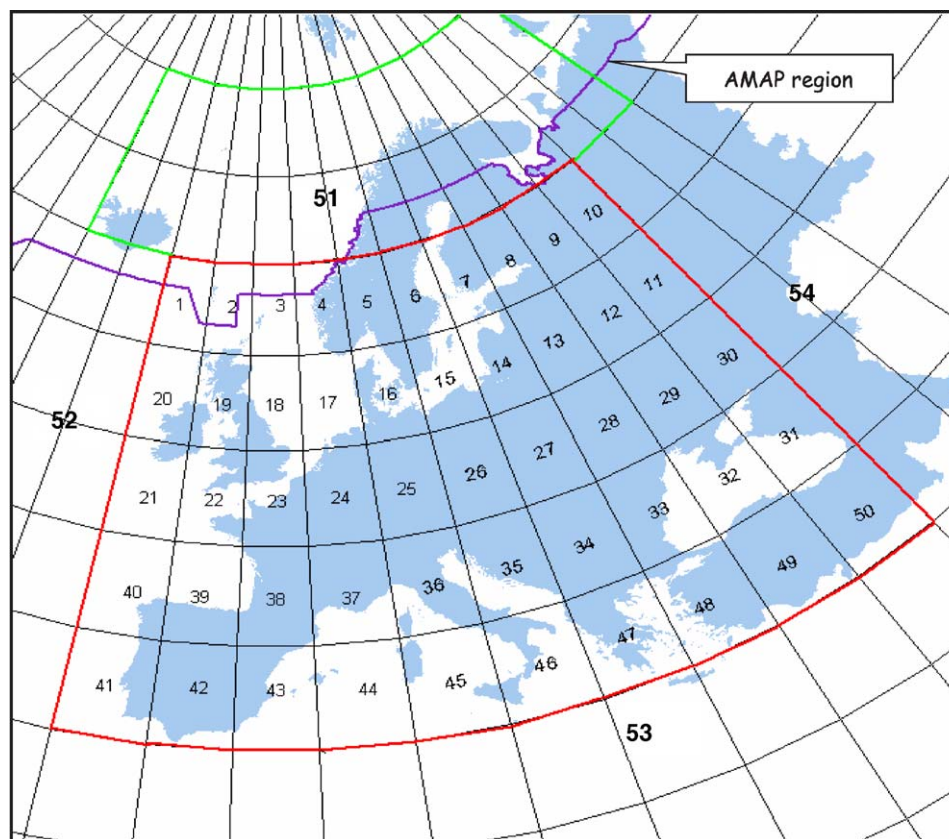


Fig. 1. EVn-BETR model segmentation.

long-term (1997–2001) wind roses for each of the inner 50 model regions. Starting from the centre of each region, one-day forward trajectories were calculated using the British Atmospheric Data Centre ECMWF trajectory service (<http://badc.nerc.ac.uk/data/ecmwf-trj/>), at the two atmospheric heights of 500 and 2000 m above sea level. The endpoints of the trajectories were then computed, producing an average wind rose for all the model segments. Finally, the wind roses were converted into a connectivity flux matrix for each atmospheric height, using a matrix technique described by Woodfine et al. (2001). In a similar way, the water mass balance was compiled; ambient air temperatures and rainfall information were also extracted from long-term environmental datasets (Leemans and Cramer, 1991; Hansen and Poulain, 1996; Vorosmarty et al., 1998). It is obvious that within EVn-BETR, the environmental distribution of chemicals is governed by long-term patterns in atmospheric and aquatic transport, as well as other meteorological parameters. Within each model segment, the temperature fluctuates between

a maximum summer and a minimum winter value according to a sinusoid distribution, and a mean annual rain rate is used. Hence, the model is designed to assess the long-term distribution and fate of POPs, some of which could be close to achieving equilibrium between air and the surface (Meijer et al., 2003). All partition coefficients are temperature dependent, with regression parameters of the temperature dependency given by enthalpies of phase change. The specific parameterisation of both models assumes temperature-independent reaction half-lives for all compartments.

## 2.2. DEHM-POP

The POP version of the Danish Eulerian Hemispheric Model (DEHM-POP) is a 3-D Eulerian dynamic atmospheric chemistry transport model. The original version of DEHM was developed to study the atmospheric transport of sulphur into the Arctic (Christensen, 1997). It has been further developed to study the atmospheric transport of lead (Christensen, 1999), CO<sub>2</sub> (Geels et al., 2004)

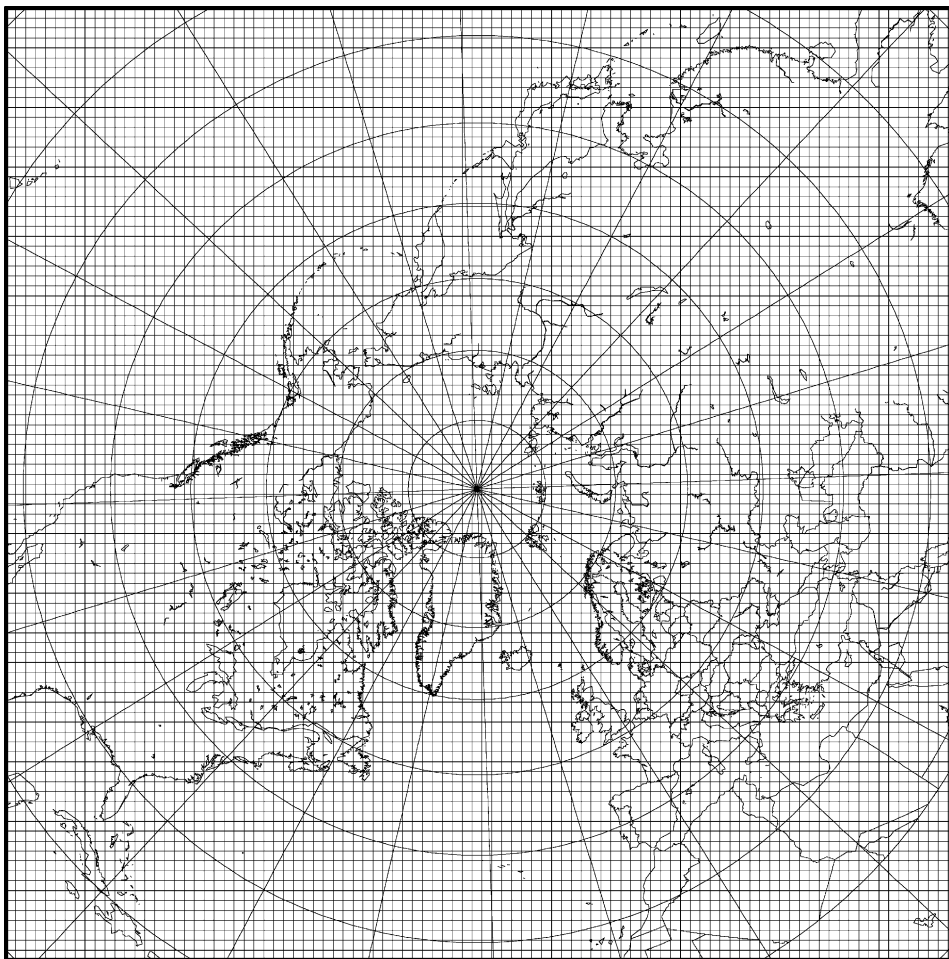


Fig. 2. DEHM-POP model grid and domain.

and mercury (Skov et al., 2004), and to include a chemical scheme with 60 components (Frohn et al., 2002). The model domain comprises the majority of the Northern Hemisphere and it is defined on a regular grid using a polar-stereographic projection with horizontal resolution of  $150\text{ km} \times 150\text{ km}$  at  $60^\circ\text{N}$  (Fig. 2). The model version used in this study has 18 unevenly distributed vertical layers described in terrain-following  $\sigma$ -coordinates. A soil module and an ocean module are introduced in DEHM-POP to account for the air-surface exchange of POPs arising from their semi-volatile nature (Hansen et al., 2004). DEHM-POP uses dynamic meteorological data as input to describe the atmospheric processes. Meteorological data are obtained from a numerical weather prediction model, MM5v2 (Grell et al., 1995), which supplies data on the wind velocity, temperature and humidity in each DEHM-POP grid cell with a temporal resolution of

3 h. These data are used to calculate horizontal and vertical advection and diffusion in the atmosphere and precipitation. MM5v2 uses the global meteorological TOGA data set from the European Centre for Medium Range Weather Forecasts on a  $2.5^\circ \times 2.5^\circ$  grid, with a time resolution of 12 h as input. DEHM-POP was successfully applied to study the atmospheric distribution of  $\alpha$ -HCH for the period 1991–1998 (Hansen et al., 2004).

### 2.3. Model similarities and differences

Differences in input parameters and process descriptions between the two models were minimised to facilitate this inter-comparison and interpretation of simulation results. The number of model compartments and compartmental segments followed the one of the less resolved model. Thus the number of environmental surface compartments

of EVn-BETR was reduced to match that of DEHM-POP. Similarly, the lowermost 8 atmospheric layers in DEHM-POP were averaged, corresponding to the lower air compartment (between 0 and 1000 m) in EVn-BETR and upper air concentrations were averaged from DEHM-POP layers 9–11 between 1000 and 2000 m. Regional concentrations were compared by averaging the concentrations in DEHM-POP grid cells within each of the EVn-BETR regions in the horizontal dimension.

The vegetation compartment of EVn-BETR was effectively neutralised by setting the vegetation cover of soil to zero. This is likely to cause a decrease in the computed air-to-surface flux, but, since all calculations were comparative/relative in nature, this was of minor importance. Freshwater and sediment volumes were set to zero.

The depths of the surface compartments in the two models were also set to the same value. The degradation rates and octanol–water ( $K_{OW}$ ) and temperature-dependent air–water ( $K_{AW}$ ) partition coefficient data were standardised; other transport parameters were chosen depending on whether they were commonly used in the two models. Table 1 presents the environmental and physical–chemical input used in this inter-comparison exercise.

As described above, horizontal and vertical advection and diffusion is calculated using long-term averaged meteorological data in EVn-BETR and dynamic data in DEHM-POP. Precipitation is described using a constant rain rate in EVn-BETR and as intermittent precipitation events using the dynamic input from the meteorological model in DEHM-POP. The original model descriptions for wet deposition were maintained in order to quantify the influence of these different parameterisations on the model output. Hence DEHM-POP distinguishes between below-cloud and in-cloud scavenging, with the latter process being more efficient due to higher droplet density in clouds (Christensen, 1997). EVn-BETR distinguishes between snow and rain scavenging, with the former being higher than the latter, whereas the same scavenging coefficients for rain and snow are used in DEHM-POP.

In DEHM-POP the air–soil and air–ocean gas exchange fluxes are driven by a deviation of chemical equilibrium between air and soil/ocean water, respectively. Stagnant two-film models determine the exchange velocities for the two media. The air–surface exchange processes in DEHM-POP are adapted from a zonally averaged multimedia

Table 1  
Normalised input data for the models

Standard model input	Value	Reference
Log $K_{ow}$	3.81	Mackay (2001)
Air reaction half-life (h)	1420	Mackay (2001)
Water reaction half-life (h)	43 800	Strand and Hov (1996)
Soil reaction half-life (h)	4380	Strand and Hov (1996)
Soil density ( $\text{kg m}^{-3}$ )	1350	Jury et al. (1983)
Soil organic carbon content	0.0125	Jury et al. (1983)
Soil depth (m)	0.15	Jury et al. (1983)
Ocean depth (m)	75	Strand and Hov (1996)
Temperature dependent $K_{AW}$		Kucklick et al. (1991)
<i>EVn-BETR-specific properties</i>		
Aqueous solubility ( $\text{g m}^{-3}$ )	1	Mackay (2001)
Molar mass	290.85	Mackay (2001)
Melting point ( $^{\circ}\text{C}$ )	157.5	Mackay (2001)
Rain scavenging ratio	100 000	Own value
<i>DEHM-POP-specific properties</i>		
In-cloud scavenging coefficient	100 000	Christensen (1997)
Below-cloud scavenging coefficient	70 000	Christensen (1997)

model (Strand and Hov, 1996). EVn-BETR, being a fugacity model, applies several transport parameters ( $D$  values, in  $\text{mol Pa}^{-1} \text{h}^{-1}$ ) to describe the magnitude of intermedia exchange processes. These  $D$  values can be compared to rate constants; when multiplied by fugacity (or partial pressure, in Pa) they give rates of transport (Mackay, 2001). They are calculated as the result of an inflow rate ( $\text{m}^3 \text{h}^{-1}$ ) multiplied by fugacity capacity (or the capacity of the chemical to remain in the medium of release, in  $\text{mol m}^{-3} \text{Pa}^{-1}$ ). It also includes exchange between adjacent ocean compartments by sea currents. The ocean compartments are stagnant in DEHM-POP. The original description of the air–surface gas exchange processes was retained in both models. These processes are described in detail in MacLeod et al. (2001); Prevedouros et al. (2004b) for EVn-BETR and in Hansen et al. (2004) for DEHM-POP.

#### 2.4. The modelled compound

The  $\alpha$ -isomer of the insecticide hexachlorocyclohexane (HCH) is used as the test chemical in the model simulations.  $\alpha$ -HCH is the major component of Technical-HCH, which was used extensively

worldwide from the mid-1940s, with an estimated global usage of 9.4 million tonnes (Li et al., 2003). The use of Technical-HCH is now banned or severely restricted in most countries.  $\alpha$ -HCH has a moderately high vapour pressure and a relatively high water solubility and is thus, mainly present as a gas in air or dissolved in water (Walker et al., 1999). It is considered to be purely in the gas phase in this inter-comparison exercise, which also further facilitates this inter-comparison and interpretation of simulation results. Reliable emission estimates derived by Li et al. (2000) exist for this chemical and model output can be directly compared to extensive monitoring data.

### 3. Results and discussion

The influence of different model descriptions on the fate of  $\alpha$ -HCH was evaluated by first investigating the importance of the different air removal processes, advection–diffusion, precipitation and air–soil and air–water gas exchange. The influence of the inferred differences was then examined by making two long-term simulations with hypothetical and realistic emission scenarios.

#### 3.1. Atmospheric removal processes

The efficiency of the four atmospheric removal processes: advection–diffusion, precipitation, air–soil gas exchange, and air–water gas exchange was tested by running the two models with only one of these processes active at a time and with combinations of two of them. The atmospheric dilution,

defined as the percentage of an initial concentration remaining in a region after a simulated time of 2, 7 and 30 days, was averaged within the EVn-BETR model domain and compared between the two models to highlight the influence of different loss processes (Table 2).

In each of the 10 simulations, an initial  $\alpha$ -HCH concentration of  $100 \text{ pgm}^{-3}$  was assumed in the lowermost 1 km of air; no further chemical present in water and soil or in air above 1 km height was assumed. In EVn-BETR, dilution was calculated from the lower air compartment (0–1 km). For the DEHM-POP model the averaged dilution was calculated from the lowermost layer (0–50 m), since the air–surface exchange processes are only active between the surface compartment and the lowermost air layer. The dilution is expected to be slightly different from a 50 m and a 1000 m thick layer. Higher dilution in the thicker layer is expected to arise from both advection and precipitation due to increased wind velocity and scavenging potential (derived from the in-cloud scavenging) with height. Similar differences are expected to arise from the air–surface gas exchange processes, which are only active between the surface compartment and the lowermost air layer. A 50 m layer will be depleted faster than a 1 km layer, hence the average dilution will appear to be greater from the 50 m layer than from the 1000 m one. Another uncertainty of this study arises because air–surface exchange processes depend on the concentration gradient between the air and the surface media. Thus, using a scenario with no initial concentration in the two surface media results in a maximum estimate of the

Table 2

Average dilution of air concentrations within the EVn-BETR model domain from individual air removal processes and combinations of two processes

Process <sup>a</sup>	DEHM-POP			EVn-BETR		
	2 days (%)	7 days (%)	30 days (%)	2 days (%)	7 days (%)	30 days (%)
A	65.1	91.5	98.8	3.1	10.0	39.8
P	21.6	55.1	92.0	6.6	20.7	59.5
AW	71.7	75.6	77.7	46.0	71.2	97.5
AS	3.3	9.0	25.9	2.7	9.0	33.3
A + P	71.3	97.4	100.0	6.7	19.0	54.0
A + AW	74.9	96.3	99.6	49.5	87.6	99.3
A + AS	65.1	91.5	98.8	3.8	11.8	44.3
P + AW	77.9	89.9	99.1	49.7	85.1	98.4
P + AS	23.8	59.1	93.9	6.9	21.7	61.4
AW + AS	73.0	78.9	87.0	46.4	81.4	97.7

<sup>a</sup>A—advection–diffusion, P—precipitation, AW—air–water gas exchange, AS—air–soil gas exchange.

atmospheric removal efficiency for this process. The average dilution within the model area is lower than for other processes since for example the air–ocean exchange is not active in regions without ocean water. The following section evaluates the relative model responses to chemical loss mechanisms and, as such, the results should be seen in their correct perspective.

### 3.1.1. Advection–diffusion

The most efficient atmospheric removal process in the DEHM-POP model is advection–diffusion with 91.5% on average removed from the domain after 7 days (Table 2). The dilution is largest near the borders of the domain in the beginning of the simulated period. The difference between regions evens out with time. This reflects that the model domain is almost completely depleted of  $\alpha$ -HCH after 30 days. Advection appears to be less efficient for EVn-BETR than for DEHM-POP.  $\alpha$ -HCH was diluted 10% on average after 7 days, with as low as 8% dilution in the central model regions and up to 13% in the north. After 30 days of simulation, the model generated an average air dilution of 40%, 35% in the central regions and up to 45% in the border regions. The relatively low dilution due to advection can be attributed to the high influence of advected air from all surrounding neighbouring regions. The EVn-BETR regions have atmospheric residence times of between 24 and 48 h and only around 6–7% of the concentration derives from the initial  $100 \text{ pg m}^{-3}$  in each region at the end of 1 month; the remainder is attributed to interregional inflows. Advected air from all surrounding adjacent regions therefore helps replenish the air concentrations to a greater extent than in DEHM-POP, where only neighbouring regions upwind support air concentrations.

### 3.1.2. Precipitation

The most efficient air removal process for EVn-BETR is precipitation. EVn-BETR uses long-term rain rates, which are assumed to remain constant throughout the year. The average dilution after 7 and 30 days of simulation was 21% and 60%, respectively for EVn-BETR. Differences of a factor of 6 were observed between regions at the end of the 30 days simulation, according to the rain rate of each region. The dilution was highest in Norway, presumably affected by snow scavenging. Air levels in southern Europe were the least affected by precipitation. Precipitation is described as intermit-

tent rainfall events in DEHM-POP as prescribed from the dynamic meteorological data, with the individual rainfall events being very efficient in removing  $\alpha$ -HCH from air. A region can therefore be depleted within a day. This also creates large spatial differences, as regions without rainfall events experience no dilution. The resulting average dilution was 55% and 92% after 7 and 30 days, respectively. The regional difference increases through the 30-day period, reflecting the large difference in air concentrations created by the intermittent rainfall events.

### 3.1.3. Air–surface gas exchange

The air–water gas exchange process in DEHM-POP appears to be a very efficient removal mechanism, with almost all chemical removed from the atmosphere above oceans within the first day. The resulting average dilution, reaching 78% after 30 days, is misleading, because in some regions there are cells with no ocean compartments. There is therefore minimal dilution in these cells. The assumed 75 m deep well-mixed surface ocean layer in the model has a large storage and uptake capacity of  $\alpha$ -HCH. This probably results in very fast dilutions of the air compartments over ocean. The air concentration gets diluted slightly faster in the northern part of the model domain, which reflects the temperature dependence of the gas-exchange process. The effect of the air–water gas exchange on air concentrations in EVn-BETR is also very significant. An average 46% of dilution throughout the model domain was found after 2 simulated days, increasing to 71% and 98% at the end of 7 and 30 days, respectively. Air–water exchange dominated the regions at the northwest of the model domain, due to the larger ocean compartments. Regions with large oceanic compartments in the South European area are affected to a lesser degree due to the temperature-driven process.

The least efficient air removal process in the two models is the air–soil gas exchange, with both models predicting almost the same dilution of about 3% after 2 days, 9% after 7 days and around 30% after 30 days of simulation (Table 2). Highest dilution was found in the northern part of the model domain. We should note at this point that both models used the same soil organic carbon (OC) content for all model segments. Region-specific OC content would be expected to increase the projected regional difference and, possibly produce larger discrepancies between the models.

### 3.1.4. Combinations of atmospheric removal processes

When two removal processes were combined in DEHM-POP, the average dilution was enhanced, e.g. the combination of advection–diffusion and precipitation effectively removed all chemicals in the model domain within 30 simulated days, whereas the average dilution due to the individual processes were 98.8% and 92%, respectively. The pattern was not so clear in the EVn-BETR model. Enhanced dilutions were also observed for combinations of some of the processes, such as the air–soil exchange combined with advection or precipitation. Whereas, when advection and precipitation were combined, the average dilution was smaller than the dilution due to the precipitation only (Table 2). This finding confirmed the influence of advection on sustaining the ambient air levels. The regional difference was minimised once advection was also present. This, again, clearly highlights the influence of advection, both in terms of predicted levels and regional differences in EVn-BETR.

### 3.1.5. Concluding remarks on the influence of atmospheric removal processes

The atmospheric removal processes appear to be more efficient in DEHM-POP than in EVn-BETR, both individually and in combination. This is due to the dynamic input used in DEHM-POP, as opposed to the averaged environmental data used as input in EVn-BETR. For example, the less efficient advection process in EVn-BETR resulted in regional atmospheric concentrations dominated by air advected from all surrounding neighbouring regions. The use of intermittent rainfall events in DEHM-POP can have two effects; a rainfall event is a more efficient removal process than long-term rain rates, but long dry spells can result in lower dilution on average. Inclusion of intermittent precipitation events, instead of constant precipitation rates, was shown to have a large effect on concentrations in multimedia fate models (Hertwich, 2001; Stroebe et al., 2004b). The combination of removal processes led to enhanced dilution in the DEHM-POP model, while the pattern was not so straightforward in the EVn-BETR model; in some cases the combined processes led to enhanced and in others to reduced dilution. This is believed to arise due to the averaged environmental data used as input. Similar non-predictive effects have been observed in a recent study on the effect of using time-averaged environmental data as input in environmental fate models (Lammel, 2004).

## 3.2. Hypothetical emission scenario

A full year simulation, beginning in spring, with hypothetical emissions of 1000 kg of  $\alpha$ -HCH emitted in the lowermost 1000 m of the atmospheric compartments in all regions was made. This emission input was evenly distributed throughout the simulated year; no background concentration was assumed in this simulation. The following sections will present modelled summer and winter concentrations in air, soil and water (averaged values over three months), as well as the generated spatial and seasonal variability. In this way, the influence of the various chemical dispersion and other loss processes, as described before, can be evaluated in terms of generated levels and the way the two models predict environmental distributions and seasonal trends. We argue that valuable insights into the characterisation of chemical fate can be extracted from such exercises.

### 3.2.1. Atmospheric levels and variability

For each season the mean upper and lower air concentration within the model domain is computed. These are presented in Table 3 together with the maximum and minimum concentrations and corresponding regions and with the computed spatial variability (SV), defined as the ratio between maximum and minimum concentrations within the model domain, and the seasonal variability (SeV), defined as the ratio between average summer and winter concentrations within the model domain. Fig. 3 shows the computed summer and winter average concentrations in the lower atmospheric compartment normalised with the mean concentration within the model domain for each model. Both models predict increased atmospheric loadings towards the northeast of the model domain for both summer and winter. The lowest concentrations were found in the northwestern regions, in accordance with the predominant European circulation pattern. Thus, both models predict minimum concentrations in southwest Ireland, with the EVn-BETR model predicting a factor of 2–3 higher concentrations than DEHM-POP for the two atmospheric compartments (Table 3). The difference in the maximum concentrations predicted by the two models is less than a factor of 3. The lower air concentrations of DEHM-POP are attributed to its more efficient air removal processes as described in Section 3.1. The largest discrepancies between the models were found in regions 23–29 (central

Table 3

Predicted maximum, minimum and mean  $\alpha$ -HCH atmospheric concentration ( $\text{pg m}^{-3}$ ) and oceanic concentrations ( $\text{pg l}^{-1}$ )

	Summer		Winter	
	EVn-BETR	DEHM-POP	EVn-BETR	DEHM-POP
Mean upper air	19.2	10.1	15.0	5.9
Max upper air	31.6	16.5	23.7	10.1
Region	29 (Ukraine)	29 (Ukraine)	28 (C Ukraine)	10 (E Siberia)
Min upper air	8.6	2.33	6.8	1.82
Region	21 (SW Ireland)	21 (SW Ireland)	21 (SW Ireland)	21 (SW Ireland)
Upper air SV	3.7	7.1	3.5	5.5
Upper air SeV	1.27	1.77	1.27	1.77
Mean lower air	31.7	15.5	25.6	16.1
Max lower air	61.2	19.9	46.1	26.3
Region	12 (Russia)	14 (Baltic Rep.)	27 (C Europe)	12 (Russia)
Min lower air	11.2	7.8	9.8	4.0
Region	21 (SW Ireland)	21 (SW Ireland)	21 (SW Ireland)	1 (One)
Lower air SV	5.5	2.5	4.7	6.6
Lower air SeV	1.22	1.08	1.22	1.08
Mean Ocean	14.0	14.0	36.4	38.7
Max Ocean	32.0	21.7	90.6	61.4
Region	8 (E Finland)	17 (North Sea)	8 (E Finland)	14 (Baltic Rep.)
Min Ocean	2.7	5.7	4.4	15.7
Region	4 (W Norway)	42 (C Spain)	4 (W Norway)	42 (C Spain)
Ocean SV	12.1	3.8	20.6	3.9
Ocean SeV	0.45	0.37	0.45	0.37

SV: Spatial variability, SeV: Seasonal variability. Region numbers can be seen in Fig. 1.

Europe), where EVn-BETR predicted relatively higher values than DEHM-POP and in regions 1–5 (northern Europe) and 40–50 (southern Europe), where DEHM-POP generated relative higher concentrations than EVn-BETR (Fig. 3). This is attributed to the atmospheric removal processes that are more efficient closer to the borders of the model domain in EVn-BETR as shown by the dilution experiments in Section 3.1, which is also confirmed by a mass flux analysis performed for this model.

The average spatial variability (SV) for the atmospheric compartments follows the concentration distribution pattern. EVn-BETR predicted an SV of 3.5–5.5 in air throughout Europe, while SV was 2.5–7.1 in DEHM-POP. Due to higher wind velocities in the upper layer of EVn-BETR, the atmospheric transport is more rapid, resulting in smaller SV in that compartment; the SV decreased from 4.7–5.5 (lower air) to 3.5–3.7 (upper air). EVn-BETR also predicted higher SV in air concentrations during summer than winter. A similar SV pattern was expected for DEHM-POP, but the SV was more variable due to the changing transport pattern originating from the dynamic input.

The average seasonal variability (SeV) was also similar in the two models. However, whereas the summer concentrations are higher than winter concentrations in all EVn-BETR regions, the average winter lower air concentrations were higher than the average summer lower air concentrations and there were 26 regions in both the lower and the upper atmospheric compartments in the DEHM-POP model with higher average winter than summer levels. This is probably caused by the dynamic input in DEHM-POP, where the short-term transport and precipitation pattern is varying and seasonal differences in air concentrations can occur, which was confirmed by repeating the simulation with DEHM-POP for another year, and thus another transport pattern.

The good agreement between the two models in both predicted concentration pattern, SV and SeV indicates that high vertical resolution is of less importance when predicting long-term average air concentration patterns. This supports findings from previous model experiments where a highly sophisticated air-chemistry transport model with 33 vertical layers was reduced to 4 atmospheric layers with comparable results (Strand and Hov, 1996).

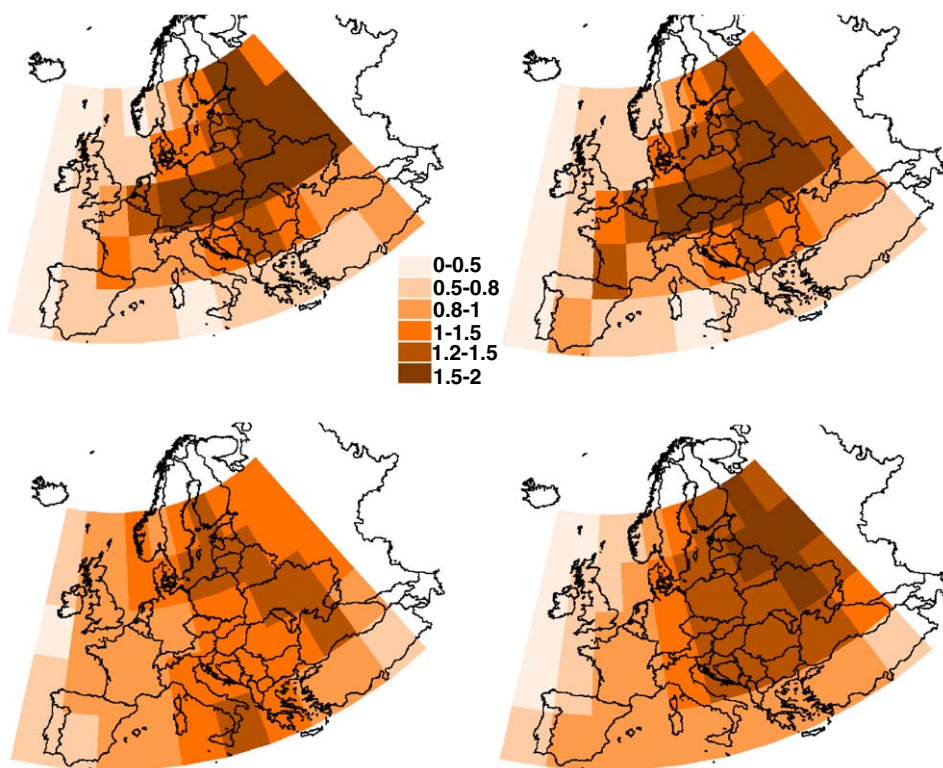


Fig. 3. Average summer (left) and winter (right)  $\alpha$ -HCH concentrations in lower air compartments for EVn-BETR (top) and DEHM-POP (bottom) for the hypothetical emission scenario with equal emissions in each region. Air concentrations are normalised with the mean concentration for each model.

However, when looking at smaller scales and/or regions, some differences especially seasonal ones, can only be highlighted by a dynamic model with a higher vertical resolution.

### 3.2.2. Concentrations and variability in oceans

Average ocean concentrations were predicted to be the same in the two models. Water concentrations closely reflected lower air concentrations in EVn-BETR, with higher concentrations towards the northeast and lower in the western part of the model domain. The ocean concentrations in DEHM-POP showed generally high values in the north and low values in the south because of the temperature dependence of the air–ocean gas exchange process.

Another process that can influence the concentrations is the ocean currents in the EVn-BETR model, which will remove chemicals from regions close to the border of the model domain. Because there are no currents in the DEHM-POP model this can result in a more rapid build-up of concentrations.

This is supported by the findings of low concentrations in five regions in the northern and western part of the domain in EVn-BETR, which were lower than in the corresponding regions in DEHM-POP. Ocean concentrations were predicted to be an average factor of 2.5 higher in winter than summer in both models, which is believed to reflect increased concentrations due to net air–ocean transfer.

EVn-BETR predicted higher SV values for water than DEHM-POP; regional differences during winter were as high as a factor of 20. Large water concentration differences between regions were generated due to low predicted levels in the north and west. DEHM-POP also predicted an increase in SV from summer to winter, but produced lower SV than EVn-BETR ( $<4$ ).

### 3.2.3. Soil

The SV pattern changed when looking at soil distributions, with mean soil concentrations a factor of 12 (summer) and 5 (winter) higher in DEHM-POP than in EVn-BETR. The higher DEHM-POP

soil concentrations point towards more efficient net flux from air to soil for this model. Since the air–soil exchange process was shown to result in similar air dilution, this difference may have arisen from the intermittent precipitation process. The soil concentrations in EVn-BETR closely reflected the lower air concentrations as seen with the ocean compartment, believed to reflect the assumed (constant) precipitation rates. DEHM-POP suggested that northeast soils are likely to accumulate  $\alpha$ -HCH at a high degree, as well as Scandinavian, and the Alpine region soils. The high concentrations in the last two regions can be attributed to increased deposition of  $\alpha$ -HCH with precipitation, since both are mountain regions. EVn-BETR predicted highest soil loadings for the northeast, followed by central European and Scandinavian soils. Again, this is the result of deposition processes and not sorption to the soil OC content.

The SV was higher in the EVn-BETR model, i.e. 10–17, while only 7–8 for DEHM-POP. Both models predicted an increase in SV during winter. These results are comparable to those of the ocean compartment and can be explained by the different characterisation of precipitation. Again, higher winter than summer concentrations were exhibited by soil, believed to show a build up of concentrations due to a net air to soil transfer. EVn-BETR predicted an average of 4 times higher levels in winter than summer, whilst DEHM-POP predicted a factor of 2.

### 3.3. Realistic emission scenario

To test the predictive capabilities of the two models, year-long simulations with realistic  $\alpha$ -HCH emissions and initial concentrations in soil and ocean water, as estimated from measurements, were conducted. Care should be taken when interpreting the model results from these simulations, since surface descriptions and environmental input were simplified. Surface compartments such as vegetation and fresh water were omitted and other environmental input parameters such as soil OC content were kept constant.

Emission estimates from the year 2000 by Li et al. (2000) were used as input. These data were calculated by estimating volatilisation from 2000 usage, as well as input from previous years' usage (Li et al., 2000). The derived emission estimates were redistributed from the original  $1^\circ \times 1^\circ$  resolution to the DEHM-POP model grid and used as

input for DEHM-POP. Emission input for EVn-BETR was calculated by averaging the emissions in the DEHM-POP grid cells within each EVn-BETR region. Highest emissions (672 kg) were found in region 45 (see Fig. 1), derived from usage in Tunisia, and in regions 34, 33, 27, and 28, derived from usage in Romania. The emissions were evenly distributed throughout the simulated year and mixed to a height of 1000 m.

To account for  $\alpha$ -HCH residues from past deposition, literature values for soil and water concentrations were adopted. A value of  $1 \text{ ng g}^{-1}$  was selected as a representative background soil burden, with soil measurements from Europe for the late 1990s varying between 0.2 and  $30.0 \text{ ng g}^{-1}$  (Manz et al., 2001; Covaci et al., 2001; Wenzel et al., 2002). Measurement data from the North Sea, Kattegat, and the Black Sea (Bethan et al., 2001; Maldonado and Bayona, 2002; Sundqvist et al., 2004) suggested oceanic water concentrations of  $0.002\text{--}4.6 \text{ ng l}^{-1}$ . An average of  $0.3 \text{ ng l}^{-1}$  was adopted for regions with an oceanic compartment. No initial concentration was used in the atmosphere due to the short mixing time.

Average predicted summer air concentrations in EVn-BETR ranged from  $9.7\text{--}92 \text{ pg m}^{-3}$  across Europe, with an average of  $49 \text{ pg m}^{-3}$ . Highest concentrations were evident in central and eastern Europe and lowest concentrations in the north-western part of the model domain. There was a factor of 10 difference between maximum and minimum concentrations within the model domain. The average lower air compartment concentration in DEHM-POP was a factor of 3 lower than EVn-BETR, i.e.  $15.8 \text{ pg m}^{-3}$ , with a range of  $4.7\text{--}62 \text{ pg m}^{-3}$ . In general the concentrations were more uniform within the model domain than in EVn-BETR, with high concentrations compared to the average in a few regions coinciding with major source regions. This suggests that primary emissions may play a more important role in supporting air concentrations in DEHM-POP than in EVn-BETR. This is in line with the more efficient air removal processes found in the dilution experiments (Section 3.1.). The SV of 13 for DEHM-POP was close to the EVn-BETR value.

The predicted normalised distribution patterns in lower air were also different. Fig. 4 shows the concentration in each region, normalised with the average concentration for each model. Relatively high concentrations are predicted by DEHM-POP for regions 33–34 and 44–47 (see Fig. 1 for region

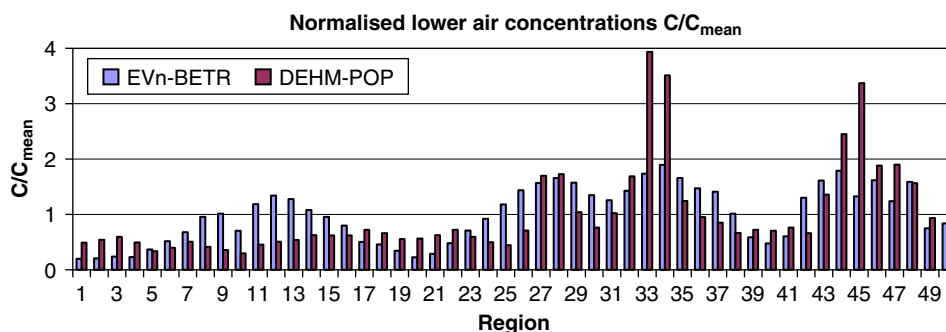


Fig. 4.  $\alpha$ -HCH concentrations in the lower air compartments normalised with mean concentration for each model for the realistic emission scenario simulation. Region numbers corresponds to regions in Fig. 1.

number). These regions were all major source regions. EVn-BETR predicted lower concentrations relative to DEHM-POP in the northwestern and western part of the model domain, which could indicate that ocean currents are transporting chemicals away from this part of the domain, leading to a depletion of the overlying air compartments. EVn-BETR predicted higher concentrations relative to DEHM-POP in regions 8–16, 24–26 and 35–38, i.e. in the northeast and central Europe. The EVn-BETR distribution pattern is very similar to the distribution pattern for the hypothetical emission scenario simulation, with greatest discrepancy in the southern regions. This distribution pattern is the result of a combination of the prevailing wind direction, leading to transport towards the northeastern part of the domain and the increased dilution in regions close to the borders of the model domain, as seen in the dilution experiments (Section 3.1.).

The average upper air concentrations were also higher in EVn-BETR by about a factor of 3. The distribution pattern followed closely the respective lower air for both models. The average ocean water concentration was about 30% lower in EVn-BETR than in DEHM-POP. Low EVn-BETR concentrations were found in border regions. This indicates the influence of ocean currents transporting chemicals away from the model domain, which was confirmed by a mass flux analysis for EVn-BETR. Large variations between regions were found in EVn-BETR, whereas the SV was low in DEHM-POP. This indicates that an insignificant amount of chemical compared to the inventory is deposited to the ocean in DEHM-POP in this simulation. The average soil concentrations were almost the same in the two models and there was an insignificant SV in

soil concentrations in either of the models, caused mainly by the normalisation of the soil organic carbon content.

Air concentration data from four monitoring stations, two in Sweden (Rörvik and Aspvreten), one in southern Norway (Lista) and one in the Czech Republic (Kosetice) were used to evaluate the model results (Berg et al., 2001; Aas et al., 2003). The 3-month summer averages of these measurements are presented in Table 4, together with the average model results from the respective regions. EVn-BETR predicts higher concentrations in Rörvik and Kosetice with a factor 2 and 4, respectively and predicts lower concentrations in Lista and Aspvreten by a factor 2 and 3, respectively. DEHM-POP predicts a factor of 2 lower concentrations for the stations, except for Aspvreten that showed very high measured values—a factor 8 higher than predicted by DEHM-POP. It is interesting to note that measured air concentrations in the Czech Republic were the lowest, despite their proximity to major primary emission sources. This could indicate that there are primary or secondary sources, which are not accounted for by the emission data or by the initial concentrations used as input in the model simulations.

To evaluate spatial patterns, the normalised modelled concentrations were compared to data from a passive air sampling campaign that was carried out across Europe (PASAE) lasting 6 weeks between June and July 2002 (Jaward et al., 2004). A total of 71 polyurethane foam (PUF) discs were deployed in both urban and rural sites throughout Europe, concurrently sampling ambient air.  $\alpha$ -HCH was among the quantified compounds, measured at detectable levels in 19 of the 50 model regions. In regions with more than one passive sampler, the

arithmetic mean value was selected as a representative concentration for the region. The average summer model predictions for the lower atmospheric compartment were compared to these measurements. The concentrations in the 19 regions, normalised to the mean for both models and passive air samplers are shown in Fig. 5. Relatively higher concentrations were measured in region 11 (Russia) than predicted by the models. This indicates either local contamination, not accounted for in the emission data, or model and/or measurement errors, or, possibly, a combination of all. Concentrations relatively higher than measured are predicted by both models in regions 27, 35, and 36, which are all close to regions with large emissions. This indicates either that the emission estimates are too high, and/or that the models or the emission estimates have a too coarse resolution. The latter

will re-distribute too high values into regions in the model with no real emissions and measured values may thus not be representative of the whole grid cell. In the other regions the predicted concentrations are close to the measured values for either one or both models (Fig. 5).

### 3.3.1. Comparison with other model estimates

A number of multimedia fate models have been used to study the fate of  $\alpha$ -HCH on a global scale. Wania and Mackay (1995) and Strand and Hov (1996) have reported representative examples of such models. However, their zonally averaged structure makes direct comparisons of concentrations difficult. The BETR-World model is built on the same model framework as EVn-BETR. The model divides the world into 25 regions following both climatic and continental or political borders (Toose et al., 2004). It has been used to study the environmental fate of  $\alpha$ -HCH for a 50-year period. BETR-World predicted  $\alpha$ -HCH air concentrations in Europe (which constitutes one region in the model) of around  $10 \text{ pg m}^{-3}$  in the late 1990s (Toose et al., 2004). POPCYCLING-Baltic is a regional multimedia model covering the Baltic Sea environment. It has been used to study the fate of  $\alpha$ -, and  $\gamma$ -HCH during 1970–2000 (Breivik and Wania, 2002). The model predicted  $\alpha$ -HCH concentrations in air of about  $10$ – $100 \text{ pg m}^{-3}$ , which compares favourably with measured air concentrations at stations in the Baltic Sea area (Breivik and Wania, 2002).

Table 4  
Summer averaged measured and modelled  $\alpha$ -HCH air concentrations ( $\text{pg m}^{-3}$ )

Station	Region	Measurement	EVn-BETR <sup>a</sup>	DEHM-POP <sup>b</sup>
Kosetice	26	17	70	10
Lista	4	24	11	12
Rörvik	16	20	39	10
Aspvreten	6	81	25	10

<sup>a</sup>EVn-BETR values are averaged for the corresponding region.

<sup>b</sup>DEHM-POP values are calculated from daily averaged concentrations extracted from the model by interpolation of the four nearest grid points for each site.

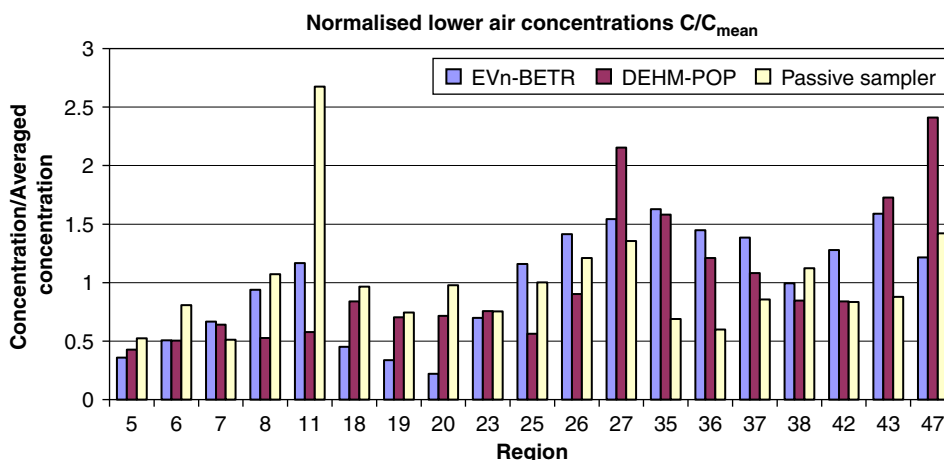


Fig. 5.  $\alpha$ -HCH concentrations in the lower air compartments normalised with the mean concentration for the two models for the realistic emission scenario simulation and for the passive air samplers. Region numbers corresponds to regions in Fig. 1. Correlation coefficients are EVn-BETR:  $r = 0.23$ ; DEHM-POP:  $r = 0.12$ . If region 11 is omitted, the correlation coefficients are EVn-BETR:  $r = 0.30$ ; DEHM-POP:  $r = 0.52$ , the latter significant with a significance level of 1%.

#### 4. Summary and concluding remarks

As far as we are aware, this paper presents the results of the first direct inter-comparison in terms of process description and transport algorithms between a fugacity-based multimedia box model (EVn-BETR) and a fully dynamic atmospheric chemistry transport model (DEHM-POP) applied to study environmental fate of POPs. Input to the two models was homogenised to a certain degree, while the original chemical distribution algorithms were retained. The assessment of individual air removal processes revealed an apparent difference in the atmospheric advection process as well as the important influence of precipitation and the differences produced when intermittent rain events were used instead of average rain rates. However, caution should be taken when generalising these results for other POPs, since  $\alpha$ -HCH is known to be among the more water soluble POPs. Both models were applied to simulate the fate of  $\alpha$ -HCH, with higher air levels predicted by EVn-BETR, which is believed to result from a less effective advection algorithm compared to DEHM-POP. One of the interesting findings of this study was the similar concentration patterns and generated spatial and seasonal variability when emitting a hypothetical amount of  $\alpha$ -HCH in each model region. This indicates that a coarse horizontal and temporal resolution probably adequately describe the long-term fate of  $\alpha$ -HCH. The short term and small-scale variability that the more detailed 3-D atmospheric chemistry transport model offers the opportunity to study have not been the issue of this study. Regarding the models' predictive capabilities, both accounted for measured air levels and, more importantly, captured the measured European spatial variability. Ocean currents were seen as a possible mechanism for transporting  $\alpha$ -HCH away from Europe for the EVn-BETR model.

Model inter-comparison exercises enhance scientific collaboration helping to highlight areas of uncertainty and different modelling philosophies. Such inter-comparisons are essential if models are to be used with confidence and transparency by decision-makers. Future inter-comparisons should address: varying important soil properties; the incorporation of other environmental compartments, notably vegetation, and the fate of other chemicals (e.g. particle-bound compounds). Finally, additional work is planned where the original model structures will be retained and the results

of the original and normalised “versions” will be compared.

#### Acknowledgements

KMH was partly funded by the Danish Research Training Council through the Copenhagen Global Change Initiative (COGCI). Lancaster University is grateful to the UK Department of the Environment, Food and Rural Affairs (DEFRA) Air Quality Division for financial support. We thank Dr. Foday Jaward for passive air sampling data and Dr. Jørgen Brandt (NERI) for comments on the manuscript.

#### References

- Aas, W., Solberg, S., Berg, T., Manø, Yttri; K. E., 2003. Monitoring of long range transported air pollutants. Annual report for 2002. SFT report 877/2003 NILU or 23/2003, Norwegian Institute for Air Research, Kjeller.
- Bennett, D.H., Scheringer, M., McKone, T.E., Hungerbühler, K., 2001. Predicting long-range transport: a systematic evaluation of two multimedia transport models. *Environmental Science and Technology* 35 (6), 1181–1189.
- Berg, T., Hjøllbrekke, A. G., Larsen, R., 2001. Heavy metals and pops within the EMEP region 1999, EMEP/CCC 9/2001.
- Bethan, B., Dannecker, W., Gerwig, H., Hühnerfuss, H., Schulz, M., 2001. Seasonal dependence of the chiral composition of  $\alpha$ -HCH in coastal deposition at the North Sea. *Chemosphere* 44, 591–597.
- Beyer, A., Scheringer, M., Schulze, C., Matthies, M., 2001. Comparing representations of the environmental spatial scale of organic chemicals. *Environmental Toxicology and Chemistry* 20 (4), 922–927.
- Breivik, K., Wania, F., 2002. Evaluating a model of the historical behavior of two hexachlorocyclohexanes in the Baltic Sea environment. *Environmental Science and Technology* 36 (5), 1014–1023.
- Christensen, J.H., 1997. The Danish Eulerian Hemispheric Model—a three-dimensional air pollution model used for the Arctic. *Atmospheric Environment* 31 (24), 4169–4191.
- Christensen, J. H., 1999. An overview of modelling the Arctic mass budget of metals and sulphur: emphasis on source apportionment of atmospheric burden and deposition, In: *Modelling and Sources: A Workshop on Techniques and Associated Uncertainties in Quantifying the Origin and Long-range Transport of Contaminants to the Arctic*. Report and extended abstracts of the workshop, Bergen, 14–16 June 1999. AMAP report 99:4. see also <http://www.amap.no/>.
- Covaci, A., Hura, C., Schepens, P., 2001. Selected persistent organochlorine pollutants in Romania. *The Science of the Total Environment* 280, 143–152.
- Frohn, L.M., Christensen, J.H., Brandt, J., 2002. Development of a high-resolution nested air pollution model—the numerical approach. *Journal of Computational Physics* 179, 68–94.
- Geels, C., Doney, S.C., Dargaville, R., Brandt, J., Christensen, J.H., 2004. Investigating the sources of synoptic variability in atmospheric CO<sub>2</sub> measurements over the Northern

- Hemisphere continents: a regional model study. *Tellus* 56B (1), 35–50.
- Grell, G. A., Dudhia, J., Stauffer, D. R., 1995. A description of the fifth-generation Penn State NCAR Mesoscale Model (MM5), NCAR/TN-398+STR, NCAR Technical Note, pp. 122, Mesoscale and Microscale Meteorology Division, National Center for Atmospheric Research, Boulder, CO.
- Hansen, D.V., Poulain, P.M., 1996. Quality control and interpolations of WOCE-TOGA drifter data. *Journal of Atmospheric and Oceanic Technology* 13, 900–909.
- Hansen, K.M., Christensen, J.H., Brandt, J., Frohn, L.M., Geels, C., 2004. Modelling atmospheric transport of  $\alpha$ -hexachlorocyclohexane in the Northern Hemisphere with a 3-d dynamical model: DEHM-POP. *Atmospheric Chemistry and Physics* 4, 1125–1137.
- Hertwich, E.G., 2001. Intermittent rainfall in dynamic multimedia fate modelling. *Environmental Science and Technology* 35 (5), 936–940.
- Jaward, F.M., Farrar, N.J., Harner, T., Sweetman, A.J., Jones, K.C., 2004. Passive air sampling of PCBs, PBDEs, and organochlorine pesticides across Europe. *Environmental Science and Technology* 38 (1), 34–41.
- Jury, W.A., Spencer, W.F., Farmer, W.J., 1983. Behavior assessment model for trace organics in soil: I. Model description. *Journal of Environmental Quality* 12 (4), 558–564.
- Koziol, A.S., Pudykiewicz, J.A., 2001. Global-scale environmental transport of persistent organic pollutants. *Chemosphere* 45, 1181–1200.
- Kucklick, J.R., Hinckley, D.A., Bidleman, T.F., 1991. Determination of Henry's law constants for hexachlorocyclohexanes in distilled water and artificial seawater as a function of temperature. *Marine Chemistry* 34, 197–209.
- Lammel, G., 2004. Effects of time-averaging climate parameters on predicted multicompartamental fate of pesticides and POPs. *Environmental Pollution* 128, 291–302.
- Lammel, G., Feichter, J., Leip, A., 2001. Long-range transport and multimedia partitioning of semivolatile organic compounds: a case study on two modern agrochemicals. Report no. 324. Max Planck Institute for Meteorology.
- Leemans, R., Cramer, W., 1991. The IIASA database for mean monthly values of temperature, precipitation and cloudiness of a global terrestrial grid. International Institute for Applied Systems Analysis (IIASA). RR-91-18.
- Li, Y.-F., Scholtz, M.T., van Heyst, B.J., 2000. Global gridded emission inventories of  $\alpha$ -hexachlorocyclohexane. *Journal of Geophysical Research* 105 (D5), 6621–6632.
- Li, Y.-F., Scholtz, M.T., van Heyst, B.J., 2003. Global gridded emission inventories of  $\alpha$ -hexachlorocyclohexane. *Environmental Science and Technology* 37 (16), 3493–3498.
- Ma, J., Daggupaty, S., Harner, T., Li, Y.-F., 2003. Impacts of Lindane usage in the Canadian prairies on the Great Lakes ecosystem. I. Coupled atmospheric transport model and modeled concentrations in air and soil. *Environmental Science and Technology* 37 (17), 3774–3781.
- Mackay, D., 2001. *Multimedia Environmental Models: The Fugacity Approach*, second ed. Lewis Publishers, Boca Raton.
- MacLeod, M., Woodfine, D.G., Mackay, D., McKone, T., Bennet, D., Maddalena, R., 2001. BETR North America: a regionally segmented multimedia contaminant fate model for North America. *Environmental Science and Pollution Research* 8 (3), 156–163.
- Malanichev, A., Mantseva, E., Shatalov, V., Strukov, B., Vulykh, N., 2004. Numerical evaluation of the PCBs transport over the Northern Hemisphere. *Environmental Pollution* 128 (1–2), 279–289.
- Maldonado, C., Bayona, J.M., 2002. Organochlorine compounds in the North-western Black Sea water: distribution and water column process. *Estuarine, Coastal and Shelf Science* 54, 527–540.
- Manz, M., Wenzel, K.-D., Dietze, U., Schüürmann, G., 2001. Persistent organic pollutants in agricultural soils of central Germany. *The Science of the Total Environment* 277, 187–198.
- Meijer, S.N., Ockenden, W.A., Sweetman, A.J., Breivik, K., Grimalt, J.O., Jones, K.C., 2003. Global distribution and budget of PCBs and HCB in background surface soils: implications for sources and environmental processes. *Environmental Science and Technology* 37 (4), 667–672.
- Prevedouros, K., Jones, K.C., Sweetman, A.J., 2004a. European-scale modeling of concentrations and distribution of polybrominated diphenyl ethers in the pentabromodiphenyl ether product. *Environmental Science and Technology* 38 (22), 5993–6001.
- Prevedouros, K., MacLeod, M., Jones, K.C., Sweetman, A.J., 2004b. Modelling the fate of persistent organic pollutants in Europe: parameterisation of a gridded distribution model. *Environmental Pollution* 128 (1–2), 251–261.
- Scheringer, M., Wegmann, F., Fenner, K., Hungerbühler, K., 2000. Investigation of the cold condensation of persistent organic pollutants with a global multimedia fate model. *Environmental Science and Technology* 34 (9), 1842–1850.
- Shatalov, V., Mantseva, E., Baart, A., Bartlett, P., Breivik, K., Christensen, J. H., Dutchak, S., Kallweit, D., Farret, R., Fedyunin, M., Gong, S., Hansen, K. M., Holoubek, I., Huang, P., Jones, K. C., Matthies, M., Petersen, G., Prevedouros, K., Pudykiewicz, J., Roemer, M., Salzmann, M., Scheringer, M., Stocker, J., Strukov, B., Suzuki, N., Sweetman, A. J., van de Meent, D., Wegmann, F., 2004. POP Model Intercomparison Study, Stage I. Comparison of descriptions of main processes determining POP behaviour in various environmental compartments. MSC-E Technical Report 1/2004.
- Skov, H., Christensen, J.H., Goodsite, M.E., Heidam, N.Z., Jensen, B., Wählin, P., Geernaert, G., 2004. Fate of elemental mercury in the Arctic during atmospheric mercury depletion episodes and the load of atmospheric mercury to the Arctic. *Environmental Science and Technology* 38 (8), 2373–2382.
- Strand, A., Hov, Ø., 1996. A model strategy for the simulation of chlorinated hydrocarbon distributions in the global environment. *Water, Air and Soil Pollution* 86, 283–316.
- Stroebe, M., Scheringer, M., Held, H., Hungerbühler, K., 2004a. Inter-comparison of multimedia modeling approaches: modes of transport, measures of long range transport potential and the spatial remote state. *Science of the Total Environment* 321, 1–20.
- Stroebe, M., Scheringer, M., Hertwich, E.G., 2004b. Comment on “intermittent rainfall in dynamic multimedia fate modeling”. *Environmental Science and Technology* 38 (20), 5484.
- Sundqvist, K.L., Wingfors, H., Brorström-Lundén, E., Wiberg, K., 2004. Air-sea gas exchange of HCHs and PCBs and

- enantiomers of  $\alpha$ -HCH in the Kattegat Sea region. *Environmental Pollution* 128 (1–2), 73–83.
- Toose, L., Woodfine, D.G., MacLeod, M., Mackay, D., Gouin, J., 2004. BETR-World: a geographically explicit model of chemical fate: application to transport of  $\alpha$ -HCH to the Arctic. *Environmental Pollution* 128 (1–2), 223–240.
- van Jaarsveld, J.A., van Pul, W.A.J., de Leeuw, F.A.A.M., 1997. Modelling transport and deposition of persistent organic pollutants in the European region. *Atmospheric Environment* 31 (7), 1011–1024.
- Vorosmarty, C. J., Fekete, B. M., Tucker, B. A., 1998. Global river discharge database (RivDis), v. 1.1. <http://www-eosdis.ornl.gov>.
- Walker, K., Vallero, D.A., Lewis, R.G., 1999. Factors influencing the distribution of Lindane and other hexachlorocyclohexanes in the environment. *Environmental Science and Technology* 33 (24), 4373–4378.
- Wania, F., 1999. Differences, similarities, and complementarity of various approaches to modelling persistent organic pollutant distribution in the environment. In: Proceedings of the WMO/EMEP/UNEP Workshop on Modelling of Atmospheric Transport and Deposition of Persistent Organic Pollutants and Heavy Metals, vol. 1., pp. 115–140.
- Wania, F., Mackay, D., 1995. A global distribution model for persistent organic chemicals. *The Science of the Total Environment* 160/161, 211–232.
- Wania, F., Mackay, D., 2000. A comparison of overall persistence values and atmospheric travel distances calculated by various multi-media fate models. WECC Report, WECC Wania Environmental Chemists Corp., Toronto, Canada, under Chlorine Chemistry Contracts No. 9461 and 9462.
- Wania, F., Dugani, C.B., 2003. Assessing the long-range transport potential of polybrominated diphenyl ethers: a comparison of four multimedia models. *Environmental Toxicology and Chemistry* 22 (6), 1252–1261.
- Wenzel, K.-D., Manz, M., Hubert, A., Schüürmann, G., 2002. Fate of POPs (DDX, HCHs, PCBs) in upper soil layers of pine forests. *Science of the Total Environment* 286, 143–154.
- Woodfine, D., MacLeod, M., Mackay, D., Brimacombe, J.R., 2001. Development of continental scale multimedia contaminant fate models: integrating GIS. *Environmental Science and Pollution Research* 8 (3), 164–172.